HHS Public Access

Author manuscript

*Compr Physiol*. Author manuscript; available in PMC 2022 December 24.

Published in final edited form as:

*Compr Physiol*. ; 11(4): 2371–2432. doi:10.1002/cphy.c200028.

# Regulation of the Cerebral Circulation During Development

**Raymond C. Koehler***

Department of Anesthesiology and Critical Care Medicine, Johns Hopkins University, Baltimore, Maryland, USA

## Abstract

The cerebral microcirculation undergoes dynamic changes in parallel with the development of neurons, glia, and their energy metabolism throughout gestation and postnatally. Cerebral blood flow (CBF), oxygen consumption, and glucose consumption are as low as 20% of adult levels in humans born prematurely but eventually exceed adult levels at ages 3 to 11 years, which coincide with the period of continued brain growth, synapse formation, synapse pruning, and myelination. Neurovascular coupling to sensory activation is present but attenuated at birth. By 2 postnatal months, the increase in CBF often is disproportionately smaller than the increase in oxygen consumption, in contrast to the relative hyperemia seen in adults. Vascular smooth muscle myogenic tone increases in parallel with developmental increases in arterial pressure. CBF autoregulatory response to increased arterial pressure is intact at birth but has a more limited range with arterial hypotension. Hypoxia-induced vasodilation in preterm fetal sheep with low oxygen consumption does not sustain cerebral oxygen transport, but the response becomes better developed for sustaining oxygen transport by term. Nitric oxide tonically inhibits vasomotor tone, and glutamate receptor activation can evoke its release in lambs and piglets. In piglets, astrocyte-derived carbon monoxide plays a central role in vasodilation evoked by glutamate, ADP, and seizures, and prostanoids play a large role in endothelial-dependent and hypercapnic vasodilation. Overall, homeostatic mechanisms of CBF regulation in response to arterial pressure, neuronal activity, carbon dioxide, and oxygenation are present at birth but continue to develop postnatally as neurovascular signaling pathways are dynamically altered and integrated.

## Introduction

Vascular physiologists traditionally integrate blood flow, vessel diameter, and vessel circumferential wall tension data by constructing conceptual models of homeostatic regulation that incorporate biophysical properties and molecular signaling within cell compartments and between cell types. These models take on increasing complexity as newer layers of cell signaling are unraveled and the nonlinear properties of multiple feedback and feed-forward signaling are revealed. Complexity is further increased when one examines the response of a brain region composed of heterogeneous cell populations or microcirculatory units that behave in a stochastic fashion. In terms of macroscopic cerebral blood flow (CBF) regulation, the most commonly considered input function variables in our homeostatic models are arterial blood pressure (ABP), basal energy metabolism,

*Correspondence to rkoehler@jhmi.edu.

neuronal activity, arterial partial pressure of carbon dioxide ($PCO_2$), arterial oxygen content ($CaO_2$), vascular neurogenic and hormonal influences, endothelial shear stress, and other endothelial-dependent factors. It is upon these conceptual physiologic models of CBF regulation for adult brain that we now add another layer of complexity for the developing brain in which the entire homeostatic regulatory system changes with time. All of the aforementioned input functions, the biophysical properties of the macrocirculation and microcirculation, and the numerous signaling pathways that control vascular tone all change throughout development. Angiogenesis is coordinated with neurogenesis. Extraparenchymal cerebral arteries that connect the microcirculation to the systemic circulation must adapt to the progressive increase in arterial pressure during development. The blood-brain barrier (BBB) must regulate the brain's interstitial fluid composition appropriately when plasma concentrations of energy substrates, glutamate (GLU) and other amino acids, hormones, and growth factors fluctuate. Energy demand increases as the brain grows, neuronal circuits are formed, synapses are pruned, and spontaneous neuronal activity increases. The fetal brain develops in an intrauterine environment with limited sensory input and an arterial oxyhemoglobin saturation of 60% to 70% and then experiences an abrupt transition at birth. Some of the signaling pathways that are prominent in adult brain can be less important in immature brain, whereas other signaling pathways appear more prominent in the immature brain. Hence, the vascular regulatory system is not stationary, and one needs to integrate many variables that change throughout development to understand the regulation of the cerebral circulation at different stages.

Our knowledge about the physiologic regulation of cerebral circulation during development has advanced considerably over recent decades in humans and animal models. Advances in humans have been facilitated with the use of positron emission tomography (PET), near-infrared spectroscopy (NIRS), and new magnetic resonance imaging (MRI) techniques. Much of our knowledge regarding prenatal regulation of the cerebral circulation is derived from the chronically instrumented fetal sheep model, whereas that obtained in postnatal animals is largely derived from neonatal lambs and piglets. In addition, better imaging techniques have more recently permitted study of the rodent cerebral circulation during development. The objective of this article is to synthesize historical and recent data on the regulation of the cerebral circulation during development and assess the degree to which common principles have emerged, which enhances our understanding of the development of this critical vascular bed.

We focus on the major themes of cerebrovascular physiology: (i) the relationship between CBF, cerebral metabolic rate of oxygen ($CMRO_2$), and cerebral metabolic rate of glucose (CMRGluc), also known as metabolic coupling; (ii) the coupling of vascular tone to neuronal activity, also known as neurovascular coupling; (iii) the vascular response to changes in cerebral perfusion pressure (CPP), also known as autoregulation; (iv) modulation of smooth muscle tone by factors released from the endothelium and astrocytes; (v) the vascular response to changes in arterial $PCO_2$, also known as $CO_2$ reactivity; and (vi) the vascular response to changes in the partial pressure of oxygen ($PO_2$), whether it is a decrease (hypoxia) or an increase (hyperoxia), and to changes in $CaO_2$, whether induced by changes in $PO_2$ or hemoglobin concentration. Understanding developmental changes in CBF is complex because of concurrent and interdependent changes in (i) energy metabolism; (ii)

neuronal connectivity, neurotransmitter release, and neurotransmitter receptors; (iii) mean arterial blood pressure (MAP); (iv) vascular and perivascular nonneuronal cell maturation; and (v) arterial blood gases, hematocrit, and $O_2$ affinity of hemoglobin after parturition.

## Changes in Cerebral Blood Flow During Development

### Cerebral blood flow during childhood

The main techniques that have been applied for the measurement of CBF in children include the Kety-Schmidt nitrous oxide tissue uptake technique that started in the 1950s, radiolabeled xenon clearance techniques in the 1980s, PET techniques in the 1980s, NIRS techniques in the 1990s, and multiple MRI techniques in the 2000s. Transcranial Doppler ultrasound measurements of blood velocity in large cerebral arteries have also been used to assess physiologic vascular regulation within the same subject. $CMRO_2$ has been derived with direct sampling of jugular venous bulb blood and with PET, NIRS, and MRI techniques. CMRGluc has been measured with the PET technique. Together, these techniques provide a picture of the relationship between blood flow and energy metabolism during development.

Normal levels of CBF are considered to be in the range of 54 to 60 mL/min/100 g of tissue for young adult males and about 10% higher for young adult females (221, 222, 300). Early measurements of global CBF in unsedated children utilized arterial and jugular bulb sampling to analyze the uptake of the diffusible indicator nitrous oxide administered by face mask. In 1957, Kennedy and Sokoloff (221) reported an average CBF of 106 mL/min/100 g in nine children ranging in age from 3 to 11 years old (Figure 1). This value was 77% greater than the average value of 60 mL/min/100 g obtained with the same technique in young adults. Others reported values of 65 to 69 mL/min/100 g in infants and older children under anesthesia for surgery (392, 393). These lower values reflect a decrease in energy demand with general anesthesia, but the values still exceed the levels of awake adults.

Greater regional resolution was subsequently obtained with single-photon emission computed tomography (SPECT) after intravenous injection of the tracer $^{133}Xe$. In 1992, Chiron et al. (96) reported on regional CBF in 42 children ranging in age from 2 days to 19 years with 60% of the subjects less than 2 years old. Global CBF in infants was near the adult level of 50 mL/min/100 g, gradually increased by 40% to 70 mL/min/100 g by 4 years, and remained at this elevated level through 8 years before slowly declining back to the adult level of 51 mL/min/100 g at 22 years of age (Figure 2). However, distinct regional differences were present. All regions of cerebral cortex had CBF below adult levels at 2 to 45 days of age, whereas thalamus, cerebellar vermis, and cerebellar hemispheres had CBF at or moderately exceeding the adult levels for these regions. Within cerebral cortex, adult levels of CBF for each region were attained at different times: 2 to 4 months for primary sensorimotor (SM) cortex, 2 to 6 months for primary visual cortex, 4 to 5 months for auditory cortex, 7 to 10 months for parietotemporal association cortex, 12 months for the pole of the temporal lobe, approximately 16 months for Brocca's area, and 13 to 24 months for prefrontal association cortex. Interestingly, CBF in all cortical regions continued to increase; by 5 years of age, CBF exceeded adult levels by approximately 70%. Thereafter, CBF gradually declined but remained elevated above adult levels throughout adolescence.

CBF in thalamus, cerebellar vermis, and cerebellar hemisphere exceeded adult CBF by approximately 25% to 33% in infants and remained elevated throughout most of childhood.

In another study of 24 children ranging in age from 10 days to 16 years, Takahashi et al. (408) confirmed a similar temporal-spatial pattern of CBF during development with PET imaging. CBF in cerebral cortex increased from levels below adult values in infants to levels 20% to 70% above adult values by 3 to 8 years of age, and CBF in thalamus, cerebellum, and brainstem increased from near-adult levels in infants to levels 40% to 60% above adult values at 3 to 8 years of age (Figure 3). In both the SPECT- and PET-based studies, the overall temporal-spatial pattern of CBF is thought to reflect the temporal-spatial pattern of developmental changes in energy metabolism. Thus, these studies of regional CBF confirmed the elevated global CBF seen at 3 to 11 years of age decades earlier with the nitrous oxide technique and extended the originate findings to describe different temporal patterns in different brain regions.

Although CBF has been noted to decline during adolescence, arterial spin labeling MRI has been used to quantify the time course of this decline (388). Interestingly, both males and females show a decline in early adolescence; however, females then display an increase in CBF at midpuberty in brain regions related to executive function (Figure 4). The regional specificity of these postpubertal sex differences suggests that differences in neuronal connectivity and function may form the basis of sex differences in the CBF trajectory during late brain development. Effects of sex hormones on vascular function and lower postpubertal hematocrit may also contribute to higher CBF in females. Another consideration is a sex difference in gray matter density (GMD) during adolescent development. Gradations in the T1 MR image are considered to reflect the density of gray matter in each voxel. Relative to the GMD of 8-year-old males, GMD in adolescent females outpaces males, whereas gray matter volume (GMV) is higher in males (Figure 4B) (156). Thus, the higher CBF per volume of tissue in late adolescent females may be supporting a higher density of gray matter.

Collectively, the literature on CBF during childhood indicates progressive increases in CBF in a region-specific manner over the first few years of life, with peak levels sustained over approximately 4 to 11 years of age. During adolescence, CBF gradually declines in a sex-specific manner until adult levels are attained at approximately 22 years of age. The increase in CBF in cerebral cortex is delayed relative to subcortical regions, but it then exceeds adult levels in cortex to a greater extent than that in subcortical regions. Region-specific developmental increases in CBF that exceed those of adults have also been described in rats at postnatal day (PND) 17 (331), in dogs at PND 20 to 60 (220), and in 1-week-old lambs (227, 230, 383). These developmental patterns have been assumed to correspond to species-specific developmental periods of enhanced neuronal activity, neurotransmitter synthesis and metabolism, synaptic proliferation and plasticity, development of glial function, and myelination.

## Cerebral blood flow in neonates

The clinical definition of a newborn is a baby less than 24-h old, whereas the formal definition of a neonate is a baby 1 to 30 days old. In general, studies of CBF in neonates

historically began after those in older children because techniques that could be used in neonates were limited. Although CBF measurements are not available for human fetuses, some insights into the effect of early development have been obtained by studying neonates born prematurely. The general finding is that neonates born prematurely have lower CBF than those born at term and that CBF then increases considerably during the first few postnatal months. One of the early studies of CBF in human neonates utilized the $^{133}$Xe clearance technique in which exposure to radiation is limited to a few minutes before clearance by the lungs. In preterm babies born at 29 to 34 weeks postmenstrual age (PMA) who had a normal neurological exam and were studied 1 to 7 weeks after birth, cortical gray matter blood flow averaged 88 ± 20 mL/min/100 g (±SD) and mixed gray and white matter compartment flow was 46±14 mL/min/100 g (473). Much of the variability was attributable to hematocrit (474). Much lower values were reported in sick preterm neonates when measurements were made within a few days of birth instead of several weeks. With the $^{133}$Xe clearance technique, Skov et al. (399) reported that neonates born over a wide range of 27 to 39 weeks PMA had CBF in a range of 5 to 30 mL/min/100 g with a median of 15 mL/min/100 g, whereas Bucher et al. (75) reported that neonates born within a more narrow 26 to 29-week PMA range had CBF values in a more narrow range of 10 to 17 mL/min/100 g. In both studies, CBF was also quantitated with a NIRS technique that utilized a sudden increase in arterial hemoglobin saturation as an arterial input tracer. A reasonable correspondence of the noninvasive NIRS technique with the $^{133}$Xe technique was demonstrated.

Limited CBF data in neonates has been obtained using PET scans to measure the kinetics in arterial blood and brain after intravenous injection of $^{15}$O-labeled water. In 16 preterm neonates born at 26 to 36 weeks PMA and studied at 2 to 39 days of age, Altman et al. (11) reported CBF that ranged widely from 5 to 23 mL/min/100 g. Some of this variability was due to the variation in PMA and disease states. The majority of subjects had intraventricular hemorrhage, and some had experienced hypoxia-ischemia, patent ductus arteriosus, or previous extracorporeal membrane oxygenation (ECMO) with ligation of a common carotid artery. Despite having CBF that was low compared to that in older children and adults, many had good neurologic outcome, suggesting that the threshold for ischemia is at a low CBF level in premature newborns. Indeed, a follow-up study (10) indicated much lower $CMRO_2$ compared to that in older children and adults. Using the same PET techniques in 14 neonates who were born at term with hypoxic-ischemic encephalopathy or required previous ECMO, CBF measured at 2 to 39 days of age ranged from 9 to 73 mL/min/100 g (11). Again, some with the lowest CBF and $CMRO_2$ had normal outcome.

More recently, two MRI techniques have been developed to measure brain perfusion in neonates. Because these techniques are noninvasive and do not require radioactive tracers, they are becoming more frequently used to provide detailed information about preterm and term neonates with neurologic and nonneurologic disorders.

One of the MRI techniques applies the arterial-spin labeling technique developed for adults with some modifications to account for the slower carotid artery-to-capillary transit times in neonates. This technique has the advantage of providing regional perfusion measurements and can be used to identify areas of focal stroke (116). De Vis et al. (115) applied arterial

spin labeling to sedated preterm infants born at 24 to 32 weeks of gestation. Global CBF was 7±2 mL/min/100 g when measured at 30 to 33 weeks PMA and 12±3 mL/min/100 g when measured at 40 to 43 weeks PMA. In those born at term and measured at 3 months, CBF was 29±8 mL/min/100 g. In basal ganglia, the corresponding CBF values were higher than global CBF: 20±6, 29±9, and 49±8 mL/min/100 g. In term neonates who suffered a hypoxic-ischemic event at birth, CBF in basal ganglia, a region particularly vulnerable to cell death, was even higher after the ischemic event (median CBF 63, range 28-108 mL/min/100 g) than it was in uninjured term neonates (median CBF 28, range 12-51 mL/min/100 g) (113). This higher basal ganglia CBF correlated with death or cerebral palsy at 9 to 18 months. It should be noted that the global CBF values detected with arterial spin labeling MRI tended to be lower than those obtained with the $^{133}$Xe clearance technique, possibly because of poorer signal/noise ratio with the MRI technique at low flows and the use of sedatives. On the other hand, the $^{133}$Xe technique can overestimate CBF when the tissue is not saturated with tracer because diffusion between gray and white matter compartments alters the washout curve.

In another study with arterial spin labeling, Tortora et al. (415) reported that preterm infants born at less than 32 weeks PMA with normal brain MRI and studied at 39 to 41 weeks PMA had significantly higher global CBF (median CBF 9, range 6-13 mL/min/100 g) than those with periventricular white matter damage on MRI (median CBF 6, range 2-10 mL/min/100 g). This difference was present in much of the cortical gray matter, thereby indicating that the blood flow deficit extended beyond the white matter lesion. Interestingly, CBF in the preterm infants with normal brain MRI was also greater than that in neonates born at term with normal brain MRI and studied at an equivalent PMA (median CBF 7, range 4-12 mL/min/100 g). Whether this higher CBF in the preterm infants at equivalent PMA is the result of accelerated postnatal development energy demand or differences in physiologic parameters, such as hematocrit, MAP, and blood gases, is unclear.

Another MRI technique measures blood velocity by the phase shift of the magnetic spins of translocated protons in the internal carotid and vertebral arteries. The velocity measurements and the images of arterial diameter are used to calculate global CBF (290). With this technique, CBF was reported to be 14±5 mL/min/100 g in neonates at 35 to 42 weeks PMA. Interestingly, a significant correlation was observed between CBF and PMA over this age range such that CBF increased approximately 1.2 mL/min/100 g per week (343). Collectively, these studies using distinct techniques indicate that CBF in preterm neonates is an order of magnitude lower than that in adults and that CBF is somewhat higher in term neonates but still only 20% of adult values. Thus, much of the developmental increase in CBF occurs postnatally in humans.

Figure 5 displays CBF throughout human development spanning preterm newborns to 22 years of age based on mean values from several studies (96, 114, 115, 290, 343). The pace of increase in CBF is greatest through the first 6 postnatal months, after which CBF increases more slowly through 3 years of age. Then, CBF gradually declines after 12 years of age. Also shown in Figure 5 are the corresponding values of MAP. MAP increases throughout the prenatal and early postnatal periods and continues to progressively increase throughout the rest of childhood. Normal values of intracranial pressure (ICP) are not available in healthy

newborns and older children although major changes are unlikely. Assuming that ICP is about 6 mmHg at all ages, CPP (CPP=MAP–ICP) could be estimated and cerebrovascular resistance (CVR) calculated as a function of age. As shown in Figure 5, marked reductions in CVR occur prenatally and through the first 6 postnatal months as the increase in CBF outpaces the increase in MAP. This decrease in CVR is related to brisk angiogenesis and arteriogenesis during this period. CVR then remains at low values through at least 3 to 12 years of age, after which MAP continues to increase while CBF decreases. The resulting increase in CVR is likely the result of continual thickening of the arterial smooth muscle and increases in myogenic tone. As discussed in the following section, decreases in cerebral energy metabolism occur beyond 12 years, which would be expected to increase basal vascular tone.

## Cerebral Energy Metabolism During Development

### Cerebral oxygen consumption during development

A fundamental concept in cerebrovascular physiology is that the delivery of $O_2$ is matched to the $O_2$ consumption such that tissue $PO_2$ at the most distant mitochondria from a capillary is regulated at a level well above the minimum $PO_2$ needed for oxidative phosphorylation. By regulating tissue $PO_2$ well above that needed for cytochrome oxidase activity, the tissue has a safety reserve for meeting dynamic fluctuations in energy consumption on a timescale faster than vascular smooth muscle (VSM) can respond to change CBF. The average tissue $PO_2$ depends on the balance of $O_2$ consumption and $O_2$ delivery to the mitochondria. The latter depends on several factors including the amount of $O_2$ transported to the microcirculation ($CaO_2$ × CBF), the hemoglobin affinity for $O_2$, capillary surface area, and capillary density. All of these factors change during development.

$CMRO_2$ increases during development in parallel with the growth of the brain and maturation of synaptic connectivity and activity. As brain growth subsides, $CMRO_2$ also declines to adult levels. For example, early work with the nitrous oxide method of global CBF measurement indicated that $CMRO_2$ in children 3 to 11 years old is 230 μmol $O_2$/min/100 g tissue (Figure 1), which exceeds the value of approximately 180 μmol $O_2$/min/100 g detected with this technique in young adults (221) and reported with other techniques (300). These values also exceed those obtained in an early study of infants and toddlers with developmental impairment of mental ability arising from hydrocephalus, seizures, and cerebral palsy (149). Early work in which maximum regional $O_2$ consumption was measured *ex vivo* indicated region-specific increases in $O_2$ consumption capacity over the first 6 postnatal weeks to levels exceeding those in adult dog brain (190). Corresponding temporal changes in regional CBF were later reported in immature dog brain (220). In sheep, which exhibit more rapid prenatal brain development, global $CMRO_2$ is approximately 55%, 75%, and 140% of adult levels at 60% of gestation (0.6 gestation), 0.9 gestation, and 1-week after birth, respectively (160, 210, 230, 382). These changes in $CMRO_2$ are accompanied by parallel developmental changes in CBF, with CBF in 1-week-old lambs exceeding that in adult sheep (230). This overshoot is analogous to the overshoot in CBF and $CMRO_2$ seen in humans later in childhood, as shown for different brain regions in children of different ages (Figure 3). However, compared to sheep and dogs, this age-dependent increase in

$CMRO_2$ is extended over a longer period in humans because the period of postnatal brain development is prolonged. For example, an early study of $CMRO_2$ measured with PET reported values in the range of 3 to 24 μmol $O_2$/min/100 g in preterm neonates born at 26 to 32 weeks PMA and in the range of 18 to 58 μmol $O_2$/min/100 g in term neonates born at 40 weeks PMA (10). Although all of these neonates were sick at the time of imaging, some had normal neurologic outcome. In another study of neonates born at 24 to 41 weeks PMA and receiving intensive care, $CMRO_2$ derived from a NIRS technique ranged from 9 to 79 μmol/min/100 g; $CMRO_2$ and cerebral $O_2$ transport ($CaO_2$ × CBF) have a positive correlation with PMA (475). In the very preterm neonates (25 weeks PMA), the NIRS technique indicated an increase in $CMRO_2$ and cerebral $O_2$ transport over the first 3 days after birth, which presumably represents an early adaptation to the extrauterine environment in these sick neonates (224).

Over the first 6 weeks after preterm birth, $CMRO_2$ continues to increase at a rate of approximately 10% per week (379). Liu et al. (290) used MRI to measure $T_2$ relaxation of sagittal sinus blood that was calibrated against $O_2$ saturation. When combined with a phase contrast measure of global CBF, the calculated global $CMRO_2$ averaged 38 μmol/min/100 g and was found to increase linearly between 35 and 42 weeks PMA (studied approximately 3 weeks after birth) with a slope of 5.2 μmol $O_2$/min/100 g per week (Figure 6). This increase in $CMRO_2$ paralleled the increase in CBF with little change in venous $O_2$ saturation. Likewise, de Vis et al. (114) used a different MRI technique and reported higher $CMRO_2$ in term neonates than in preterm neonates. Overall, studies in human neonates indicate that $CMRO_2$ is less than 20% of adult values in preterm neonates and about 35% of adult levels in term neonates (112).

Beyond the neonatal period, PET imaging demonstrated regional increases in $CMRO_2$ during the first year after birth to approximately 50% to 80% of adult levels (408). Adult levels are nearly fully attained at 1 to 3 years, but delays are longer in frontal and visual association (VA) cortex. At 3 to 16 years of age, $CMRO_2$ increased to peak levels 20% to 40% above adult values throughout most brain regions other than frontal association (FA) cortex, which is thought to have continued synaptic development beyond 16 years. Thus, the regional $CMRO_2$ data obtained with PET confirmed the global $CMRO_2$ data obtained earlier with the nitrous oxide method in children over this age range. In general, CBF also increases during development in parallel with the increase in $CMRO_2$ and then declines slightly after the teenage years. The oxygen extraction fraction (OEF), which equals $CMRO_2$/(CBF × arterial $O_2$ content), remains relatively constant at approximately 0.35 after birth (290) and throughout childhood (408), although one study reported a postnatal increase in OEF over the first 3 months after birth (114), which might be related to postnatal decreases in hemoglobin $O_2$ affinity (228). Within the brain, this coupling of CBF to energy metabolic rate at equivalent levels of arterial $O_2$ content ($CaO_2$) also holds at a regional level (408).

A specialized NIRS technique has been developed in which the incident light intensity is modulated at 110 MHz, and different detector distances are used to calculate the path length of the light. This frequency-domain NIRS technique enables users to estimate deoxyhemoglobin and oxyhemoglobin contents in the cortex in absolute units rather than the relative units obtained with standard continuous-wave NIRS. It also allows an estimation

of CBF, cerebral blood volume (CBV), and, when combined with the technique of diffuse correlation spectroscopy, $CMRO_2$. In neonates born prematurely at PMA ranging from 24 to 37 weeks, CBF and $CMRO_2$ increased progressively over 6 postnatal weeks (379). However, tissue hemoglobin and tissue oxyhemoglobin saturation ($HbO_2$) decreased without a change in CBV over the 6-week period (Figure 7). In a follow-up study (380), the decreases in tissue hemoglobin and $HbO_2$ corresponded better with postnatal age than with PMA, suggesting that the decrease in tissue hemoglobin is likely the result of a postnatal decrease in hematocrit and that the decrease in tissue $HbO_2$ is likely the result of the replacement of high $O_2$-affinity fetal hemoglobin with lower affinity adult hemoglobin. In contrast, the CBF and $CMRO_2$ were shown to correlate better with the PMA than with the chronologic age after birth, suggesting that they are determined by brain maturation rather than by red blood cell (RBC) transition.

The NIRS technique also revealed differences among cortical regions. In a population of 55 premature neonates and 15 full-term neonates, some of whom had various disorders, CBF measured at approximately 3.6 postnatal weeks was higher in temporal and parietal lobes than in frontal lobes, and the right lobes had higher CBF than the left lobes in males (286). In a later study of 30 healthy term newborns at approximately PND 3, CBF and $CMRO_2$ were 15% higher in the right hemisphere, but females had 25% to 30% higher values than males in association with lower tissue hemoglobin concentration and lower tissue $HbO_2$ (136). These apparent changes in sex differences between preterm and term neonates will require further confirmation. The frequency-domain NIRS technique has also been used to track CBV over the first 12 months after birth in 47 healthy infants (143). After an early postnatal decrease in tissue total hemoglobin attributable to transient postnatal anemia, tissue hemoglobin content increased progressively through 40 weeks of age. Using the measured blood hemoglobin concentration, CBV was calculated. CBV did not display an initial postnatal dip but rather increased progressively through 40 weeks of age. This increase was similar in all cortical lobes and is presumed to reflect increased vascular density, a progressive decrease in vascular resistance, and increased CBF. Because the tissue oxyhemoglobin saturation was not markedly increased, the increased CBF is presumed to be coupled to a developmental increase in $CMRO_2$.

The developmental increase in $CMRO_2$ is thought to be matched to developmental increases in mitochondrial density. Regional maturation of oxidative metabolic capacity has been analyzed in the cat with cytochrome oxidase histochemistry (196). Adult levels were attained as early as 7 days in some motor regions, whereas other regions required 30 days. Interestingly, regions such as basal ganglia and thalamus attained histochemical activity that exceeded adult levels, possibly reflecting augmented metabolic demand for growth and synaptic proliferation. In piglets, selectively high levels of cytochrome oxidase histochemical activity in SM cortex, basal ganglia, and thalamus corresponded to selective vulnerability of these regions to hypoxia-ischemia (303–305). Term human newborns also exhibit selective vulnerability to hypoxia-ischemia in these brain regions (52, 316), suggesting a relationship between vulnerability and regional metabolic energy demand.

## Cerebral glucose consumption during development

Glucose is the primary energy substrate for the adult brain, but some species utilize other substrates, such as ketones, lactate, and fatty acids, early in development (105, 312). The [$^{14}$C]-2-deoxglucose autoradiographic technique and the corresponding 2-deoxy-2[$^{18}$F]fluoro-D-glucose PET imaging permit good regional spatial resolution of CMRGluc. These techniques show region-specific increases in CMRGluc postnatally in rat (330), cat (98), dog (220), sheep (1), monkey (207), and humans (99, 100). At birth, CMRGluc is below that seen in the adult brain (Figure 8). In humans, for example, CMRGluc at birth is about 70% of adult levels in cerebral cortex and 80% to 90% of adult levels in brainstem and cerebellum (100). Part of the low glucose consumption is attributable to the use of alternative energy substrates seen in some (105) but not all species (161, 187). However, part is due to region-specific differences in maturation of synaptic connectivity and spontaneous activity.

As with $CMRO_2$, CMRGluc increases during postnatal development to levels exceeding that in adult brain (Figure 8). In cerebral cortex, peak levels are attained at approximately PND 21 to 35 in rat, PND 60 to 180 in cat (98), PND 60 to 180 in vervet monkey (207), and 0.5 to 5 years in humans (97, 100). These periods of high CMRGluc are thought to correspond to the period of greatest brain growth, synapse formation, synapse plasticity, and associated increases in electrical activity during cortical development. High levels of protein synthesis between PND 15 and PND 90 in cat brain to levels exceeding those in adult cat support this concept (197). In humans, remarkably, the CMRGluc level in the neocortex of infants and toddlers approaches twice that observed in adult neocortex (Figure 8). Moreover, this relative difference exceeds that of $CMRO_2$, which is approximately 20% to 40% higher in infants and toddlers than in adults. This contrast between CMRGluc and $CMRO_2$ suggests that excess aerobic glycolysis is used to support high levels of protein and lipid production for synapse and neurotransmitter turnover, electrical activity, and neuronal plasticity during this period of cortical development. Some glucose likely enters the pentose phosphate pathway for nucleic acid synthesis. In humans, this increase in CMRGluc to levels exceeding adult values occurs in all major brain regions, but it is less pronounced in brainstem and cerebellum, possibly because connectivity matures at an earlier developmental stage in phylogenetically older regions than in cerebral cortex. Within cerebral cortex, CMRGluc increases sooner in primary SM cortex than in other regions of neocortex, followed by increases in primary auditory and visual cortex and lastly by association cortex and frontal cortex (97, 99, 100). This temporal-spatial pattern is, in general, similar to that seen with CBF during human development. However, the time of peak CMRGluc (330) is later than the time of peak CBF in the rat (331), suggesting that the temporal correspondence is not necessarily precise.

## Energy budget

In humans, the ratio of brain weight to body weight is highest at birth and then declines as the body grows faster than the brain. This observation led to the assumption that the ratio of brain energy metabolism to total body resting metabolism is also greatest at birth. However, this assumption has proved incorrect. With the use of MRI, the volume of different brain regions during human development can be determined and combined

with regionally specific CMRGluc measurements to calculate absolute values of total brain glucose consumption more precisely. The estimated absolute amount of glucose consumed by the entire brain was shown to increase during development to peak values of 167 g/day in males and 146 g/day in females at 5 years of age followed by gradual declines to 88 g/day in adult males and 80 g/day in adult females (Figures 9A and 9B) (241). By converting energy requirements into glucose equivalents for whole-body maintenance functions, an equivalent resting rate of daily glucose consumption for the whole body can be calculated. As a percent of the resting whole body energy requirements at each age, the corresponding total brain glucose uptake in males and females are 53% and 60% at birth, 31% and 40% at 6 months, and 66% and 65% at 4.2 to 4.4 years (Figures 9C and 9D, solid lines). Thus, the fractional energy requirement of the brain peaks well beyond birth. A similar conclusion is reached when one uses a daily whole-body energy requirement that also includes physical activity and growth; brain glucose consumption utilizes 35% and 39% at birth, 25% and 27% at 7 months, and 43% and 44% at 3.8 to 4.0 years in males and females, respectively (Figures 9C and 9D, dashed lines). Interestingly, the period of greatest fractional glucose uptake by the brain corresponds to the period of slowest rate of the overall body growth (Figures 9E and 9F). The subsequent decline in the brain fractional glucose uptake corresponds approximately to the pubertal period of maximum body growth, which occurs earlier in females (424). One interpretation of these data is that the slow body growth in early human development relative to that of other mammals is an evolutionary adaptation attributable to a metabolic trade-off for the prolonged high-energy requirement for human brain development and for diversion of glucose into synthetic pathways (241).

In mature gray matter, considerably more than half of energy consumption is utilized in synapses for neurotransmission, including neurotransmitter synthesis, release, and reuptake, postsynaptic membrane ion changes, and downstream signaling (179, 198). The remainder is used to support basic cell functions related to molecular synthesis and degradation and maintaining resting membrane potential and basic cell function. Data from quiescent PND 21 rat hippocampal slices suggests that actin polymerization and depolymerization, microtubule turnover, and lipid synthesis are the major energy consumers of the nonsignaling cell function component, whereas protein synthesis is a minor component when there is no electrical activity (131). As neurons and glia grow in size and number and change shape, energy used to support lipid synthesis, actin and microtubule turnover, and mitochondrial biogenesis and trafficking is expected to increase progressively and contribute to the prepuberty overshoot in $CMRO_2$ and CMRGluc. Likewise, the developmental increase in the density of *N*-methyl-D-aspartate (NMDA) and α-amino-3-hydroxy-5-methyl-4-isoxazolepropionic acid (AMPA) receptors and the number of dendritic spines will also make a major contribution to the 10-fold increase in whole brain energy consumption between preterm newborns and prepubertal children. The decline in energy demand from puberty to adulthood is attributed to synaptic pruning and a decrease in biosynthetic processes as the brain achieves a stable size. Moreover, the progressive increases in energy demand occur at different rates in different brain regions as connectivity matures along the caudal-rostral axis. Thus, synaptic activity and presumably $CMRO_2$ will increase later in hippocampus and cerebral cortex than in brainstem, thalamus, and basal

ganglia. Within the cerebral cortex, primary SM regions increase their mitochondrial density earlier than do the secondary association cortex and frontal cortex.

## Neurovascular Coupling During Development

### Functional MRI studies in humans during development

In adult animals, neuronal activation of cerebral cortex leads to a small increase in the local $CMRO_2$, a larger percent increase in local CMRGluc, and an increase in CBF that is approximately proportional to the increase in CMRGluc and greater than the percent increase in $CMRO_2$. Consequently, the local vascular oxyhemoglobin concentration increases and deoxyhemoglobin decreases, providing a positive MRI blood oxygen level-dependent (BOLD) signal that is used to identify neuronal activation by functional MRI. Functional MRI has been used extensively to map areas of adult human brain that are activated by various paradigms of SM and cognitive tasks. Attempts have also been made to map activation during early developmental stages. Remarkably, positive BOLD responses seen in neonates are converted to negative BOLD responses in infants and then revert to positive BOLD responses later in childhood.

The negative BOLD response seen in young children reflects a mismatch of CBF and $CMRO_2$. For example, a study of four sedated children, ages 4 to 71 months, detected no increase in perfusion measured with arterial water spin labeling MRI in occipital cortex during photic stimulation (Figure 10A), resulting in a negative BOLD response (64). Yamada et al. (467, 468) reported that photic stimulation in barbiturate-sedated 0 to 7-week-old neonates and infants produced a positive BOLD response in occipital cortex, whereas stimulation in 8 to 22-week-old infants produced a negative BOLD signal (Figure 10B). They attributed this switch in the signal response to the developmental increase in synaptic density and basal CMRGluc that occurs in this region at 2 months (99, 100) and a greater percent increase in $CMRO_2$ during activation (324). Others reported that the negative BOLD response encompassed a larger area during later development through 48 months of age (65), which is likely related to maturation of secondary visual cortex areas (302).

With tactile stimulation, Arichi et al. (15) reported a positive BOLD response in contralateral cortex in both preterm and term neonates (Figure 11A). However, the amplitude of the BOLD response was smaller in preterm and term neonates than in adults, and the time to the peak response was longer in preterm neonates than in term neonates and longer in term neonates than in adults (14). A more detailed analysis of the BOLD response at different PMA revealed a positive BOLD response as early as 31 weeks PMA with the time to the peak BOLD response progressively decreasing from 15 s at 31 weeks PMA to 8 s at 43 weeks PMA (8). Interestingly, the cortical area with a positive BOLD response also increased progressively from 31 weeks through the term equivalent age (Figure 11B). Decreases in latency, increases in amplitude, and increases in the area of foreleg activation in the BOLD response have been reported in the rat between PND 13 to 15 and PND 20 to 30 (103). Others have reported the presence of bilateral positive and negative BOLD responses in different somatosensory cortical regions with passive hand movements in neonates, whereas a positive contralateral BOLD response emerged at 3 to 9 months of age (132, 133). Furthermore, with auditory stimulation, most neonates displayed

a negative BOLD response in temporal lobe, whereas a minority displayed a positive BOLD response (12). Collectively, functional MRI studies indicate that neurovascular coupling to passive visual, tactile, and auditory stimulation is incompletely developed at birth and that consistent, adult-like positive BOLD responses in the corresponding primary sensory cortex can take several months or even years to fully develop.

## Functional near-infrared spectroscopy studies in humans during development

NIRS offers an alternative noninvasive technology for evaluating neurovascular coupling. While the BOLD signal is sensitive to the concentration of deoxyhemoglobin, NIRS provides information on dynamic changes in deoxyhemoglobin, oxyhemoglobin, and total hemoglobin. In preterm neonates born at 33 to 34 weeks PMA and studied during sleep within 2.5 weeks of birth, NIRS showed increases in oxyhemoglobin and total hemoglobin and decreases in deoxyhemoglobin in sensory cortex after tactile stimulation of the hand (381). In addition, diffuse correlation spectroscopy at the hemoglobin isosbestic wavelength was used to measure changes in CBV and then derive a measure of the relative change in CBF from the empirical relationship between CBF and CBV (381). This CBF measure showed an increase beginning at 3 s and peaking at 9 s from the start of the 5-s stimulation period (Figure 11C). These latencies are somewhat longer than the 1 to 2-s delay and 5-s peak response typically seen in adult brain. Relative changes in $CMRO_2$ were calculated from the change in CBF and OEF. Although the OEF decreased, $CMRO_2$ was estimated to increase in parallel with the transient increase in CBF. Collectively, these data support an intact neurovascular coupling mechanism in sensory cortex of preterm neonates that responds to passive tactile stimulation, albeit with slower latency and time constant than in adult cortex. These data with NIRS corroborate the slow, positive BOLD response to tactile stimulation observed by Arichi et al. (14, 15) in preterm and term neonates.

Developmental studies have also been performed using NIRS in occipital cortex with photic stimulation. In two-thirds of term neonates, photic stimulation during natural sleep produced significant increases in oxyhemoglobin and decreases in deoxyhemoglobin (218), responses that are directionally similar to those in adults. These observations have been confirmed in term newborns with the use of a higher density array of optodes (283). In 83% of 2% to 4-month-old infants studied in the awake state, photic stimulation with a rapidly alternating checkerboard pattern produced increases in oxyhemoglobin, although decreases in deoxyhemoglobin were less consistent (406). In contrast, stroboscopic photic stimulation in infants at ages of 29 to 111 days elicited decreases in oxyhemoglobin and total hemoglobin (240). Overall, the NIRS data with visual activation in neonates tends to agree with the positive BOLD responses seen in most of this age group, whereas the NIRS data in infants appears to have some inconsistency. Some of this inconsistency may be related to the developmental switch from positive to negative BOLD responses reported to occur at 8 weeks of age (467, 468), to the lower spatial resolution of the NIRS technique, and possibly to differences in the nature of the photic stimulation (e.g., checkerboard patterns elicit activation of edge discriminator neurons).

Another consideration is that studies were performed in the awake state, the natural sleep state, or with sedatives and anesthetics. Natural sleep after feeding is often used to avoid

motion artifacts and potential blood pressure transients during movements. However, it remains unclear how natural sleep might affect neurovascular coupling in the immature brain. In adult rats, different classes of anesthetics can have a profound effect on the CBF response. The increase in CBF with whisker stimulation is considerably greater in awake rats than in rats anesthetized with chloralose, which was commonly used in rodent neurovascular studies (327), and the response is further depressed by gas inhalation anesthetics (157). Many, but not all, studies that have shown a decrease in oxyhemoglobin with NIRS or a decrease in the BOLD signal with functional MRI were performed on babies anesthetized or sedated with barbiturates, chloral hydrate, or gas inhalation anesthetics or were performed during sleep (see Table 3 of Liao et al. (283) and review by Kozberg and Hillman (234)). Thus, it is possible that anesthesia or sleep state may have blunted the increase in CBF sufficiently to attenuate the increase in oxyhemoglobin measured with NIRS and the decrease in deoxyhemoglobin measured with functional MRI or to nearly block the response and thereby result in an inverted response. However, even in studies of awake subjects, an adult-like response is not seen in a portion of the subjects, or an inverted response is obtained, especially in older infants. Therefore, the bulk of the evidence in this field generally indicates that (i) the vascular response to sensory activation is not as strong in neonates as in adults, possibly because neuronal networks within cerebral cortex are still forming, some regions have low cytochrome oxidase activity indicative of low mitochondrial density, and myelination required for rapid conduction between regions is incomplete and (ii) in older infants with higher baseline CBF and $CMRO_2$, the increase in CBF is inadequate to match the increase in $CMRO_2$ during activation. However, this mismatch does not necessarily imply that $PO_2$ at the mitochondria most distant from a capillary drops to critically low levels because the distribution of RBCs within the capillary networks at the higher baseline CBF seen at this developmental stage may mitigate the occurrence of patches of tissue with low $PO_2$.

## Neurovascular coupling studies in immature animals

Neurovascular coupling has also been studied during development in rodents. A single stimulation of whiskers in PND seven mice produced a 1% to 2% transient increase in perfusion over whisker barrel cortex (476). This increase is smaller than the response in adult mice. Moreover, repetitive whisker stimulation produced a prolonged decrease in perfusion during the stimulation period after the brief initial increase. This response differed from the sustained increase observed in PND 30 mice. In a study of PND 12 to 13 rats, electrical stimulation of the hind paw produced an increase in deoxyhemoglobin and decreases in oxyhemoglobin and total hemoglobin (235). By PND 15 to 18, small transient increases in oxyhemoglobin and total hemoglobin became evident followed by decreases as seen at PND 12 to 13. These responses differed from those observed in adult rats, wherein oxyhemoglobin and total hemoglobin increased and deoxyhemoglobin decreased. In a similar paradigm carried out in PND 7 to 8 and PND 10 to 13 mice, the responses of laser-speckle flow, deoxyhemoglobin, and oxyhemoglobin were small during the stimulation and were inverted after the stimulation compared to the responses in adult rats (Figure 12). Evoked cortical neuronal activity, as reported by GCaMP imaging, was present in all three age groups, suggesting that the lack of a blood flow response in the immature brain is not due to a lack of neuronal activation, although the activation

occurred sooner and lasted longer over a larger area in adult cortex (236). However, evoked responses of flavin adenine dinucleotide fluorescence, a marker of oxidative metabolism, were smaller in immature brain, indicating a smaller area of an evoked mitochondrial metabolic response. With maturation, highly localized neuronal activation converted to a more widespread neuronal activation and metabolic pattern in both contralateral and ipsilateral cortex and eventually to a larger and more rapid CBF response that resulted in increased rather than decreased oxygenation (236). This conversion is postulated to correlate with increased synaptic connectivity to association cortical regions that are known to have delayed mitochondrial development; moreover, the more rapid neuronal response in mature brain is postulated to correspond to developmental increases in myelination. Thus, the work in PND 7 to 18 rodents, whose brain development is thought generally to correspond to that of human newborns and infants, indicates that a small degree of vasodilation or even vasoconstriction in the cerebral vasculature leads to decreased oxygenation during sensory activation of cerebral cortex early in development. An adult-like pattern becomes evident by PND 30, which is thought to correspond to early juvenile development in humans.

In adult brain, neurovascular coupling is associated with a local increase in CMRGluc. As noted above in the section on CMRGluc, the basal CMRGluc during development can increase to as much as twice the adult basal level. This raises the question of whether the high basal level of CMRGluc, which is thought to be attributed to synapse and neurotransmitter turnover, electrical activity, and neuronal plasticity, has already engaged a high level of neurovascular coupling such that additional neuronal activity produces minor additional vasodilatory responses.

## Mechanisms of neurovascular coupling in mature brain

The precise mechanisms that account for changes in neurovascular coupling during development have not been well explored, but advances have been made over the past 20 years in identifying mechanisms in the mature rodent brain, as summarized below and in Figure 13. In mature brain, neuronal activation leads to an increase in RBC velocity in less than 1 s in association with an increase in $CMRO_2$ and a decrease in $PO_2$ that precedes detectable changes in arteriolar diameter. The increased RBC velocity is thought to be related to an increase in RBC deformability associated with the rapid initial increase in deoxyhemoglobin (450). The mechanism likely involves increased deoxyhemoglobin binding to anion transport protein, band3, which releases ankyrin and its associated cytoskeletal proteins from the cell membrane (400). Then within 1 to 2 s, vessels at the transition from the most distal arterioles to capillaries begin to dilate (94, 189). The dilatory response eventually ascends to penetrating arterioles and pial arterioles over a period of 2 to 5 s. Because damage to a short segment of endothelium blocks ascending dilation in response to sensory stimulation, signaling through endothelial gap junctions, release of endothelial $Ca^{2+}$ stores, opening of intermediate Ca-activated $K^+$ channels, and release of endothelial-derived hyperpolarizing factor are thought to contribute to this ascending dilation (94).

Some evidence suggests that a rapid relaxation of circumferential capillary pericytes at 1 to 2 s permits an increase in capillary diameter sufficient to decrease segmental

hydraulic resistance in selective capillaries and decrease the amount of RBC deformation required for passage (169, 368). Others suggest that the cell with circumferential encasing of the capillary is a smooth muscle cell containing α-smooth muscle actin rather than a circumferential pericyte containing smooth muscle actin (189). This difference in interpretation appears to rest upon the definition of a pericyte. Traditionally, pericytes are ascribed to have long, thin processes extending longitudinally along the capillary wall and are distinguished morphologically by the “bump-on-a-log” appearance of their nucleus and soma along the outside of the vessel, which differs from the smooth outer wall of VSM. Biochemically, pericytes are distinguished by their expression of platelet-derived growth factor receptor β and the proteoglycan NG2 ligand of this receptor. As proposed by Attwell et al. (46), cells with these morphological and biochemical markers can be further divided into subclasses based on geometrical features: those possessing a circumferential orientation are seen predominantly at the transition from the end arteriole to the capillary; those with long longitudinal processes are seen throughout the capillary network, especially in the middle of the capillary network, and are thought to monitor the integrity of the BBB; and those with a stellate appearance are seen predominantly on venules, where transendothelial migration of immune cells is prominent. Furthermore, the layer of smooth muscle cells along an arteriole is continuous, whereas the platelet-derived growth factor receptor β/NG2-positive cells with circumferentially oriented α-smooth muscle actin at the capillary transition are interspersed along the axial direction (189). Functionally, relaxation of this subclass of pericytes is thought to reduce the heterogeneity of RBC flux within a capillary network and thereby assure a sufficient $O_2$ diffusion gradient to reach the most distant mitochondria within that capillary network.

The early dilation at the transition from the end arterioles and proximal capillaries precedes dilation of penetrating pial arterioles and results in a small increase in CBV. However, because the upstream penetrating arterioles and pial arterioles represent the largest component of CVR, the increase in regional CBF resulting from pericyte-induced capillary dilation is relatively small in this early vascular response phase. With the moderate increase in $CMRO_2$ exceeding the early increase in CBF during early neuronal activation, paramagnetic deoxyhemoglobin content initially increases. Consequently, a small, brief negative BOLD signal can sometimes be detected preceding the large, positive BOLD signal that normally occurs later when penetrating arterioles dilate, the increase in CBF exceeds the increase in $CMRO_2$, and deoxyhemoglobin content decreases.

The early relaxation of pericytes and end-arteriolar smooth muscle is preceded by increases in $Ca^{2+}$ occurring within 100 ms of sensory stimulation in nearby astrocytes, including their foot processes (287). Interestingly, this rapid increase in $Ca^{2+}$ in the astrocyte soma and processes requires glutamatergic transmission whereas that in the astrocyte foot process depends on GABAergic transmission (288). Low concentrations of an NMDA antagonist sufficient to block the increase in astrocyte soma $Ca^{2+}$ did alter the CBF response, whereas a GABA-A receptor agonist sufficient to increase astrocyte foot process $Ca^{2+}$ increased local CBF. Evidence in brain slices indicates that circumferential pericyte relaxation is mediated by increased extracellular ATP and subsequent activation of P2X1 receptors on astrocytes, which then leads to local increases in astrocyte $Ca^{2+}$, mobilization of arachidonic acid (AA) by phospholipase D2 and diacylglycerol lipase (DGL) activity, and formation of

prostaglandin (PG) $E_2$ by cyclooxygenase-1 (COX-1) (318). The pericyte relaxation appears to be mediated by $PGE_2$ stimulation of PGE2 receptor 4 (EP4) on pericytes. The dilation on first-order capillaries is associated with decreases in pericyte $Ca^{2+}$ (223) and is propagated along the capillary by a purinergic mechanism that is thought to be astrocyte based (87).

Subpopulations of GABAergic interneurons containing neuronal nitric oxide synthase (NOS) and peptidergic coneurotransmitters and receiving cholinergic or serotonergic afferents have processes that come into contact with the blood vessel adventitia and astrocyte foot processes (90). In brain slices, the peptidergic neurotransmitter vasoactive intestinal peptide has vasodilatory properties, whereas neuropeptide Y and somatostatin have vasoconstrictor properties (90). *In vivo*, stimulation of basal forebrain elicits global vasodilation requiring GABA-A receptor signaling (226). While NOS activation in interneurons is involved in neurovascular coupling (130), an essential role of the peptide neurotransmitters themselves in physiological neurovascular coupling *in vivo* remains to be determined (89). Nevertheless, GABA-A receptor transmission is essential for the rapid increase in $Ca^{2+}$ seen at 100 ms in astrocyte foot processes, but not in other astrocyte processes or soma, after whisker pad stimulation (288). This observation implicates interneuron signaling to astrocyte foot processes, which then leads to pericyte relaxation around capillaries and smooth muscle relaxation around arterioles, possibly mediated by peptidergic transmitters. Thus, an interplay of interneurons, astrocytes, and pericytes are considered to be important components of the neurovascular unit, contributing to the early neurovascular response to neural activation.

When sensory activation is sustained, blood flow continues to increase until a steady-state response is attained in approximately 5 s. This additional hyperemia is largely attributable to arteriolar smooth muscle relaxation mediated by AA metabolites, adenosine, large conductance calcium-activated $K^+$ ($BK_{Ca}$) channels in astrocyte foot processes (141), inward-rectifier $K^+$ ($K_{ir}$) channels in VSM (141), and the action of neuronally derived nitric oxide (NO) on VSM. One of the AA metabolites are the epoxyeicosatrienoic acids (EETs) derived from specific cytochrome P450s (CYP) with epoxygenase activity (247, 366, 367). The latter are localized primarily in astrocytes, especially on foot processes near small arterioles (6, 7, 318). EETs produced in astrocytes can open the $BK_{Ca}$ channels (154, 188, 469). The resulting release of $K^+$ from the end feet is thought to produce activation of $K_{ir}$ channels on adjacent VSM (141, 159). In addition to $BK_{Ca}$ channels, activation of TRPV4 channels (122) and intermediate $K_{Ca}$ 3.1 channels (298) in astrocyte end feet plays a role in coupling with VSM. Their exact mechanism of action is unclear, but extracellular AA, which can be released as a coneurotransmitter, serves as a ligand on TRPV4 channels and generates the release of ATP (397). Extracellular ATP can stimulate $Ca^{2+}$ signaling in adjacent astrocytes, thereby increasing the astrocyte pool that releases vasodilators. Furthermore, breakdown of extracellular ATP by astrocytic ectonucleotidases increases extracellular adenosine that acts on $A_{2A}$ and $A_{2B}$ receptors. Adenosine $A_{2B}$ receptors contribute to the steady-state increase in blood flow (396), and the $A_{2A}$ receptors appear to be more important in upstream pial arteriole dilation (314). Although astrocytes can induce pericyte relaxation by $PGE_2$ generated from COX-1 activity, this activity is thought to provide a relatively constant level of inhibitory vascular tone in upstream arteriolar smooth muscle (292, 384). Synthesis of EETs, in contrast, is presumed to respond to dynamic

changes in astrocyte $Ca^{2+}$ and AA mobilization. Additional information on the role of EETs and other CYP-derived lipid mediators is provided in another *Comprehensive Physiology* review (174).

Neuronally derived mediators are also important. For example, $PGE_2$ derived from COX-2 activity in pyramidal neurons plays a role in the increased blood flow during neuronal activation in rodent brain (243, 332). Furthermore, GLU activation of NMDA receptors stimulates neuronal NOS, and the diffusible NO can act on VSM to cause relaxation of arterioles. NO can produce vasorelaxation through two mechanisms. First, NO can activate soluble guanylyl cyclase (GC) in VSM and generate cyclic GMP. This mechanism is thought to account for part of the early dilation produced by stimulation of interneurons in the close vicinity of VSM (89). Second, NO can also inhibit the cytochrome P450 enzymes that synthesize the lipid vasoconstrictor 20-hydroxyeicosatetraenoic acid (20-HETE) derived from AA (9) in VSM. Because 20-HETE acts to close $BK_{Ca}$ channels (152, 173) and maintain myogenic tone in the face of increased transmural pressure, inhibition of 20-HETE synthesis by NO will permit the mediators of vasodilation to fully function when upstream pial arterioles dilate and increase transmural pressure in downstream penetrating arterioles. Blood flow and vessel diameter responses with pharmacologic inhibitors of 20-HETE and NOS support the latter mechanism in that the attenuation of the vascular response by a NOS inhibitor is absent when a 20-HETE synthesis inhibitor is present (169, 293). The interaction of NO on 20-HETE synthesis might occur not only in VSM but also in astrocytes, which have been shown to possess the ability to synthesize 20-HETE that can then close $BK_{Ca}$ channels in astrocytes and VSM (155). By inhibiting 20-HETE synthesis, NO serves as a permissive enabler of vasodilation (289) when sensory stimulation is sustained. It should also be noted that the increase in tissue NO during 4 s of neuronal activation is brief (<2 s) compared to the duration of vasodilation (76), although the action of NO may be sustained beyond 2 s if the time constant for NO to dissociate from the heme moieties on GC and cytochrome P450 is considerably longer than the time constant to associate with heme.
In summary, we now know of many signaling components required for the neurovascular coupling response in mature brain, although the complexity of the signaling interactions in the different cell types and segments of the neurovascular unit remain to be fully resolved.

One caveat concerning the role of NO in neurovascular coupling is that studies showing a reduction in the CBF response to neural activation with administration of a NOS inhibitor have been performed primarily with laser-Doppler flow measurements of RBC movement in anesthetized animals. However when studied in unanesthetized rats with the radiolabeled iodoantipyrine technique that measures plasma inflow, no significant effects of NOS inhibitors on the hyperemic response were seen (3, 165, 327, 446). In unanesthetized human adults administered a nonselective NOS isoform inhibitor, one study failed to find a diminution of the frontal cortex CBF response (measured with a PET tracer) to a complex finger movement paradigm (453), whereas another study reported a 30% diminution in the posterior cerebral artery velocity response to visual activation (193). Moreover, anesthetized mice lacking the nNOS isoform have an intact neurovascular coupling response, suggesting compensation by other pathways (301). Thus, the precise role of NO in neurovascular coupling has not been completely resolved.

## Mechanisms of neurovascular coupling in immature brain

Exactly when each of the aforementioned signaling components becomes fully developed in the immature brain is an open question. Because the initial increase in CBF during sensory activation in the neonate is delayed by more than 2 s, the early capillary and precapillary arteriole dilation that is responsible for the initial increase in CBF may not be well developed in the neonate. As discussed in later sections, arterial pressure and myogenic tone is lower in neonatal vessels, and smooth muscle thickness increases first in the more proximal arterial vessels. Thus, there may be less myogenic tone in the pericytes and end arterioles for neurovascular mediators to inhibit, resulting in the CBF response being delayed until penetrating and pial arterioles are recruited. Furthermore, the lack of an increase in oxyhemoglobin and a positive BOLD response in infants beyond 8 weeks of age suggests that coupling mechanisms dependent on neuronal and astrocyte ATP, AA metabolite, NO, and extracellular adenosine signaling mechanisms are not yet fully integrated and synchronized.

Some data related to signaling by adenosine, NO, and carbon monoxide (CO) have been obtained in lambs and piglets. In fetal sheep, for example, pial arteries exhibit a robust dilatory response to adenosine $A_2$ agonists as early as 0.65 gestation (238), and 2-chloroadenosine is capable of increasing CBF in 1-week-old lambs (336). In newborn piglets, an increase in striatal microdialysate adenosine can be detected after local electrical stimulation or administration of kainate, and the administration of an adenosine antagonist attenuated the increase in CBF evoked by kainate (391). Thus, some aspects of adenosine signaling are present at midgestation and postnatally.

Immunohistochemistry has indicated that endothelial NOS is present in fetal sheep microvessels as early as 0.4 gestation and that expression increases as vascular density increases during development (334). Neuronal NOS is present in cortical subplate neuropil at 0.4 gestation and appears in neurite soma and processes at 0.5 gestation in fetal sheep (334). Discrete punctate staining on maturing nonpyramidal cells increases between 0.6 and 0.9 gestation. The temporal expression pattern differs in subcortical regions where an overshoot in immunostaining occurs at 0.5 to 0.6 gestation. The developmental pattern in human brain appears analogous to that in fetal sheep. In frontal cortex of human fetuses, NADPH-diaphorase histochemistry implies the presence of NOS in cortical subplate neurons by 13 weeks' gestation and an adult-like pattern throughout cerebral cortex and white matter by 32 weeks (471). Interestingly, a unique population of small GABAergic interneurons with light NADPH-diaphorase staining is present in higher order mammals, including neurons in Layers II to IV of adult monkey brain (472) and humans (412), but this phenotype is not present in rodent brain (470). In human fetuses, this second population of neurons develops relatively late, as staining increases between 32 and 40 weeks' gestation (471).

Brain NOS catalytic activity develops prenatally in sheep, pre- and postnatally in guinea pig, and postnatally in rats (295). In fetal sheep, nitrate and nitrite are detectable in cortical microdialysates at 0.6 and 0.9 gestation (375). *Ex vivo* tissue activity of NOS increases progressively after 0.5 gestation, with adult levels being attained at 0.9 gestation in cerebral cortex and striatum and at 0.8 gestation in hippocampus; adult levels are already attained by

0.5 gestation in thalamus, cerebellum, and medulla (335). The fourfold increase in cortical NOS activity between midgestation and late gestation corresponds to the developmental increase in CBF (Figure 14). Administration of a NOS inhibitor decreases CBF at both 0.63 and 0.92 gestation without reducing $CMRO_2$, thereby indicating that NO exerts a tonic vasodilatory effect by midgestation. The developmental increase in NOS catalytic activity also corresponds to increased cortical expression of AMPA, kainate, and metabotropic glutamate receptors (mGLUR) (147) and astrocytic expression of the glutamate transporter GLT1 (337). Thus, developmental expression of NOS in mature neurons and NOS activity are coordinated with the development of glutamatergic neurotransmission.

Vascular coupling to glutamatergic signaling has been evaluated primarily by application of NMDA. Fetal sheep at 0.65 and 0.9 gestation and 1-week-old lambs exhibit an increase in cortical blood flow in response to NMDA that is attenuated by administration of a NOS inhibitor (177, 336). The increase in cortical blood flow was greater at 0.9 gestation than at 0.65 gestation, consistent with the developmental increase in NOS activity. As described in greater detail in the “Carbon monoxide signaling” section, astrocyte-derived CO plays a prominent role in the pial arteriole dilation response to GLU and ADP in newborn piglets. Metabotropic GluR5 receptors are expressed on astrocytes during early development (403) and can contribute to neurovascular coupling (292, 294, 396) and activation of heme oxygenase-2 (HO-2) known to be expressed in astrocytes of immature piglet brain (280, 466). Likewise, extracellular ADP can also stimulate HO-2 in astrocytes in piglet brain (215). It is unclear how long during development the HO-2-dependent mechanisms remain active and whether CO plays a role in neurovascular coupling in early development in species other than swine. For example, administration of an HO inhibitor did not reduce pial arteriole dilation to ADP in adult rat or to acetylcholine in adult cat, except in the presence of a chemically stabilized cell-free hemoglobin polymer in the plasma (372). On the other hand, inhibition of HO is reported to reduce the CBF response to kainate-induced seizures in adult rat (320), pial arteriole dilation to topical administration of AMPA in adult rat (339), and pial arteriole dilation to acetylcholine in adult mouse (370). Thus, CO can play a role in cerebrovascular regulation in specific circumstances in mature brain.

Nevertheless, more research is needed to improve our understanding of when the various signaling components in capillaries, parenchymal arterioles, and pial arterioles become active during development. Such research will broaden our view of neurovascular coupling by helping us to elucidate the mechanisms that underlie the switch from positive to negative BOLD response in infants and the eventual reversal back to a positive BOLD response in children.

## Neurovascular coupling and angiogenesis

In fetal sheep at 0.4 gestation, the cerebral cortex is lissencephalic with two layers, and microvessels are spaced at an average of 250 μm apart in two-dimensional images from 30-μm sections (124). By 0.85 gestation, when spontaneous electrical activity is present, microvessel spacing in the six-layer neocortex is reduced to about 50 μm, and vessel density has increased sevenfold. In rabbit cortex, capillary density increases between PND 8 and PND 17 in the deep cortical layers, whereas adult levels are already present in the superficial

layers by PND 1 (Figure 15) (417). In contrast, cytochrome oxidase activity and CBF increase between PND 8 and PND 17 in both the superficial and deep layers. By PND 17, capillary density and cytochrome oxidase activity are better correlated spatially and approach adult levels, although CBF is still only about half that of adult levels (417). The further increase in CBF between PND 17 and adulthood without a corresponding large additional increase in capillary density and cytochrome oxidase likely reflects increased control of columnar blood flow by penetrating arteriole resistance in the face of increasing arterial pressure. In deep layers, the relative increase in capillary density between PND1 and PND17 is greater than the relative change in cytochrome oxidase, suggesting that metabolic energy demand is driving angiogenesis at this stage.

Growth of blood vessels during development is coordinated with neuronal growth through crosstalk among vascular endothelial growth factors, ephrins, and semaphorins (4). CD95 ligand secreted by central nervous system macrophages helps orchestrate this synchronized neuronal dendritic and capillary branching (95). Furthermore, neuronal activity during development also influences angiogenesis. In rodents, whiskers have a large representation in SM cortex, and each individual whisker has a one-to-one correspondence with a distinct cortical column known as a whisker barrel. Each barrel has high cytochrome oxidase activity relative to that of the surrounding cortex between each barrel. Thalamocortical projections to layer IV of whisker barrels increase in mice between PND 0 and PND 14 in association with an increase in vascular density and branching points (242). Deafferentation of whiskers before PND 5 or genetic impairment of neurotransmitter release from thalamocortical axons decreased vascular density at PND 14. Stimulation of the whiskers for 15 min per day from PND 14 through PND 21 increased vessel density at PND 21. These data support a role for thalamocortical activation in developmental angiogenesis in layer IV of primary SM cortex. Thus, neuronal activity, metabolic activity, and angiogenesis are well coordinated during development.

## Myogenic Responses and Autoregulation During Development

### Arterial structure development

Intracranial vessels from human embryos and fetuses less than 24 weeks PMA have been examined with electron microscopy (146). Vessels with a single layer of irregularly shaped endothelial cells connected with junctional complexes can be seen at 7 weeks, whereas intima, media, and adventitia layers appear at 9 weeks. By 12 weeks, large arteries contain 2 to 4 layers of smooth muscle cells with large nuclei. Fibroblasts, collagen, and elastic fibers appear at around 20 weeks PMA (146). At 24 weeks, the proximal middle cerebral artery (MCA) displays endothelial cells lining a thick and undulating internal elastic lamina; circumferentially oriented smooth muscle cells with large nuclei, collagen, and fine elastic fibers in the media extracellular matrix; and nerve fibers in the adventitia (56). In the first branch of the distal MCA, the internal elastic lamina is thinner and smoother. By 32 weeks PMA, the extracellular matrix between smooth muscle layers and collagen bundles in the adventitia expands in the distal MCA. At 37 weeks, the smooth muscle cells appear to expand their cytoplasm compartment.

Structural and functional changes have been explored in depth in sheep during development. The external elastic membrane first appears in the carotid arteries at 0.6 gestation, and passive stiffness increases linearly through the remaining gestation (377). In 3 to 7-day-old lambs, the common carotid artery, MCA, posterior communicating artery, and basilar artery are thicker and stiffer than those of the fetal sheep that are near term (364). Most segments are capable of attaining greater maximum tension and active stress soon after birth. MAP increases from approximately 45 to 60 mmHg over this time and likely provides a stimulus for increased VSM mass in the most proximal arteries and for synthesis of extracellular matrix proteins in both extra- and intracranial arteries (365). Increased oxygenation after birth increases arterial tone and may also provide a stimulus. Moreover, the transition at birth produces proportionately greater increases in thickness, stiffness, and maximum tension in the common carotid artery than in the intracranial artery (364). This finding is consistent with the concept that extracranial arteries contribute to overall CVR to a greater extent after birth when arterial pressure progressively increases.

During the transition from the neonatal to the adult period in sheep, MAP increases from approximately 60 to 90-100 mmHg. This transition is associated with continued increases in arterial wall thickness and maximum tension (362, 364). Again, the percent increase in wall thickness of the common carotid artery exceeded that of intracranial arteries. However, the percent increase in maximum tension generated in the common carotid artery was less than that in the intracranial arteries. This finding is consistent with the concept that intracranial arteries have a larger dynamic range for regulating wall tension.

## Myogenic tone

Myogenic tone refers to the circumferential wall tension developed in response to an increase in transmural pressure across the blood vessel. It is a function of the number of VSM cell layers, the thickness of the smooth muscle, and the orientation of the cytoskeletal contractile elements. Increases in transmural pressure lead to VSM membrane depolarization, opening of voltage-dependent $Ca^{2+}$ channels (VDCC), and activation of downstream protein kinase C signaling. Activation of $BK_{Ca}$ channels and voltage-sensitive $K^+$ ($BK_V$) channels can limit depolarization and developed tension (297, 410). However, concurrent mobilization of AA leads to the formation of 20-HETE, which inhibits $BK_{Ca}$ channels and enables depolarization and an increase in myogenic tone (152). These mechanisms have been explored, in part, in immature cerebral arteries.

Segments of isolated MCA and basilar arteries from human newborns at PMA 23 weeks to term were obtained soon after death from noncerebral causes at 1 h to 34 days after birth (58). Most segments developed spontaneous tone at pressures lower than those seen in adult arteries. When arterial segments were pressurized, tone was maintained. As intraluminal pressure was increased from 30 to 80 mmHg, internal diameter decreased as expected from a myogenic response (Figure 16). The diameter was smaller than the passive diameter-pressure relationship obtained in the absence of external $Ca^{2+}$. Thus, human cerebral arteries gain the ability to generate a myogenic response early in development.

As in humans, cerebral arteries from PND 5 mice develop active tone at lower transmural pressure than those from mature mice (150). With increasing transmural pressure, cerebral

arteries from PND 1 to 2 rats display a decrease in diameter and a global increase in intracellular $Ca^{2+}$ that is sensitive to an inhibitor of VDCC (163). At PND 14, the increase in intracellular $Ca^{2+}$ is greater than that observed in mature rat arteries over a low transmural pressure range (92). These findings are consistent with the concept that myogenic tone is optimized to operate over the lower arterial pressure range seen in immature animals.

Development of contractile mechanisms has been investigated in fetal, newborn, and adult sheep. Isolated MCA and posterior communicating arteries from fetal and newborn sheep develop spontaneous tone that depends on the amount of stretch (129, 387). The maximum tension generated by high external $K^+$-induced depolarization increases during development in accordance with the increase in VSM mass (362, 364), but the myogenic tone as a percent of the maximum tension is similar in fetal and adult posterior communicating arteries (387). Observations in permeabilized arteries indicate that fetal arteries are more dependent on $Ca^{2+}$ sensitization than are adult arteries, whereas myosin light-chain phosphorylation is similar for the same degree of relative stretch (387). Activation of protein kinase C increases $Ca^{2+}$ sensitivity in cerebral arteries of near-term fetal sheep, and 5-hydroxytryptamine increases $Ca^{2+}$ sensitivity through small G-proteins and Rho kinase, similar to what occurs in adult arteries (5).

In the basilar artery, the $Ca^{2+}$ mass that is sensitive to release by inositol triphosphate and thought to be activated by agonists was similar in near-term fetal and adult sheep, whereas the $Ca^{2+}$ mass that is sensitive to release by ryanodine and the remaining $Ca^{2+}$ mass decreased in the adult basilar artery (329). Although ryanodine receptors are present in very immature cerebral arteries from PND 1 to 2 rats, they rarely evoke detectable $Ca^{2+}$ sparks, possibly because they are not yet organized in clusters near $BK_{Ca}$ channels (163). At this age, addition of the $BK_{Ca}$ inhibitor iberiotoxin has no effect on myogenic tone, whereas it increases the tone in adult rat cerebral arteries (163). In the more mature near-term fetal sheep, iberiotoxin and an inhibitor of $K_V$ channels are capable of enhancing stretch-dependent tone in branches of the MCA (410). Thus, these channels partially counter arterial tone induced by stretch, although the effect is still less than that in the corresponding adult arteries. Furthermore, a developmental change in the $BK_{Ca}$ channel appears to occur postnatally in sheep. The activity of $BK_{Ca}$ channels in fetal arteries is enhanced by a lower set point for $Ca^{2+}$ activation (284) that may result from the phosphorylation state (285). This difference may allow these channels to respond to smaller $Ca^{2+}$ sparks.

Another developmental VSM change relates to soluble GC. Its activity and protein expression in cerebral arteries is higher in neonatal lambs than in adult sheep (452), and cGMP decreases the $Ca^{2+}$ response to 5-hydroxytryptamine and the myofilament $Ca^{2+}$ sensitivity in fetal basilar artery (328). The enhanced soluble GC activity and its downstream effects on myofilament $Ca^{2+}$ sensitivity may contribute to the finding that postnatal CBF is high relative to that in adults. In neonatal piglets, cGMP and cAMP are detectable in cortical cerebrospinal fluid (CSF) and increase during hypercapnia-induced dilation of pial arteries (355). Phosphodiesterase inhibitors produce pial artery dilation during normocapnia and further dilation during hypercapnia. Piglet cerebral VSM cAMP is stimulated by the stable $PGI_2$ analog, iloprost, and by $PGE_2$, isoproterenol, and pituitary adenylate cyclase-activating polypeptide (348, 356, 414). Iloprost also increases cGMP (354). The dilator effects of

iloprost and $PGE_2$ are not additive (349), possibly because of convergence on cyclic nucleotide signaling. When microvessel VSM from neonatal and adult pigs was compared, the increase in cAMP in response to iloprost and the increase in cGMP in response to nitroprusside were similar (351), but developmental changes in endothelial-derived NO did occur (see section titled “Endothelial and astrocyte vasoactive signaling”). Overall, myogenic tone develops in cerebral arteries early in development, but the tone can be modulated by many factors that change during development. Many of these factors are extrinsic to VSM.

## Autoregulation of cerebral blood flow

Autoregulation refers to the ability of cerebrovascular smooth muscle cells to change their tone when CPP fluctuates such that changes in CBF are minimized. CPP is generally defined as MAP minus ICP. When CPP increases, myogenic tone increases in response to an increase in transmural pressure. This increase in tone not only prevents distension of the arteries but can produce decreases in diameter that increase CVR and limit the increase in CBF. Likewise, when CPP decreases, the resulting decrease in transmural pressure decreases myogenic tone. Moreover, if the decrease in CPP is severe, vasodilators can be released from brain parenchymal cells. Together, the decrease in myogenic tone and the released vasodilators produce increases in cerebral artery diameter and consequent decreases in CVR that limit the decreases in CBF. Aspects of CBF regulation specifically during hemorrhage have been previously reviewed in *Comprehensive Physiology* (376). With ideal autoregulation, CBF is maintained constant over a wide range of CPP. However, in any individual, the slope of this relationship is often not zero and can be variable. The degree of autoregulation can vary from no change in CVR [with the percent change in CBF equal to the percent change in CPP (i.e., no autoregulation)] to perfect autoregulation in which the percent change in CVR equals the percent change in CPP (with no change in CBF). A review of studies in which CBF velocity and end-tidal $CO_2$ were measured in human adults during induced changes in MAP indicated that the percent change in CBF velocity per percent change in MAP was 0.39±0.30 for increases in MAP and 0.64±1.16 for decreases in MAP (after correcting for changes in $PCO_2$) (338). This review of the literature indicates not only variability among individuals but also considerable variability in autoregulatory function among studies that present the average responses among individuals. Thus, when examining autoregulatory function during development, one must view the data from the perspective that autoregulatory function is also likely to be highly heterogeneous among individual children.

Although cerebrovascular autoregulation has been studied at various ages of human development, most studies have been done during surgery with general anesthesia or in disorders such as neonatal hypoxic-ischemic encephalopathy and traumatic brain injury (TBI). Physiological studies have been done in fetal sheep and postnatal dogs, piglets, lambs, and rabbits. Translation of studies on animals to humans requires some assessment of how the stage of brain development and blood pressure in a particular species corresponds to human development. By synthesizing the animal and human autoregulatory data, one can postulate an ideal set of autoregulatory curves at different stages of human development (Figure 17). These curves take into account the known levels of CBF at normotensive

pressures and the range of MAP that would normally be experienced at different stages of development. As CPP decreases from normotensive levels, CBF decreases proportionately less over the autoregulatory range until a downward inflection point is reached where further decreases in CPP result in larger decreases in CBF. This inflection point is called the lower limit of autoregulation (LLA). The positive x-intercept where CBF falls to zero is called the critical closing pressure. With increases in CPP above normotensive levels, CBF increases proportionately less than the increase in CPP until an upward inflection point is reached. This upward inflection point is termed the upper limit of autoregulation (ULA). Several features should be noted in these curves. First, as the normal level of blood pressure increases during development, the corresponding LLA and ULA also increase. Second, the normal level of blood pressure at a particular age tends to be closer to the LLA than the ULA, thereby indicating a greater range to autoregulate during acute hypertensive episodes than during acute hypotensive episodes. Third, the slopes of the autoregulatory curves between the LLA and ULA may be flat in some individuals or much higher in other individuals, and the graphs represent a population average, and it is unclear how much the slopes change during development. The autoregulatory slopes may be affected by anesthesia and energy metabolism. Nevertheless, this set of autoregulatory curves provides a model for understanding the effects of perfusion pressure on CBF when the absolute levels of CBF and CPP have large changes during development. The data that contribute to this conceptual framework are described below.

**Autoregulation in neonatal animals—**In 1980, Hernandez et al. (185) reported that CBF measurements made in anesthetized newborn dogs over a range of 27 to 97 mmHg remained within 10% of the normal CBF of 24 mL/min/100 g at the baseline MAP of 57 mmHg. In another study, regional CBF was found to be relatively constant over a MAP range of 35 to 75 mmHg (360). Above 75 mmHg, CBF increased more in thalamus, mesencephalic nuclei, and rostral germinal matrix than in other gray and white matter regions. Because canine brain at birth is in a relatively immature state that is thought to correspond to preterm humans, these studies suggest that autoregulation is an early ontogenetic property of the brain.

Later studies of neonatal animals primarily used the more precocious piglet and lamb. In one of the first autoregulation studies in neonatal piglets, Laptook et al. (244) found that decreasing MAP from 90 to 39 mmHg by hemorrhage decreased cortical CBF by 36% and brainstem CBF by 14%. Because the percent decreases in CBF were smaller than the percent decrease in MAP, CVR decreased regionally, but these were insufficient to sustain CBF. However, it should be noted that the baseline MAP of 90 mmHg was relatively high for the 5-day-old piglets. In another study in which baseline MAP was 57 mmHg in unanesthetized newborn piglets, decreasing MAP to 36 mmHg with hemorrhage did not change CBF or $CMRO_2$, thereby implying effective autoregulation with as much as a 37% decrease in MAP (262). However, hemorrhage moderately decreased arterial $O_2$ content in these studies, thereby complicating interpretation of autoregulatory capacity. In newborn lambs in which the decrease in hemoglobin was prevented by transfusion of autologous RBCs after hemorrhage, CBF was found to autoregulate down to MAP levels of 25 mmHg, implying a fairly low MAP limit for sustaining perfusion (342). An alternative approach

for producing hypotension without a decrease in hematocrit is inflation of a balloon in the inferior vena cava. Laser-Doppler flowmetry measurements in anesthetized piglets showed that CBF autoregulated during progressive decreases in CPP from 60 mmHg at baseline down to 30 mmHg, below which the estimated CVR continued to decrease, but the decrease was no longer able to sustain CBF (70). Furthermore, autoregulatory responses remained intact down to a CPP of 30 to 40 mmHg at 6 to 48 h after resuscitation in a piglet model of asphyxic cardiac arrest (249, 252). In nonischemic piglets with hemorrhagic hypotension, increases in interstitial adenosine have been reported when cerebral $O_2$ transport begins to decline. These increases likely contribute to additional decreases in CVR below the LLA (358).

Hemorrhagic hypotension in piglets leads to pial arteriolar dilation, as visualized through a closed cranial window (259). Both $K_{ATP}$ and $BK_{Ca}$ channels mediate the dilation (27). The dilation is associated with an increase in $PGE_2$ and 6-keto-$PGF_{1\alpha}$, a stable metabolite of $PGI_2$. Administration of indomethacin after the onset of hypotension blocks the increase in perivascular prostanoids and pial arteriolar diameter (259) and causes a decrease in CBF and $CMRO_2$ (262). The endothelium is an important source of $PGI_2$, and damage to the endothelium with the light/dye procedure limits pial arteriolar dilation during hemorrhage (127). These results indicate that increased endothelial production of vasodilatory prostanoids participates in autoregulatory vasodilation in newborn piglets. Unexpectedly, administration of indomethacin immediately before the onset of hemorrhage did not impair the subsequent autoregulatory response, suggesting recruitment of other mechanisms. Another mechanism involves the generation of CO by HO-2. Hemorrhagic hypotension in piglets increased the concentration of CO in the CSF, and inhibitors of HO blocked the increase in pial arteriolar diameter (217). As discussed below, CO can be generated in piglet astrocytes and endothelium, and more work needs to be done to better understand the factors that modulate vascular tone during arterial hypotension.

Collectively, these studies in neonatal dogs, piglets, and lambs demonstrate that reactive decreases in CVR result in only minor decreases in CBF down to a CPP of 25 to 40 mmHg. Below this range, some additional decrease in CVR may occur, but it is no longer proportional to the decrease in CPP. As a result, CBF falls significantly below a CPP of 25 to 40 mmHg as vasodilatory reserve becomes exhausted. This LLA inflection point is less than the 50-mmHg lower limit ascribed to adult animals. Developmental differences in the LLA are consistent with the concept that the blood pressure range for autoregulation adapts to the developmental increase in MAP.

It should be noted that the LLA depends on the vasodilatory reserve present at the MAP where the animal normally operates. For example, when vasodilatory reserve is exhausted by hypercapnia, CBF falls passively with subsequent decreases in MAP (401). This reserve will depend on the countering vasodilatory influence of $CMRO_2$. At any given MAP, an increase in $CMRO_2$ decreases CVR and vasodilatory reserve, whereas a decrease in $CMRO_2$ has the opposite effect. Most studies of autoregulation in animals are performed with general anesthesia, which typically produces about a 30% reduction in $CMRO_2$. Thus, one study in awake lambs estimated an LLA closer to 40 mmHg, whereas barbiturate coma, which decreased $CMRO_2$ by approximately 50%, extended the lower limit to about 25 mmHg

(120). This LLA in comatose lambs was less than that observed in comatose adult sheep and supports the concept of inherent developmental differences in the MAP range for autoregulation when differences in $CMRO_2$ are minimized.

Fewer studies have examined the effect of increases in MAP in neonatal animals. In PND 1 rabbits with norepinephrine-induced hypertension or hemorrhage-induced hypotension, CBF was nearly pressure passive in frontal cortex, but CBF in medulla exhibited moderate autoregulation over a MAP range of 20 to 60 mmHg (416). In frontal cortex, autoregulation developed over the MAP range of 30 to 40 mmHg at PND 8 and over the 40 to 70 mmHg range at PND 17, whereas adult rabbits exhibited tight autoregulation over the MAP range of 40 to 150 mmHg. Patchy areas of marked hyperemia were seen in PND 1 and 8 cortex with severe hypertension. It should be noted that cytochrome oxidase and capillary density are still below adult levels in rabbit cortex at PND 8 and that CBF is approximately 30% of adult levels, whereas these parameters are close to adult rabbit levels in PND 1 medulla (417). In contrast, more robust autoregulation to increases in MAP have been reported in postnatal dogs and pigs. With pharmacologically induced hypertension in newborn dogs, CBF was relatively constant until MAP increased above 100 mmHg (185). In newborn piglets, metaraminol-induced increases in MAP from 68 to 118 mmHg resulted in a 20% increase in CBF; this increase was prevented by pretreatment with atropine, suggesting an active cholinergic component that attenuated the autoregulatory response (74). Using balloon inflation in the descending aorta to increase cephalic MAP, a doubling of CPP from 60 to 120 mmHg in piglets increased CVR by approximately 66% and CBF by approximately 20% (252). This autoregulatory response remained intact after asphyxic cardiac arrest (252) and treatment with hypothermia (245). In the piglet, the precise pressure at which autoregulatory breakthrough occurs is difficult to determine because the piglet heart cannot maintain pressures exceeding 120 mmHg in the presence of anesthesia. Nevertheless, these data indicate that the neonatal dog and piglet have a broad range of autoregulation, especially above the normal MAP at this developmental age, whereas the rabbit, with its delayed postnatal capillary and metabolic cortical development, has delayed development of autoregulation.

**Autoregulation in fetal animals—**A critical issue is whether cerebral autoregulation exists in the fetus, where arterial $PO_2$ is about 25 mmHg and arterial $O_2$ saturation of hemoglobin is about 60% to 70%. This level of oxygenation decreases cerebral vascular tone compared to postnatal oxygenation levels (162). In sheep, MAP is about 35 mmHg at 0.6 gestation, 45 to 50 mmHg at 0.9 gestation, 50 to 60 mmHg after birth, 60 to 70 mmHg by 1 week after birth, 90 mmHg at 3 weeks, and 90 to 100 mmHg in adulthood. The relatively low MAP in the fetus at submaximal arterial $O_2$ saturation raises the question of whether the autoregulatory range is limited *in utero*.

One of the first studies of autoregulation in the fetus was performed by Tweed et al. (420), who catheterized the fetus for microsphere-determined blood flow at 0.9 gestation in unanesthetized sheep. They found that hemorrhagic hypotension sufficient to decrease MAP by 20% (from 52 to 41 mmHg) produced a nonsignificant decrease in cortical CBF of 9%, thereby implying active vasodilation. In a follow-up study, autoregulatory responses were found to relate dichotomously to the baseline arterial $O_2$ saturation (419). Fetal sheep with

an arterial $O_2$ saturation greater than 57% (mean of 63%) exhibited a nonsignificant 5% decrease in CBF in response to a 26% decrease in MAP, whereas those with an arterial $O_2$ saturation less than 57% (mean of 45%) exhibited a 41% decrease in CBF in response to a 31% decrease in MAP. In another study, linear regression analysis of the percent change of CBF from the pooled data suggested that the LLA was approximately 45 mmHg, which was close to the baseline MAP of 49 mmHg in this cohort (405). However, some of the near-term fetuses in this study had an arterial $O_2$ saturation less than 57%, which may have influenced the breakpoint determined in the linear regression analysis. Another way to reduce CPP is to infuse artificial CSF into the lateral ventricle to produce global increases in ICP. With this methodology, stepwise reductions of CPP from 45 to 33 and to 28 mmHg in fetal sheep at 0.9 gestation with an arterial $O_2$ saturation of 60% produced no significant change in CBF except in cerebellum (184). At a CPP of 28 mmHg, CVR significantly decreased and resulted in only a 15% nonsignificant lowering of the average CBF, which was not sufficient to reduce $O_2$ uptake. Thus, the near-term fetus does have some ability to autoregulate CBF in the face of moderate decreases in MAP or increases in ICP when the fetal oxygenation state is normal, but this ability becomes impaired at subnormal oxygenation.

Available data on autoregulation at midgestation are limited. In fetal sheep at 0.6 gestation with an arterial $O_2$ saturation of 65%, a 27% decrease in MAP from 37 to 27 mmHg produced by hemorrhagic hypotension resulted in a 20% decrease in cortical CBF, indicating a small decrease in CVR (405). Linear regression analysis of the percent change of CBF from the pooled data suggested that the LLA was close to the baseline MAP of 37 mmHg. When CSF was infused into fetal sheep with an arterial $O_2$ saturation of 68% at 0.6 gestation, stepwise decreases in CPP from 35 to 25 and 18 mmHg resulted in decreases in CBF in cerebral cortex (184). CBF was sustained in brainstem, cerebellum, and thalamus at a CPP of 25 mmHg, indicating some autoregulatory capacity in subcortical regions at this developmental stage. Interestingly, the 0.6 gestation responses in cerebral cortex were dichotomized by arterial $O_2$ saturation. Those with an average arterial $O_2$ saturation of 73% demonstrated autoregulation down to a CPP of 25 mmHg, whereas those with an average arterial $O_2$ saturation of 61% exhibited no autoregulation at this CPP. Thus, as in the near-term fetus, the midgestation fetus can exhibit modest autoregulation to decreases in CPP when the oxygenation state is relatively high.

A few studies have examined autoregulation responses to both increases and decreases in MAP in fetal sheep. One approach was to occlude blood flow around the brachiocephalic trunk and aortic isthmus. In 0.8-gestation fetal sheep that had undergone baroreceptor denervation, the control cephalic MAP was 54 mmHg. CBF exhibited an autoregulatory plateau between 45 and 80 mmHg; pressure-passive decreases in CBF occurred below 45 mmHg and pressure-passive increases occurred between 80 and 90 mmHg (344). The latter pressures would normally not occur in fetuses with intact baroreceptors because the maximum pressor response elicited by endogenous sympathoadrenal and humoral activation is about 70 mmHg, and blood flow is diverted to the placenta during the fetal pressor response (176). Together, these studies in fetal sheep show that the range of CBF autoregulation lies mostly above the operating point of MAP and that autoregulatory vasodilatory reserve during decreases in MAP are limited and dependent on the level of fetal oxygenation. However, one study failed to show autoregulation during fetal hypertension

(191). In this study of 0.9-gestation fetal sheep, ganglionic blockade was induced with hexamethonium, and hypertension was induced with angiotensin. It is unclear whether the combination of these drugs could have influenced the autoregulatory response.

Because the fetal autoregulatory response depends on the level of oxygenation, another consideration is whether decreasing oxygenation after birth to the level experienced before birth influences autoregulation. One study investigated this question in postnatal lambs by measuring CBF during stepwise increases in ICP. Arterial $O_2$ saturation was kept at either 50% or greater than 95% during the generation of the autoregulatory curve (63). Unexpectedly, no significant changes in CBF occurred in either group as CPP was reduced to approximately 25 mmHg, despite the fact that baseline CBF was doubled and CVR was halved in the hypoxic group. A limitation of this study is that the barbiturate anesthesia used in this experiment increases baseline CVR, which may have extended the LLA. Nevertheless, this study suggests that a level of hypoxia more severe than 50% arterial $O_2$ saturation is required to impair the autoregulation response to CPP decreases in the neonate.

In the studies described above, either upstream MAP or downstream ICP was manipulated to generate autoregulatory curves. Studies in adult animals indicate that the LLA has a similar CPP whether CPP is decreased by reducing MAP or increasing ICP (168, 313). However, little is known about the lower limit when MAP is decreased in a state of intracranial hypertension. This situation is relevant for neonates and infants whose ICP is elevated from edema or hydrocephalus. In such cases, it was unclear how well CBF would autoregulate with changes in MAP. Brady et al. (68) addressed this question by increasing ICP in piglets to 20 or 40 mmHg with ventricular infusion of artificial CSF and then slowly decreasing MAP by inflating a balloon catheter in the inferior vena cava. When the cortical laser Doppler flow change was plotted against CPP, breakpoint analysis for the LLA was not fixed despite inclusion of ICP in the calculation of CPP. Rather, the lower limit increased approximately 0.6 mmHg for each 1 mmHg increase in ICP. This shift to the right of the autoregulatory curve may be explained by a mathematical model of vascular distensibility and collapse of vessels at low distending pressure. If the critical closing pressure at which vessels begin to collapse and decrease their diameter has a Gaussian distribution, the dispersion of when vessels begin to decrease diameter and increase their resistance will become more broad at higher ICP (2).

**Autoregulation in human neonates and children—**Assessing autoregulation in healthy neonates and older children by direct CBF measurements is limited by the difficulty of making repeated CBF measurements and safety concerns surrounding CPP manipulation. One study used transcranial Doppler measurements of blood velocity in the MCA and basilar artery of healthy, 10 to 15-year-old children during MAP decreases that occurred during the transition from supine to upright position (429). MAP estimated at the base of the brain decreased to an average of 22 mmHg. The autoregulatory index (ARI), calculated as the ratio of the percent change in CVR to the percent change in MAP, averaged 0.95, with most children exhibiting an ARI > 0.9, thereby indicating good autoregulation.

Studies of autoregulation in younger children have largely been restricted to those being monitored during surgery or in the intensive care unit. Many of these studies used

indirect measures of CBV or CBF and then calculated a correlation coefficient of these indirect measures with variations in MAP after filtering high frequencies to exclude cardiac pulsations. The main indices that have been used in pediatrics include the pressure-reactivity index (PRx) based on changes in ICP, the hemoglobin volume index (HVx) derived from NIRS measurement of tissue hemoglobin changes, and the cerebral oximetry index (COx) based on changes in NIRS measurement of tissue $HbO_2$ changes (70, 250, 323, 477). The PRx and HVx indices assume that autoregulatory vasoconstriction during arterial hypertension and vasodilation during hypotension produce changes in CBV, ICP, and tissue hemoglobin concentration that are inversely related to MAP. Thus, ICP and hemoglobin concentration should have a negative correlation coefficient with MAP perturbations when autoregulation is intact and a positive correlation coefficient when autoregulation is impaired. The COx index assumes that $O_2$ extraction is inversely related to CBF and that $CMRO_2$ is unaltered over the averaging window of 5 to 10 min. Thus, the correlation coefficient of tissue $HbO_2$ should approach zero when there is no change in CBF during perturbations in CPP and become progressively positive as CBF and cerebral venous and tissue $HbO_2$ vary directly with changes in MAP (impaired autoregulation). Receiver-operating characteristic analysis in piglets showed that the LLA was best predicted by a COx of approximately 0.4 (69, 70). Because the PRx requires ICP monitoring, its application is typically restricted to children with TBI. The COx and HVx techniques are based on noninvasive NIRS monitoring and have been applied to neonates in the intensive care unit and to older children undergoing surgery.

In a study of preterm newborns at 25 to 29 PMA with median MAP of approximately 35 mmHg (range approximately 25–50 mmHg), the majority had a COx correlation coefficient less than 0.5 throughout the monitoring period of 6 to 18 h after birth (47). Less than one-third experienced a COx>0.5 for more than 10% of the time. In another study of preterm newborns, many of whom had intraventricular hemorrhage, the MAP at which COx was greater than 0.5 varied considerably (20–50 mmHg) (158). On average, COx increased from 0.1 at 40 mmHg to 0.5 at 20 mmHg. Thus, most preterm newborns operate predominantly within a MAP range of intact autoregulatory vasoreactivity, although the degree of autoregulation can vary considerably. These findings raise the possibility that MAP management in the intensive care unit may be best served by targeting the MAP at which the COx is minimized in an individual patient rather than using only population-based guidelines.

The HVx index has been used to monitor autoregulation in term newborns with hypoxic-ischemic encephalopathy during and after hypothermic treatment. An optimal MAP was defined as the MAP at which the HVx was at a distinct minimum, which corresponds to the MAP at which vascular reactivity to MAP perturbations is maximal for each subject. The percent of time that a patient's MAP was lower than the optimal MAP correlated with later abnormalities of apparent diffusion scalars on the MRI in white matter, basal ganglia, and paracentral gyri and with 2-year neurodevelopmental outcome (77, 251, 409). Acute outcome in children resuscitated from cardiac arrest also showed a relationship with the patient's MAP deviation from the optimal MAP for autoregulation (248).

COx has been measured in anesthetized children (age range of 0-222 months; median 25 months) before, during, and after cardiopulmonary bypass for cardiac repair surgery (71). The lowest COx was in the 50 to 75 mmHg MAP range (Figure 18). A COx of 0.4 in these cardiac surgical patients corresponded to an average MAP of 42 mmHg (range 20–55 mmHg). This LLA assumed at a COx of 0.4 is significantly less than the 66-mmHg lower limit observed with the same analysis in adult patients undergoing cardiopulmonary bypass (66, 213). When the HVx index was used, a similar LLA of 41 mmHg was obtained (126), again less than the 66-mmHg lower limit obtained with this index in adult surgical patients (125). These studies support the concept of a developmental increase in the LLA, although the sample size was too small to determine the precise relationship with age. Several studies have examined autoregulation in children after TBI, as discussed in a later section. Therefore, PRx, HVx, and COx have proven useful for assessing cerebrovascular autoregulatory vasoreactivity in the neonatal and pediatric intensive care setting and during surgical procedures.

**Frequency response of autoregulation—**The time constant for autoregulation has been assessed by imposing approximate step changes in MAP. Direct visualization of pial arteriole diameter in anesthetized adult animals indicates that the time constant for the response to changes in transmural pressure is in the range of 3 to 10 s (62, 232, 404). Another approach for assessing autoregulatory dynamics is to perform spectral analysis. In human adults, the transfer function gain between arterial pressure and CBF velocity is minimal at approximately 0.03 Hz, and the phase angle is maximal in this frequency range (421). At frequencies higher than 0.07 Hz, the coherence between CBF fluctuations and arterial pressure fluctuations increases. Thus, autoregulation in adults dampens blood pressure effects on CBF when the periodicity is greater than approximately 14 s. In preterm newborns at 24 to 28 weeks PMA, the transfer function gain was minimal at about 0.08 Hz (432), suggesting a somewhat faster autoregulatory response than in adults.

Instead of performing spectral analysis, one can produce a forcing function at a single frequency. In anesthetized piglets, sinusoidal variations in positive end-expiratory airway pressure produced quasi-sinusoidal fluctuations in MAP and ICP, but the ICP was out of phase with the MAP (67). A shift from a large absolute phase angle (indicative of good autoregulation) to a smaller phase angle occurred when the MAP fell below the LLA. The residual phase angle observed below the LLA presumably represents the phase lag between changes in blood flow and changes in ICP induced by changes in blood volume. When the frequency of the sinusoidal variations was increased from one to six cycles per minute at normal MAP, the phase angle decreased from 156° to 40° (Figure 19), which corresponded to the low phase angle seen when MAP was below the LLA (144). The cutoff frequency (0.03 Hz) for the ICP response is slower than those associated with the myogenic response (0.1–0.3 Hz) and the NIRS-based tissue oximetry response (0.05–0.25 Hz), which is indirectly related to CBF (341). Because the change in ICP is directly related to the change in CBV, which is related to the time integral of inflow minus outflow, the change in ICP will inherently have a slower time constant than the change in CBF. Thus, changes in the phase angle can provide useful information about loss of autoregulation, but the actual

phase angle will differ depending on whether the metric is based on a CBV measurement, tissue hemoglobin oxygenation measurement, or MCA blood velocity measurement.

Frequency domain analysis of the NIRS-derived tissue deoxyhemoglobin signal has been analyzed in the 0.05 to 0.25 Hz frequency band in premature newborns (341). The period that the NIRS signal exhibited high coherence with MAP was longer in those with intraventricular hemorrhage, suggesting that more time was spent in the MAP range where blood flow was passively related to MAP. In term newborns, coherence was also increased in those who experienced hypoxia-ischemia (307). Another approach involves calculating the transfer function gain from the cross-power spectra of the MAP input with NIRS-derived changes in tissue $HbO_2$ (432). The ability to dampen tissue $HbO_2$ fluctuations during MAP fluctuations increases between 24–25 weeks PMA and 26–28 weeks PMA. This methodology also reveals impaired attenuation of tissue $HbO_2$ fluctuations in premature newborns with intraventricular hemorrhage.

Therefore, different types of methodologies indicate that autoregulation is limited in very premature newborns and that the strength and range of autoregulation gradually increase during late gestation and throughout childhood as MAP and arterial VSM mass increase.

## Sympathetic Nervous System

### Sympathetic effects in adult cerebral circulation

In several adult animal species, sympathetic nervous stimulation produces constriction of the carotid and large cerebral arteries with progressively less constriction in branches of the cerebral arteries (55, 82). Pressure within pial arteries decreases, but CBF does not change, thereby indicating that a selective increase in upstream large arterial resistance is counterbalanced by a decrease in downstream small arteriolar resistance (53). In rabbit, a longitudinal decrease in sensitivity to norepinephrine occurs abruptly near where the vertebral and internal carotid arteries enter the skull (54). In addition, the density of adrenergic receptors decreases between the main cerebral arteries and their branches, and the maximum tension of intracranial arteries evoked by norepinephrine is much less than the maximum tension evoked by a high concentration of depolarizing KCl (55). Likewise, the catecholamine content and the density of nerve fibers in the border between the adventitia and media layers are much less in isolated human pial arteries than in meningeal or superior temporal arteries (57). In a study by Bevan et al. (57) electrical activation of intramural nerves increased tension of pial arteries to only 1% of maximum, and application of 10 μmol/liter norepinephrine produced an increase in tension equivalent to 21% of the maximum. The smaller response to electrical activation presumably reflects a nerve fiber catecholamine content that is low, possibly in part because of postmortem degradation. These responses to activation and norepinephrine were not augmented by a NOS inhibitor or indomethacin, suggesting that a concomitant increase in NO or prostanoids does not mask the sensitivity to adrenergic stimuli.

Human pial arteries are insensitive to β-adrenergic agonists, and their response to norepinephrine was blocked by an α-adrenergic antagonist but not a β-adrenergic antagonist (57). In cat, application of norepinephrine to isolated basilar artery produced VSM

depolarization and contraction, whereas application to small pial arteries produced VSM hyperpolarization and relaxation that was blocked by a β-adrenergic antagonist (172), suggesting some species difference within pial arteries. Penetrating arterioles neither constrict nor dilate in response to norepinephrine (111). Thus, in the adult brain, the effect of noradrenergic stimulation is highly dependent on the arterial segment. The greater potency in the larger arteries is thought to protect the microcirculation from increases in arterial pressure while exerting little effect on CBF. However, some species variation has been observed in that norepinephrine produced β-adrenergic relaxation in large cerebral arteries of pigs (253, 462) and in pial arteries of cats (172).

### Sympathetic effects during development

Information on adrenergic responsivity in arteries from immature human brain is limited. Bevan et al. (56) measured responses of MCA and basilar arteries isolated within 2 days of death from eight infants who ranged in birth age from 23 weeks PMA to term and died between 1 h and PND 34. Catecholamine-containing nerve fibers were already present at 23 to 24 weeks PMA in the adventitia layer (Figure 20). At all ages, electrical activation of intramural nerves increased tension to an average of 13% of the artery's maximum. This response was blocked with an α-adrenergic antagonist. Application of norepinephrine produced an increase in tension equivalent to 43% of the maximum. Both the electrical and pharmacologic responses were greater than those seen in human adult MCA and pial arteries (57). In contrast to the adult arteries, indomethacin enhanced basal tone (58) and the contractile response to norepinephrine in both premature and postnatal infants (56). Thus, adrenergic constriction is enhanced in the perinatal period and appears to be modulated by prostanoids.

The effect of sympathetic stimulation and the responses of cerebral arteries to norepinephrine have been studied during development in baboons, sheep, and pigs. The carotid artery and the major forebrain arteries of the fetal, neonatal, and adult sheep express $\alpha_1$-adrenergic receptors (299). The isolated forebrain arteries were shown to constrict in response to norepinephrine (129). This constriction was blocked with an $\alpha_1$- but not with an $\alpha_2$-adrenergic receptor antagonist. The constrictor response was absent in the basilar artery of near-term fetal sheep and newborn lambs (444), suggesting preferential adrenergic constriction in the anterior circulation. The density of $\alpha_1$ receptors on the forebrain cerebral arteries and their constriction response to norepinephrine are less than that in the carotid artery (299). However, the receptor density in the fetal cerebral arteries generally is greater than that in adult sheep cerebral arteries (299). The pial arterial response to norepinephrine and to superior cervical ganglion stimulation has been reported *in vivo* through closed cranial windows in anesthetized fetal sheep (Figure 21). The pial arterial constriction response to topical norepinephrine is greater in preterm fetuses than in near-term fetuses and neonatal lambs, whereas a moderate dilator response is seen in adult sheep (442). The constrictor response is blocked with an $\alpha_1$-adrenergic antagonist. Moreover, electrical stimulation of the superior cervical ganglion in near-term fetal sheep decreases pial arterial diameter as much as 20% (442). Interestingly, the MCA and pial arteries at 0.6 to 0.8 gestation are more sensitive than those at 0.8 to 0.9 gestation (442, 444). The decreased constrictor sensitivity to norepinephrine in the MCA of 0.8 to 0.9-gestation fetal sheep is

partly attributed to an upregulation of β-adrenergic relaxation by norepinephrine and an increase in basal NO (444). Thus, the intracerebral expression of $\alpha_1$-adrenergic receptors and their physiologic response are downregulated as development progresses in sheep, and $\alpha_1$-adrenergic constriction is lost in the smaller pial arteries by adulthood.

In baboons, norepinephrine and phenylephrine produced constriction of the MCA at 0.75 gestation and in term newborns and adults (180). However, sensitivity decreased by one order of magnitude between the newborn and adult MCA, suggesting a decrease in agonist affinity for the α-adrenergic receptor. The β-adrenergic agonist isoproterenol produced relaxation in cerebral arteries from fetus and newborn but little response in adult cerebral arteries. Thus, the baboon and sheep express general similarities in that both α-adrenergic constriction and β-adrenergic relaxation of large cerebral arteries diminish beyond midgestation in the sheep and beyond late gestation in the baboon.

In the newborn piglet, noradrenergic responses have been studied *in vivo* in the pial arteries through closed cranial windows. Stimulation of the superior cervical ganglion or application of norepinephrine, phenylephrine, or clonidine produces pial artery constriction (78, 81). In contrast to sheep, constriction in response to sympathetic stimulation and norepinephrine appears to be mediated by primarily $\alpha_2$- and not $\alpha_1$-adrenergic receptors (78, 79). It is unclear whether $\alpha_2$-mediated constriction in pial arteries persists during maturation in swine.

The role of the sympathetic nervous system in the regulation of CBF has been studied by using microspheres to measure regional CBF. In neonatal piglets, sympathetic stimulation produces as much as a 15% decrease in CBF in cerebrum, which is much less than the concurrent 93% decrease in blood flow to the masseter muscle (440). The decrease in CBF was attenuated by an $\alpha_1$-adrenergic antagonist but not by an $\alpha_2$-adrenergic antagonist (438). This observation suggests that the effect of sympathetic stimulation on increasing resistance in the carotid and forebrain large arteries plays a more prominent role in controlling CBF than $\alpha_2$-adrenergic constriction in pial arteries.

Dopamine and dobutamine infusions are often used to support arterial pressure in neonates. Of interest is the observation that rather than producing vasoconstriction, dobutamine produces β-adrenergic-mediated dilation of pial arteries in association with an increase in cGMP in neonatal piglets (373).

In neonatal lambs, stimulation of the superior cervical ganglia during systemic hypoxia was shown to decrease CBF by as much as 25%, an effect that was blocked by an $\alpha_1$-adrenergic antagonist (439). However, administration of the $\alpha_1$-adrenergic antagonist during hypoxia did not increase CBF, thereby indicating that any increase in sympathetic activity is not sufficient to restrict CBF during hypoxia. In more extreme situations when sympathetic activity is expected to be high, such as during airway occlusion and seizures, sympathetic denervation does result in higher CBF (164, 239). The magnitude of the decrease in CBF during sympathetic stimulation is augmented when the cerebral vessels are dilated, such as during hypercapnia (440) and hypoxia (439). Therefore, $\alpha_1$-adrenergic vasoconstriction in sheep is most evident preterm, and the constrictor response diminishes later in development

as $\alpha_1$-adrenergic receptor density declines, especially in the more distal pial arteries, and as β-adrenergic and NO vasodilatory influences mature. Nevertheless, the sympathetic nervous system can limit CBF in profound dilatory states arising from hypercapnia, hypoxia, asphyxia, and seizures in near-term and postnatal animals.

In summary, (i) adrenergic vasoconstriction is attenuated in intracranial cerebral arteries compared to that in extracranial cephalic arteries, (ii) within the intracranial network, adrenergic sensitivity diminishes further between the major cerebral arteries and their branches, and (iii) for intracranial arteries, sympathetic constriction appears to be more prominent in the perinatal period than in adulthood. One can speculate that more potent constriction of large cerebral arteries in immature brain serves to limit increases in microvascular pressure during arterial hypertension at a stage when the extracellular matrix and basement membrane are underdeveloped.

## Endothelium and Astrocyte Vascular Regulation

### Blood-brain barrier development

Molecules are transported between plasma and interstitial fluid compartments via facilitated and active transporters on the luminal and abluminal surfaces of endothelial cells, formation of vesicles at the endothelial plasma membrane, and diffusion through intercellular clefts between endothelial cells. Glucose uptake is facilitated by the GLUT1 transporter on cerebral endothelium and by GLUT3 in neurons. In accordance with the postnatal increase in CMRGluc, GLUT3 increases progressively from PND 1 through PND 30 in rat, whereas most of the increase in GLUT1 occurs between PND 14 and PND 30 (425–427). The latter period corresponds to the transition from endothelium with thick cytoplasm and abundant smooth endoplasmic reticulum and Golgi apparatus to endothelium with thinner cytoplasm, a continuous basement membrane (119), and a doubling of capillary density (104). Rodents also use ketones as metabolic substrates during the period of suckling when their diet is high in fat (106, 107, 322). Expression of monocarboxylic transporter-1, which transports ketones, lactate, and pyruvate, is elevated in cerebral microvessels during this period (428). After weaning, microvessel expression of this transporter decreases, while the GLUT1 expression rapidly increases. However, in human newborns, brain ketone uptake is small relative to glucose uptake (105), and it is less clear whether a major developmental switch in endothelial expression of monocarboxylic transporters occurs.

In human fetuses, the GLUT1 transporter is already evident on the abluminal and lateral endothelial surfaces at 12 weeks' gestation and increases further at 18 weeks when interdigitation between adjacent endothelial cells develops (435). Other transporters, such as the basic and neutral amino acid transporters, are present in rat pup brains (322) and operate at a capacity equivalent to that of adult brain (106). The ontogeny of these transporters has not been reported in human brain. P-glycoprotein, which exerts xenobiotic protection, is detectable as diffuse staining in cerebral endothelial cytoplasm at 12 weeks of gestation, as punctate staining in luminal and some abluminal membranes at 18 weeks, and as punctate staining that colocalizes with abluminal phosphorylated caveolin at 22 weeks (433). Luminal localization is consistent with its role in limiting influx of toxins, and its

abluminal localization is consistent with its role in augmenting efflux of toxins. Other details of BBB transporters during development have been reviewed elsewhere (105, 312).

The barrier function of cerebral endothelium is attributed to tight junctions between adjacent endothelial cells. These cells are mechanically linked at adherens junctions composed of transmembrane VE cadherin, junction-associated molecules, PECAM, and other proteins. Tight junctions between endothelial cells limit diffusion of molecules and ions, conveying a high electrical resistance between the luminal and abluminal sides of the cerebral endothelium. The high electrical resistance is attributed to transmembrane proteins of the claudin family, especially claudin-5 and claudin-3. The claudins form heteropolymers with the transmembrane protein occluden to fill the intercellular cleft. These heteropolymers are anchored intracellularly by adapter proteins of the zona occludens family and other junction-associated molecules. Signaling from luminal endothelial receptors can effect changes in tight junction permeability via $Ca^{2+}$ signaling and alterations in the actin cytoskeleton and the zona occludens scaffolding of the heteropolymers.

Developmental studies of barrier permeability have been performed primarily in rats, rabbits, and sheep. In rats, much of the decrease in BBB permeability occurs postnatally, in line with the overall postnatal brain development. For example, permeability of radiolabeled rubidium (Rb), which is used as a surrogate for $K^+$ permeability, decreases substantially between 21-day gestation in fetal rats and PND 2, with continued reductions occurring beyond weaning at PND 21 (219). Uptake of radiolabeled sucrose and inulin also decreases markedly between 4 days before birth and PND 3, with further decreases occurring through the suckling period beyond weaning (138). In fetal sheep, however, much of the decrease in BBB permeability occurs early in gestation. A large decrease in penetration of radiolabeled sucrose occurs between 0.35 and 0.5 gestation, with a further decrease by 0.85 gestation (134). Extravascular concentration of albumin and other plasma proteins decreases with a similar time course (123). Intercellular tight junctions are apparent on electron microscopy by 0.4 gestation (124), but the endothelial cells do not yet have a mature appearance. The cells exhibit plasma membrane protrusions into the lumen, abundant cytoplasmic vesicles, and a poorly defined basement membrane. Additionally, the extracellular space is large, and astrocyte processes do not completely envelop the vessels. However, by 0.85 gestation, the endothelial cells have a normal thin cytoplasm with fewer vesicles and no fenestrations, a well-formed basement membrane, extensive astrocyte foot process abutment, and fewer pericyte processes.

The inert neutral amino acid α-aminoisobutyric acid has been used as a low-molecular-weight tracer (MW = 104) because it is taken up into brain cells but not metabolized or rapidly released. Because the tracer remains trapped in brain cells, backflux can be neglected, and a transfer constant can be calculated simply from tracer accumulation over an extended circulation time period. In rabbits, the transfer constant from blood to brain was relatively high at PND 1 (10-fold greater than in adults) but approached adult levels by PND 17 (418). In fetal sheep at 0.6 and 0.9 gestation, the α-aminoisobutyric acid transfer constant was relatively low compared to that in non-BBB tissue (402), consistent with the restriction of sucrose by 0.5 gestation (134). Interestingly, further decreases in the transfer constant occurred in all brain regions at 3 and 24 days after birth (Figure 22). In cerebrum,

an additional decrease in the transfer constant was seen between 24-day-old lambs and adult sheep. However, it is worth noting that the transfer constant depends on capillary surface area as well as permeability, and it is unknown if surface area declines in association with the known decrease in CBF over this late developmental period. Dopamine is commonly used in neonatal practice to maintain MAP, but there is some concern regarding possible effects of hypertension on the BBB. Nonetheless, the α-aminoisobutyric acid transfer constant did not increase with a 30% increase in MAP induced by dopamine infusion in fetal sheep at 0.6 or 0.9 gestation (178). The transfer constant is also low in neonatal piglets, although increases have been detected after cardiac arrest and resuscitation (389, 390).

Limited information is available on BBB development in human fetuses. Electron micrographs of human fetal brains indicate the presence of tight junctions as early as 8 weeks' gestation (319). Claudin-5 and occludin are detected primarily in the cerebral endothelial cytoplasm at 12 weeks of gestation and begin to form linear beads along the membrane by 14 weeks (434). A mature membrane localization is apparent at 18 weeks (Figure 23). Although functional permeability of these tight junctions in early gestation is unknown, these observations suggest that mechanical features of the tight junctions are present by the time of viability of premature newborns. By term, normal neonates do not exhibit enhancement with gadolinium-based contrast agents (51), suggesting that barrier function is intact. Among mammalian species, physical barrier function between endothelial cells can develop early or late in gestation in coordination with early or late neuronal development for that particular species. Presumably, the barrier function limits non-lipid-soluble molecules from the systemic circulation from interfering with the brain's developmental cues, network circuit formation, and neurotransmission. The development of the physical barrier, in turn, is coordinated with the expression of endothelial transporters to permit selective influx and efflux of substrates and metabolites.

## Endothelial and astrocyte vasoactive signaling

In most mature cerebral and peripheral arteries and arterioles, acetylcholine, bradykinin, ADP, and some other purinergic molecules bind to their respective receptors on endothelium. In response, signaling molecules such as NO, $PGI_2$, EETs, and $K^+$ are released and act on VSM to produce relaxation. Furthermore, increases in shear stress on the endothelial glycocalyx can activate mechanoreceptors that also generate vasoactive releasing factors. Factors that produce hyperpolarization of VSM, such as $K^+$ and EETs, are thought to play a more prominent role in small, intraparenchymal arterioles. However, most investigations of endothelial-dependent vasodilation during development have focused on isolated large cerebral arteries or on pial arterioles *in vivo* with the closed cranial window technique. Prostanoids and NO are the primary endothelial relaxing factors in these vessels during development.

**Nitric oxide—**NO plays a key role in regulating vascular tone in the brain and throughout the cardiovascular system under physiologic and patholphysiologic conditions, as reviewed elsewhere (61). In sheep, endothelial cells and smooth muscle cells of the major cerebral arteries increase in both length and width between birth and adulthood (128, 365). Endothelial NOS (NOS III) abundance and enzymatic activity, normalized by luminal

surface area of the carotid artery, also increase during ovine development as does shear-induced NO release (451). Endothelial NOS is present in intraparenchymal vessels by 0.4 gestation in fetal sheep (334). In large cerebral arteries, endothelial NOS expression increases during maturation and then decreases in adult arteries (457). However, dilation in response to the divalent cation ionophore A23187 is greater in the major isolated cerebral arteries of adult sheep than in those of fetal or neonatal lambs (457, 458). Likewise, the amount of NO generated in adult cerebral arteries is greater than that generated by fetal cerebral arteries (451), whether normalized by luminal surface area or endothelial nitric oxide synthase (eNOS) abundance, for similar levels of shear stress or A23187 (Figure 24). In contrast, dilation in response to ADP is similar in neonatal and adult sheep (457), and the NO generated by ADP exposure in fetal and adult arteries are comparable (451). Thus, NOS abundance does not necessarily correlate with endothelial-dependent dilation, possibly because not all of the NOS are in the proper location for effective signal transduction. Furthermore, maturation appears to depend on the nature of the stimulus.

Both expression and activity of NOS are lower in endothelial microvessels from piglets than in those from adult pigs (351). Acetylcholine and bradykinin were shown to stimulate NOS activity in microvessels at both ages, but the stimulated activity was greater in the adult microvessels. In isolated pressurized MCA from newborn piglets, dilation in response to decreased transmural pressure was blocked by deendothelialization, NOS inhibition, or a $BK_{Ca}$ channel antagonist, and constriction in response to increased transmural pressure was blocked by deendothelialization or an endothelin A receptor antagonist (306). Indomethacin had a minor effect. Thus, the endothelium and NO can play a role in the integrated myogenic response of large cerebral arteries of newborn piglets.

Interestingly, transient expression of inducible NOS (NOS II) has been observed in microvessels of rat brainstem and thalamus at embryonic day 17 and again in cerebellar white matter, cerebral cortex, thalamus, striatum, and hippocampus at PND 5 to 10 (148). Expression was undetectable in adult rat brain. The protein expression appeared to localize with endothelium, including penetrating arterioles. The assay for NOS activity confirmed a $Ca^{2+}$-independent component in microvessels at PND 7. The functional consequence of this transient activity during development is unknown, but a constant production of NO by inducible NOS might interfere with dynamic NO signaling from neuronal and endothelial NOS during this period of angiogenesis.

**Prostanoids—**PGs and thromboxanes are derived from the metabolism of AA by COX. The main isoforms are COX-1 and COX-2. Traditionally, COX-1 is considered to be constitutively expressed, and COX-2 to be induced during inflammation. However in brain, subsets of neurons constitutively express COX-2, and COX-2 expression has also been reported in cerebral endothelium in immature brain. In the extracranial vertebral artery from human neonates, prostanoid-dependent vasodilator tone is prominent (93). The COX inhibitor indomethacin produces contraction in isolated cerebral arteries from perinatal humans (58), thereby indicating a net dilating influence of prostanoids in immature large cerebral arteries. In piglet cranial windows, the CSF was shown to contain not only $PGI_2$ metabolite 6-keto-$PGF_{1\alpha}$ but also abundant amounts of $PGE_2$ and $PGF_{2\alpha}$; however, $PGD_2$ was not detectable (85). COX activity was similar in microvessels isolated from neonatal

and adult pig brain and primarily attributed to COX-2 (351). In endothelial cells cultured from neonatal and adult pigs, acetylcholine, bradykinin, and a calcium ionophore increased $PGE_2$ production to a similar extent at both ages (351). Likewise, cultured microvascular endothelial cells derived from human autopsy cortex and cerebellum at 22 to 26 weeks PMA displayed COX activity with the generation of 6-keto-$PGF_{1\alpha}$ and $PGE_2$ that was primarily attributed to COX-2 (350). In piglet cerebrovascular endothelial cells, coculture with smooth muscle increased expression and activity of COX-2 but not COX-1 (346), suggesting that COX-2 expression may be upregulated selectively in endothelium of arteries and arterioles. In addition, interleuken-1β augmented COX-2 activity and preferentially increased $PGE_2$ production in both cortical and cerebellar human endothelial cells; it also augmented COX-1 activity in cerebellar endothelial cells (350). Similar effects of interleuken-1β have been observed *in vivo* in piglet cortical CSF in association with pial artery dilation (398). Hence, endothelial-derived prostanoids play an important role in regulating VSM tone in large arteries, pial arteries, and microvascular arterioles early in development.

Large arteries from fetal baboons have been found to possess enhanced vasoactivity. The relaxation produced by $PGE_1$, $PGE_2$, and $PGF_{2\alpha}$ was more potent in preconstricted cerebral arteries isolated from baboons at 0.75 and term gestation than in those isolated from adult baboons (181). At high concentrations, $PGE_1$, $PGE_2$, and $PGF_{2\alpha}$ produced a more potent constrictor response in adult arteries. $PGI_2$ produced relaxation at all ages, but the sensitivity at low concentrations was greater in the premature vessels. Moreover, the $EC_{25}$ was lower for $PGE_1$ and $PGE_2$ than for $PGI_2$ in immature arteries, although the maximal relaxation was greater for $PGI_2$. Thus, the nonhuman primate shows major developmental changes in prostanoid reactivity of large cerebral arteries.

**Endothelial cholinergic signaling—**In adults, luminal exposure of most arteries to acetylcholine elicits relaxation mediated by endothelial muscarinic receptors linked to $Ca^{2+}$/calmodulin activation of NOS. The resulting NO or nitrosothiol is transferred to VSM, where it stimulates soluble GC. Restricting acetylcholine to the abluminal surface or applying it after endothelial injury usually produces a constrictor response. In cerebral arteries from immature animals, both dilator and constrictor responses have been reported. This variation depends on species and arterial segment. In humans and fetal sheep, vasodilation predominates, whereas in baboons and piglets, vasoconstriction predominates.

In sheep, application of acetylcholine to cranial windows produced dilation of pial arteries at 0.7 and 0.9 gestation and at 1 to 2 postnatal weeks of age with an $EC_{50}$ of 0.1 to 0.3 μmol/liter (441). In piglet cranial windows, application of 0.1 μmol/liter produced a heterogeneous response that consisted of moderate dilation in 45% of arteries, constriction in 19% of arteries, and little change in the remaining arteries (436). As the concentration increased, more arteries constricted than dilated, and the constrictor response was attenuated by indomethacin. Activation of thromboxane A2 receptors is thought to play a permissive role in the acetylcholine constrictor response (37). Interestingly, after cerebral ischemia and reperfusion, acetylcholine-induced increases in prostanoids were reduced, and pial arteries dilated in response to acetylcholine (260). In healthy neonatal piglets, administration of a NOS inhibitor had no effect on the constrictor response to acetylcholine, whereas in juvenile pigs, acetylcholine produced a brief constrictor response that was sensitive to indomethacin

followed by a dilator response that was sensitive to a NOS inhibitor (45, 480). Thus, NOS-dependent vasodilation in pial arteries is developmentally delayed in swine. Part of this developmental delay may be explained by downstream signaling. Cerebral arterioles in newborn piglets have a low expression of the β-subunit of $BK_{Ca}$ channels, which are thought to be required for full expression of NO-dependent relaxation (463, 465). However, when COX activity was suppressed for a week, NOS-dependent dilation in response to acetylcholine became prominent (478), thereby indicating that the developmental role of NOS signaling can be accelerated. In contrast to endothelial NOS, neuronal NOS expression and activity is higher in cortex from newborn piglets than from adult pigs (121). This elevated NOS expression was associated with higher COX-2 expression in piglet cortex. Chronically inhibiting COX or blocking EP3 receptors downregulated neuronal NOS. Thus, the interaction of prostanoids with NOS during development differs between endothelial and neuronal NOS.

**Carbon monoxide signaling—**The role of CO in vascular regulation has been extensively studied in the laboratories of Leffler et al. (276). The signaling mechanisms are shown schematically in Figure 25. The metabolism of heme by HO generates CO, biliverdin, and free iron. The amount of CO produced by HO in the body is too small to have a significant effect on raising carboxyhemoglobin (COHb) in the blood above 2%. However, dynamic increases in CO by HO activity can reduce VSM tone in some circumstances by increasing cGMP and opening $BK_{Ca}$ channels. Prolonged increases in CO can also produce a biphasic response and delayed constriction by inhibiting NO production (225). A reduction in NO production by HO activity has also been reported in adult rat pial arterioles (205). In piglets, endogenous production of CO is thought to limit the vasoconstriction elicited by hypocapnia and hypertension (461) and to augment the vasodilation evoked by arterial hypotension (217). Although CO can produce relaxation of VSM by increasing cGMP, it has also been shown to produce hyperpolarization of rat tail VSM cells by an interaction requiring histidine groups of the α-subunit of the $BK_{Ca}$ channel (447–449, 463). In piglet cerebral arteries, CO also interacts with the α-subunit of $BK_{Ca}$ channels by a mechanism involving binding of CO to a heme moiety on the channel (209). This binding increases the efficacy with which $Ca^{2+}$ sparks activate the channel (208) by increasing $Ca^{2+}$ sensitivity (465) independently of ryanodine receptors (279). Application of exogenous CO or an HO substrate to piglet cranial windows dilates pial arteries, and $BK_{Ca}$ channel inhibitors block this dilation (271). Moreover, both prostacyclin and NO are required to enable the CO-induced dilation. The enabling effect of NO, which appears to be related to a minimal cGMP requirement (50, 231), is seen in newborn and 7-week-old piglets but is lost in 3 to 4-month-old pigs in whom dilation evoked by exogenous CO is less potent (195). The reduction of CO-induced vasodilation in adult pigs is consistent with the low potency of CO compared to NO seen in adult arteries from other species (13, 73, 205). Furthermore, pial arteriolar dilation in response to $PGE_2$ in piglets requires HO activity (216). Thus, considerable crosstalk exists between CO and other signaling pathways in piglets.

In mature brain, the constitutive HO isoform, HO-2, is enriched in neurons, where it appears to play a role in neurovascular signaling during AMPA receptor activation in adult rats (339). In newborn piglets, HO-2 is also present in astrocytes and endothelium.

Experimental evidence from cultured piglet astrocytes, fresh brain slices, and selectively damaged astrocytes *in vivo* implicates astrocyte HO-2 as the main source of CO responsible for vasodilation in response to GLU and ADP (Figure 25). For example, exposure of the glia limitans to an astrocyte toxin blocks GLU- and ADP-evoked production of CO and pial arteriolar dilation without blocking the dilatory response to isoproterenol or bradykinin (215, 275). Addition of GLU to cultured piglet astrocytes produces an increase in astrocyte $Ca^{2+}$ and CO production (464) and activates $BK_{Ca}$ channels in piglet vascular myocytes that are in contact with the astrocytes. These effects are absent when an HO inhibitor is added to astrocytes or when GLU is added to myocytes without astrocytes (280). In arterioles of fresh piglet brain slices, GLU increases $Ca^{2+}$ sparks, decreases global $Ca^{2+}$, and increases vessel diameter. All of these effects are blunted by an HO inhibitor (280, 466). Thus, astrocyte-derived CO is a key signaling molecule within the neurovascular unit that modulates arteriole tone in neonatal piglets and is thought to be involved in neurovascular coupling in the immature brain (Figure 13).

In addition to astrocytes, the endothelium can also play a role in GLU-evoked vasodilation in piglets. Microvessels freshly isolated from piglet brain express HO-2 and not HO-1, whereas piglet cerebral endothelial cultures express both isoforms (352). Treatment of the cultures with a glucocorticoid increases HO-2 expression and decreases COX-2 without changing HO-1 or NOS expression. Incubation of the cells with GLU led to specific high-affinity GLU binding in the membrane fraction and stimulated the generation of CO, suggesting coupling of HO activity to an endothelial GLU receptor (352). Displacement by NMDA and AMPA/kainate receptor ligands and stimulation of CO production by AMPA/kainate and NMDA receptor agonists further support a coupling with GLU receptors (347). The activation of HO in cerebral microvessels requires NO (254) and depends on a tyrosine kinase-mediated pathway rather than a protein kinase C-mediated pathway (255, 256). In isolated, pressurized pial arteries (200 μm), dilation was evoked by a CO donor, GLU, or NMDA receptor agonist (142). The dilation produced by GLU and the NMDA receptor agonist was blocked with an HO inhibitor or by denuding the endothelium. *In vivo*, application of AMPA, kainate, and NMDA receptor agonists produced pial artery dilation that was largely attenuated by treatment with an HO inhibitor (378). Thus, GLU can evoke endothelial-dependent vasodilation requiring HO generation of CO in piglet pial arteries. However, it should be appreciated that astrocytes are in a better position for sensing neuronally released GLU than is endothelium, which is exposed to a relatively constant and higher level of plasma GLU.

In summary, vasoactive molecules derived from the endothelium, astrocytes, and neurons play a prominent role in modulating vascular myogenic tone during development. $PGI_2$ and $PGE_2$ are involved in tonic and dynamic inhibition of myogenic tone, and COX-2 is a major source of these vasodilators. Tonic release of NO also inhibits myogenic tone, but cholinergic coupling to endothelial NOS is not fully developed at birth in swine. HO-2-derived CO in astrocytes and endothelium plays a significant role in dynamic inhibition of myogenic tone in the neonatal period, at least in swine. CO mediates vasodilation to ADP, GLU, and seizures, but not to bradykinin or β-adrenergic activation, and the vasodilation is attributed to activation of VSM $BK_{Ca}$ channels. However, whether CO plays a similarly significant role in human neonates is not known.

## Cerebrovascular Reactivity to Carbon Dioxide

In adults, vascular reactivity in response to $CO_2$ is greater in the cerebral circulation than in most other vascular beds, as has been reviewed in detail in a previous publication in *Comprehensive Physiology* (194). Cerebrovascular smooth muscle responds to changes in extracellular pH and is also influenced by intracellular pH and $HCO_3^-$ ions (60). CBF increases in response to hypercapnia in fetal sheep at 0.6 and 0.9 gestation and in 1-week-old lambs, but the change in CBF in absolute flow units (mL/min/100 g) per mmHg $PCO_2$ rises progressively from 1.9 at 0.6 gestation to 3.5 at 0.9 gestation, to 5.2 in one-week-old lambs, and to 6.2 in adult sheep (183, 383). Low CBF reactivity has also been described in newborn monkey (374) and newborn dog (91, 166, 186). In piglets, increases in CBF during hypercapnia are lower in cerebrum than in subcortical and hindbrain structures (170), whereas decreases in CBF during hypocapnia are greater in cerebrum (171). The possibility that enhanced sympathetic activity in neonatal animals restrains CBF in cerebrum during hypercapnia is not supported by data, which have shown that neither an α-adrenergic antagonist nor cordotomy affects $CO_2$ reactivity in piglets (321).

Developmental increases in vascular $CO_2$ reactivity can be related, in part, to developmental increases in $CMRO_2$ because the change in CBF normalized by $CMRO_2$ is approximately equivalent in 0.6 gestation, 0.9 gestation, and 1-week-old lambs despite a fourfold increase in $CMRO_2$ over these development stages (183, 383). Because baseline CBF correlates with $CMRO_2$, $CO_2$ reactivity is also related to basal CBF. Thus, the relative increase in cortical laser-Doppler flow per mmHg $PCO_2$ is similar at 0.65 and 0.9 gestation (177). Interestingly, inhibition of NOS decreased baseline laser-Doppler flow in both 0.65- and 0.9-gestation fetuses but did not reduce the relative cerebrovascular reactivity to $CO_2$ at either age. However in adult sheep, both the absolute and relative change in CBF per mmHg $PCO_2$ increased further from that observed in 1-week-old lambs. Thus, mechanisms in addition to basal $O_2$ consumption, which is coupled to $CO_2$ production, contribute to further postnatal maturation of $CO_2$ reactivity.

Mechanisms of postnatal cerebral arteriole $CO_2$ reactivity have been best studied with closed cranial windows in piglets. The VSM relaxation induced by hypercapnia in newborn piglets is mediated by activation of $BK_{Ca}$ and $K_{ATP}$ channels and modulated by endothelial factors (333). As with arterial hypotension, hypercapnia produced an increase in perivascular vasodilatory prostanoids, $PGE_2$, and the $PGI_2$-stable metabolite 6-keto-$F_{1\alpha}$ (270). Indomethacin blocked the hypercapnia-induced prostanoid response and the increase in pial arteriolar diameter (443) but had no effect on the hypocapnia-induced decrease in arteriolar diameter (317). When starting from an arterial $PCO_2$ of 15 mmHg, increasing arterial $PCO_2$ back to normocapnia increased arteriolar diameter, but this dilatory response was not blocked by indomethacin. Thus, in the newborn piglet, prostanoids contribute to $CO_2$ reactivity only in the absolute hypercapnia range and do not contribute to vasodilation in response to a positive directional change of $PCO_2$ within the low $PCO_2$ range.

Several lines of evidence indicate that the endothelium plays an important role in neonatal $CO_2$ reactivity. For example, damage to the endothelium *in vivo* with the light/dye technique blocks hypercapnic vasodilation (269), and piglet cerebral microvascular

endothelium *in vitro* increases $PGI_2$ production in response to hypercapnia (200) and decreases in intracellular pH (199). Although the calcium ionophore increased endothelial prostanoid production, acidosis did not appear to increase intracellular $Ca^{2+}$ in endothelium. Additionally, increases in $PCO_2$ in piglet cerebrovascular smooth muscle or glia cultures did not cause an increase in release of $PGE_2$ or 6-keto-$PGF_{1\alpha}$ (200). Thus, endothelium is the main source of prostanoids that contribute to pial arteriolar dilation in response to hypercapnia in the newborn piglet.

Prostanoids may provide more of a permissive action than a mediator role because keeping a small perivascular concentration of $PGE_2$ (437) or the $PGI_2$ analog iloprost restores hypercapnic reactivity after blocking synthesis or injuring the endothelium (265, 268, 269, 371) and because $PGI_2$ permits decreases in pH to increase cAMP in piglet VSM cells (257). Furthermore, 0.1 nmol/liter iloprost can act through other second messengers involving inositol trisphosphate and diacylglycerol formation (359). The permissive effect of $PGI_2$ dissipates in juvenile piglets when NO-derived cGMP appears to serve as a permissive factor (459, 460, 480). After cerebral ischemia in newborn piglets, hypercapnia no longer increases perivascular prostanoids, and the dilator response of pial arterioles to hypercapnia is absent, whereas the dilator response to $PGE_2$ is retained (258, 260). Application of AA restored 6-keto-$PGF_{1\alpha}$ and other prostanoid levels and also restored the dilator response to hypercapnia (266, 267). Together, these data indicate that prostanoid synthesis is required for hypercapnic vasodilation in neonatal piglets.

In mature brain, hypercapnia can also activate acid-sensitive ion channel 1a in neurons and lead to stimulation of neuronal NOS sufficient to augment hypercapnic vasodilation (135). Whether this mechanism is operative in the immature brain or whether it becomes operative only in mature brain and is responsible for the greater $CO_2$ responsivity in adult brain is unknown.

Another pathway implicated in modulating hypercapnic reactivity involves hydrogen sulfide ($H_2S$). Increases in $H_2S$ can be detected in CSF during hypercapnia, and an inhibitor of cystathionine $\gamma$-lyase (CSE), which is expressed in piglet blood vessels, reduced hypercapnic vasodilation (274). $H_2S$ acts by opening $K_{ATP}$ channels present in piglet VSM (281) and by promoting the activation of $Ca^{2+}$ sparks with secondary effects on $BK_{Ca}$ channel opening (282). In summary, the endothelium plays a prominent role in hypercapnic dilation of pial arterioles in newborn piglets, as summarized in Figure 26. Endothelial-derived $PGI_2$ enables the dilation evoked by hypercapnia. Both $K_{ATP}$ and $BK_{Ca}$ channels contribute to hypercapnic dilation of pial arterioles in newborn piglets (333), and $H_2S$ derived from endothelial CSE participates in the activation of these channels.

## Cerebrovascular Reactivity to Oxygenation

The CBF response to changes in oxygenation represents an integration of multiple factors, including CPP, arterial $PO_2$, hematocrit, $O_2$ affinity of hemoglobin, and $CMRO_2$, all of which influence tissue $PO_2$. A review of the literature in human adults exposed to hypoxic hypoxia indicates that the increase in CBF offsets the decrease in $CaO_2$ such that cerebral $O_2$

transport (CBF × $CaO_2$) does not decline, whereas induction of hemodilution does produce a modest decline in cerebral $O_2$ transport (192).

### Alterations in arterial $PO_2$

The cephalic arterial $PO_2$ *in utero* is approximately 25 Torr. Because fetal hemoglobin has a high $O_2$ affinity, the arterial oxyhemoglobin saturation supplying the brain is approximately 70%. However, small decrements in fetal arterial $PO_2$ result in large decrements in $O_2$ saturation because the fetal hemoglobin operates near the steep portion of the $O_2$-dissociation curve. Thus, small impairments in placental $O_2$ exchange can exert a large effect on $CaO_2$. Studies in 0.9-gestation fetal sheep indicate robust cerebral vasodilation in response to decreases in $CaO_2$, whether produced by decreasing maternal inspired $O_2$ or by hemodilution as a result of fetal blood exchange transfusion with an albumin solution (211, 382). With either hypoxic hypoxia or anemic hypoxia, the increase in CBF is related reciprocally with the decrease in $CaO_2$ such that bulk cerebral $O_2$ transport is sustained (212). This homeostatic mechanism maintains global $CMRO_2$ and high energy phosphates in the fetal brain unless $CaO_2$ falls to very low levels (<1.5 mmol $O_2$/liter) (210, 211) or arterial pressure decreases (411, 445). At a $CaO_2$ of about 1.5 mmol/liter, tissue $PO_2$ in the fetal sheep brain has been reported to approach 1.5 Torr, which is in the range that limits oxidative phosphorylation (59). With the maintenance of $CMRO_2$ and cerebral $O_2$ transport above this critical $CaO_2$, OEF (equivalent to ratio of $CMRO_2$ to cerebral $O_2$ transport) also remains nearly constant over a wide range of $CaO_2$ in near-term fetal sheep (382), 1-week-old lambs (227), and adult sheep (230). Figures 27A–27C shows the mean regression curves from these studies and illustrates the robust CBF response to hypoxia that is sufficient to maintain $O_2$ transport and OEF by 0.9 gestation in fetal sheep.

The CBF response to acute hypoxia has also been examined in fetal sheep at 0.6 gestation. At this developmental stage, CBF, cerebral $O_2$ transport, $CMRO_2$, and CMRGluc are approximately 25% to 30% of the normal values seen at 0.9 gestation (160). Interestingly, OEF is 0.30, which is comparable to that at 0.9 gestation. With decreases in arterial $PO_2$ and $CaO_2$, CBF increases (206), but the increase is insufficient to maintain cerebral $O_2$ transport (Figures 27A–27C). Consequently, an increase in OEF is required to sustain the low level of $CMRO_2$ at 0.6 gestation (161). When hypoxia is induced by partial restriction of uterine blood flow and the duration of hypoxia is extended to 12 h, the moderate increase in CBF is sustained (311). As with acute hypoxia, cerebral $O_2$ transport initially declines. However, the uterine blood flow restriction also induces fetal respiratory acidosis. As the acidosis spontaneously normalizes beyond 3 h, cerebral $O_2$ transport improves and returns to baseline levels by 12 h. Thus, an interaction with fetal pH may occur when fetal hypoxia is prolonged.

After birth, arterial $PO_2$ and $CaO_2$ increase as a result of the transition from placental to pulmonary $O_2$ supply. To isolate the effect of increasing arterial $PO_2$ without the increase in external sensory stimulation, near-term fetal sheep were ventilated *in utero* through a chronically implanted endotracheal tube (162, 423). Ventilation with a low $O_2$ mixture that did not change fetal arterial $PO_2$ or $CaO_2$ had little effect on CBF, cerebral $O_2$ transport, $CMRO_2$, or OEF, thereby indicating that fetal lung inflation, *per se*, has little effect on

cerebral hemodynamics (162). Ventilation with a high $O_2$ mixture that increased fetal arterial $PO_2$ and $CaO_2$ decreased CBF but had no major effect on cerebral $O_2$ transport, $CMRO_2$, or OEF. Thus, as when arterial $PO_2$ decreases, cerebral $O_2$ transport is also tightly controlled when arterial $PO_2$ increases. Moreover, $CMRO_2$ is lower in fetal lambs at 0.9 gestation than in lambs at 1 week of age. The fact that $CMRO_2$ did not increase acutely with increases in arterial $PO_2$ indicates that the low oxygenation state *in utero* is not limiting $CMRO_2$. Furthermore, the active regulation of cerebral $O_2$ transport is supported by data showing a 30% decrease in the diameter of pial arteries on the surface of the fetal brain when the fetal arterial $PO_2$ was increased from 20-25 mmHg to 80-100 mmHg with *in utero* ventilation of a high $O_2$ mixture (340). Thus, homeostatic mechanisms are present near-term for defending brain oxygenation against increases or decreases in arterial $PO_2$.

### Alterations in $CMRO_2$

As discussed above, $CMRO_2$ increases as the brain continues to develop through early childhood. Developmental increases in $CMRO_2$ are matched by increases in CBF and cerebral $O_2$ transport. In sheep, this developmental increase in $CMRO_2$ occurs rapidly, and $CMRO_2$ and cerebral $O_2$ transport in 1-week-old lambs already exceed the corresponding values in adult sheep by 20% (230). With induction of hypoxia, the increase in CBF is sufficient to sustain cerebral $O_2$ transport, $CMRO_2$, and OEF in both lambs and adult sheep (Figures 27A–27C), but the $O_2$ transport is higher in lambs. Together, these observations imply that the postnatal CBF response to hypoxia is related to the $CMRO_2$ at that developmental stage. To gain more insight into the effect of $CMRO_2$ on the CBF response to hypoxia, pentobarbital coma with an isoelectric EEG was induced in 1-week-old lambs and adult sheep (120). Coma caused an approximately 50% decrease in $CMRO_2$, CBF, and cerebral $O_2$ transport in both age groups with no change in OEF. During subsequent induction of hypoxia, the increase in CBF was less than that in awake animals but was sufficient to sustain a constant cerebral $O_2$ transport at its lower comatose level. OEF remained constant during hypoxia. Although direct vascular effects of high barbiturate doses cannot be excluded, the data support the concept that cerebral $O_2$ transport remains coupled to $CMRO_2$ during hypoxia over a large reduction in $CMRO_2$.

### Alterations in hematocrit and $O_2$ affinity of hemoglobin

In addition to $CMRO_2$, other regulatory factors change in the postnatal period. For example, fetal hemoglobin is replaced by adult hemoglobin, which has a lower $O_2$ affinity (higher $P_{50}$, the $PO_2$ at 50% oxyhemoglobin saturation). The transition from RBCs with fetal hemoglobin to those with adult hemoglobin results in a transient decline in hematocrit in the early postnatal period. One way to experimentally isolate the effects of decreased $CaO_2$ from decreased arterial $PO_2$ is to decrease hematocrit. In newborn lambs, the relationship of CBF to $CaO_2$ is equivalent with hypoxic and anemic hypoxia, thereby indicating that cerebral $O_2$ transport is well regulated in both cases (212). However, because anemia decreases blood viscosity, the amount of vasodilation required to increase CBF is less than that with hypoxic hypoxia. To separate effects of hematocrit from $CaO_2$, moderately anemic lambs with a hematocrit of 20% were exchange transfused with methemoglobin-containing RBCs to increase hematocrit to 38% without increasing the $O_2$-carrying capacity (201). CBF was found to decrease about half as much as that in anemic lambs exchange transfused with

oxyhemoglobin-containing RBCs. Thus, about half of the change in CBF under anemic conditions is attributed to rheological effects, and the remaining half is attributed to active vasodilation from hypoxia. Similar conclusions are reached when hematocrit is increased from 30% to 55% (308). Part of the decrease in CBF with polycythemia is attributed to rheological effects, and part is attributed to increased oxygenation. The influence of anemia's rheological effect is greater when cerebral arterioles are already dilated by hypercapnia and less when cerebral arterioles are already constricted by hypocapnia (202). Thus, one needs to factor in the postnatal decrease in hematocrit when evaluating postnatal increases in CBF.

Another way to experimentally isolate the effects of decreased $CaO_2$ from decreased arterial $PO_2$ is to reduce $CaO_2$ by ventilating the animal with CO, while keeping arterial $PO_2$ constant. Graded levels of up to 60% COHb produced graded increases in CBF in newborn lambs (227). However, for equivalent decreases in arterial oxyhemoglobin saturation, the increase in CBF during CO-induced hypoxia was greater than that induced by decreases in arterial $PO_2$. This enhanced response to CO hypoxia resulted in an increase in cerebral $O_2$ transport, no change in $CMRO_2$, and a decrease in OEF. Similar differences in $O_2$ transport and OEF between hypoxic and CO hypoxia were observed in adult sheep (230). Interestingly, the decrease in sagittal sinus $PO_2$ was equivalent for the same decrease in $CaO_2$ during hypoxic and CO hypoxia in lambs (227). A greater increase in CBF without a smaller drop in venous $PO_2$ can be explained by the binding of CO to one or more of the heme subunits, which increases the $O_2$ affinity of the remaining heme subunits and thereby decreases the $P_{50}$. These observations imply that a decrease in the hemoglobin $P_{50}$ augments the CBF response to a decrease in $CaO_2$ such that cerebral venous $PO_2$ is identical, and by inference, cerebral tissue $PO_2$ is similar in the two types of hypoxia. To determine whether this is a fortuitous observation or if the degree of cerebral vasodilation is adjusted to the level of venous and tissue $PO_2$, the decrease in $P_{50}$ during CO hypoxia was mitigated by first performing an exchange transfusion with high-$P_{50}$ RBCs from adult sheep and then exposing the newborn lambs to CO hypoxia (229). After the $P_{50}$ of the circulating RBCs was increased, CBF and cerebral $O_2$ transport decreased and OEF increased at normal arterial $PO_2$. Subsequent induction of CO hypoxia to a level that restored the $P_{50}$ to the lambs' baseline $P_{50}$ increased CBF, but only by an amount that restored cerebral $O_2$ transport to the baseline level (rather than by an amount that increased cerebral $O_2$ transport, as had been the case when CO hypoxia was permitted to decrease $P_{50}$ below the baseline value). Consequently, cerebral $O_2$ transport is inversely related to $P_{50}$, and OEF is positively correlated with $P_{50}$ during CO hypoxia.

These observations raise the question of whether the transition from low-$P_{50}$ fetal hemoglobin to high-$P_{50}$ adult hemoglobin influences the sensitivity of the cerebrovascular response to hypoxia induced by decreases in arterial $PO_2$. In 0.9-gestation fetal sheep with a $P_{50}$ of 15 to 20 Torr, exchange transfusion with blood from adult sheep that had a $P_{50}$ of 40 to 45 Torr resulted in a lower CBF over a wide range of $CaO_2$ induced by reducing arterial $PO_2$ (382). Similar results were obtained in 1-week-old lambs when the $P_{50}$ was increased from 26 to 37 Torr by exchange transfusion with adult sheep blood (228). In both cases, the higher $P_{50}$ was associated with a lower cerebral $O_2$ transport and a higher OEF that remained relatively constant during subsequent hypoxia (Figures 27D–27F). Indeed, as

the $P_{50}$ is increased in near-term fetus sheep and neonatal lambs, the CBF, $O_2$ transport, and OEF relationships move closer to those seen in adult sheep. Thus, the level at which cerebral $O_2$ transport is regulated is determined by the combination of $CMRO_2$ and $P_{50}$, both of which influence the tissue $PO_2$ that will determine the degree of vasodilation at a given $CaO_2$. OEF, which already accounts for developmental differences in $CMRO_2$, is primarily influenced by $P_{50}$, which appears to change the set point at which OEF is regulated over a wide range of $CaO_2$.

The relationship of OEF to $P_{50}$ when fetal hemoglobin is replaced with adult hemoglobin overlaps with the same relationship obtained when $P_{50}$ is decreased during COHb. Indeed, species differences in $O_2$ affinity of hemoglobin may explain part of the species differences in cerebral OEF. For example, adult sheep with a $P_{50}$ of 40 to 45 Torr have a cerebral OEF of approximately 0.55 (230), whereas adult humans with a $P_{50}$ of 28 Torr have an OEF of approximately 0.34. Thus, the transition from fetal to adult hemoglobin in humans does not result in as large a change in $P_{50}$ and OEF as that seen in sheep, although one study using MRI to measure cerebral venous $O_2$ saturation did report higher OEF at 1 to 3 months of age than in neonates (114). The large postnatal change in $P_{50}$ seen in sheep provides a proof of principle for the importance of $O_2$ affinity in influencing the unloading of $O_2$ in the microcirculation and consequently the tissue $PO_2$, which then feeds back to regulate arteriolar tone. In summary, when interpreting changes in CBF during the postnatal period, one needs to consider that the transition from fetal to adult hemoglobin, with its higher $P_{50}$, will promote a lower CBF and a higher OEF, whereas postnatal anemia will promote a higher CBF with little change in OEF.

## Mechanisms of arterial reactivity to oxygenation

Studies in adult rodents indicate that cerebrovascular dilation during hypoxia depends on adenosine receptors, EETs, and activation of $K_{ATP}$ channels (291, 315, 407, 413). Some studies in immature animals also support a role for these pathways. In neonatal piglets, interstitial adenosine, measured by microdialysis, increases approximately 150% in frontal cortex and thalamus when arterial $PO_2$ is acutely decreased to 20 mmHg (357). Increases in CSF concentration of the adenosine metabolites inosine and hypoxanthine correlate with the increase in CBF, and inhibiting adenosine receptors with 8-phenyltheophylline substantially reduces the increase in CBF during hypoxia in piglets (246). Kurth and Wagerle (238) compared adenosine analog-induced dilation of pial arteries by intravital microscopy through closed cranial windows in fetal sheep *in utero* at 0.65 and 0.9 gestation. Dilation was robust at both ages. Thus, an inability of pial arteries to respond to adenosine is not responsible for the smaller increase in CBF observed during hypoxia at 0.6 gestation (161).

In newborn piglets, EETs are capable of dilating pial arterioles (264), and administration of the epoxygenase inhibitor miconazole decreases the pial arteriole dilatory response to hypoxia (277). EETs can target VSM $BK_{Ca}$ channels (153), which are known to be activated by hypoxia in mature cerebral VSM (151). Additionally, the $BK_{Ca}$ channel inhibitor iberiotoxin partially reduces pial arteriolar dilation to hypoxia in neonatal piglets, thereby implicating a role for these channels (19). The opening of $BK_{Ca}$ channels appears to be

related to increases in cAMP rather than to NO and increases in cGMP (18, 21). Hypoxia also increases CO production (214), and inhibiting HO reduces pial arteriolar dilation in piglets (272). However, the contribution of CO to hypoxic vasodilation does not appear to be mediated by $BK_{Ca}$ channels or GC activity (214), suggesting that CO may interact with other pathways. Prostanoids do not appear to directly initiate hypoxic dilation of piglet pial arterioles (273). These findings imply that EET- and $BK_{Ca}$ channel-dependent mechanisms of hypoxic vasodilation are intact in newborn piglets, which are considered to be at a neurodevelopmental stage similar to that of term human neonates.

Isolated branches of the MCA in neonatal lambs dilate in response to a $K_{ATP}$ channel agonist, but sensitivity is less than that in arteries from adult sheep (363), suggesting that this channel undergoes a developmental change in large cerebral arteries. The evidence for $K_{ATP}$ channel involvement in the vasodilatory response to hypoxia is less consistent. One study in piglets reported no effect of the sulfonylurea antagonist glibenclamide on pial arteriolar dilation to hypoxia (277), whereas another study did find that glibenclamide reduced hypoxia-induced dilation of pial arterioles (20). The latter study also found that an adenosine receptor antagonist decreased pial arteriolar dilation to hypoxia and that glibenclamide attenuated the dilation to exogenous adenosine, suggesting that $K_{ATP}$ channels may mediate part of the adenosine-dependent component of hypoxic vasodilation.

The contribution of NO to hypoxic vasodilation has been studied by administering a NOS inhibitor intravenously to fetal sheep at 0.6 and 0.9 gestation. At both ages, NOS inhibition increased MAP and CVR and reduced microsphere measurement of CBF during normoxia and acute hypoxia without curtailing $CMRO_2$ (175, 422). However, CVR still decreased and CBF still increased during acute hypoxia in both age groups, and the percent increase in CBF during hypoxia from the lower normoxic baseline after NOS inhibition was similar to that without NOS inhibition (175). These results imply that NO exerts a tonic vasodilatory influence during both normoxia and hypoxia, but that it is not the prime mediator of hypoxic vasodilation at 0.6 or 0.9 gestation. A somewhat different conclusion was obtained when cerebral RBC flux was measured with a laser-Doppler flow probe chronically implanted deep in the cerebral cortex of 0.9-gestation fetal sheep. Here, the NOS inhibitor not only decreased normoxic RBC perfusion but also attenuated the percent increase in perfusion during hypoxia from the lower baseline (203). Similar results were obtained with a laser-Doppler flow probe inserted into the striatum of PND 7 and PND 14 rats, although MAP responses could not be recorded in these small pups (204). The observation that CBF further increases during reoxygenation suggests that arterial hypotension may have been present during hypoxia and then recovered during reoxygenation in the rat pups. Nevertheless, an NO electrode in the striatum indicated a concurrent increase in NO during hypoxia and reoxygenation. These results suggest that NO could serve as a mediator and not simply as a modulator of RBC perfusion at the microvascular level during perinatal hypoxia. It should be noted that the percent increase in laser-Doppler perfusion during hypoxia in fetal sheep was less than that obtained with the microsphere technique (59). It is unclear whether the further attenuation of the laser-Doppler response seen after NOS inhibition was related to differences in methodology, as microspheres are considered to measure arteriolar blood flow, whereas laser-Doppler measures RBC movement. In either case, the vasodilatory influence

of NO remained sustained for at least 3 h of hypoxia, as evident by a 15% reduction in CBF when a NOS inhibitor was administered at 3 h of hypoxia in 0.9-gestation fetal sheep (310).

In piglet pial arteries, a complex interplay of NO and vasopressin with opioid release occurs during hypoxia. For example, NO release during hypoxia acts to increase methionine enkephalin (17, 454), which then can produce vasodilation via activation of $BK_{Ca}$ channels (18, 19) and $K_{ATP}$ channels (23, 394). NO derived from neuronal NOS rather than endothelial NOS appears to drive opioid release from glia during hypoxia (22, 455, 456). Furthermore, vasopressin can stimulate the release of methionine enkephalin and leucine enkephalin (386), whereas a vasopressin antagonist attenuates the release of methionine enkephalin and leucine enkephalin as well as dilation of pial arteries during hypoxia (385). Antagonists of μ-opioid receptors (17) and δ-opioid receptors (16) blunt the hypoxia-induced dilation of pial arterioles. In contrast, antagonists of κ-opioid receptors potentiate vasodilation induced by hypoxia (17). As the duration of hypoxia was prolonged from 10 to 40 min, pial arterial dilation was noted to partially subside in association with a decline in methionine enkephalin and a rise in dynorphin, a κ-opioid receptor agonist (24). A time-dependent amplification of dynorphin's limitation of hypoxic vasodilation may be attributed to an increase in vasopressin (431). Therefore, opioids have distinct modulatory effects on the temporal response of pial arteries to hypoxia in the newborn piglet.

The transition to pulmonary ventilation at birth increases $CaO_2$ and results in a lower CBF after birth. When fetal sheep were ventilated *in utero* to increase arterial $PO_2$ to postnatal levels, CBF decreased with little change in cerebral $O_2$ transport. However, *in utero* oxygenation-induced pial artery vasoconstriction was blocked when an inhibitor of cytochrome P450 ω-hydroxylase was applied to the cranial window, suggesting that an $O_2$-dependent increase in vascular 20-HETE production is responsible for limiting hyperoxia in the brain at birth (340). CYP4A isoforms that make 20-HETE are $O_2$ dependent and are known to be present in mature cerebral arteries. Additionally, cephalic arteries in fetal sheep were found to express CYP4A proteins. After birth, an increase in endothelin may also contribute to hyperoxic vasoconstriction (26). Therefore, the mechanisms of vascular reactivity to increases and decreases in oxygenation appear to be different.

## Cerebrovascular Function During Pathophysiological States

### Seizures

Status epilepticus represents the extreme case of physiologic excitatory neurotransmission and induced neurovascular coupling. Bicuculline-induced seizures in neonatal piglets were shown to increase CBF and the cortical CSF concentration of $PGE_2$, 6-keto-$PGF_{1\alpha}$, $PGF_{2\alpha}$, and thromboxane $B_2$ (80). Pretreatment with indomethacin attenuated the increase in CBF, thereby implicating a net vasodilatory influence on these prostanoids during seizures. The contribution of CO to vasodilation has also been examined in detail. Seizures produced near-maximal dilation of 68% in pial arterioles (369) associated with increases in CSF CO (88). Topical application of an HO inhibitor to the cranial window CSF reduced dilation to 35%, whereas systemic injection of an HO inhibitor reduced dilation to 13% (369). The inhibitors did not attenuate the accompanying 75% increase in MAP, the 25% increase in arterial $PCO_2$, or the increases in perivascular CSF concentrations of cGMP and cAMP. These

results are consistent with vascular effects of CO acting independently of cyclic nucleotides. By 2 h of recovery from seizure activity, pial arteriolar responses to hypercapnia, bradykinin (endothelial-dependent), isoproterenol, and nitroprusside (endothelial-independent) dilators were intact. However, after HO inhibition, these responses were impaired (88). When the postictal recovery period was extended to 2 days, responses to these vasodilators became partially impaired in the absence of HO inhibitor treatment. This impairment was ameliorated by induction of HO-1 or administration of a CO donor prior to seizures (345, 479). Together, these data in piglets indicate that CO generated during seizures exerts a protective effect on vascular reactivity that lasts for at least 2 days.

### Hypoxia-ischemia

In a model of 45-min hypoxia (arterial $O_2$ saturation 35%) followed by 7-min airway occlusion, autoregulation was found to remain intact at 6, 24, and 48 h after reoxygenation (249, 252). After induction of moderate hypothermia starting at 2 h after reoxygenation, CBF decreased and the LLA shifted to a lower CPP (249). Furthermore, after a 20-h period of hypothermia and a 4-h period of rewarming, autoregulation to arterial hypotension remained intact (245). It should be noted that this model of hypoxia-asphyxia produces selective neuronal injury in SM cortex, striatum, and thalamus with sparing of brainstem and cerebellum (304). This pattern of injury is analogous to that commonly seen in term human newborns (117) and in newborn monkeys subjected to partial asphyxia (325). In another model in which asphyxic blood gases and acidosis were induced without severe hypotension, pial arteriolar dilation to astrocyte- and endothelial-dependent dilation was impaired at 24 and 48 h of recovery (353). This dysfunction could be ameliorated by pretreatment of a CO donor, which reduced ROS, and worsened by pretreatment of an HO inhibitor, thereby indicating that CO can exert protective effects on postasphyxic cerebrovascular reactivity.

A different pattern of injury involving the brainstem, cerebellum, and thalamus emerges after complete asphyxia when blood flow ceases for an extended period (309, 325). In piglets subjected to a more severe model in which artificial CSF was infused into the epidural space to produce 20 min of intracranial hypertension with no blood flow, CBF and $CMRO_2$ were decreased at 2 h of reoxygenation (263), and pial arterial dilation to arterial hypotension and hypercapnia were reduced in association with a loss of the CSF prostanoid responses (258, 261). Administration of exogenous AA restored the pial arteriole dilatory response to hypercapnia (267), suggesting a role for substrate limitation after the early reperfusion period (266). When piglets were exposed to 10 min of complete ischemia, the vasodilatory response to the $K_{ATP}$ channel opener aprikalim was markedly reduced at 1 h but recovered at 2 h (49). Likewise, vasodilation to NMDA was impaired at 1 h after a 10-min period of complete asphyxia (86) or complete ischemia (83), but treatment with the mitochondrial $K_{ATP}$ channel opener diazoxide preserved NMDA-induced vasodilation (118). Overall, these results indicate that periods of complete cerebral ischemia disrupt normal vascular reactivity to physiologic stimuli.

### Traumatic brain injury

TBI has a high prevalence among children. Impaired autoregulation has been noted after TBI in a subpopulation of children (72, 140, 323), especially those who had poor outcome and

were less than 4 years old (145, 167, 278, 326). One of the first studies was reported by Muizelaar et al. (323), who measured the change in CBF by the radiolabeled Xe washout technique during pharmacologically induced changes in MAP. Impaired autoregulation, defined as an ARI less than 0.5, was observed on 41% of the measurements and was more prevalent when baseline CBF was less than 33 mL/min/100 g. In most children with intact autoregulation, the change in ICP was inversely related to the change in MAP, whereas those with defective autoregulation generally exhibited a positive relationship between the change in ICP and the change of MAP. This work supported the subsequent development of the PRx index of autoregulation, which is based on the correlation coefficient of ICP with MAP. Transcranial Doppler measurements of MCA blood velocity have been used to test autoregulation during phenylephrine-induced hypertension after TBI. Neurologic status and age less than 4 years were risk factors for impaired autoregulation, which was detected in about 40% of the children (145, 430). The limitation of using transcranial Doppler is that measurements are intermittent. The use of PRx overcomes this limitation. Continuous monitoring of PRx can identify the CPP at which PRx has a minimal value for an individual patient. This minimal CPP is designated the optimal CPP because it is presumed to be the CPP at which vasoreactivity to a change in CPP is maximal. In the subset of pediatric TBI patients in which an optimal CPP could be identified, that optimal CPP correlated with the patient's age (Figure 28). However, it is noteworthy that the optimal CPP has considerable interpatient variability and that a higher average PRx value and a greater percentage of time spent with CPP deviating from its optimum for each individual patient are associated with worse outcome from TBI (72, 278). Thus, real-time monitoring of PRx and other indices of autoregulation provide an opportunity for individualized management of a patient's CPP near its optimum where vasodilator and vasoconstrictor reserve are maximal.

Impaired autoregulation has been replicated with the fluid percussion model of TBI in neonatal piglets. After TBI, dilation of pial arteries is impaired, and CBF during induced arterial hypotension is reduced. Interestingly, these effects are more prominent in male than in female piglets (233). The deficits can be partly restored by administration of an angiotensin receptor-1 antagonist (48), an ERK antagonist (233), an endothelin receptor A antagonist (38), and inhaled NO (110, 182, 361). Hypoperfusion and sustained pial arterial constriction are more prominent in newborn piglets than in 1-month-old piglets after fluid percussion TBI (28). As summarized in Figure 29, this effect has been attributed to vasopressin and endothelin-1 (ET-1) stimulation of the opioid nociception/orphanin FQ, leading to superoxide generation, activation of protein tyrosine kinase (PKT) and ERK, and impaired functionality of $K_{ATP}$ and $BK_{Ca}$ channels (25, 29–33). Inhaled NO in amounts that do not cause overt hypotension can restore autoregulation by blocking the increase in endothelin and the downsteam effects on ERK and MAPK and interleukin-6 (IL-6) (110). Increased IL-6 can impair $K^+$ channels. In the case of neonatal stroke, endogenous tissue plasminogen activator (tPA) augments NMDA receptor activation that leads to increased endothelin and IL-6 (35, 36), and similar mechanisms are likely operative after TBI (44).

Adrenergic pressor agents can be used to maintain MAP near the optimal level for vasoreactivity. Interestingly, the pressor agents can help restore pial artery dilation to subsequent dilation induced by hemorrhagic hypotension, but the effect depends on the sex and age of the piglets. For example, epinephrine infusion improves vasodilation elicited by

hemorrhage or by $K_{ATP}$ or $BK_{Ca}$ channel agonists in newborn male and female piglets and in female 4-week-old piglets but not in male 4-week-olds (42, 43). Neither norepinephrine nor phenylephrine infusion improves autoregulatory vasodilation in male newborns, but it does in female newborns and in both male and female 4-week-olds (38, 40, 41, 109). On the other hand, dopamine infusion improves post-TBI autoregulation in both sexes and both age groups (39, 108). However, it should be noted that adrenergic control of pial arterioles has a greater predominance of $\alpha_2$-adrenergic constrictor and β-adrenergic dilator effects in piglets than in other species and that dopamine acts primarily through β-adrenergic receptors. Thus, some caution is required in translating these findings on pressor agents to humans. In addition to disturbances in autoregulation, TBI can impair the function of microvessels with regard to the BBB, vasogenic edema, and inflammation (296), but this aspect has been primarily studied in adult animal models.

## Future Directions

- *Neuronal network formation*. Complex networks of excitatory and inhibitory neurons undergo dynamic organization that depends on use and interactions with other networks. Further work is needed to understand how maturation of network formation affects tissue energy demands, angiogenesis, and the various aspects of blood flow regulation.
- *Neurovascular coupling*. As neuronal networks develop and interconnect, a better understanding is needed of how the mechanisms of neurovascular coupling become integrated during different stages of development. Changes in signaling pathways during development need to be better explored in multiple species, especially in the context of the switch to negative BOLD responses in infants.
- *Pericytes*. Pericytes play a role in angiogenesis, BBB development, and monitoring endothelial function, but more insights are needed with regard to their role in the control of capillary blood flow during development.
- *CO and $H_2S$*. While CO and $H_2S$ have been well studied in the regulation of pial arterioles in newborn piglets, their role in regulating penetrating arterioles and in species other than swine during development is understudied.
- *Hypoxia, hypercapnia, and hypotension*. Signaling mechanisms of vasodilation can differ with hypoxia, hypercapnia, and arterial hypotension, but how each of these mechanisms become integrated among cell types in the neurovascular unit during development still requires more elucidation in multiple species.
- *Endothelium*. Endothelial cells are often lumped into a single phenotype. It will be of interest to better understand the development of different endothelial phenotypes along different segments of the vascular tree and the role of extracellular vesicles in altering the phenotype, especially in pro-inflammatory states.
- *BBB*. Formation of the BBB during development has largely focused on permeability through endothelial clefts, but more research should focus on

transendothelial transport mechanisms and how they are affected by various neurologic disorders during development.

- *Microglia*. Some work has been done on how the maturation of microglia influences the vulnerability of the BBB during development (137, 139, 237), but how microglia maturation influences physiological regulation of the cerebral circulation has been largely unexplored.
- *Vascular mitochondria*. It is becoming recognized that mitochondria in microvessels and large arteries can play a role in vascular control and in preconditioning by various forms of stress (84, 101), but changes in vascular mitochondria protein expression and the impact on vascular function during development remain largely unexplored.
- *Maternal health*. Maternal nutrition and inflammatory conditions in the intrauterine environment can affect not only neuronal development but also endothelial phenotype and the propensity for endothelial dysfunction later in life (102). This area needs further investigation.
- *Effect of sex*. Different aspects of brain development vary by sex, and some studies of the cerebral circulation and energy metabolism during human development have segregated the data by sex. While studies of the cerebral circulation during development in rodents, piglets, and fetal and newborn lambs generally included both sexes, these data generally have not been separated by sex. Thus, it is largely unknown whether sex affects prepubertal developmental control of the cerebral circulation under normal physiologic conditions. However, under conditions of acute brain injury, sex differences in the restoration of autoregulation become apparent according to the properties of the pressor agent, as discussed in the Traumatic brain injury section. These observations suggest the presence of inherent underlying sex differences in vascular signaling in the newborn brain that can be revealed after an acute injury. Therefore, more attention should be paid to sex differences in vascular control mechanisms during development.
- *Microbiome*. There is a need for a better understanding of how the change in the gut microbiome during development might influence the cerebral circulation. Studies have been performed concerning the maternal microbiome effect on maternal inflammatory state that then influences fetal brain development, BBB development, and neurologic and psychiatric disorders later in life (395). However, studies are lacking on whether the maternal microbiome or inflammatory status of the placenta influences the regulation of fetal CBF. After birth, the fetal gut is no longer sterile, and some research has been done on the effect of the gut microbiome on neural development. But again, the role of postnatal gut microbiome on cerebrovascular physiological regulation has not been well investigated.

## Conclusions

Many of the physiologic principles of CBF regulation observed in adult brain pertain to immature brain, but the responses to physiologic perturbations are often weaker and dependent on the developmental stage. $CMRO_2$ is very low at birth in humans but eventually exceeds adult levels at 3 to 11 years of age. CBF is metabolically coupled to the developmental increases in $CMRO_2$ such that OEF changes little during development, other than that accompanying the postnatal increase in hemoglobin $P_{50}$. CBF is also coupled to developmental increases in CMRGluc, but the relative increase in CMRGluc exceeds the relative increase in $CMRO_2$, presumably because a significant portion of glucose enters the synthetic pathways during the prepubertal timespan of brain growth and synaptic plasticity.

Neurovascular coupling is present in primary sensory cortex at birth, but the response is slow, and the amplitude is low compared to responses in adult brain. This slower, diminished response in neonates is likely related to a lower energy demand and to a smaller area of activation due to underdeveloped interconnections among cortical regions. Moreover, responses in infants can become inadequate to match the increase in $CMRO_2$, resulting in an increase in deoxyhemoglobin content and a negative BOLD MRI signal, the mechanisms of which remain unknown. However, the increase in deoxyhemoglobin might not be considered harmful because the level of CBF at this stage of development already exceeds adult levels of CBF, and the changes in the BOLD response represent only a small change in oxyhemoglobin saturation that is unlikely to impair mitochondrial respiration.

Myogenic tone is present early in development and increases in concert with developmental increases in arterial pressure and thickening of the VSM media layer. Evidence indicates that autoregulatory function is present at birth in term humans and in the several large animal species that have been studied. Data in fetal sheep suggest that MAP operates *in utero* close to the LLA, which is sensitive to the arterial $O_2$ saturation. Strong autoregulatory responses to increases in MAP are evident in postnatal animals. Studies on large cerebral arteries of human newborns and fetal sheep indicate that adrenergic constrictor capability is present at birth and may actually be enhanced compared to that of adults. Some species differences exist in that piglets rely more on $\alpha_2$- than on $\alpha_1$-mediated constriction, and β-adrenergic vasodilation is strong in swine.

Endothelial cells undergo a change in morphology during development as angiogenesis subsides and communication with pericytes and glia matures. Formation of tight junctions and decreases in BBB permeability are early events during neural development. Fully mature levels of very low permeability to small, nonlipid molecules are attained relatively late, although continued formation of new leaky capillaries may contribute to this delay. Endothelial-dependent dilation can be observed in fetuses and neonates of large animal species, but the magnitude and signaling pathways can change during later development.

Studies in animals indicate that CBF reactivity to hypercapnia is lower in cerebrum than in brainstem during the perinatal period. However, reactivity in cerebrum increases progressively throughout development and attains the high reactivity seen in adults despite the highest $CMRO_2$ occurring before adulthood. Prostanoids can play a permissive function

in the hypercapnia-induced dilation of pial arterioles in newborn piglets, whereas NO takes on a more prominent permissive role later in development. Endothelial-derived $H_2S$ has been implicated in hypercapnic vasodilation.

The fetus grows in an intrauterine environment with arterial $PO_2$ just several Torr above the fetal hemoglobin $P_{50}$ such that small decrements in arterial $PO_2$ result in large decrements in $CaO_2$. Cerebral vasodilation in response to decreased $CaO_2$ is observed early in fetal development, but the response largely matures at the developmental stage when $CMRO_2$ transitions approximately from 30% to 70% of adult levels. At the low energy demand state, the increase in CBF does not fully compensate for the decrease in $CaO_2$, and cerebral $O_2$ transport falls, whereas in the higher energy demand state, cerebral $O_2$ transport is well regulated.

It is evident that the different cell types in the brain contribute to the vascular response to physiological perturbation in a well-integrated manner. Moreover, each cell type has a different maturation profile as the brain increases in size and connectivity. Likewise, cerebrovascular reactivity develops over a period of weeks to years, depending on the species. In light of this protracted ontogeny, one needs to be cautious when interpreting primary cell culture studies in which the cells are typically derived from fetal or newborn animals. Cultures may be left for 14 days *in vitro* to allow maturation, but a fully mature phenotype may not be achieved, especially in the absence of signaling from the full complement of other cell types in the brain. Cocultures and slice cultures overcome some of these limitations, but one still has to consider that the developmental program has not been completely executed among all cell types in these model systems to fully recapitulate the *in vivo* cerebrovascular responses.

Overall, a picture emerges in which regulation of the cerebral circulation matures at a different pace for each category of physiologic stimuli, as summarized qualitatively in the schematic diagram (Figure 30). Much of the diffusion restriction by the BBB develops early and is followed by vascular responsivity to hypoxia. Developmental increases in CBF, $CMRO_2$, and CMRGluc have a longer time course, and vascular reactivity to $CO_2$, while present at an early stage, has a protracted time course to reach full maturity. Vascular responses to neuronal activation are also only partially developed at birth, and more research is required to better understand the developmental trajectory of the complex signaling mechanisms required for a fully mature and integrated neurovascular coupling response.

## Acknowledgments

The author is grateful to Claire Levine, M.S., E.L.S, for her editorial assistance.

The author's research in perinatal physiology has been supported by grants from the National Institutes of Health R01 NS060703, R01 HL139543, and R21 NS095036.

## List of Abbreviations

| | |
|---|---|
| **20-HETE** | 20-hydroxyeicosatetraenoic acid |
| **AMPA** | α-amino-3-hydroxy-5-methyl-4-isoxazolepropionic acid |

| | |
|---|---|
| **ARI** | autoregulatory index |
| **BBB** | blood-brain barrier |
| **$BK_{Ca}$** | large conductance calcium-activated $K^+$ channel |
| **$BK_V$** | voltage-sensitive $K^+$ channels |
| **BOLD** | blood oxygen level-dependent |
| **$CaO_2$** | arterial oxygen content |
| **CBF** | cerebral blood flow |
| **CBV** | cerebral blood volume |
| **CMRGluc** | cerebral metabolic rate of glucose |
| **$CMRO_2$** | cerebral metabolic rate of oxygen |
| **CO** | carbon monoxide |
| **COHb** | carboxyhemoglobin |
| **COX** | cyclooxygenase |
| **COx** | cerebral oximetry index |
| **CPP** | cerebral perfusion pressure |
| **CSF** | cerebrospinal fluid |
| **CVR** | cerebrovascular resistance |
| **CYP** | cytochrome P450 |
| **ECMO** | extracorporeal membrane oxygenation |
| **EET** | epoxyeicosatrienoic acid |
| **EP4** | prostaglandin E2 receptor 4 |
| **$HbO_2$** | hemoglobin oxygen saturation |
| **HVx** | hemoglobin volume index |
| **ICP** | intracranial pressure |
| **$K_{ir}$** | inward-rectifier $K^+$ channel |
| **LLA** | lower limit of autoregulation |
| **MAP** | mean arterial blood pressure |
| **MCA** | middle cerebral artery |
| **MRI** | magnetic resonance imaging |

| | |
|---|---|
| **NIRS** | near-infrared spectroscopy |
| **NMDA** | *N*-methyl-D-aspartate |
| **NO** | nitric oxide |
| **NOS** | nitric oxide synthase |
| **OEF** | oxygen extraction fraction |
| **$PCO_2$** | partial pressure of carbon dioxide |
| **PET** | positron emission tomography |
| **PG** | prostaglandin |
| **PMA** | postmenstrual age |
| **PND** | postnatal day |
| **$PO_2$** | partial pressure of oxygen |
| **PRx** | pressure-reactivity index |
| **Rb** | Rubidium |
| **RBC** | red blood cell |
| **SPECT** | single-photon emission computed tomography |
| **TBI** | traumatic brain injury |
| **VSM** | vascular smooth muscle |

## References


1. Abrams RM, Ito M, Frisinger JE, Patlak CS, Pettigrew KD, Kennedy C. Local cerebral glucose utilization in fetal and neonatal sheep. Am J Physiol Regul Integr Comp Physiol 246: R608–R618, 1984.
2. Acosta S, Penny DJ, Brady KM, Rusin CG. An effective model of cerebrovascular pressure reactivity and blood flow autoregulation. Microvasc Res 115: 34–43, 2018. DOI: 10.1016/j.mvr.2017.08.006. [PubMed: 28847705]
3. Adachi K, Takahashi S, Melzer P, Campos KL, Nelson T, Kennedy C, Sokoloff L. Increases in local cerebral blood flow associated with somatosensory activation are not mediated by NO. Am J Physiol Heart Circ Physiol 267: H2155–H2162, 1994.
4. Adams RH, Eichmann A. Axon guidance molecules in vascular patterning. Cold Spring Harb Perspect Biol 2: a001875, 2010. DOI: 10.1101/cshperspect.a001875. [PubMed: 20452960]
5. Akopov SE, Zhang L, Pearce WJ. Regulation of $Ca^{2+}$ sensitization by PKC and rho proteins in ovine cerebral arteries: Effects of artery size and age. Am J Physiol 275: H930–H939, 1998. [PubMed: 9724297]
6. Alkayed NJ, Birks EK, Narayanan J, Petrie KA, Kohler-Cabot AE, Harder DR. Role of P-450 arachidonic acid expoygenase in the response of cerebral blood flow to glutamate in rats. Stroke 28: 1066–1072, 1997. [PubMed: 9158651]
7. Alkayed NJ, Narayanan J, Gebremedhin D, Medhora M, Roman RJ, Harder DR. Molecular characterization of an arachidonic acid epoxygenase in rat brain astrocytes. Stroke 27: 971–979, 1996. [PubMed: 8623121]

8. Allievi AG, Arichi T, Tusor N, Kimpton J, Arulkumaran S, Counsell SJ, Edwards AD, Burdet E. Maturation of sensori-motor functional responses in the preterm brain. Cereb Cortex 26: 402–413, 2016. DOI: 10.1093/cercor/bhv203. [PubMed: 26491066]
9. Alonso-Galicia M, Hudetz AG, Shen H, Harder DR, Roman RJ. Contribution of 20-HETE to vasodilator actions of nitric oxide in the cerebral microcirculation. Stroke 30: 2727–2734, 1999. [PubMed: 10583004]
10. Altman DI, Perlman JM, Volpe JJ, Powers WJ. Cerebral oxygen metabolism in newborns. Pediatrics 92: 99–104, 1993. [PubMed: 8516092]
11. Altman DI, Powers WJ, Perlman JM, Herscovitch P, Volpe SL, Volpe JJ. Cerebral blood flow requirement for brain viability in newborn infants is lower than in adults. Ann Neurol 24: 218–226, 1988. [PubMed: 3263081]
12. Anderson AW, Marois R, Colson ER, Peterson BS, Duncan CC, Ehrenkranz RA, Schneider KC, Gore JC, Ment LR. Neonatal auditory activation detected by functional magnetic resonance imaging. Magn Reson Imaging 19: 1–5, 2001. [PubMed: 11295339]
13. Andresen JJ, Shafi NI, Durante W, Bryan RM Jr. Effects of carbon monoxide and heme oxygenase inhibitors in cerebral vessels of rats and mice. Am J Physiol Heart Circ Physiol 291: H223–H230, 2006. DOI: 10.1152/ajpheart.00058.2006. [PubMed: 16489113]
14. Arichi T, Fagiolo G, Varela M, Melendez-Calderon A, Allievi A, Merchant N, Tusor N, Counsell SJ, Burdet E, Beckmann CF, Edwards AD. Development of BOLD signal hemodynamic responses in the human brain. NeuroImage 63: 663–673, 2012. DOI: 10.1016/j.neuroimage.2012.06.054. [PubMed: 22776460]
15. Arichi T, Moraux A, Melendez A, Doria V, Groppo M, Merchant N, Combs S, Burdet E, Larkman DJ, Counsell SJ, Beckmann CF, Edwards AD. Somatosensory cortical activation identified by functional MRI in preterm and term infants. NeuroImage 49: 2063–2071, 2010. DOI: 10.1016/j.neuroimage.2009.10.038. [PubMed: 19854281]
16. Armstead WM. The contribution of delta 1- and delta 2-opioid receptors to hypoxia-induced pial artery dilation in the newborn pig. J Cereb Blood Flow Metab 15: 539–546, 1995. DOI: 10.1038/jcbfm.1995.67. [PubMed: 7714013]
17. Armstead WM. Opioids and nitric oxide contribute to hypoxia-induced pial arterial vasodilation in newborn pigs. Am J Physiol Heart Circ Physiol 268: H226–H232, 1995.
18. Armstead WM. Role of activation of calcium-sensitive $K^+$ channels and cAMP in opioid-induced pial artery dilation. Brain Res 747: 252–258, 1997. [PubMed: 9046000]
19. Armstead WM. Role of activation of calcium-sensitive $K^+$ channels in NO- and hypoxia-induced pial artery vasodilation. Am J Physiol Heart Circ Physiol 272: H1785–H1790, 1997. DOI: 10.1152/ajpheart.1997.272.4.H1785.
20. Armstead WM. Role of nitric oxide, cyclic nucleotides, and the activation of ATP-sensitive $K^+$ channels in the contribution of adenosine to hypoxia-induced pial artery dilation. J Cereb Blood Flow Metab 17: 100–108, 1997. DOI: 10.1097/00004647-199701000-00013. [PubMed: 8978392]
21. Armstead WM. Contribution of $K_{Ca}$ channel activation to hypoxic cerebrovasodilation does not involve NO. Brain Res 799: 44–48, 1998. [PubMed: 9666071]
22. Armstead WM. Nitric oxide contributes to opioid release from glia during hypoxia. Brain Res 813: 398–401, 1998. [PubMed: 9838202]
23. Armstead WM. Relationship among NO, the $K_{ATP}$ channel, and opioids in hypoxic pial artery dilation. Am J Physiol Heart Circ Physiol 275: H988–H994, 1998.
24. Armstead WM. Role of opioids in hypoxic pial artery dilation is stimulus duration dependent. Am J Physiol Heart Circ Physiol 275: H861–H867, 1998.
25. Armstead WM. Age-dependent impairment of K(ATP) channel function following brain injury. J Neurotrauma 16: 391–402, 1999. DOI: 10.1089/neu.1999.16.391. [PubMed: 10369559]
26. Armstead WM. Endothelin-1 contributes to normocapnic hyperoxic pial artery vasoconstriction. Brain Res 842: 252–255, 1999. [PubMed: 10526121]
27. Armstead WM. Hypotension dilates pial arteries by $K_{ATP}$ and $K_{Ca}$ channel activation. Brain Res 816: 158–164, 1999. [PubMed: 9878717]

28. Armstead WM. Role of nociceptin/orphanin FQ in age-dependent cerebral hemodynamic effects of brain injury. J Neurotrauma 17:751–764, 2000. DOI: 10.1089/neu.2000.17.751. [PubMed: 11011815]
29. Armstead WM. Endothelin-induced cyclooxygenase-dependent superoxide generation contributes to $K^+$ channel functional impairment after brain injury. J Neurotrauma 18: 1039–1048, 2001. DOI: 10.1089/08977150152693737. [PubMed: 11686491]
30. Armstead WM. Vasopressin-induced protein kinase C-dependent superoxide generation contributes to ATP-sensitive potassium channel but not calcium-sensitive potassium channel function impairment after brain injury. Stroke 32: 1408–1414, 2001. [PubMed: 11387506]
31. Armstead WM. Vasopressin induced cyclooxygenase dependent superoxide generation contributes to K(+) channel function impairment after brain injury. Brain Res 910: 19–28, 2001. [PubMed: 11489250]
32. Armstead WM. Age-dependent NOC/oFQ contribution to impaired hypotensive cerebral hemodynamics after brain injury. J Neurotrauma 19: 1193–1202, 2002. DOI: 10.1089/08977150260337994. [PubMed: 12427328]
33. Armstead WM. Protein tyrosine kinase and mitogen-activated protein kinase activation contribute to K(ATP) and K(ca) channel impairment after brain injury. Brain Res 943: 276–282, 2002. [PubMed: 12101050]
34. Armstead WM. Age and cerebral circulation. Pathophysiology 12: 5–15, 2005. DOI: 10.1016/j.pathophys.2005.01.002. [PubMed: 15927820]
35. Armstead WM, Hekierski H, Pastor P, Yarovoi S, Higazi AA, Cines DB. Release of IL-6 after stroke contributes to impaired cerebral autoregulation and hippocampal neuronal necrosis through NMDA receptor activation and upregulation of ET-1 and JNK. Transl Stroke Res 10: 104–111, 2019. DOI: 10.1007/s12975-018-0617-z. [PubMed: 29476447]
36. Armstead WM, Hekierski H, Yarovoi S, Higazi AA, Cines DB. tPA variant tPA-A(296-299) prevents impairment of cerebral autoregulation and necrosis of hippocampal neurons after stroke by inhibiting upregulation of ET-1. J Neurosci Res 96: 128–137, 2018. DOI: 10.1002/jnr.24112. [PubMed: 28703856]
37. Armstead WM, Mirro R, Busija DW, Leffler CW. Permissive role of prostanoids in acetylcholine-induced cerebral vasoconstriction. J Pharmacol Exp Ther 251: 1012–1019, 1989. [PubMed: 2532248]
38. Armstead WM, Riley J, Vavilala MS. TBI sex dependently upregulates ET-1 to impair autoregulation, which is aggravated by phenylephrine in males but is abrogated in females. J Neurotrauma 29: 1483–1490, 2012. DOI: 10.1089/neu.2011.2248. [PubMed: 22335188]
39. Armstead WM, Riley J, Vavilala MS. Dopamine prevents impairment of autoregulation after traumatic brain injury in the newborn pig through inhibition of Up-regulation of endothelin-1 and extracellular signal-regulated kinase mitogen-activated protein kinase. Pediatr Crit Care Med 14: e103–e111, 2013. DOI: 10.1097/PCC.0b013e3182712b44. [PubMed: 23314184]
40. Armstead WM, Riley J, Vavilala MS. Norepinephrine protects cerebral autoregulation and reduces hippocampal necrosis after traumatic brain injury via blockade of ERK MAPK and IL-6 in juvenile pigs. J Neurotrauma 33: 1761–1767, 2016. DOI: 10.1089/neu.2015.4290. [PubMed: 26597684]
41. Armstead WM, Riley J, Vavilala MS. Preferential protection of cerebral autoregulation and reduction of hippocampal necrosis with norepinephrine after traumatic brain injury in female piglets. Pediatr Crit Care Med 17: e130–e137, 2016. DOI: 10.1097/PCC.0000000000000603. [PubMed: 26741414]
42. Armstead WM, Riley J, Vavilala MS. K channel impairment determines sex and age differences in epinephrine-mediated outcomes after brain injury. J Neurosci Res 95: 1917–1926, 2017. DOI: 10.1002/jnr.24063. [PubMed: 28397372]
43. Armstead WM, Riley J, Vavilala MS. Sex and age differences in epinephrine mechanisms and outcomes after brain injury. J Neurotrauma 34: 1666–1675, 2017. DOI: 10.1089/neu.2016.4770. [PubMed: 27912253]

44. Armstead WM, Vavilala MS. Translational approach towards determining the role of cerebral autoregulation in outcome after traumatic brain injury. Exp Neurol 317: 291–297, 2019. DOI: 10.1016/j.expneurol.2019.03.015. [PubMed: 30928388]
45. Armstead WM, Zuckerman SL, Shibata M, Parfenova H, Leffler CW. Different pial arteriolar responses to acetylcholine in the newborn and juvenile pig. J Cereb Blood Flow Metab 14: 1088–1095, 1994. DOI: 10.1038/jcbfm.1994.142. [PubMed: 7523428]
46. Attwell D, Mishra A, Hall CN, O'Farrell FM, Dalkara T. What is a pericyte? J Cereb Blood Flow Metab 36: 451–455, 2016. DOI: 10.1177/0271678X15610340. [PubMed: 26661200]
47. Baerts W, van Bel F, Thewissen L, Derks JB, Lemmers PM. Tocolytic indomethacin: Effects on neonatal haemodynamics and cerebral autoregulation in the preterm newborn. Arch Dis Child Fetal Neonatal Ed 98: F419–F423, 2013. DOI: 10.1136/archdischild-2012-302532. [PubMed: 23482639]
48. Baranov D, Armstead WM. Selective blockade of AT1 receptor attenuates impairment of hypotensive autoregulation and improves cerebral blood flow after brain injury in the newborn pig. Anesthesiology 99: 1118–1124, 2003. [PubMed: 14576548]
49. Bari F, Louis TM, Meng W, Busija DW. Global ischemia impairs ATP-sensitive $K^+$ channel function in cerebral arterioles in piglets. Stroke 27: 1874–1880; discussion 1880-1871, 1996. [PubMed: 8841347]
50. Barkoudah E, Jaggar JH, Leffler CW. The permissive role of endothelial NO in CO-induced cerebrovascular dilation. Am J Physiol Heart Circ Physiol 287: H1459–H1465, 2004. [PubMed: 15191891]
51. Barkovich AJ, Latal-Hajnal B, Partridge JC, Sola A, Ferriero DM. MR contrast enhancement of the normal neonatal brain. AJNR Am J Neuroradiol 18: 1713–1717, 1997. [PubMed: 9367320]
52. Barkovich AJ, Westmark K, Partridge C, Sola A, Ferriero DM. Perinatal asphyxia: MR findings in the first 10 days. Am J Neuroradiol 16: 427–438, 1995. [PubMed: 7793360]
53. Baumbach GL, Heistad DD. Effects of sympathetic stimulation and changes in arterial pressure on segmental resistance of cerebral vessels in rabbits and cats. Circ Res 52: 527–533, 1983. [PubMed: 6851007]
54. Bevan JA. Sites of transition between functional systemic and cerebral arteries of rabbits occur at embryological junctional sites. Science 204: 635–637, 1979. [PubMed: 432670]
55. Bevan JA, Duckworth J, Laher I, Oriowo MA, McPherson GA, Bevan RD. Sympathetic control of cerebral arteries: Specialization in receptor type, reserve, affinity, and distribution. FASEB J 1: 193–198, 1987. [PubMed: 2887477]
56. Bevan R, Dodge J, Nichols P, Poseno T, Vijayakumaran E, Wellman T, Bevan JA. Responsiveness of human infant cerebral arteries to sympathetic nerve stimulation and vasoactive agents. Pediatr Res 44:730–739, 1998. DOI: 10.1203/00006450-199811000-00016. [PubMed: 9803455]
57. Bevan RD, Dodge J, Nichols P, Penar PL, Walters CL, Wellman T, Bevan JA. Weakness of sympathetic neural control of human pial compared with superficial temporal arteries reflects low innervation density and poor sympathetic responsiveness. Stroke 29: 212–221, 1998. [PubMed: 9445353]
58. Bevan RD, Vijayakumaran E, Gentry A, Wellman T, Bevan JA. Intrinsic tone of cerebral artery segments of human infants between 23 weeks of gestation and term. Pediatr Res 43: 20–27, 1998. DOI: 10.1203/00006450-199804001-00125. [PubMed: 9432108]
59. Bishai JM, Blood AB, Hunter CJ, Longo LD, Power GG. Fetal lamb cerebral blood flow (CBF) and oxygen tensions during hypoxia: A comparison of laser Doppler and microsphere measurements of CBF. J Physiol 546: 869–878, 2003. [PubMed: 12563011]
60. Boedtkjer E. Acid-base regulation and sensing: Accelerators and brakes in metabolic regulation of cerebrovascular tone. J Cereb Blood Flow Metab 38: 588–602, 2018. DOI: 10.1177/0271678X17733868. [PubMed: 28984162]
61. Bohlen HG. Nitric oxide and the cardiovascular system. Compr Physiol 5: 808–823, 2015. DOI: 10.1002/c140052. [PubMed: 25880514]
62. Bohlen HG, Harper SL. Evidence of myogenic vascular control in the rat cerebral cortex. Circ Res 55: 554–559, 1984. [PubMed: 6478557]

63. Borel CO, Backofen JE, Koehler RC, Jones MD Jr, Traystman RJ. Cerebral blood flow autoregulation during intracranial hypertension in hypoxic lambs. Am J Physiol Heart Circ Physiol 253: H1342–H1348, 1987.
64. Born AP, Rostrnp E, Miranda MJ, Larsson HB, Lou HC. Visual cortex reactivity in sedated children examined with perfusion MRI (FAIR). Magn Reson Imaging 20: 199–205, 2002. [PubMed: 12034341]
65. Born P, Leth H, Miranda MJ, Rostrup E, Stensgaard A, Peitersen B, Larsson HB, Lou HC. Visual activation in infants and young children studied by functional magnetic resonance imaging. Pediatr Res 44:578–583, 1998. DOI: 10.1203/00006450-199810000-00018. [PubMed: 9773849]
66. Brady K, Joshi B, Zweifel C, Smielewski P, Czosnyka M, Easley RB, Hogue CW Jr. Real-time continuous monitoring of cerebral blood flow autoregulation using near-infrared spectroscopy in patients undergoing cardiopulmonary bypass. Stroke 41: 1951–1956, 2010. [PubMed: 20651274]
67. Brady KM, Easley RB, Kibler K, Kaczka DW, Andropoulos D, Fraser CD 3rd, Smielewski P, Czosnyka M, Adams GJ, Rhee CJ, Rusin CG. Positive end-expiratory pressure oscillation facilitates brain vascular reactivity monitoring. J Appl Physiol 113: 1362–1368, 2012. DOI: 10.1152/japplphysiol.00853.2012. [PubMed: 22984248]
68. Brady KM, Lee JK, Kibler KK, Easley RB, Koehler RC, Czosnyka M, Smielewski P, Shaffner DH. The lower limit of cerebral blood flow autoregulation is increased with elevated intracranial pressure. Anesth Analg 108: 1278–1283, 2009. [PubMed: 19299800]
69. Brady KM, Lee JK, Kibler KK, Easley RB, Koehler RC, Shaffner DH. Continuous measurement of autoregulation by spontaneous fluctuations in cerebral perfusion pressure: Comparison of 3 methods. Stroke 39: 2531–2537, 2008. [PubMed: 18669896]
70. Brady KM, Lee JK, Kibler KK, Smielewski P, Czosnyka M, Easley RB, Koehler RC, Shaffner DH. Continuous time-domain analysis of cerebrovascular autoregulation using near-infrared spectroscopy. Stroke 38: 2818–2825, 2007. [PubMed: 17761921]
71. Brady KM, Mytar JO, Lee JK, Cameron DE, Vricella LA, Thompson WR, Hogue CW, Easley RB. Monitoring cerebral blood flow pressure autoregulation in pediatric patients during cardiac surgery. Stroke 41: 1957–1962, 2010. [PubMed: 20651273]
72. Brady KM, Shaffner DH, Lee JK, Easley RB, Smielewski P, Czosnyka M, Jallo GI, Guerguerian AM. Continuous monitoring of cerebrovascular pressure reactivity after traumatic brain injury in children. Pediatrics 124: e1205–e1212, 2009. [PubMed: 19948619]
73. Brian JE Jr, Heistad DD, Faraci FM. Effect of carbon monoxide on rabbit cerebral arteries. Stroke 25: 639–643, 1994. [PubMed: 8128519]
74. Brubakk AM, Bratlid D, Oh W, Yao AC, Stonestreet BS. Atropine prevents increases in brain blood flow during hypertension in newborn piglets. Pediatr Res 18: 1121–1126, 1984. DOI: 10.1203/00006450-198411000-00013. [PubMed: 6514438]
75. Bucher HU, Edwards AD, Lipp AE, Duc G. Comparison between near infrared spectroscopy and 133Xenon clearance for estimation of cerebral blood flow in critically ill preterm infants. Pediatr Res 33: 56–60, 1993. DOI: 10.1203/00006450-199301000-00012. [PubMed: 8433862]
76. Buerk DG, Ances BM, Greenberg JH, Detre JA. Temporal dynamics of brain tissue nitric oxide during functional forepaw stimulation in rats. NeuroImage 18: 1–9, 2003. [PubMed: 12507439]
77. Burton VJ, Gerner G, Cristofalo E, Chung SE, Jennings JM, Parkinson C, Koehler RC, Chavez-Valdez R, Johnston MV, Northington FJ, Lee JK. A pilot cohort study of cerebral autoregulation and 2-year neurodevelopmental outcomes in neonates with hypoxic-ischemic encephalopathy who received therapeutic hypothermia. BMC Neurol 15: 209, 2015. DOI: 10.1186/s12883-015-0464-4. [PubMed: 26486728]
78. Busija DW, Leffler CW. Exogenous norepinephrine constricts cerebral arterioles via alpha 2-adrenoceptors in newborn pigs. J Cereb Blood Flow Metab 7: 184–188, 1987. [PubMed: 3031091]
79. Busija DW, Leffler CW. Postjunctional alpha 2-adrenoceptors in pial arteries of anesthetized newborn pigs. Dev Pharmacol Ther 10: 36–46, 1987. [PubMed: 3034531]
80. Busija DW, Leffler CW. Role of prostanoids in cerebrovascular responses during seizures in piglets. Am J Physiol Heart Circ Physiol 256: H120–H125, 1989.

81. Busija DW, Leffler CW, Wagerle LC. Responses of newborn pig pial arteries to sympathetic nervous stimulation and exogenous norepinephrine. Pediatr Res 19: 1210–1214, 1985. [PubMed: 4069832]
82. Busija DW, Marcus ML, Heistad DD. Pial artery diameter and blood flow velocity during sympathetic stimulation in cats. J Cereb Blood Flow Metab 2: 363–367, 1982. [PubMed: 7096460]
83. Busija DW, Meng W, Bari F, McGough PS, Errico RA, Tobin JR, Louis TM. Effects of ischemia on cerebrovascular responses to *N*-methyl-D-aspartate in piglets. Am J Physiol Heart Circ Physiol 270: H1225–H1230, 1996. DOI: 10.1152/ajpheart.1996.270.4.H1225.
84. Busija DW, Rutkai I, Dutta S, Katakam PV. Role of mitochondria in cerebral vascular function: energy production, cellular protection, and regulation of vascular tone. Compr Physiol 6: 1529–1548, 2016. DOI: 10.1002/c150051. [PubMed: 27347901]
85. Busija DW, Wagerle LC, Pourcyrous M, Leffler CW. Acetylcholine dramatically increases prostanoid synthesis in piglet parietal cortex. Brain Res 439: 122–126, 1988. [PubMed: 3359178]
86. Busija DW, Wei M. Altered cerebrovascular responsiveness to *N*-methyl-D-aspartate after asphyxia in piglets. Am J Physiol Heart Circ Physiol 265: H389–H394, 1993.
87. Cai C, Fordsmann JC, Jensen SH, Gesslein B, Lonstrup M, Hald BO, Zambach SA, Brodin B, Lauritzen MJ. Stimulation-induced increases in cerebral blood flow and local capillary vasoconstriction depend on conducted vascular responses. Proc Natl Acad Sci U S A 115: E5796–E5804, 2018. DOI: 10.1073/pnas.1707702115. [PubMed: 29866853]
88. Carratu P, Pourcyrous M, Fedinec A, Leffler CW, Parfenova H. Endogenous heme oxygenase prevents impairment of cerebral vascular functions caused by seizures. Am J Physiol Heart Circ Physiol 285: H1148–H1157, 2003. [PubMed: 12915392]
89. Cauli B, Hamel E. Revisiting the role of neurons in neurovascular coupling. Front Neuroenergetics 2:9, 2010. DOI: 10.3389/fnene.2010.00009. [PubMed: 20616884]
90. Cauli B, Tong XK, Rancillac A, Serluca N, Lambolez B, Rossier J, Hamel E. Cortical GABA interneurons in neurovascular coupling: Relays for subcortical vasoactive pathways. J Neurosci 24: 8940–8949, 2004. DOI: 10.1523/JNEUROSCI.3065-04.2004. [PubMed: 15483113]
91. Cavazutti M, Duffy TE. Regulation of local cerebral blood flow in normal and hypoxic newborn dogs. Ann Neurol 11: 247–257, 1982. [PubMed: 6807192]
92. Charles SM, Zhang L, Longo LD, Buchholz JN, Pearce WJ. Postnatal maturation attenuates pressure-evoked myogenic tone and stretch-induced increases in $Ca^{2+}$ in rat cerebral arteries. Am J Physiol Regul Integr Comp Physiol 293: R737–R744, 2007. DOI: 10.1152/ajpregu.00869.2006. [PubMed: 17553845]
93. Charpie JR, Schreur KD, Papadopoulos SM, Webb RC. Endothelium dependency of contractile activity differs in infant and adult vertebral arteries. J Clin Invest 93: 1339–1343, 1994. DOI: 10.1172/JCI117093. [PubMed: 8132776]
94. Chen BR, Kozberg MG, Bouchard MB, Shaik MA, Hillman EM. A critical role for the vascular endothelium in functional neurovascular coupling in the brain. J Am Heart Assoc 3: e000787, 2014. DOI: 10.1161/JAHA.114.000787. [PubMed: 24926076]
95. Chen S, Tisch N, Kegel M, Yerbes R, Hermann R, Hudalla H, Zuliani C, Gulculer GS, Zwadlo K, von Engelhardt J, Ruiz de Almodovar C, Martin-Villalba A. CNS macrophages control neurovascular development via CD95L. Cell Rep 19: 1378–1393, 2017. DOI: 10.1016/j.celrep.2017.04.056. [PubMed: 28514658]
96. Chiron C, Raynaud C, Maziere B, Zilbovicius M, Laflamme L, Masure MC, Dulac O, Bourguignon M, Syrota A. Changes in regional cerebral blood flow during brain maturation in children and adolescents. J Nucl Med 33: 696–703, 1992. [PubMed: 1569478]
97. Chugani HT. Biological basis of emotions: Brain systems and brain development. Pediatrics 102: 1225–1229, 1998. [PubMed: 9794959]
98. Chugani HT, Hovda DA, Villablanca JR, Phelps ME, Xu WF. Metabolic maturation of the brain: A study of local cerebral glucose utilization in the developing cat. J Cereb Blood Flow Metab 11: 35–47, 1991. DOI: 10.1038/jcbfm.1991.4. [PubMed: 1984003]
99. Chugani HT, Phelps ME. Maturational changes in cerebral function in infants determined by 18FDG positron emission tomography. Science 231: 840–843, 1986. [PubMed: 3945811]

100. Chugani HT, Phelps ME, Mazziotta JC. Positron emission tomography study of human brain functional development. Ann Neurol 22: 487–497, 1987. DOI: 10.1002/ana.410220408. [PubMed: 3501693]
101. Cikic S, Chandra PK, Harman JC, Rutkai I, Katakam PV, Guidry JJ, Gidday JM, Busija DW. Sexual differences in mitochondrial and related proteins in rat cerebral microvessels: A proteomic approach. J Cereb Blood Flow Metab 41: 397–412, 2021. DOI: 10.1177/0271678X20915127. [PubMed: 32241204]
102. Clough GF. Developmental conditioning of the vasculature. Compr Physiol 5: 397–438, 2015. DOI: 10.1002/c140037. [PubMed: 25589274]
103. Colonnese MT, Phillips MA, Constantine-Paton M, Kaila K, Jasanoff A. Development of hemodynamic responses and functional connectivity in rat somatosensory cortex. Nat Neurosci 11: 72–79, 2008. DOI: 10.1038/nn2017. [PubMed: 18037883]
104. Craigie EH. Postnatal changes in vascularity in the cerebral cortex of the male albino rat. J Comp Neurol 39: 301–324, 1925.
105. Cremer JE. Nutrients for the brain: Problems in supply. Early Hum Dev 5: 117–132, 1981. [PubMed: 7018883]
106. Cremer JE, Braun LD, Oldendorf WH. Changes during development in transport processes of the blood-brain barrier. Biochim Biophys Acta 448: 633–637, 1976. [PubMed: 823975]
107. Cremer JE, Cunningham VJ, Pardridge WM, Braun LD, Oldendorf WH. Kinetics of blood-brain barrier transport of pyruvate, lactate and glucose in suckling, weanling and adultrats. J Neurochem 33: 439–445, 1979. [PubMed: 469534]
108. Curvello V, Hekierski H, Pastor P, Vavilala MS, Armstead WM. Dopamine protects cerebral autoregulation and prevents hippocampal necrosis after traumatic brain injury via block of ERK MAPK in juvenile pigs. Brain Res 1670: 118–124, 2017. DOI: 10.1016/j.brainres.2017.06.010. [PubMed: 28625390]
109. Curvello V, Hekierski H, Riley J, Vavilala M, Armstead WM. Sex and age differences in phenylephrine mechanisms and outcomes after piglet brain injury. Pediatr Res 82: 108–113, 2017. DOI: 10.1038/pr.2017.83. [PubMed: 28355201]
110. Curvello V, Pastor P, Hekierski H, Armstead WM. Inhaled nitric oxide protects cerebral autoregulation and reduces hippocampal necrosis after traumatic brain injury through inhibition of ET-1, ERK MAPK and IL-6 upregulation in pigs. Neurocrit Care 30: 467–477, 2019. DOI: 10.1007/s12028-018-0638-1. [PubMed: 30386963]
111. Dacey RG Jr, Duling BR. Effect of norepinephrine on penetrating arterioles of rat cerebral cortex. Am J Physiol Heart Circ Physiol 246: H380–H385, 1984. DOI: 10.1152/ajpheart.1984.246.3.H380.
112. De Vis JB, Alderliesten T, Hendrikse J, Petersen ET, Benders MJ. Magnetic resonance imaging based noninvasive measurements of brain hemodynamics in neonates: A review. Pediatr Res 80: 641–650, 2016. DOI: 10.1038/pr.2016.146. [PubMed: 27434119]
113. De Vis JB, Hendrikse J, Petersen ET, de Vries LS, van Bel F, Alderliesten T, Negro S, Groenendaal F, Benders MJ. Arterial spin-labelling perfusion MRI and outcome in neonates with hypoxic-ischemic encephalopathy. Eur Radiol 25: 113–121, 2015. DOI: 10.1007/s00330-014-3352-1. [PubMed: 25097129]
114. De Vis JB, Petersen ET, Alderliesten T, Groenendaal F, de Vries LS, van Bel F, Benders MJ, Hendrikse J. Non-invasive MRI measurements of venous oxygenation, oxygen extraction fraction and oxygen consumption in neonates. NeuroImage 95: 185–192, 2014. DOI: 10.1016/j.neuroimage.2014.03.060. [PubMed: 24685437]
115. De Vis JB, Petersen ET, de Vries LS, Groenendaal F, Kersbergen KJ, Alderliesten T, Hendrikse J, Benders MJ. Regional changes in brain perfusion during brain maturation measured non-invasively with Arterial Spin Labeling MRI in neonates. Eur J Radiol 82: 538–543, 2013. DOI: 10.1016/j.ejrad.2012.10.013. [PubMed: 23199750]
116. De Vis JB, Petersen ET, Kersbergen KJ, Alderliesten T, de Vries LS, van Bel F, Groenendaal F, Lemmers PM, Hendrikse J, Benders MJ. Evaluation of perinatal arterial ischemic stroke using noninvasive arterial spin labeling perfusion MRI. Pediatr Res 74: 307–313, 2013. DOI: 10.1038/pr.2013.111. [PubMed: 23797533]

117. de Vries LS, Groenendaal F. Patterns of neonatal hypoxic-ischaemic brain injury. Neuroradiology 52:555–566, 2010. DOI: 10.1007/s00234-010-0674-9. [PubMed: 20390260]
118. Domoki F, Perciaccante JV, Veltkamp R, Bari F, Busija DW. Mitochondrial potassium channel opener diazoxide preserves neuronal-vascular function after cerebral ischemia in newborn pigs. Stroke 30: 2713–2718; discussion 2718-2719, 1999. [PubMed: 10583002]
119. Donahue S, Pappas GD. The fine structure of capillaries in the cerebral cortex of the rat at various stages of development. Am J Anat 108: 331–347, 1961. DOI: 10.1002/aja.1001080307. [PubMed: 13887158]
120. Donegan JH, Traystman RJ, Koehler RC, Jones MD Jr, Rogers MC. Cerebrovascular hypoxic and autoregulatory responses during reduced brain metabolism. Am J Physiol Heart Circ Physiol 249: H421–H429, 1985.
121. Dumont I, Peri KG, Hardy P, Hou X, Martinez-Bermudez AK, Molotchnikoff S, Varma DR, Chemtob S. $PGE_2$, via EP3 receptors, regulates brain nitric oxide synthase in the perinatal period. Am J Physiol Regul Integr Comp Physiol 275: R1812–R1821, 1998.
122. Dunn KM, Hill-Eubanks DC, Liedtke WB, Nelson MT. TRPV4 channels stimulate $Ca^{2+}$-induced $Ca^{2+}$ release in astrocytic endfeet and amplify neurovascular coupling responses. Proc Natl Acad Sci U S A 110: 6157–6162, 2013. DOI: 10.1073/pnas.1216514110. [PubMed: 23530219]
123. Dziegielewska KM, Evans CA, Lorscheider FL, Malinowska DH, Mollgard K, Reynolds ML, Saunders NR. Plasma proteins in fetal sheep brain: Blood-brain barrier and intracerebral distribution. J Physiol 318: 239–250, 1981. [PubMed: 6172581]
124. Dziegielewska KM, Evans CAN, Malinowska DH, Mollgard K, Reynolds JM, Reynolds ML, Saunders NR. Studies of the development of brain barrier systems to lipid insoluble molecules in fetal sheep. J Physiol Lond 292:207–231, 1979. [PubMed: 490348]
125. Easley RB, Kibler KK, Brady KM, Joshi B, Ono M, Brown C, Hogue CW. Continuous cerebrovascular reactivity monitoring and autoregulation monitoring identify similar lower limits of autoregulation in patients undergoing cardiopulmonary bypass. Neurol Res 35: 344–354, 2013. DOI: 10.1179/1743132812Y.0000000145. [PubMed: 23540403]
126. Easley RB, Marino BS, Jennings J, Cassedy AE, Kibler KK, Brady KM, Andropoulos DB, Brunetti M, Hogue CW, Heitmiller ES, Lee JK, Spaeth J, Everett AD. Impaired cerebral autoregulation and elevation in plasma glial fibrillary acidic protein level during cardiopulmonary bypass surgery for CHD. Cardiol Young 28: 55–65, 2018. DOI: 10.1017/S1047951117001573. [PubMed: 28835309]
127. Eidson TH, Edrington JL, Albuquerque ML, Zuckerman SL, Leffler CW. Light/dye microvascular injury eliminates pial arteriolar dilation in hypotensive piglets. Pediatr Res 37: 10–14, 1995. [PubMed: 7700723]
128. Elliott CF, Pearce WJ. Effects of maturation on cell water, protein, and DNA content in ovine cerebral arteries. J Appl Physiol (1985) 79:831–837, 1995. DOI: 10.1152/jappl.1995.79.3.831. [PubMed: 8567525]
129. Elliott SR, Pearce WJ. Effects of maturation on alpha-adrenergic receptor affinity and occupancy in small cerebral arteries. Am J Physiol Heart Circ Physiol 267:H757–H763, 1994. DOI: 10.1152/ajpheart.1994.267.2.H757.
130. Enager P, Piilgaard H, Offenhauser N, Kocharyan A, Fernandes P, Hamel E, Lauritzen M. Pathway-specific variations in neurovascular and neurometabolic coupling in rat primary somatosensory cortex. J Cereb Blood Flow Metab 29: 976–986, 2009. DOI: 10.1038/jcbfm.2009.23. [PubMed: 19337274]
131. Engl E, Jolivet R, Hall CN, Attwell D. Non-signalling energy use in the developing rat brain. J Cereb Blood Flow Metab 37: 951–966, 2017. DOI: 10.1177/0271678X16648710. [PubMed: 27170699]
132. Erberich SG, Friedlich P, Seri I, Nelson MD Jr, Bluml S. Functional MRI in neonates using neonatal head coil and MR compatible incubator. NeuroImage 20: 683–692, 2003. DOI: 10.1016/S1053-8119(03)00370-7. [PubMed: 14568444]
133. Erberich SG, Panigrahy A, Friedlich P, Seri I, Nelson MD, Gilles F. Somatosensory lateralization in the newborn brain. NeuroImage 29: 155–161, 2006. DOI: 10.1016/j.neuroimage.2005.07.024. [PubMed: 16112875]

134. Evans CAN, Reynolds JM, Reynolds ML, Saunders NR, Segal MB. The development of a blood-brain barrier mechanism in fetal sheep. J Physiol Lond 238: 371–386, 1974. [PubMed: 4601383]

135. Faraci FM, Taugher RJ, Lynch C, Fan R, Gupta S, Wemmie JA. Acid-sensing ion channels: Novel mediators of cerebral vascular responses. Circ Res 125: 907–920, 2019. DOI: 10.1161/CIRCRESAHA.119.315024. [PubMed: 31451088]

136. Farzam P, Buckley EM, Lin PY, Hagan K, Grant PE, Inder TE, Carp SA, Franceschini MA. Shedding light on the neonatal brain: Probing cerebral hemodynamics by diffuse optical spectroscopic methods. Sci Rep 7: 15786, 2017. DOI: 10.1038/s41598-017-15995-1. [PubMed: 29150648]

137. Faustino JV, Wang X, Johnson CE, Klibanov A, Derugin N, Wendland MF, Vexler ZS. Microglial cells contribute to endogenous brain defenses after acute neonatal focal stroke. J Neurosci 31:12992–13001, 2011. DOI: 10.1523/JNEUROSCI.2102-11.2011. [PubMed: 21900578]

138. Ferguson RK, Woodbury DM. Penetration of 14C-inulin and 14C-sucrose into brain, cerebrospinal fluid, and skeletal muscle of developing rats. Exp Brain Res 7: 181–194, 1969. [PubMed: 5795246]

139. Fernandez-Lopez D, Faustino J, Klibanov AL, Derugin N, Blanchard E, Simon F, Leib SL, Vexler ZS. Microglial cells prevent hemorrhage in neonatal focal arterial stroke. J Neurosci 36: 2881–2893, 2016. DOI: 10.1523/JNEUROSCI.0140-15.2016. [PubMed: 26961944]

140. Figaji AA, Zwane E, Fieggen AG, Argent AC, Le Roux PD, Siesjo P, Peter JC. Pressure autoregulation, intracranial pressure, and brain tissue oxygenation in children with severe traumatic brain injury. J Neurosurg Pediatr 4: 420–428, 2009. DOI: 10.3171/2009.6.PEDS096. [PubMed: 19877773]

141. Filosa JA, Bonev AD, Straub SV, Meredith AL, Wilkerson MK, Aldrich RW, Nelson MT. Local potassium signaling couples neuronal activity to vasodilation in the brain. Nat Neurosci 9: 1397–1403, 2006. [PubMed: 17013381]

142. Fiumana E, Parfenova H, Jagger JH, Leffler CW. Carbon monoxide mediates vasodilator effects of glutamate in isolated pressurized cerebral arterioles of newborn pigs. Am J Physiol Heart Circ Physiol 284: H1073–H1079, 2003. [PubMed: 12666665]

143. Franceschini MA, Thaker S, Themelis G, Krishnamoorthy KK, Bortfeld H, Diamond SG, Boas DA, Arvin K, Grant PE. Assessment of infant brain development with frequency-domain near-infrared spectroscopy. Pediatr Res 61: 546–551, 2007. DOI: 10.1203/pdr.0b013e318045be99. [PubMed: 17413855]

144. Fraser CD 3rd, Brady KM, Rhee CJ, Easley RB, Kibler K, Smielewski P, Czosnyka M, Kaczka DW, Andropoulos DB, Rusin C. The frequency response of cerebral autoregulation. J Appl Physiol 115: 52–56, 2013. DOI: 10.1152/japplphysiol.00068.2013. [PubMed: 23681909]

145. Freeman SS, Udomphorn Y, Armstead WM, Fisk DM, Vavilala MS. Young age as a risk factor for impaired cerebral autoregulation after moderate to severe pediatric traumatic brain injury. Anesthesiology 108: 588–595, 2008. DOI: 10.1097/ALN.0b013e31816725d7. [PubMed: 18362589]

146. Fujimoto K. 'Medial defects' in the prenatal human cerebral arteries: an electron microscopic study. Stroke 27: 706–708, 1996. [PubMed: 8614935]

147. Furuta A, Martin LJ. Laminar segregation of the cortical plate during corticogenesis is accompanied by changes in glutamate receptor expression. J Neurobiol 39: 67–80, 1999. [PubMed: 10213454]

148. Galea E, Reis DJ, Xu H, Feinstein DL. Transient expression of calcium-independent nitric oxide synthase in blood vessels during brain development. FASEB J 9: 1632–1637, 1995. [PubMed: 8529843]

149. Garfunkel JM, Baird HW 3rd, Ziegler J. The relationship of oxygen consumption of cerebral functional activity. J Pediatr 44: 64–72, 1954. [PubMed: 13131199]

150. Geary GG, Buchholz JN, Pearce WJ. Maturation depresses mouse cerebrovascular tone through endothelium-dependent mechanisms. Am J Physiol Regul Integr Comp Physiol 284: R734–R741, 2003. DOI: 10.1152/ajpregu.00510.2002. [PubMed: 12468443]

151. Gebremedhin D, Bonnet P, Greene AS, England SK, Rusch NJ, Lombard JH, Harder DR. Hypoxia increases the activity of $Ca^{2+}$-sensitive $K^+$ channels in cat cerebral arterial muscle cell membranes. Pflugers Arch 428: 621–630, 1994. [PubMed: 7838685]
152. Gebremedhin D, Lange AR, Lowry TF, Taheri MR, Birks EK, Hudetz AG, Narayanan J, Falck JR, Okamoto H, Roman RJ, Nithipatikom K, Campbell WB, Harder DR. Production of 20-HETE and its role in autoregulation of cerebral blood flow. Circ Res 87: 60–65, 2000. [PubMed: 10884373]
153. Gebremedhin D, Ma YH, Falck JR, Roman RJ, VanRollins M, Harder DR. Mechanism of action of cerebral epoxyeicosatrienoic acids on cerebral arterial smooth muscle. Am J Physiol Heart Circ Physiol 263: H519–H525, 1992.
154. Gebremedhin D, Yamaura K, Zhang C, Bylund J, Koehler RC, Harder DR. Metabotropic glutamate receptor activation enhances the activities of two types of $Ca^{2+}$ -activated $K^+$ channels in rat hippocampal astrocytes. J Neurosci 23: 1678–1687, 2003. [PubMed: 12629172]
155. Gebremedhin D, Zhang DX, Carver KA, Rau N, Rarick KR, Roman RJ, Harder DR. Expression of CYP 4A omega-hydroxylase and formation of 20-hydroxyeicosatetreanoic acid (20-HETE) in cultured rat brain astrocytes. Prostaglandins Other Lipid Mediat 124: 16–26, 2016. DOI: 10.1016/j.prostaglandins.2016.04.003. [PubMed: 27174801]
156. Gennatas ED, Avants BB, Wolf DH, Satterthwaite TD, Ruparel K, Ciric R, Hakonarson H, Gur RE, Gur RC. Age-related effects and sex differences in gray matter density, volume, mass, and cortical thickness from childhood to young adulthood. J Neurosci 37: 5065–5073, 2017. DOI: 10.1523/JNEUROSCI.3550-16.2017. [PubMed: 28432144]
157. Gerrits RJ, Stein EA, Greene AS. Anesthesia alters NO-mediated functional hyperemia. Brain Res 907: 20–26, 2001. [PubMed: 11430881]
158. Gilmore MM, Stone BS, Shepard JA, Czosnyka M, Easley RB, Brady KM. Relationship between cerebrovascular dysautoregulation and arterial blood pressure in the premature infant. J Perinatol 31: 722–729, 2011. [PubMed: 21372795]
159. Girouard H, Bonev AD, Hannah RM, Meredith A, Aldrich RW, Nelson MT. Astrocytic endfoot $Ca^{2+}$ and BK channels determine both arteriolar dilation and constriction. Proc Natl Acad Sci U S A 107: 3811–3816, 2010. [PubMed: 20133576]
160. Gleason CA, Hamm C, Jones MD Jr. Cerebral blood flow, oxygenation, and carbohydrate metabolism in immature fetal sheep in utero. Am J Physiol Regul Integr Comp Physiol 256: R1264–R1268, 1989.
161. Gleason CA, Hamm C, Jones MD Jr. Effect of acute hypoxemia on brain blood flow and oxygen metabolism in immature fetal sheep. Am J Physiol Heart Circ Physiol 258: H1064–H1069, 1990.
162. Gleason CA, Jones MD Jr, Traystman RJ, Notter RH. Fetal cerebral responses to ventilation and oxygenation in utero. Am J Physiol Regul Integr Comp Physiol 255: R1049–R1054, 1988.
163. Gollasch M, Wellman GC, Knot HJ, Jaggar JH, Damon DH, Bonev AD, Nelson MT. Ontogeny of local sarcoplasmic reticulum $Ca^{2+}$ signals in cerebral arteries: $Ca^{2+}$ sparks as elementary physiological events. Circ Res 83: 1104–1114, 1998. [PubMed: 9831705]
164. Goplerud JM, Wagerle LC, Delivoria-Papadopoulos M. Sympathetic nerve modulation of regional cerebral blood flow during asphyxia in newborn piglets. Am J Physiol Heart Circ Physiol 260: H1575–H1580, 1991. DOI: 10.1152/ajpheart.1991.260.5.H1575.
165. Gotoh J, Kuang TY, Nakao Y, Cohen DM, Melzer P, Itoh Y, Pak H, Pettigrew K, Sokoloff L. Regional differences in mechanisms of cerebral circulatory response to neuronal activation. Am J Physiol Heart Circ Physiol 280: H821–H829, 2001. [PubMed: 11158982]
166. Gregoire NM, Gjedde A, Plum F, Duffy TE. Cerebral blood flow and cerebral metabolic rates for oxygen, glucose, and ketone bodies in new-born dogs. J Neurochem 30: 63–69, 1978. [PubMed: 340616]
167. Guiza F, Meyfroidt G, Lo TY, Jones PA, Van den Berghe G, Depreitere B. Continuous optimal CPP based on minute-by-minute monitoring data: A study of a pediatric population. Acta Neurochir Suppl 122: 187–191, 2016. DOI: 10.1007/978-3-319-22533-3_38. [PubMed: 27165904]
168. Haggendal E, Lofgren J, Nilsson NJ, Zwetnow NN. Effects of varied cerebrospinal fluid pressure on cerebral blood flow in dogs. Acta Physiol Scand 79: 262–271, 1970. [PubMed: 4916937]

169. Hall CN, Reynell C, Gesslein B, Hamilton NB, Mishra A, Sutherland BA, O'Farrell FM, Buchan AM, Lauritzen M, Attwell D. Capillary pericytes regulate cerebral blood flow in health and disease. Nature 508: 55–60, 2014. DOI: 10.1038/nature13165. [PubMed: 24670647]

170. Hansen NB, Brubakk AM, Bratlid D, Oh W, Stonestreet BS. The effects of variations in $PaCO_2$ on brain blood flow and cardiac output in the newborn piglet. Pediatr Res 18: 1132–1136, 1984. DOI: 10.1203/00006450-198411000-00015. [PubMed: 6440112]

171. Hansen NB, Nowicki PT, Miller RR, Malone T, Bickers RG, Menke JA. Alterations in cerebral blood flow and oxygen consumption during prolonged hypocarbia. Pediatr Res 20: 147–150, 1986. DOI: 10.1203/00006450-198602000-00010. [PubMed: 3080728]

172. Harder DR, Abel PW, Hermsmeyer K. Membrane electrical mechanism of basilar artery constriction and pial artery dilation by norepinephrine. Circ Res 49: 1237–1242, 1981. [PubMed: 7307242]

173. Harder DR, Gebremedhin D, Narayanan J, Jefcoat C, Falck JR, Campbell WB, Roman R. Formation and action of a p-450 4A metabolite of arachidonic acid in cat cerebral microvessels. Am J Physiol Heart Circ Physiol 266: H2098–H2107, 1994.

174. Harder DR, Rarick KR, Gebremedhin D, Cohen SS. Regulation of cerebral blood flow: Response to cytochrome P450 lipid metabolites. Compr Physiol 8: 801–821, 2018. DOI: 10.1002/c170025. [PubMed: 29687906]

175. Harris AP, Helou S, Gleason CA, Traystman RJ, Koehler RC. Fetal cerebral and peripheral circulatory responses to hypoxia after nitric oxide synthase inhibition. Am J Physiol Regul Integr Comp Physiol 281: R381–R390, 2001. [PubMed: 11448839]

176. Harris AP, Koehler RC, Gleason CA, Jones MD Jr, Traystman RJ. Cerebral and peripheral circulatory responses to intracranial hypertension in fetal sheep. Circ Res 64: 991–1000, 1989. [PubMed: 2706763]

177. Harris AP, Ohata H, Koehler RC. Role of nitric oxide in cerebrovascular reactivity to NMDA and hypercapnia during prenatal development in sheep. Int J Dev Neurosci 26: 47–55, 2008. [PubMed: 17935926]

178. Harris AP, Robinson R, Koehler RC, Traystman RJ, Gleason CA. Blood-brain barrier permeability during dopamine-induced hypertension in fetal sheep. J Appl Physiol 91: 123–129, 2001. [PubMed: 11408422]

179. Harris JJ, Jolivet R, Attwell D. Synaptic energy use and supply. Neuron 75: 762–777, 2012. DOI: 10.1016/j.neuron.2012.08.019. [PubMed: 22958818]

180. Hayashi S, Park MK, Kuehl TJ. Higher sensitivity of cerebral arteries isolated from premature and newborn baboons to adrenergic and cholinergic stimulation. Life Sci 35: 253–260, 1984. [PubMed: 6748852]

181. Hayashi S, Park MK, Kuehl TJ. Relaxant and contractile responses to prostaglandins in premature, newborn and adult baboon cerebral arteries. J Pharmacol Exp Ther 233: 628–635, 1985. [PubMed: 4009485]

182. Hekierski H, Pastor P, Curvello V, Armstead WM. Inhaled nitric oxide protects cerebral autoregulation and reduces hippocampal neuronal cell necrosis after traumatic brain injury in newborn and juvenile pigs. J Neurotrauma 36: 630–638, 2019. DOI: 10.1089/neu.2018.5824. [PubMed: 30051755]

183. Helou SM, Hudak ML, Jones MD Jr. Cerebral blood flow response to hypercapnia in immature fetal sheep. Am J Physiol Heart Circ Physiol 261: H1366–H1370, 1991.

184. Helou SM, Koehler RC, Gleason CA, Jones MD Jr, Traystman RJ. Cerebrovascular autoregulation during fetal development in sheep. Am J Physiol Heart Circ Physiol 266: H1069–H1074, 1994.

185. Hernandez MJ, Brennan RW, Bowman GS. Autoregulation of cerebral blood flow in the newborn dog. Brain Res 184: 199–202, 1980. [PubMed: 7357418]

186. Hernandez MJ, Brennan RW, Vannucci RC, Bowman GS. Cerebral blood flow and oxygen consumption in the newborn dog. Am J Physiol Regul Integr Comp Physiol 234: R209–R215, 1978.

187. Hernandez MJ, Vannucci RC, Salcedo A, Brennan RW. Cerebral blood flow and metabolism during hypoglycemia in newborn dogs. J Neurochem 35: 622–628, 1980. [PubMed: 7452278]

188. Higashimori H, Blanco VM, Tuniki VR, Falck JR, Filosa JA. Role of epoxyeicosatrienoic acids as autocrine metabolites in glutamate-mediated $K^+$ signaling in perivascular astrocytes. Am J Physiol Cell Physiol 299: C1068–C1078, 2010. [PubMed: 20844244]

189. Hill RA, Tong L, Yuan P, Murikinati S, Gupta S, Grutzendler J. Regional blood flow in the normal and ischemic brain is controlled by arteriolar smooth muscle cell contractility and not by capillary pericytes. Neuron 87: 95–110, 2015. DOI: 10.1016/j.neuron.2015.06.001. [PubMed: 26119027]

190. Himwich HE, Fazekas JF. Comparative studies of the metabolism of the brain of infant and adult dogs. Am J Phys 132: 454–459, 1941.

191. Hohimer AR, Bissonnette JM. Effects of cephalic hypotension, hypertension, and barbiturates on fetal cerebral flood flow and metabolism. Am J Obstet Gynecol 161: 1344–1351, 1989. [PubMed: 2589461]

192. Hoiland RL, Bain AR, Rieger MG, Bailey DM, Ainslie PN. Hypoxemia, oxygen content, and the regulation of cerebral blood flow. Am J Physiol Regul Integr Comp Physiol 310: R398–R413, 2016. DOI: 10.1152/ajpregu.00270.2015. [PubMed: 26676248]

193. Hoiland RL, Caldwell HG, Howe CA, Nowak-Fluck D, Stacey BS, Bailey DM, Paton JFR, Green DJ, Sekhon MS, Macleod DB, Ainslie PN. Nitric oxide is fundamental to neurovascular coupling in humans. J Physiol 598: 4927–4939, 2020. DOI: 10.1113/JP280162. [PubMed: 32785972]

194. Hoiland RL, Fisher JA, Ainslie PN. Regulation of the cerebral circulation by arterial carbon dioxide. Compr Physiol 9: 1101–1154, 2019. DOI: 10.1002/c180021. [PubMed: 31187899]

195. Holt DC, Fedinec AL, Vaughn AN, Leffler CW. Age and species dependence of pial arteriolar responses to topical carbon monoxide in vivo. Exp Biol Med (Maywood) 232: 1465–1469, 2007. [PubMed: 18040071]

196. Hovda DA, Chugani HT, Villablanca JR, Badie B, Sutton RL. Maturation of cerebral oxidative metabolism in the cat: A cytochrome oxidase histochemistry study. J Cereb Blood Flow Metab 12: 1039–1048, 1992. DOI: 10.1038/jcbfm.1992.141. [PubMed: 1328263]

197. Hovda DA, Villablanca JR, Chugani HT, Barrio JR. Metabolic maturation of the brain: A study of local cerebral protein synthesis in the developing cat. Brain Res 1113: 54–63, 2006. DOI: 10.1016/j.brainres.2006.07.083. [PubMed: 16934237]

198. Howarth C, Gleeson P, Attwell D. Updated energy budgets for neural computation in the neocortex and cerebellum. J Cereb Blood Flow Metab 32: 1222–1232, 2012. DOI: 10.1038/jcbfm.2012.35. [PubMed: 22434069]

199. Hsu P, Albuquerque ML, Leffler CW. Mechanisms of hypercapnia-stimulated PG production in piglet cerebral microvascular endothelial cells. Am J Physiol Heart Circ Physiol 268: H591–H603, 1995. DOI: 10.1152/ajpheart.1995.268.2.H591.

200. Hsu P, Shibata M, Leffler CW. Prostanoid synthesis in response to high $CO_2$ in newborn pig brain microvascular endothelial cells. Am J Physiol Heart Circ Physiol 264: H1485–H1492, 1993. DOI: 10.1152/ajpheart.1993.264.5.H1485.

201. Hudak ML, Koehler RC, Rosenberg AA, Traystman RJ, Jones MD Jr. Effect of hematocrit on cerebral blood flow. Am J Physiol Heart Circ Physiol 251: H63–H70, 1986.

202. Hudak ML, Tang YL, Massik J, Koehler RC, Traystman RJ, Jones MD Jr. Base-line $O_2$ extraction influences cerebral blood flow response to hematocrit. Am J Physiol Heart Circ Physiol 254: H156–H162, 1988.

203. Hunter CJ, Blood AB, White CR, Pearce WJ, Power GG. Role of nitric oxide in hypoxic cerebral vasodilatation in the ovine fetus. J Physiol 549: 625–633, 2003. DOI: 10.1113/jphysiol.2002.038034. [PubMed: 12665609]

204. Ioroi T, Yonetani M, Nakamura H. Effects of hypoxia and reoxygenation on nitric oxide production and cerebral blood flow in developing rat striatum. Pediatr Res 43: 733–737, 1998. [PubMed: 9621981]

205. Ishikawa M, Kajimura M, Adachi T, Maruyama K, Makino N, Goda N, Yamaguchi T, Sekizuka E, Suematsu M. Carbon monoxide from heme oxygenase-2 is a tonic regulator against NO-dependent vasodilatation in the adult rat cerebral microcirculation. Circ Res 97: e104–e114, 2005. DOI: 10.1161/01.RES.0000196681.34485.ec. [PubMed: 16293786]

206. Iwamoto HS, Kaufman T, Keil LC, Rudolph AM. Responses to acute hypoxemia in fetal sheep at 0.6-0.7 gestation. Am J Physiol Heart Circ Physiol 256: H613–H620, 1989.

207. Jacobs B, Chugani HT, Allada V, Chen S, Phelps ME, Pollack DB, Raleigh MJ. Developmental changes in brain metabolism in sedated rhesus macaques and vervet monkeys revealed by positron emission tomography. Cereb Cortex 5: 222–233, 1995. [PubMed: 7613078]

208. Jaggar JH, Leffler CW, Cheranov SY, Tcheranova D, Shuyu E, Cheng X. Carbon monoxide dilates cerebral arterioles by enhancing the coupling of $Ca^{2+}$ sparks to $Ca^{2+}$-activated $K^+$ channels. Circ Res 91: 610–617, 2002. [PubMed: 12364389]

209. Jaggar JH, Li A, Parfenova H, Liu J, Umstot ES, Dopico AM, Leffler CW. Heme is a carbon monoxide receptor for large-conductance $Ca^{2+}$-activated $K^+$ channels. Circ Res 97: 805–812, 2005. [PubMed: 16166559]

210. Jones M Jr, Sheldon RE, Peeters LL, Meschia G, Battaglia FC, Makowski EL. Fetal cerebral oxygen consumption at different levels of oxygenation. J Appl Physiol 43: 1080–1084, 1977. DOI: 10.1152/jappl.1977.43.6.1080. [PubMed: 606693]

211. Jones MD Jr, Sheldon RE, Peeters LL, Makowski EL, Meschia G. Regulation of cerebral blood flow in the ovine fetus. Am J Physiol Heart Circ Physiol 235: H162–H166, 1978.

212. Jones MD Jr, Traystman RJ, Simmons MA, Molteni RA. Effects of changes in arterial $O_2$ content on cerebral blood flow in the lamb. Am J Physiol Heart Circ Physiol 240: H209–H215, 1981.

213. Joshi B, Ono M, Brown C, Brady K, Easley RB, Yenokyan G, Gottesman RF, Hogue CW. Predicting the limits of cerebral autoregulation during cardiopulmonary bypass. Anesth Analg 114: 503–510, 2012. DOI: 10.1213/ANE.0b013e31823d292a. [PubMed: 22104067]

214. Kanu A, Leffler CW. Carbon monoxide and $Ca^{2+}$-activated $K^+$ channels in cerebral arteriolar responses to glutamate and hypoxia in newborn pigs. Am J Physiol Heart Circ Physiol 293: H3193–H3200, 2007. [PubMed: 17766483]

215. Kanu A, Leffler CW. Roles of glia limitans astrocytes and carbon monoxide in adenosine diphosphate-induced pial arteriolar dilation in newborn pigs. Stroke 40: 930–935, 2009. [PubMed: 19164779]

216. Kanu A, Leffler CW. Arachidonic acid- and prostaglandin E2-induced cerebral vasodilation is mediated by carbon monoxide, independent of reactive oxygen species in piglets. Am J Physiol Heart Circ Physiol 301: H2482–H2487, 2011. [PubMed: 21984542]

217. Kanu A, Whitfield J, Leffler CW. Carbon monoxide contributes to hypotension-induced cerebrovascular vasodilation in piglets. Am J Physiol Heart Circ Physiol 291: H2409–H2414, 2006. [PubMed: 16751286]

218. Karen T, Morren G, Haensse D, Bauschatz AS, Bucher HU, Wolf M. Hemodynamic response to visual stimulation in newborn infants using functional near-infrared spectroscopy. Hum Brain Mapp 29: 453–460, 2008. DOI: 10.1002/hbm.20411. [PubMed: 17525986]

219. Keep RF, Ennis SR, Beer ME, Betz AL. Developmental changes in blood-brain barrier potassium permeability in the rat: Relation to brain growth. J Physiol 488 (Pt 2): 439–448, 1995. [PubMed: 8568682]

220. Kennedy C, Grave GD, Juhle JW, Sokoloff L. Changes in blood flow in the component structures of the dog brain during postnatal maturation. J Neurochem 19: 2423–2433, 1972. [PubMed: 4676486]

221. Kennedy C, Sokoloff L. An adaptation of the nitrous oxide method to the study of the cerebral circulation in children; normal values for cerebral blood flow and cerebral metabolic rate in childhood. J Clin Invest 36: 1130–1137, 1957. DOI: 10.1172/JCI103509. [PubMed: 13449166]

222. Kety SS, Schmidt CF. The nitrous nxide method for the quantitative determination of cerebral bloodflow in man: Theory, procedure and normal values. J Clin Invest 27:476–483, 1948. DOI: 10.1172/JCI101994. [PubMed: 16695568]

223. Khennouf L, Gesslein B, Brazhe A, Octeau JC, Kutuzov N, Khakh BS, Lauritzen M. Active role of capillary pericytes during stimulation-induced activity and spreading depolarization. Brain 141: 2032–2046, 2018. DOI: 10.1093/brain/awy143. [PubMed: 30053174]

224. Kissack CM, Garr R, Wardle SP, Weindling AM. Cerebral fractional oxygen extraction is inversely correlated with oxygen delivery in the sick, newborn, preterm infant. J Cereb Blood Flow Metab 25: 545–553, 2005. DOI: 10.1038/sj.jcbfm.9600046. [PubMed: 15744253]

225. Knecht KR, Milam S, Wilkinson DA, Fedinec AL, Leffler CW. Time-dependent action of carbon monoxide on the newborn cerebrovascular circulation. Am J Physiol Heart Circ Physiol 299: H70–H75, 2010. [PubMed: 20435844]

226. Kocharyan A, Fernandes P, Tong XK, Vaucher E, Hamel E. Specific subtypes of cortical GABA interneurons contribute to the neurovascular coupling response to basal forebrain stimulation. J Cereb Blood Flow Metab 28: 221–231, 2008. DOI: 10.1038/sj.jcbfm.9600558. [PubMed: 17895909]

227. Koehler RC, Jones MD Jr, Traystman RJ. Cerebral circulatory response to carbon monoxide and hypoxic hypoxia in the lamb. Am J Physiol Heart Circ Physiol 243: H27–H32, 1982.

228. Koehler RC, Traystman RJ, Jones MD Jr. Influence of reduced oxygemoglobin affinity on cerebrovascular response to hypoxic hypoxia. Am J Physiol Heart Circ Physiol 251: H756–H763, 1986.

229. Koehler RC, Traystman RJ, Rosenberg AA, Hudak ML, Jones MD Jr. Role of $O_2$-hemoglobin affinity on cerebrovascular response to carbon monoxide hypoxia. Am J Physiol Heart Circ Physiol 245: H1019–H1023, 1983.

230. Koehler RC, Traystman RJ, Zeger S, Rogers MC, Jones MD Jr. Comparison of cerebrovascular response to hypoxic and carbon monoxide hypoxia in newborn and adult sheep. J Cereb Blood Flow Metab 4: 115–122, 1984. [PubMed: 6420426]

231. Koneru P, Leffler CW. Role of cGMP in carbon monoxide-induced cerebral vasodilation in piglets. Am J Physiol Heart Circ Physiol 286: H304–H309, 2004. [PubMed: 14684363]

232. Kontos HA, Wei EP, Navari RM, Levasseur JE, Rosenblum WI, Patterson JL Jr. Responses of cerebral arteries and arterioles to acute hypotension and hypertension. Am J Physiol Heart Circ Physiol 234: H371–H383, 1978.

233. Kosty J, Riley J, Liang J, Armstead WM. Influence of sex and ERK MAPK on the pressure reactivity index in newborn piglets after fluid percussion injury. Transl Stroke Res 3: 460–465, 2012. DOI: 10.1007/s12975-012-0196-3. [PubMed: 23525515]

234. Kozberg M, Hillman E. Neurovascular coupling and energy metabolism in the developing brain. Prog Brain Res 225: 213–242, 2016. DOI: 10.1016/bs.pbr.2016.02.002. [PubMed: 27130418]

235. Kozberg MG, Chen BR, DeLeo SE, Bouchard MB, Hillman EM. Resolving the transition from negative to positive blood oxygen level-dependent responses in the developing brain. Proc Natl Acad Sci USA 110: 4380–4385, 2013. DOI: 10.1073/pnas.1212785110. [PubMed: 23426630]

236. Kozberg MG, Ma Y, Shaik MA, Kim SH, Hillman EM. Rapid postnatal expansion of neural networks occurs in an environment of altered neurovascular and neurometabolic coupling. J Neurosci 36: 6704–6717, 2016. DOI: 10.1523/JNEUROSCI.2363-15.2016. [PubMed: 27335402]

237. Kratzer I, Chip S, Vexler ZS. Barrier mechanisms in neonatal stroke. Front Neurosci 8: 359, 2014. DOI: 10.3389/fnins.2014.00359. [PubMed: 25426016]

238. Kurth CD, Wagerle LC. Cerebrovascular reactivity to adenosine analogues in 0.6-0.7 gestation and near-term fetal sheep. Am J Physiol Heart Circ Physiol 262: H1338–H1342, 1992.

239. Kurth CD, Wagerle LC, Delivoria-Papadopoulos M. Sympathetic regulation of cerebral blood flow during seizures in newborn lambs. Am J Physiol Heart Circ Physiol 255: H563–H568, 1988. DOI: 10.1152/ajpheart.1988.255.3.H563.

240. Kusaka T, Kawada K, Okubo K, Nagano K, Namba M, Okada H, Imai T, Isobe K, Itoh S. Noninvasive optical imaging in the visual cortex in young infants. Hum Brain Mapp 22: 122–132, 2004. DOI: 10.1002/hbm.20020. [PubMed: 15108300]

241. Kuzawa CW, Chugani HT, Grossman LI, Lipovich L, Muzik O, Hof PR, Wildman DE, Sherwood CC, Leonard WR, Lange N. Metabolic costs and evolutionary implications of human brain development. Proc Natl Acad Sci U S A 111: 13010–13015, 2014. DOI: 10.1073/pnas.1323099111. [PubMed: 25157149]

242. Lacoste B, Comin CH, Ben-Zvi A, Kaeser PS, Xu X, Costa Lda F, Gu C. Sensory-related neural activity regulates the structure of vascular networks in the cerebral cortex. Neuron 83: 1117–1130, 2014. DOI: 10.1016/j.neuron.2014.07.034. [PubMed: 25155955]

243. Lacroix A, Toussay X, Anenberg E, Lecrux C, Ferreiros N, Karagiannis A, Plaisier F, Chausson P, Jarlier F, Burgess SA, Hillman EM, Tegeder I, Murphy TH, Hamel E, Cauli B. COX-2-derived prostaglandin E2 produced by pyramidal neurons contributes to neurovascular

coupling in the rodent cerebral cortex. J Neurosci 35: 11791–11810, 2015. DOI: 10.1523/JNEUROSCI.0651-15.2015. [PubMed: 26311764]

244. Laptook AR, Stonestreet BS, Oh W. Brain blood flow and $O_2$ delivery during hemorrhagic hypotension in the piglet. Pediatr Res 17: 77–80, 1983. [PubMed: 6835718]
245. Larson AC, Jamrogowicz JL, Kulikowicz E, Wang B, Yang ZJ, Shaffner DH, Koehler RC, Lee JK. Cerebrovascular autoregulation after rewarming from hypothermia in a neonatal swine model of asphyxic brain injury. J Appl Physiol 115: 1433–1442, 2013. DOI: 10.1152/japplphysiol.00238.2013. [PubMed: 24009008]
246. Laudignon N, Farri E, Beharry K, Rex J, Aranda JV. Influence of adenosine on cerebral blood flow during hypoxic hypoxia in the newborn piglet. J Appl Physiol 68: 1534–1541, 1990. [PubMed: 2347792]
247. Lecrux C, Toussay X, Kocharyan A, Fernandes P, Neupane S, Levesque M, Plaisier F, Shmuel A, Cauli B, Hamel E. Pyramidal neurons are “neurogenic hubs” in the neurovascular coupling response to whisker stimulation. J Neurosci 31: 9836–9847, 2011. [PubMed: 21734275]
248. Lee JK, Brady KM, Chung SE, Jennings JM, Whitaker EE, Aganga D, Easley RB, Heitmiller K, Jamrogowicz JL, Larson AC, Lee JH, Jordan LC, Hogue CW, Lehmann CU, Bembea Mm, Hunt EA, Koehler RC, Shaffner DH. A pilot study of cerebrovascular reactivity autoregulation after pediatric cardiac arrest. Resuscitation 85: 1387–1393, 2014. DOI: 10.1016/j.resuscitation.2014.07.006. [PubMed: 25046743]
249. Lee JK, Brady KM, Mytar JO, Kibler KK, Carter EL, Hirsch KG, Hogue CW, Easley RB, Jordan LC, Smielewski P, Czosnyka M, Shaffner DH, Koehler RC. Cerebral blood flow and cerebrovascular autoregulation in a swine model of pediatric cardiac arrest and hypothermia. Crit Care Med 39: 2337–2345, 2011. [PubMed: 21705904]
250. Lee JK, Kibler KK, Benni PB, Easley RB, Czosnyka M, Smielewski P, Koehler RC, Shaffner DH, Brady KM. Cerebrovascular reactivity measured by near-infrared spectroscopy. Stroke 40: 1820–1826, 2009. [PubMed: 19286593]
251. Lee JK, Poretti A, Perin J, Huisman T, Parkinson C, Chavez-Valdez R, O’Connor M, Reyes M, Armstrong J, Jennings JM, Gilmore MM, Koehler RC, Northington FJ, Tekes A. Optimizing cerebral autoregulation may decrease neonatal regional hypoxic-ischemic brain injury. Dev Neurosci 39: 248–256, 2017. DOI: 10.1159/000452833. [PubMed: 27978510]
252. Lee JK, Yang ZJ, Wang B, Larson AC, Jamrogowicz JL, Kulikowicz E, Kibler KK, Mytar JO, Carter EL, Burman HT, Brady KM, Smielewski P, Czosnyka M, Koehler RC, Shaffner DH. Noninvasive autoregulation monitoring in a swine model of pediatric cardiac arrest. Anesth Analg 114: 825–836, 2012. [PubMed: 22314692]
253. Lee TJ, Kinkead LR, Sarwinski S. Norepinephrine and acetylcholine transmitter mechanisms in large cerebral arteries of the pig. J Cereb Blood Flow Metab 2: 439–450, 1982. DOI: 10.1038/jcbfm.1982.50. [PubMed: 7142308]
254. Leffler CW, Balabanova L, Fedinec AL, Parfenova H. Nitric oxide increases carbon monoxide production by piglet cerebral microvessels. Am J Physiol Heart Circ Physiol 289: H1442–H1447, 2005. [PubMed: 15964921]
255. Leffler CW, Balabanova L, Fedinec AL, Waters CM, Parfenova H. Mechanism of glutamate stimulation of CO production in cerebral microvessels. Am J Physiol Heart Circ Physiol 285: H74–H80, 2003. [PubMed: 12623781]
256. Leffler CW, Balabanova L, Sullivan D, Wang X, Fedinec AL, Parfenova H. Regulation of CO production in cerebral microvessels of newborn pigs. Am J Physiol Heart Circ Physiol 285: H292–H297, 2003. [PubMed: 12623784]
257. Leffler CW, Balabanova L, Williams KK. cAMP production by piglet cerebral vascular smooth muscle cells: pH(o), pH(i), and permissive action of PGI(2). Am J Physiol Heart Circ Physiol 277: H1878–H1883, 1999.
258. Leffler CW, Beasley DG, Busija DW. Cerebral ischemia alters cerebral microvascular reactivity in newborn pigs. Am J Physiol Heart Circ Physiol 257: H266–H271, 1989.
259. Leffler CW, Busija DW. Prostanoids and pial arteriolar diameter in hypotensive newborn pigs. Am J Physiol Heart Circ Physiol 252: H687–H691, 1987.

260. Leffler CW, Busija DW, Armstead WM, Mirro R, Beasley DG. Ischemia alters cerebral vascular responses to hypercapnia and acetylcholine in piglets. Pediatr Res 25: 180–183, 1989. [PubMed: 2919133]

261. Leffler CW, Busija DW, Beasley DG, Armstead WM, Mirro R. Postischemic cerebral microvascular responses to norepinephrine and hypotension in newborn pigs. Stroke 20: 541–546, 1989. [PubMed: 2929031]

262. Leffler CW, Busija DW, Beasley DG, Fletcher AM. Maintenance of cerebral circulation during hemorrhagic hypotension in newborn pigs: Role of prostanoids. Circ Res 59: 562–567, 1986. [PubMed: 3542278]

263. Leffler CW, Busija DW, Mirro R, Armstead WM, Beasley DG. Effects of ischemia on brain blood flow and oxygen consumption of newborn pigs. Am J Physiol Heart Circ Physiol 257: H1917–H1926, 1989.

264. Leffler CW, Fedinec AL. Newborn piglet cerebral microvascular responses to epoxyeicosatrienoic acids. Am J Physiol Heart Circ Physiol 273: H333–H338, 1997. DOI: 10.1152/ajpheart.1997.273.1.H333.

265. Leffler CW, Fedinec AL, Shibata M. Prostacyclin receptor activation and pial arteriolar dilation after endothelial injury in piglets. Stroke 26: 2103–2110; discussion 2110-2111, 1995. [PubMed: 7482658]

266. Leffler CW, Mirro R, Armstead WM, Busija DW, Thelin O. Prostanoid synthesis and vascular responses to exogenous arachidonic acid following cerebral ischemia in piglets. Prostaglandins 40: 241–248, 1990. [PubMed: 2123354]

267. Leffler CW, Mirro R, Armstead WM, Shibata M. Topical arachidonic acid restores pial arteriolar dilation to hypercapnia of postischemic newborn pig brain. Am J Physiol Heart Circ Physiol 263: H746–H751, 1992.

268. Leffler CW, Mirro R, Pharris LJ, Shibata M. Permissive role of prostacyclin in cerebral vasodilation to hypercapnia in newborn pigs. Am J Physiol Heart Circ Physiol 267: H285–H291, 1994.

269. Leffler CW, Mirro R, Shanklin DR, Armstead WM, Shibata M. Light/dye microvascular injury selectively eliminates hypercapnia-induced pial arteriolar dilation in newborn pigs. Am J Physiol Heart Circ Physiol 266: H623–H630, 1994. DOI: 10.1152/ajpheart.1994.266.2.H623.

270. Leffler CW, Mirro R, Shibata M, Parfenova H, Armstead WM, Zuckerman S. Effects of indomethacin on cerebral vasodilator responses to arachidonic acid and hypercapniain newborn pigs. Pediatr Res 33:609–614, 1993. DOI: 10.1203/00006450-199306000-00016. [PubMed: 8378120]

271. Leffler CW, Nasjletti A, Johnson RA, Fedinec AL. Contributions of prostacyclin and nitric oxide to carbon monoxide-induced cerebrovascular dilation in piglets. Am J Physiol Heart Circ Physiol 280: H1490–H1495, 2001. [PubMed: 11247758]

272. Leffler CW, Nasjletti A, Yu C, Johnson RA, Fedinec AL, Walker N. Carbon monoxide and cerebral microvascular tone in newborn pigs. Am J Physiol Heart Circ Physiol 276: H1641–H1646, 1999.

273. Leffler CW, Parfenova H. Cerebral arteriolar dilation to hypoxia: Role of prostanoids. Am J Physiol Heart Circ Physiol 272: H418–H424, 1997. DOI: 10.1152/ajpheart.1997.272.1.H418.

274. Leffler CW, Parfenova H, Basuroy S, Jaggar JH, Umstot ES, Fedinec AL. Hydrogen sulfide and cerebral microvascular tone in newborn pigs. Am J Physiol Heart Circ Physiol 300: H440–H447, 2011. [PubMed: 21131483]

275. Leffler CW, Parfenova H, Fedinec AL, Basuroy S, Tcheranova D. Contributions of astrocytes and CO to pial arteriolar dilation to glutamate in newborn pigs. Am J Physiol Heart Circ Physiol 291: H2897–H2904, 2006. [PubMed: 16891404]

276. Leffler CW, Parfenova H, Jaggar JH. Carbon monoxide as an endogenous vascular modulator. Am J Physiol Heart Circ Physiol 301: H1–H11, 2011. [PubMed: 21498777]

277. Leffler CW, Smith JS, Edrington JL, Zuckerman SL, Parfenova H. Mechanisms of hypoxia-induced cerebrovascular dilation in the newborn pig. Am J Physiol Heart Circ Physiol 272: H1323–H1332, 1997. DOI: 10.1152/ajpheart.1997.272.3.H1323.

278. Lewis PM, Czosnyka M, Carter BG, Rosenfeld JV, Paul E, Singhal N, Butt W. Cerebrovascular pressure reactivity in children with traumatic brain injury. Pediatr Crit Care Med 16: 739–749, 2015. DOI: 10.1097/PCC.0000000000000471. [PubMed: 26132743]

279. Li A, Adebiyi A, Leffler CW, Jaggar JH. $K_{Ca}$ channel insensitivity to $Ca^{2+}$ sparks underlies fractional uncoupling in newborn cerebral artery smooth muscle cells. Am J Physiol Heart Circ Physiol 291: H1118–H1125, 2006. [PubMed: 16603686]

280. Li A, Xi Q, Umstot ES, Bellner L, Schwartzman ML, Jaggar JH, Leffler CW. Astrocyte-derived CO is a diffusible messenger that mediates glutamate-induced cerebral arteriolar dilation by activating smooth muscle cell $K_{Ca}$ channels. Circ Res 102: 234–241, 2008. [PubMed: 17991880]

281. Liang GH, Adebiyi A, Leo MD, McNally EM, Leffler CW, Jaggar JH. Hydrogen sulfide dilates cerebral arterioles by activating smooth muscle cell plasma membrane KATP channels. Am J Physiol Heart Circ Physiol 300: H2088–H2095, 2011. [PubMed: 21421823]

282. Liang GH, Xi Q, Leffler CW, Jaggar JH. Hydrogen sulfide activates Ca(2)(+) sparks to induce cerebral arteriole dilatation. J Physiol 590: 2709–2720, 2012. [PubMed: 22508960]

283. Liao SM, Gregg NM, White BR, Zeff BW, Bjerkaas KA, Inder TE, Culver JP. Neonatal hemodynamic response to visual cortex activity: High-density near-infrared spectroscopy study. J Biomed Opt 15: 026010, 2010. DOI: 10.1117/1.3369809. [PubMed: 20459255]

284. Lin MT, Hessinger DA, Pearce WJ, Longo LD. Developmental differences in $Ca^{2+}$-activated $K^+$ channel activity in ovine basilar artery. Am J Physiol Heart Circ Physiol 285: H701–H709, 2003. DOI: 10.1152/ajpheart.00138.2003. [PubMed: 12689856]

285. Lin MT, Longo LD, Pearce WJ, Hessinger DA. $Ca^{2+}$-activated $K^+$ channel-associated phosphatase and kinase activities during development. Am J Physiol Heart Circ Physiol 289: H414–H425, 2005. DOI: 10.1152/ajpheart.01079.2004. [PubMed: 15708961]

286. Lin PY, Roche-Labarbe N, Dehaes M, Fenoglio A, Grant PE, Franceschini MA. Regional and hemispheric asymmetries of cerebral hemodynamic and oxygen metabolism in newborns. Cereb Cortex 23: 339–348, 2013. DOI: 10.1093/cercor/bhs023. [PubMed: 22328446]

287. Lind BL, Brazhe AR, Jessen SB, Tan FC, Lauritzen MJ. Rapid stimulus-evoked astrocyte $Ca^{2+}$ elevations and hemodynamic responses in mouse somatosensory cortex in vivo. Proc Natl Acad Sci U S A 110: E4678–E4687, 2013. DOI: 10.1073/pnas.1310065110. [PubMed: 24218625]

288. Lind BL, Jessen SB, Lonstrup M, Josephine C, Bonvento G, Lauritzen M. Fast Ca(2+) responses in astrocyte end-feet and neurovascular coupling in mice. Glia 66: 348–358, 2018. DOI: 10.1002/glia.23246. [PubMed: 29058353]

289. Lindauer U, Megow D, Matsuda H, Dirnagl U. Nitric oxide: A modulator, but not a mediator, of neurovascular coupling in rat somatosensory cortex. Am J Physiol Heart Circ Physiol 277: H799–H811, 1999.

290. Liu P, Huang H, Rollins N, Chalak LF, Jeon T, Halovanic C, Lu H. Quantitative assessment of global cerebral metabolic rate of oxygen ($CMRO_2$) in neonates using MRI. NMR Biomed 27: 332–340, 2014. DOI: 10.1002/nbm.3067. [PubMed: 24399806]

291. Liu X, Gebremedhin D, Harder DR, Koehler RC. Contribution of epoxyeicosatrienoic acids to the cerebral blood flow response to hypoxemia. J Appl Physiol 119: 1202–1209, 2015. DOI: 10.1152/japplphysiol.01043.2014. [PubMed: 25792716]

292. Liu X, Li C, Falck JR, Harder DR, Koehler RC. Relative contribution of cyclooxygenases, epoxyeicosatrienoic acids, and pH to the cerebral blood flow response to vibrissal stimulation. Am J Physiol Heart Circ Physiol 302: H1075–H1085, 2012. [PubMed: 22198176]

293. Liu X, Li C, Falck JR, Roman RJ, Harder DR, Koehler RC. Interaction of nitric oxide, 20-HETE, and EETs during functional hyperemia in whisker barrel cortex. Am J Physiol Heart Circ Physiol 295: H619–H631, 2008. [PubMed: 18502903]

294. Liu X, Li C, Gebremedhin D, Hwang SH, Hammock BD, Falck JR, Roman RJ, Harder DR, Koehler RC. Epoxyeicosatrienoic acid-dependent cerebral vasodilation evoked by metabotropic glutamate receptor activation *in vivo*. Am J Physiol Heart Circ Physiol 301: H373–H381, 2011. [PubMed: 21602473]

295. Lizasoain I, Weiner CP, Knowles RG, Moncada S. The ontogeny of cerebral and cerebellar nitric oxide synthase in the guinea pig and rat. Pediatr Res 39: 779–783, 1996. DOI: 10.1203/00006450-199605000-00006. [PubMed: 8726228]

296. Logsdon AF, Lucke-Wold BP, Turner RC, Huber JD, Rosen CL, Simpkins JW. Role of microvascular disruption in brain damage from traumatic brain injury. Compr Physiol 5: 1147–1160, 2015. DOI: 10.1002/c140057. [PubMed: 26140712]

297. Lohn M, Lauterbach B, Haller H, Pongs O, Luft FC, Gollasch M. Beta(1)-subunit of BK channels regulates arterial wall[Ca(2+)] and diameter in mouse cerebral arteries. J Appl Physiol 91: 1350–1354, 2001. DOI: 10.1152/jappl.2001.91.3.1350. [PubMed: 11509535]

298. Longden TA, Dunn Km, Draheim HJ, Nelson MT, Weston AH, Edwards G. Intermediate-conductance calcium-activated potassium channels participate in neurovascular coupling. Br J Pharmacol 164: 922–933, 2011. DOI: 10.1111/j.1476-5381.2011.01447.x. [PubMed: 21506954]

299. Longo LD, Ueno N, Zhao Y, Pearce WJ, Zhang L. Developmental changes in alpha 1-adrenergic receptors, IP3 responses, and NE-induced contraction in cerebral arteries. Am J Physiol Heart Circ Physiol 271: H2313–H2319, 1996. DOI: 10.1152/ajpheart.1996.271.6.H2313.

300. Lu H, Xu F, Rodrigue KM, Kennedy KM, Cheng Y, Flicker B, Hebrank AC, Uh J, Park DC. Alterations in cerebral metabolic rate and blood supply across the adult lifespan. Cereb Cortex 21: 1426–1434, 2011. DOI: 10.1093/cercor/bhq224. [PubMed: 21051551]

301. Ma J, Ayata C, Huang PL, Fishman MC, Moskowitz MA. Regional cerebral blood flow response to vibrissal stimulation in mice lacking type I NOS gene expression. Am J Physiol Heart Circ Physiol 270: H1085–H1090, 1996.

302. Martin E, Joeri P, Loenneker T, Ekatodramis D, Vitacco D, Hennig J, Marcar VL. Visual processing in infants and children studied using functional MRI. Pediatr Res 46: 135–140, 1999. [PubMed: 10447104]

303. Martin LJ, Brambrink A, Koehler RC, Traystman RJ. Neonatal asphyxic brain injury is neural system preferential and targets sensory-motor networks. In: Stevenson DK, Sunshine P, editors. Fetal and Neonatal Brain Injury: Mechanisms, Management and the Risks of Practice. Oxford: Oxford University Press, 1997, p. 374–399.

304. Martin LJ, Brambrink A, Koehler RC, Traystman RJ. Primary sensory and forebrain motor systems in the newborn brain are preferentially damaged by hypoxia-ischemia. J Comp Neurol 377: 262–285, 1997. [PubMed: 8986885]

305. Martin LJ, Brambrink AM, Price AC, Kaiser A, Agnew DM, Ichord RN, Traystman RJ. Neuronal death in newborn striatum after hypoxia-ischemiais necrosis and evolves with oxidative stress. Neurobiol Dis 7: 169–191, 2000. [PubMed: 10860783]

306. Martinez-Orgado J, Gonzalez R, Alonso MJ, Rodriguez-Martinez MA, Sanchez-Ferrer CF, Marin J. Endothelial factors and autoregulation during pressure changes in isolated newborn piglet cerebral arteries. Pediatr Res 44: 161–167, 1998. DOI: 10.1203/00006450-19980800000004. [PubMed: 9702908]

307. Massaro AN, Govindan RB, Vezina G, Chang T, Andescavage NN, Wang Y, Al-Shargabi T, Metzler M, Harris K, du Plessis AJ. Impaired cerebral autoregulation and brain injury in newborns with hypoxic-ischemic encephalopathy treated with hypothermia. J Neurophysiol 114: 818–824, 2015. DOI: 10.1152/jn.00353.2015. [PubMed: 26063779]

308. Massik J, Tang YL, Hudak ML, Koehler RC, Traystman RJ, Jones MD Jr. Effect of hematocrit on cerebral blood flow with induced polycythemia. J Appl Physiol 62: 1090–1096, 1987. [PubMed: 3571067]

309. McAdams RM, Fleiss B, Traudt C, Schwendimann L, Snyder JM, Haynes RL, Natarajan N, Gressens P, Juul SE. Long-term neuropathological changes associated with cerebral palsy in a nonhuman primate model of hypoxic-ischemic encephalopathy. Dev Neurosci 39: 124–140, 2017. DOI: 10.1159/000470903. [PubMed: 28486224]

310. McCrabb GJ, Harding R. Role of nitric oxide in the regulation of cerebral blood flow in the ovine foetus. Clin Exp Pharmacol Physiol 23: 855–860, 1996. [PubMed: 8911725]

311. McCrabb GJ, Harding R. Cerebral oxygen delivery is reduced during the acidaemia associated with prolonged hypoxaemia in the immature ovine fetus. Biol Neonate 71: 385–394, 1997. DOI: 10.1159/000244440. [PubMed: 9197341]

312. McKenna MC, Scafidi S, Robertson CL. Metabolic alterations in developing brain after injury: Knowns and unknowns. Neurochem Res 40: 2527–2543, 2015. DOI: 10.1007/s11064-015-1600-7. [PubMed: 26148530]

313. McPherson RW, Koehler RC, Traystman RJ. Effect of jugular venous pressure on cerebral autoregulation in dogs. Am J Physiol Heart Circ Physiol 255: H1516–H1524, 1988.

314. Meno JR, Crum AV, Winn HR. Effect of adenosine receptor blockade on pial arteriolar dilation during sciatic nerve stimulation. Am J Physiol Heart Circ Physiol 281: H2018–H2027, 2001. [PubMed: 11668063]

315. Miekisiak G, Kulik T, Kusano Y, Kung D, Chen JF, Winn HR. Cerebral blood flow response in adenosine 2a receptor knockout mice during transient hypoxic hypoxia. J Cereb Blood Flow Metab 28: 1656–1664, 2008. [PubMed: 18545261]

316. Miller SP, Ramaswamy V, Michelson D, Barkovich AJ, Holshouser B, Wycliffe N, Glidden DV, Deming D, Partridge JC, Wu YW, Ashwal S, Ferriero DM. Patterns of brain injury in term neonatal encephalopathy. J Pediatr 146: 453–460, 2005. [PubMed: 15812446]

317. Mirro R, Pharris LJ, Armstead WM, Shibata M, Leffler CW. Effects of indomethacin on newborn pig pial arteriolar responses to $PCO_2$. J Appl Physiol 75: 1300–1305, 1993.DOI: 10.1152/jappl.1993.75.3.1300. [PubMed: 8226544]

318. Mishra A, Reynolds JP, Chen Y, Gourine AV, Rusakov DA, Attwell D. Astrocytes mediate neurovascular signaling to capillary pericytes but not to arterioles. Nat Neurosci 19: 1619–1627, 2016. DOI: 10.1038/nn.4428. [PubMed: 27775719]

319. Mollgard K, Saunders NR. The development of the human blood-brain and blood-CSF barriers. Neuropathol Appl Neurobiol 12: 337–358, 1986. [PubMed: 3534622]

320. Montecot C, Seylaz J, Pinard E. Carbon monoxide regulates cerebral blood flow in epileptic seizures but not in hypercapnia. Neuroreport 9: 2341–2346, 1998. [PubMed: 9694225]

321. Moore LE, Kirsch JR, Helfaer MA, Greenberg RS, Traystman RJ. Hypercapnic blood flow reactivity not increased by alpha-blockade or cordotomy in piglets. Am J Physiol Heart Circ Physiol 262: H1884–H1890, 1992.

322. Moore TJ, Lione AP, Sugden MC, Regen DM. Beta-hydroxybutyrate transport in rat brain: Developmental and dietary modulations. Am J Phys 230:619–630, 1976. DOI: 10.1152/ajplegacy.1976.230.3.619.

323. Muizelaar JP, Ward JD, Marmarou A, Newlon PG, Wachi A. Cerebral blood flow and metabolism in severely head-injured children. Part 2: Autoregulation. J Neurosurg 71: 72–76, 1989. [PubMed: 2738644]

324. Muramoto S, Yamada H, Sadato N, Kimura H, Konishi Y, Kimura K, Tanaka M, Kochiyama T, Yonekura Y, Ito H. Age-dependent change in metabolic response to photic stimulation of the primary visual cortex in infants: Functional magnetic resonance imaging study. J Comput Assist Tomogr 26: 894–901, 2002. [PubMed: 12488732]

325. Myers RE. Two patterns of perinatal brain damage and their conditions of occurrence. Am J Obstet Gynecol 112: 246–276, 1972. [PubMed: 4621486]

326. Nagel C, Diedler J, Gerbig I, Heimberg E, Schuhmann MU, Hockel K. State of cerebrovascular autoregulation correlates with outcome in severe infant/pediatric traumatic brain injury. Acta Neurochir Suppl 122: 239–244, 2016. DOI: 10.1007/978-3-319-22533-3_48. [PubMed: 27165914]

327. Nakao Y, Itoh Y, Kuang TY, Cook M, Jehle J, Sokoloff L. Effects of anesthesia on functional activation of cerebral blood flow and metabolism. Proc Natl Acad Sci U S A 98: 7593–7598, 2001. [PubMed: 11390971]

328. Nauli SM, Ally A, Zhang L, Gerthoffer WT, Pearce WJ. Maturation attenuates the effects of cGMP on contraction, $[Ca^{2+}]_i$ and $Ca^{2+}$ sensitivity in ovine basilar arteries. Gen Pharmacol 35: 107–118, 2000. [PubMed: 11707317]

329. Nauli SM, Williams JM, Akopov SE, Zhang L, Pearce WJ. Developmental changes in ryanodine- and IP(3)-sensitive Ca(2+) pools in ovine basilar artery. Am J Physiol Cell Physiol 281: C1785–C1796, 2001. DOI: 10.1152/ajpcell.2001.281.6.C1785. [PubMed: 11698236]

330. Nehlig A, de Vasconcelos AP, Boyet S. Quantitative autoradiographic measurement of local cerebral glucose utilization in freely moving rats during postnatal development. J Neurosci 8: 2321–2333, 1988. [PubMed: 3249228]

331. Nehlig A, Pereira de Vasconcelos A, Boyet S. Postnatal changes in local cerebral blood flow measured by the quantitative autoradiographic [14C]iodoantipyrine technique in freely moving

rats. J Cereb Blood Flow Metab 9: 579–588, 1989. DOI: 10.1038/jcbfm.1989.83. [PubMed: 2777930]

332. Niwa K, Araki E, Morham SG, Ross ME, Iadecola C. Cyclooxygenase-2 contributes to functional hyperemia in whisker-barrel cortex. J Neurosci 20: 763–770, 2000. [PubMed: 10632605]
333. Nnorom CC, Davis C, Fedinec AL, Howell K, Jaggar JH, Parfenova H, Pourcyrous M, Leffler CW. Contributions of $K_{ATP}$ and $K_{Ca}$ channels to cerebral arteriolar dilation to hypercapnia in neonatal brain. Physiol Rep 2: e12127, 2014. DOI: 10.14814/phy2.12127. [PubMed: 25168876]
334. Northington FJ, Koehler RC, Traystman RJ, Martin LJ. Nitric oxide synthase 1 and nitric oxide synthase 3 protein expression is regionally and temporally regulated in fetal brain. Brain Res Dev Brain Res 95: 1–14, 1996. [PubMed: 8873971]
335. Northington FJ, Tobin JR, Harris AP, Traystman RJ, Koehler RC. Developmental and regional differences in nitric oxide synthase activity and blood flow in the sheep brain. J Cerebr Blood Flow Metab 17: 109–115, 1997.
336. Northington FJ, Tobin JR, Koehler RC, Traystman RJ. *In vivo* production of nitric oxide correlates with NMDA-induced cerebral hyperemia in newborn sheep. Am J Physiol Heart Circ Physiol 269: H215–H221, 1995.
337. Northington FJ, Traystman RJ, Koehler RC, Martin LJ. GLT1, glial glutamate transporter, is transiently expressed in neurons and develops astrocyte specificity only after midgestation in the ovine fetal brain. J Neurobiol 39:515–526, 1999. [PubMed: 10380073]
338. Numan T, Bain AR, Hoiland RL, Smirl JD, Lewis NC, Ainslie PN. Static autoregulation in humans: A review and reanalysis. Med Eng Phys 36: 1487–1495, 2014. DOI: 10.1016/j.medengphy.2014.08.001. [PubMed: 25205587]
339. Ohata H, Cao S, Koehler RC. Contribution of adenosine $A_{2A}$ and $A_{2B}$ receptors and heme oxygenase to AMPA-induced dilation of pial arterioles in rats. Am J Physiol Regul Integr Comp Physiol 291: R728–R735, 2006. [PubMed: 16601261]
340. Ohata H, Gebremedhin D, Narayanan J, Harder DR, Koehler RC. Onset of pulmonary ventilation in fetal sheep produces pial arteriolar constriction dependent on cytochrome p450 omega-hydroxylase activity. J Appl Physiol 109:412–417, 2010. [PubMed: 20489034]
341. O'Leary H, Gregas MC, Limperopoulos C, Zaretskaya I, Bassan H, Soul JS, Di Salvo DN, du Plessis AJ. Elevated cerebral pressure passivity is associated with prematurity-related intracranial hemorrhage. Pediatrics 124: 302–309, 2009. DOI: 10.1542/peds.2008-2004. [PubMed: 19564313]
342. O'Neill JT, Golden SM, Franklin GA, Alden ER. Cerebral vascular response to hemorrhagic hypotension in newborn lambs: The influence of developing anemia. Proc Soc Exp Biol Med 205: 132–139, 1994. [PubMed: 8108462]
343. Ouyang M, Liu P, Jeon T, Chalak L, Heyne R, Rollins NK, Licht DJ, Detre JA, Roberts TP, Lu H, Huang H. Heterogeneous increases of regional cerebral blood flow during preterm brain development: Preliminary assessment with pseudo-continuous arterial spin labeled perfusion MRI. NeuroImage 147: 233–242, 2017. DOI: 10.1016/j.neuroimage.2016.12.034. [PubMed: 27988320]
344. Papile LA, Rudolph AM, Heymann MA. Autoregulation of cerebral blood flow in the preterm fetal lamb. Pediatr Res 19: 159–161, 1985. [PubMed: 3982870]
345. Parfenova H, Carratu P, Tcheranova D, Fedinec A, Pourcyrous M, Leffler CW. Epileptic seizures cause extended postictal cerebral vascular dysfunction that is prevented by HO-1 overexpression. Am J Physiol Heart Circ Physiol 288: H2843–H2850, 2005. [PubMed: 15681702]
346. Parfenova H, Eidson TH, Leffler CW. Upregulation of COX-2 in cerebral microvascular endothelial cells by smooth muscle cell signals. Am J Physiol Cell Physiol 273: C277–C288, 1997.
347. Parfenova H, Fedinec A, Leffler CW. Ionotropic glutamate receptors in cerebral microvascular endothelium are functionally linked to heme oxygenase. J Cereb Blood Flow Metab 23: 190–197, 2003. [PubMed: 12571450]
348. Parfenova H, Hsu P, Leffler CW. Dilator prostanoid-induced cyclic AMP formation and release by cerebral microvascular smooth muscle cells: Inhibition by indomethacin. J Pharmacol Exp Ther 272: 44–52, 1995. [PubMed: 7529312]

349. Parfenova H, Leffler CW. Functional study on vasodilator effects of prostaglandin E2 in the newborn pig cerebral circulation. Eur J Pharmacol 278: 133–142, 1995. [PubMed: 7545580]
350. Parfenova H, Levine V, Gunther WM, Pourcyrous M, Leffler CW. COX-1 and COX-2 contributions to basal and IL-1 beta-stimulated prostanoid synthesis in human neonatal cerebral microvascular endothelial cells. Pediatr Res 52: 342–348, 2002. [PubMed: 12193665]
351. Parfenova H, Massie V, Leffler CW. Developmental changes in endothelium-derived vasorelaxant factors in cerebral circulation. Am J Physiol Heart Circ Physiol 278: H780–H788, 2000. [PubMed: 10710346]
352. Parfenova H, Neff RA III, Alonso JS, Shlopov BV, Jamal CN, Sarkisova SA, Leffler CW. Cerebral vascular endothelial heme oxygenase: Expression, localization, and activation by glutamate. Am J Physiol Cell Physiol 281: C1954–C1963, 2001. [PubMed: 11698254]
353. Parfenova H, Pourcyrous M, Fedinec AL, Liu J, Basuroy S, Leffler CW. Astrocyte-produced carbon monoxide and the carbon monoxide donor CORM-A1 protect against cerebrovascular dysfunction caused by prolonged neonatal asphyxia. Am J Physiol Heart Circ Physiol 315: H978–H988, 2018. DOI: 10.1152/ajpheart.00140.2018. [PubMed: 30028198]
354. Parfenova H, Shibata M, Zuckerman S, Leffler CW. $CO_2$ and cerebral circulation in newborn pigs: Cyclic nucleotides and prostanoids in vascular regulation. Am J Physiol Heart Circ Physiol 266: H1494–H1501, 1994. DOI: 10.1152/ajpheart.1994.266.4.H1494.
355. Parfenova H, Shibata M, Zuckerman S, Mirro R, Leffler CW. Cyclic nucleotides and cerebrovascular tone in newborn pigs. Am J Physiol Heart Circ Physiol 265: H1972–H1982, 1993.
356. Parfenova H, Zuckerman S, Leffler CW. Inhibitory effect of indomethacin on prostacyclin receptor-mediated cerebral vascular responses. Am J Physiol Heart Circ Physiol 268: H1884–H1890, 1995. DOI: 10.1152/ajpheart.1995.268.5.H1884.
357. Park TS, Van Wylen DG, Rubio R, Berne RM. Increased brain interstitial fluid adenosine concentration during hypoxia in newborn piglet. J Cereb Blood Flow Metab 7: 178–183, 1987. DOI: 10.1038/jcbfm.1987.41. [PubMed: 3558500]
358. Park TS, Van Wylen DG, Rubio R, Berne RM. Brain interstitial adenosine and sagittal sinus blood flow during systemic hypotension in piglet. J Cereb Blood Flow Metab 8: 822–828, 1988. DOI: 10.1038/jcbfm.1988.138. [PubMed: 3192647]
359. Parkinson PA, Parfenova H, Leffler CW. Phospholipase C activation by prostacyclin receptor agonist in cerebral microvascular smooth muscle cells. Proc Soc Exp Biol Med 223: 53–58, 2000. [PubMed: 10632961]
360. Pasternak JF, Groothuis DR. Autoregulation of cerebral blood flow in the newborn beagle puppy. Biol Neonate 48: 100–109, 1985. DOI: 10.1159/000242160. [PubMed: 4041504]
361. Pastor P, Curvello V, Hekierski H, Armstead WM. Inhaled nitric oxide protects cerebral autoregulation through prevention of impairment of ATP and calcium sensitive K channel mediated cerebrovasodilation after traumatic brain injury. Brain Res 1711: 1–6, 2019. DOI: 10.1016/j.brainres.2019.01.008. [PubMed: 30629942]
362. Pearce WJ, Ashwal S. Developmental changes in thickness, contractility, and hypoxic sensitivity of newborn lamb cerebral arteries. Pediatr Res 22: 192–196, 1987. DOI: 10.1203/00006450-198708000-00019. [PubMed: 3658545]
363. Pearce WJ, Elliott SR. Maturation enhances the sensitivity of ovine cerebral arteries to the ATP-sensitive potassium channel activator lemakalim. Pediatr Res 35: 729–732, 1994. DOI: 10.1203/00006450-199406000-00021. [PubMed: 7936826]
364. Pearce WJ, Hull AD, Long DM, Longo LD. Developmental changes in ovine cerebral artery composition and reactivity. Am J Physiol Regul Integr Comp Physiol 261: R458–R465, 1991. DOI: 10.1152/ajpregu.1991.261.2.R458.
365. Pearce WJ, Khorram O. Maturation and differentiation of the fetal vasculature. Clin Obstet Gynecol 56: 537–548, 2013. DOI: 10.1097/GRF.0b013e31829e5bc9. [PubMed: 23820122]
366. Peng X, Carhuapoma JR, Bhardwaj A, Alkayed NJ, Falck JR, Harder DR, Traystman RJ, Koehler RC. Suppression of cortical functional hyperemia to vibrissal stimulation in the rat by epoxygenase inhibitors. Am J Physiol Heart Circ Physiol 283: H2029–H2037, 2002. [PubMed: 12384482]

367. Peng X, Zhang C, Alkayed NJ, Harder DR, Koehler RC. Dependency of cortical functional hyperemia to forepaw stimulation on epoxygenase and nitric oxide synthase activities in rats. J Cereb Blood Flow Metab 24: 509–517, 2004. [PubMed: 15129182]

368. Peppiatt CM, Howarth C, Mobbs P, Attwell D. Bidirectional control of CNS capillary diameter by pericytes. Nature 443: 700–704, 2006. [PubMed: 17036005]

369. Pourcyrous M, Bada HS, Parfenova H, Daley ML, Korones SB, Leffler CW. Cerebrovasodilatory contribution of endogenous carbon monoxide during seizures in newborn pigs. Pediatr Res 51: 579–585, 2002. [PubMed: 11978880]

370. Qin X, Kwansa H, Bucci E, Dore S, Boehning D, Shugar D, Koehler RC. Role of heme oxygenase-2 in pial arteriolar response to acetylcholine in mice with and without transfusion of cell-free hemoglobin polymers. Am J Physiol Regul Integr Comp Physiol 295: R498–R504, 2008. [PubMed: 18495834]

371. Rama GP, Parfenova H, Leffler CW. Protein kinase Cs and tyrosine kinases in permissive action of prostacyclin on cerebrovascular regulation in newborn pigs. Pediatr Res 41: 83–89, 1997. DOI: 10.1203/00006450-199704001-00506. [PubMed: 8979294]

372. Rebel A, Cao S, Kwansa H, Dore S, Bucci E, Koehler RC. Dependence of acetylcholine and ADP dilation of pial arterioles on heme oxygenase after transfusion of cell-free polymeric hemoglobin. Am J Physiol Heart Circ Physiol 290: H1027–H1037, 2006. [PubMed: 16214847]

373. Rebich S, Devine JO, Armstead WM. Role of nitric oxide and cAMP in beta-adrenoceptor-induced pial artery vasodilation. Am J Phys 268: H1071–H1076, 1995. DOI: 10.1152/ajpheart.1995.268.3.H1071.

374. Reivich M, Brann AW Jr, Shapiro H, Rawson J, Sano N. Reactivity of cerebral vessels to $CO_2$ in the newborn rhesus monkey. Eur Neurol 6: 132–136, 1971. DOI: 10.1159/000114481. [PubMed: 5005112]

375. Reynolds JD, Zeballos GA, Penning DH, Kimura KA, Atkins B, Brien JF. Nitrate and nitrite anion concentration in the intact cerebral cortex of preterm and nearterm fetal sheep: Indirect index of *in vivo* nitric oxide formation. J Pharmacol Toxicol Methods 39: 125–128, 1998. [PubMed: 9741385]

376. Rickards CA. Cerebral blood-flow regulation during hemorrhage. Compr Physiol 5: 1585–1621, 2015. DOI: 10.1002/c140058. [PubMed: 26426461]

377. Roach MR. The static elastic properties of carotid arteries from fetal sheep. Can J Physiol Pharmacol 48: 694–708, 1970. [PubMed: 5495204]

378. Robinson JS, Fedinec AL, Leffler CW. Role of carbon monoxide in glutamate receptor-induced dilation of newborn pig pial arterioles. Am J Physiol Heart Circ Physiol 282: H2371–H2376, 2002. [PubMed: 12003848]

379. Roche-Labarbe N, Carp SA, Surova A, Patel M, Boas DA, Grant PE, Franceschini MA. Noninvasive optical measures of CBV, StO(2), CBF index, and rCMRO(2) in human premature neonates' brains in the first six weeks of life. Hum Brain Mapp 31: 341–352, 2010. DOI: 10.1002/hbm.20868. [PubMed: 19650140]

380. Roche-Labarbe N, Fenoglio A, Aggarwal A, Dehaes M, Carp SA, Franceschini MA, Grant PE. Near-infrared spectroscopy assessment of cerebral oxygen metabolism in the developing premature brain. J Cereb Blood Flow Metab 32: 481–488, 2012. DOI: 10.1038/jcbfm.2011.145. [PubMed: 22027937]

381. Roche-Labarbe N, Fenoglio A, Radhakrishnan H, Kocienski-Filip M, Carp SA, Dubb J, Boas DA, Grant PE, Franceschini MA. Somatosensory evoked changes in cerebral oxygen consumption measured non-invasively in premature neonates. Neuro Image 85 Pt 1: 279–286, 2014. DOI: 10.1016/j.neuroimage.2013.01.035. [PubMed: 23370052]

382. Rosenberg AA, Harris AP, Koehler RC, Hudak ML, Traystman RJ, Jones MD Jr. Role of $O_2$-hemoglobin affinity in the regulation of cerebral blood flow in fetal sheep. Am J Physiol Heart Circ Physiol 251: H56–H62, 1986.

383. Rosenberg AA, Jones MD Jr, Traystman RJ, Simmons MA, Molteni RA. Response of cerebral blood flow to changes in $PCO_2$ in fetal, newborn, and adult sheep. Am J Physiol Heart Circ Physiol 242: H862–H866, 1982.

384. Rosenegger DG, Tran CH, Wamsteeker Cusulin JI, Gordon GR. Tonic local brain blood flow control by astrocytes independent of phasic neurovascular coupling. J Neurosci 35: 13463–13474, 2015. DOI: 10.1523/JNEUROSCI.1780-15.2015. [PubMed: 26424891]

385. Rossberg MI, Armstead WM. Relationship between vasopressin and opioids in hypoxia induced pial artery vasodilation. Am J Physiol Heart Circ Physiol 271: H521–H527, 1996. DOI: 10.1152/ajpheart.1996.271.2.H521.

386. Rossberg MI, Armstead WM. Role of cyclic nucleotides in vasopressin-induced piglet pial artery dilation and opioid release. Pediatr Res 41: 498–504, 1997. DOI: 10.1203/00006450-199704000-00008. [PubMed: 9098851]

387. Sandoval RJ, Injeti ER, Williams JM, Georthoffer WT, Pearce WJ. Myogenic contractility is more dependent on myofilament calcium sensitization in term fetal than adult ovine cerebral arteries. Am J Physiol Heart Circ Physiol 293: H548–H556, 2007. DOI: 10.1152/ajpheart.00134.2007. [PubMed: 17384133]

388. Satterthwaite TD, Shinohara RT, Wolf DH, Hopson RD, Elliott MA, Vandekar SN, Ruparel K, Calkins ME, Roalf DR, Gennatas ED, Jackson C, Erus G, Prabhakaran K, Davatzikos C, Detre JA, Hakonarson H, Gur RC, Gur RE. Impact of puberty on the evolution of cerebral perfusion during adolescence. Proc Natl Acad Sci U S A 111: 8643–8648, 2014. DOI: 10.1073/pnas.1400178111. [PubMed: 24912164]

389. Schleien CL, Eberle B, Shaffner DH, Koehler RC, Traystman RJ. Reduced blood-brain barrier permeability after cardiac arrest by conjugated superoxide dismutase and catalase in piglets. Stroke 25: 1830–1834, 1994. [PubMed: 8073465]

390. Schleien CL, Koehler RC, Shaffner DH, Eberle B, Traystman RJ. Blood-brain barrier disruption after cardiopulmonary resuscitation in immature swine. Stroke 22: 477–483, 1991. [PubMed: 1902598]

391. Sciotti VM, Park TS, Berne RM, Van Wylen DG. Changes in extracellular adenosine during chemical or electrical brain stimulation. Brain Res 613: 16–20, 1993. [PubMed: 8348299]

392. Settergren G, Lindblad BS, Persson B. Cerebral blood flow and exchange of oxygen, glucose, ketone bodies, lactate, pyruvate and amino acids in infants. Acta Paediatr Scand 65: 343–353, 1976. [PubMed: 5840]

393. Settergren G, Lindblad BS, Persson B. Cerebral blood flow and exchange of oxygen, glucose ketone bodies, lactate, pyruvate and amino acids in anesthetized children. Acta Paediatr Scand 69: 457–465, 1980. [PubMed: 7446094]

394. Shankar V, Armstead WM. Opioids contribute to hypoxia-induced pial artery dilation through activation of ATP-sensitive $K^+$ channels. Am J Physiol Heart Circ Physiol 269: H997–H1002, 1995.

395. Sharon G, Sampson TR, Geschwind DH, Mazmanian SK. The central nervous system and the gut microbiome. Cell 167:915–932, 2016. DOI: 10.1016/j.cell.2016.10.027. [PubMed: 27814521]

396. Shi Y, Liu X, Gebremedhin D, Falck JR, Harder DR, Koehler RC. Interaction of mechanisms involving epoxyeicosatrienoic acids, adenosine receptors, and metabotropic glutamate receptors in neurovascular coupling in rat whisker barrel cortex. J Cereb Blood Flow Metab 28: 111–125, 2008. [PubMed: 17519974]

397. Shibasaki K, Ikenaka K, Tamalu F, Tominaga M, Ishizaki Y. A novel subtype of astrocytes expressing TRPV4 (transient receptor potential vanilloid 4) regulates neuronal excitability via release of gliotransmitters. J Biol Chem 289: 14470–14480, 2014. DOI: 10.1074/jbc.M114.557132. [PubMed: 24737318]

398. Shibata M, Parfenova H, Zuckerman SL, Seyer JM, Krueger JM, Leffler CW. Interleukin-1 beta peptides induce cerebral pial arteriolar dilation in anesthetized newborn pigs. Am J Physiol Regul Integr Comp Physiol 270: R1044–R1050, 1996. DOI: 10.1152/ajpregu.1996.270.5.R1044.

399. Skov L, Pryds O, Greisen G. Estimating cerebral blood flow in newborn infants: Comparison of near infrared spectroscopy and $^{133}Xe$ clearance. Pediatr Res 30: 570–573, 1991. DOI: 10.1203/00006450-199112000-00016. [PubMed: 1805154]

400. Stefanovic M, Puchulu-Campanella E, Kodippili G, Low PS. Oxygen regulates the band 3-ankyrin bridge in the human erythrocyte membrane. Biochem J 449: 143–150, 2013.DOI: 10.1042/BJ20120869. [PubMed: 23013433]

401. Stonestreet BS, Barefield ES, Piva D, Goldstein M. Effects of hyper-carbia on autoregulation of brain blood flow and cerebral metabolism in newborn piglets. Reprod Fertil Dev 7: 1381–1387, 1995. [PubMed: 8848615]

402. Stonestreet BS, Patlak CS, Pettigrew KD, Reilly CB, Cserr HF. Ontogeny of blood-brain barrier function in ovine fetuses, lambs, and adults. Am J Physiol Regul Integr Comp Physiol 271: R1594–R1601, 1996. DOI: 10.1152/ajpregu.1996.271.6.R1594.

403. Sun W, McConnell E, Pare JF, Xu Q, Chen M, Peng W, Lovatt D, Han X, Smith Y, Nedergaard M. Glutamate-dependent neuroglial calcium signaling differs between young and adult brain. Science 339: 197–200, 2013. DOI: 10.1126/science.1226740. [PubMed: 23307741]

404. Symon L, Held K, Dorsch NW. On the myogenic nature of the autoregulatory mechanism in the cerebral circulation. Eur Neurol 6: 11–18, 1971. [PubMed: 5005215]

405. Szymonowicz W, Walker AM, Yu VY, Stewart ML, Cannata J, Cussen L. Regional cerebral blood flow after hemorrhagic hypotension in the preterm, near-term, and newborn lamb. Pediatr Res 28: 361–366, 1990. DOI: 10.1203/00006450-199010000-00012. [PubMed: 2235134]

406. Taga G, Asakawa K, Maki A, Konishi Y, Koizumi H. Brain imaging in awake infants by near-infrared optical topography. Proc Natl Acad Sci U S A 100: 10722–10727, 2003. DOI: 10.1073/pnas.1932552100. [PubMed: 12960368]

407. Taguchi H, Heistad DD, Kitazono T, Faraci FM. ATP-sensitive $K^+$ channels mediate dilatation of cerebral arterioles during hypoxia. Circ Res 74: 1005–1008, 1994. [PubMed: 8156623]

408. Takahashi T, Shirane R, Sato S, Yoshimoto T. Developmental changes of cerebral blood flow and oxygen metabolism in children. Am J Neuroradiol 20: 917–922, 1999. [PubMed: 10369366]

409. Tekes A, Poretti A, Scheurkogel MM, Huisman TA, Howlett JA, Alqahtani E, Lee JH, Parkinson C, Shapiro K, Chung SE, Jennings JM, Gilmore MM, Hogue CW, Martin LJ, Koehler RC, Northington FJ, Lee JK. Apparent diffusion coefficient scalars correlate with near-infrared spectroscopy markers of cerebrovascular autoregulation in neonates cooled for perinatal hypoxic-ischemic injury. AJNR Am J Neuroradiol 36: 188–193, 2015. DOI: 10.3174/ajnr.A4083. [PubMed: 25169927]

410. Teng GQ, Nauli SM, Brayden JE, Pearce WJ. Maturation alters the contribution of potassium channels to resting and 5HT-induced tone in small cerebral arteries of the sheep. Brain Res Dev Brain Res 133: 81–91, 2002. [PubMed: 11882339]

411. Ting P, Yamaguchi S, Bacher JD, Killens RH, Myers RE. Hypoxic-ischemic cerebral necrosis in midgestational sheep fetuses: Physiopathologic correlations. Exp Neurol 80: 227–245, 1983. [PubMed: 6403369]

412. Tomimoto H, Nishimura M, Suenaga T, Nakamura S, Akiguchi I, Wakita H, Kimura J, Mayer B. Distribution of nitric oxide synthase in the human cerebral blood vessels and brain tissues. J Cereb Blood Flow Metab 14: 930–938, 1994. DOI: 10.1038/jcbfm.1994.124. [PubMed: 7523431]

413. Tomiyama Y, Brian JE Jr, Todd MM. Cerebral blood flow during hemodilution and hypoxia in rats: Role of ATP-sensitive potassium channels. Stroke 30: 1942–1947, 1999. [PubMed: 10471448]

414. Tong S, Parfenova H, Shibata M, Zuckerman S, Armstead WM, Leffler CW. Pituitary adenylate cyclase-activating polypeptide dilates cerebral arterioles of newborn pigs. Proc Soc Exp Biol Med 203:343–347, 1993. [PubMed: 8390692]

415. Tortora D, Mattei PA, Navarra R, Panara V, Salomone R, Rossi A, Detre JA, Caulo M. Prematurity and brain perfusion: Arterial spin labeling MRI. Neuroimage Clin 15: 401–407, 2017. DOI: 10.1016/j.nicl.2017.05.023. [PubMed: 28603687]

416. Tuor UI, Grewal D. Autoregulation of cerebral blood flow: Influence of local brain development and postnatal age. Am J Physiol Heart Circ Physiol 267: H2220–H2228, 1994.

417. Tuor UI, Kurpita G, Simone C. Correlation of local changes in cerebral blood flow, capillary density, and cytochrome oxidase during development. J Comp Neurol 342: 439–448, 1994. [PubMed: 8021344]

418. Tuor UI, Simone C, Bascaramurty S. Local blood-brain barrier in the newborn rabbit: Postnatal changes in a-aminoisobutyric acid transfer within medulla, cortex, and selected brain areas. J Neurochem 59: 999–1007, 1992. [PubMed: 1494922]

419. Tweed WA, Cote J, Pash M, Lou H. Arterial oxygenation determines autoregulation of cerebral blood flow in the fetal lamb. Pediatr Res 17: 246–249, 1983. DOI: 10.1203/00006450-198304000-00002. [PubMed: 6682966]

420. Tweed WA, Cote J, Wade JG, Gregory G, Mills A. Preservation of fetal brain blood flow relative to other organs during hypovolemic hypotension. Pediatr Res 16: 137–140, 1982. [PubMed: 7058079]

421. Tzeng YC, Ainslie PN. Blood pressure regulation IX: Cerebral autoregulation under blood pressure challenges. Eur J Appl Physiol 114: 545–559, 2014. DOI: 10.1007/s00421-013-2667-y. [PubMed: 23737006]

422. Van Bel F, Sola A, Roman C, Rudolph AM. Role of nitric oxide in the regulation of the cerebral circulation in the lamb fetus during normoxemia and hypoxemia. Biol Neonate 68: 200–210, 1995. [PubMed: 8534785]

423. Van Bel F, Sola A, Roman C, Rudolph AM. Perinatal regulation of the cerebral circulation: Role of nitric oxide and prostaglandins. Pediatr Res 42: 299–304, 1997. [PubMed: 9284269]

424. Vandekar SN, Shou H, Satterthwaite TD, Shinohara RT, Merikangas AK, Roalf DR, Ruparel K, Rosen A, Gennatas ED, Elliott MA, Davatzikos C, Gur RC, Gur RE, Detre JA. Sex differences in estimated brain metabolism in relation to body growth through adolescence. J Cereb Blood Flow Metab 39: 524–535, 2019. DOI: 10.1177/0271678X17737692.

425. Vannucci SJ, Clark RR, Koehler-Stec E, Li K, Smith CB, Davies P, Maher F, Simpson IA. Glucose transporter expression in brain: Relationship to cerebral glucose utilization. Dev Neurosci 20: 369–379, 1998. DOI: 10.1159/000017333. [PubMed: 9778574]

426. Vannucci SJ, Maher F, Koehler E, Simpson IA. Altered expression of GLUT-1 and GLUT-3 glucose transporters in neurohypophysis of water-deprived or diabetic rats. Am J Phys 267: E605–E611, 1994. DOI: 10.1152/ajpendo.1994.267.4.E605.

427. Vannucci SJ, Seaman LB, Brucklacher RM, Vannucci RC. Glucose transport in developing rat brain: Glucose transporter proteins, rate constants and cerebral glucose utilization. Mol Cell Biochem 140: 177–184, 1994. [PubMed: 7898489]

428. Vannucci SJ, Simpson IA. Developmental switch in brain nutrient transporter expression in the rat. Am J Physiol Endocrinol Metab 285: E1127–E1134, 2003. DOI: 10.1152/ajpendo.00187.2003. [PubMed: 14534079]

429. Vavilala MS, Kincaid MS, Muangman SL, Suz P, Rozet I, Lam AM. Gender differences in cerebral blood flow velocity and autoregulation between the anterior and posterior circulations in healthy children. Pediatr Res 58: 574–578, 2005. DOI: 10.1203/01.PDR.0000179405.30737.0F. [PubMed: 16148076]

430. Vavilala MS, Lee LA, Boddu K, Visco E, Newell DW, Zimmerman JJ, Lam AM. Cerebral autoregulation in pediatric traumatic brain injury. Pediatr Crit Care Med 5: 257–263, 2004. [PubMed: 15115564]

431. Venteicher A, Armstead WM. Vasopressin contributes to dynorphin modulation of hypoxic cerebrovasodilation. Am J Physiol Heart Circ Physiol 275:H2072–H2079, 1998. DOI: 10.1152/ajpheart.1998.275.6.H2072.

432. Vesoulis ZA, Liao SM, Trivedi SB, Ters NE, Mathur AM. A novel method for assessing cerebral autoregulation in preterm infants using transfer function analysis. Pediatr Res 79: 453–459, 2016. DOI: 10.1038/pr.2015.238. [PubMed: 26571222]

433. Virgintino D, Errede M, Girolamo F, Capobianco C, Robertson D, Vimercati A, Serio G, Di Benedetto A, Yonekawa Y, Frei K, Roncali L. Fetal blood-brain barrier P-glycoprotein contributes to brain protection during human development. J Neuropathol Exp Neurol 67: 50–61, 2008. DOI: 10.1097/nen.0b013e31815f65d9. [PubMed: 18091560]

434. Virgintino D, Errede M, Robertson D, Capobianco C, Girolamo F, Vimercati A, Bertossi M, Roncali L. Immunolocalization of tight junction proteins in the adult and developing human brain. Histochem Cell Biol 122: 51–59, 2004. DOI: 10.1007/s00418-004-0665-1. [PubMed: 15221411]

435. Virgintino D, Robertson D, Benagiano V, Errede M, Bertossi M, Ambrosi G, Roncali L. Immunogold cytochemistry of the blood-brain barrier glucose transporter GLUT1 and

endogenous albumin in the developing human brain. Brain Res Dev Brain Res 123: 95–101, 2000. [PubMed: 11020555]

436. Wagerle LC, Busija DW. Cholinergic mechanisms in the cerebral circulation of the newborn piglet: Effect of inhibitors of arachidonic acid metabolism. Circ Res 64: 1030–1036, 1989. [PubMed: 2495868]
437. Wagerle LC, Degiulio PA. Indomethacin-sensitive $CO_2$ reactivity of cerebral arterioles is restored by vasodilator prostaglandin. Am J Physiol Heart Circ Physiol 266: H1332–H1338, 1994. DOI: 10.1152/ajpheart.1994.266.4.H1332.
438. Wagerle LC, Delivoria-Papadopoulos M. Alpha-adrenergic receptor subtypes in the cerebral circulation of newborn piglets. Am J Physiol Heart Circ Physiol 252: R1092–R1098, 1987. DOI: 10.1152/ajpregu.1987.252.6.R1092.
439. Wagerle LC, Heffernan TM, Sacks LM, Delivoria-Papadopoulos M. Sympathetic effect on cerebral blood flow regulation in hypoxic newborn lambs. Am J Physiol Heart Circ Physiol 245: H487–H494, 1983. DOI: 10.1152/ajpheart.1983.245.3.H487.
440. Wagerle LC, Kumar SP, Delivoria-Papadopoulos M. Effect of sympathetic nerve stimulation on cerebral blood flow in newborn piglets. Pediatr Res 20: 131–135, 1986. DOI: 10.1203/00006450-198602000-00007. [PubMed: 3945523]
441. Wagerle LC, Kurth CD, Busija DW. Cholinergic reactivity of cerebral arteries in the developing fetal and newborn lamb. J Dev Physiol 17: 51–54, 1992. [PubMed: 1645016]
442. Wagerle LC, Kurth CD, Roth RA. Sympathetic reactivity of cerebral arteries in developing fetal lamb and adult sheep. Am J Physiol Heart Circ Physiol 258: H1432–H1438, 1990. DOI: 10.1152/ajpheart.1990.258.5.H1432.
443. Wagerle LC, Mishra OP. Mechanism of $CO_2$ response in cerebral arteries of the newborn pig: Role of phospholipase, cyclooxygenase, and lipoxygenase pathways. Circ Res 62: 1019–1026, 1988. [PubMed: 3129206]
444. Wagerle LC, Moliken W, Russo P. Nitric oxide and beta-adrenergic mechanisms modify contractile responses to norepinephrine in ovine fetal and newborn cerebral arteries. Pediatr Res 38: 237–242, 1995. DOI: 10.1203/00006450-199508000-00017. [PubMed: 7478822]
445. Wagner KR, Ting P, Westfall MV, Yamaguchi S, Bacher JD, Myers RE. Brain metabolic correlates of hypoxic-ischemic cerebral necrosis in mid-gestational sheep fetuses: Significance of hypotension. J Cereb Blood Flow Metab 6: 425–434, 1986. DOI: 10.1038/jcbfm.1986.75. [PubMed: 3733902]
446. Wang Q, Kjaer T, Jorgensen MB, Paulson OB, Lassen NA, Diemer NH, Lou HC. Nitric oxide does not act as a mediator coupling cerebral blood flow to neural activity following somatosensory stimuli in rats. Neurol Res 15: 33–36, 1993. [PubMed: 8098850]
447. Wang R, Wang Z, Wu L. Carbon monoxide-induced vasorelaxation and the underlying mechanisms. Br J Pharmacol 121: 927–934, 1997. [PubMed: 9222549]
448. Wang R, Wu L. The chemical modification of $K_{Ca}$ channels by carbon monoxide in vascular smooth muscle cells. J Biol Chem 272: 8222–8226, 1997. [PubMed: 9079640]
449. Wang R, Wu L, Wang Z. The direct effect of carbon monoxide on $K_{Ca}$ channels in vascular smooth muscle cells. Pflugers Arch 434: 285–291, 1997. [PubMed: 9178628]
450. Wei HS, Kang H, Rasheed ID, Zhou S, Lou N, Gershteyn A, McConnell ED, Wang Y, Richardson KE, Palmer AF, Xu C, Wan J, Nedergaard M. Erythrocytes are oxygen-sensing regulators of the cerebral microcirculation. Neuron 91: 851–862, 2016. DOI: 10.1016/j.neuron.2016.07.016. [PubMed: 27499087]
451. White CR, Hamade MW, Siami K, Chang MM, Mangalwadi A, Frangos JA, Pearce WJ. Maturation enhances fluid shear-induced activation of eNOS in perfused ovine carotid arteries. Am J Physiol Heart Circ Physiol 289: H2220–H2227, 2005. DOI: 10.1152/ajpheart.01013.2004. [PubMed: 15923310]
452. White CR, Hao X, Pearce WJ. Maturational differences in soluble guanylate cyclase activity in ovine carotid and cerebral arteries. Pediatr Res 47: 369–375, 2000. [PubMed: 10709737]
453. White RP, Hindley C, Bloomfield PM, Cunningham VJ, Vallance P, Brooks DJ, Markus HS. The effect of the nitric oxide synthase inhibitor L-NMMA on basal CBF and vasoneuronal

coupling in man: A PET study. J Cereb Blood Flow Metab 19: 673–678, 1999. DOI: 10.1097/00004647-199906000-00011. [PubMed: 10366198]

454. Wilderman MJ, Armstead WM. Relationship between nitric oxide and opioids in hypoxia-induced pial artery vasodilation. Am J Physiol 270: H869–H874, 1996. DOI: 10.1152/ajpheart.1996.270.3.H869. [PubMed: 8780180]
455. Wilderman MJ, Armstead WM. Role of neuronal NO synthase in relationship between NO and opioids in hypoxia-induced pial artery dilation. Am J Physiol Heart Circ Physiol 273: H1807–H1815, 1997.
456. Wilderman MJ, Armstead WM. Role of endothelial nitric oxide synthase in hypoxia-induced pial artery dilation. J Cereb Blood Flow Metab 18:531–538, 1998. DOI: 10.1097/00004647-199805000-00008. [PubMed: 9591845]
457. Williams JM, Hull AD, Pearce WJ. Maturational modulation of endothelium-dependent vasodilatation in ovine cerebral arteries. Am J Physiol Regul Integr Comp Physiol 288: R149–R157, 2005. DOI: 10.1152/ajpregu.00427.2004. [PubMed: 15358604]
458. Williams JM, Pearce WJ. Age-dependent modulation of endothelium-dependent vasodilatation by chronic hypoxia in ovine cranial arteries. J Appl Physiol (1985) 100: 225–232, 2006. DOI: 10.1152/japplphysiol.00221.2005.
459. Willis AP, Leffler CW. NO and prostanoids: Age dependence of hypercapnia and histamine-induced dilations of pig pial arterioles. Am J Physiol Heart Circ Physiol 277: H299–H307, 1999.
460. Willis AP, Leffler CW. Endothelial NO and prostanoid involvement in newborn and juvenile pig pial arteriolar vasomotor responses. Am J Physiol Heart Circ Physiol 281: H2366–H2377, 2001. DOI: 10.1152/ajpheart.2001.281.6.H2366. [PubMed: 11709401]
461. Winestone JS, Bonner C, Leffler CW. Carbon monoxide as an attenuator of vasoconstriction in piglet cerebral arterioles. Exp Biol Med (Maywood) 228: 46–50, 2003. [PubMed: 12524472]
462. Winquist RJ, Webb RC, Bohr DF. Relaxation to transmural nerve stimulation and exogenously added norepinephrine in porcine cerebral vessels. A study utilizing cerebrovascular intrinsic tone. Circ Res 51: 769–776, 1982. [PubMed: 6128083]
463. Wu L, Cao K, Lu Y, Wang R. Different mechanisms underlying the stimulation of $K_{Ca}$ channels by nitric oxide and carbon monoxide. J Clin Invest 110: 691–700, 2002. [PubMed: 12208870]
464. Xi Q, Tcheranova D, Basuroy S, Parfenova H, Jaggar JH, Leffler CW. Glutamate-induced calcium signals stimulate CO production in piglet astrocytes. Am J Physiol Heart Circ Physiol 301: H428–H433, 2011. [PubMed: 21572018]
465. Xi Q, Tcheranova D, Parfenova H, Horowitz B, Leffler CW, Jaggar JH. Carbon monoxide activates $K_{Ca}$ channels in newborn arteriole smooth muscle cells by increasing apparent $Ca^{2+}$ sensitivity of à-subunits. Am J Physiol Heart Circ Physiol 286: H610–H618, 2004. [PubMed: 14563665]
466. Xi Q, Umstot E, Zhao G, Narayanan D, Leffler CW, Jaggar JH. Glutamate regulates $Ca^{2+}$ signals in smooth muscle cells of newborn piglet brain slice arterioles through astrocyte- and heme oxygenase-dependent mechanisms. Am J Physiol Heart Circ Physiol 298: H562–H569, 2010. [PubMed: 19966053]
467. Yamada H, Sadato N, Konishi Y, Kimura K, Tanaka M, Yonekura Y, Ishii Y. A rapid brain metabolic change in infants detected by fMRI. Neuroreport 8: 3775–3778, 1997. [PubMed: 9427369]
468. Yamada H, Sadato N, Konishi Y, Muramoto S, Kimura K, Tanaka M, Yonekura Y, Ishii Y, Itoh H. A milestone for normal development of the infantile brain detected by functional MRI. Neurology 55: 218–223, 2000. [PubMed: 10908895]
469. Yamaura K, Gebremedhin D, Zhang C, Narayanan J, Hoefert K, Jacobs ER, Koehler RC, Harder DR. Contribution of epoxyeicosatrienoic acids to the hypoxia-induced activation of $Ca^{2+}$-activated $K^{+}$ channel current in cultured rat hippocampal astrocytes. Neuroscience 143: 703–716, 2006. [PubMed: 17027168]
470. Yan XX, Garey LJ. Morphological diversity of nitric oxide synthesising neurons in mammalian cerebral cortex. J Hirnforsch 38:165–172, 1997. [PubMed: 9176729]
471. Yan XX, Garey LJ, Jen LS. Prenatal development of NADPH-diaphorase-reactive neurons in human frontal cortex. Cereb Cortex 6: 737–745, 1996. [PubMed: 8921208]

472. Yan XX, Jen LS, Garey LJ. NADPH-diaphorase-positive neurons in primate cerebral cortex colocalize with GABA and calcium-binding proteins. Cereb Cortex 6: 524–529, 1996. [PubMed: 8670678]

473. Younkin DP, Reivich M, Jaggi J, Obrist W, Delivoria-Papadopoulos M. Noninvasive method of estimating human newborn regional cerebral blood flow. J Cereb Blood Flow Metab 2: 415–420, 1982. DOI: 10.1038/jcbfm.1982.47. [PubMed: 7142305]

474. Younkin DP, Reivich M, Jaggi JL, Obrist WD, Delivoria-Papadopoulos M. The effect of hematocrit and systolic blood pressure on cerebral blood flow in newborn infants. J Cereb Blood Flow Metab 7: 295–299, 1987. DOI: 10.1038/jcbfm.1987.66. [PubMed: 3584264]

475. Yoxall CW, Weindling AM. Measurement of cerebral oxygen consumption in the human neonate using near infrared spectroscopy: Cerebral oxygen consumption increases with advancing gestational age. Pediatr Res 44: 283–290, 1998. DOI: 10.1203/00006450199809000-00004. [PubMed: 9727702]

476. Zehendner CM, Tsohataridis S, Luhmann HJ, Yang JW. Developmental switch in neurovascular coupling in the immature rodent barrel cortex. PLoS One 8: e80749, 2013. DOI: 10.1371/journal.pone.0080749. [PubMed: 24224059]

477. Zeiler FA, Donnelly J, Menon DK, Smielewski P, Zweifel C, Brady K, Czosnyka M. Continuous autoregulatory indices derived from multimodal monitoring: Each one is not like the other. J Neurotrauma 34: 3070–3080, 2017. DOI: 10.1089/neu.2017.5129. [PubMed: 28571485]

478. Zhang Y, Leffler CW. Compensatory role of NO in cerebral circulation of piglets chronically treated with indomethacin. Am J Physiol Regul Integr Comp Physiol 282: R400–R410, 2002. [PubMed: 11792649]

479. Zimmermann A, Leffler CW, Tcheranova D, Fedinec AL, Parfenova H. Cerebroprotective effects of the CO-releasing molecule CORM-A1 against seizure-induced neonatal vascular injury. Am J Physiol Heart Circ Physiol 293: H2501–H2507, 2007. [PubMed: 17630349]

480. Zuckerman SL, Armstead WM, Hsu P, Shibata M, Leffler CW. Age dependence of cerebrovascular response mechanisms in domestic pigs. Am J Physiol Heart Circ Physiol 271: H535–H540, 1996.

## Didactic Synopsis

### Major Teaching Points

- In human development, cerebral blood flow (CBF) and oxygen and glucose consumption, normalized by tissue weight, increase from less than 20% of adult levels at 70% of the gestation period (0.7 gestation) to levels exceeding those of adults at 3 to 11 years of age in accordance with regional growth, synaptic plasticity, and myelination.
- Coupling of vasodilation to neuronal activity is sluggish in term neonates relative to that seen in adults. In infants, the increase in local CBF during sensory activation fails to match the increase in energy metabolism, resulting in an increase in tissue deoxyhemoglobin and a negative blood oxygen level-dependent signal on magnetic resonance imaging.
- As the mean arterial pressure increases from 35 mmHg at 0.7 gestation to adult levels, arterial smooth muscle mass, basal myogenic tone, and the myogenic response to changes in transmural pressure increase, thereby extending the range of CBF autoregulation.
- In sheep, the CBF responses to hypercapnia and hypoxia increase in relationship to the increase in oxygen consumption during development. The exception is that $CO_2$ reactivity is greater in adult sheep despite oxygen consumption being lower than that in neonatal lambs. As high-affinity fetal hemoglobin is replaced by adult hemoglobin, the CBF response to hypoxia declines for the same arterial oxygen content.
- In newborn piglets, prostanoids and heme oxygenase-derived carbon monoxide play a prominent role in vascular reactivity to a variety of physiologic stimuli, including autoregulation, neurovascular coupling, hypercapnia, and endothelial-dependent vasodilation.

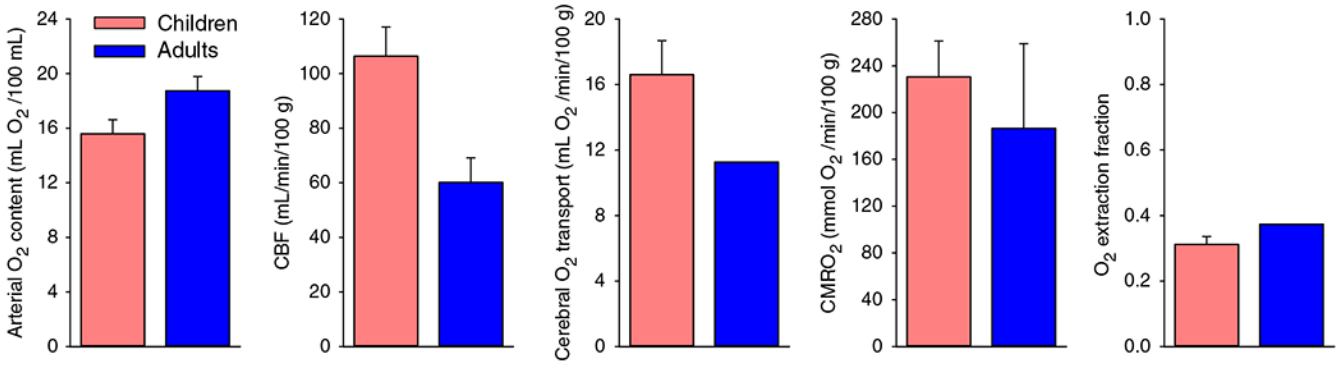


**Figure 1.**

Global cerebral blood flow (CBF) is higher at 3 to 11 years of age than in adults. Arterial $O_2$ content, CBF, cerebral $O_2$ transport, cerebral metabolic rate of $O_2$ ($CMRO_2$), and $O_2$ extraction fraction in first quantitative cerebral hemodynamic study in children with the nitrous oxide wash-in technique. Data from nine children were pooled from ages 3 to 11 years. Children at this age have higher CBF, $O_2$ transport, and $CMRO_2$, with comparable $O_2$ extraction fraction as 12 adults undergoing the same technique. Source: Adapted, with permission, from Kennedy C and Sokoloff L, 1957 (221).

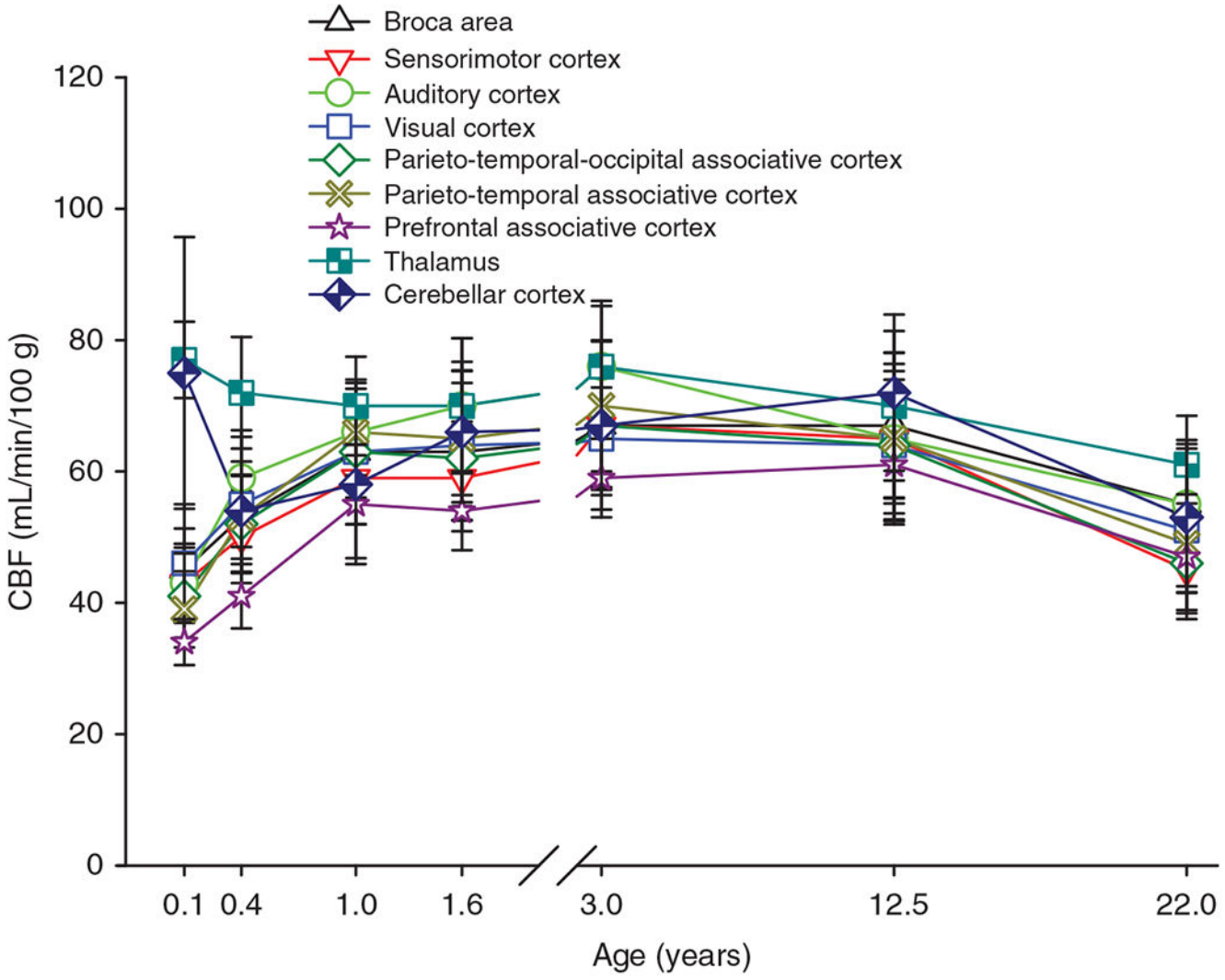


**Figure 2.**

Cerebral blood flow (CBF) throughout childhood varies by brain region. Regional CBF was measured by SPECT imaging in 42 children ranging in age from 2 days to 19 years. Data are divided into age bins with 5 to 10 children per bin, and the mean and SD are plotted against the average age for each bin. Blood flow in cortical regions increases in infants and reaches adult levels by 1 year and exceeds adult levels from 3 to 12.5 years. CBF in frontal association cortex lags other cortical regions. In thalamus, CBF is already above adult levels in infants. Source: Adapted, with permission, from Chiron C, et al., 1992 (96).

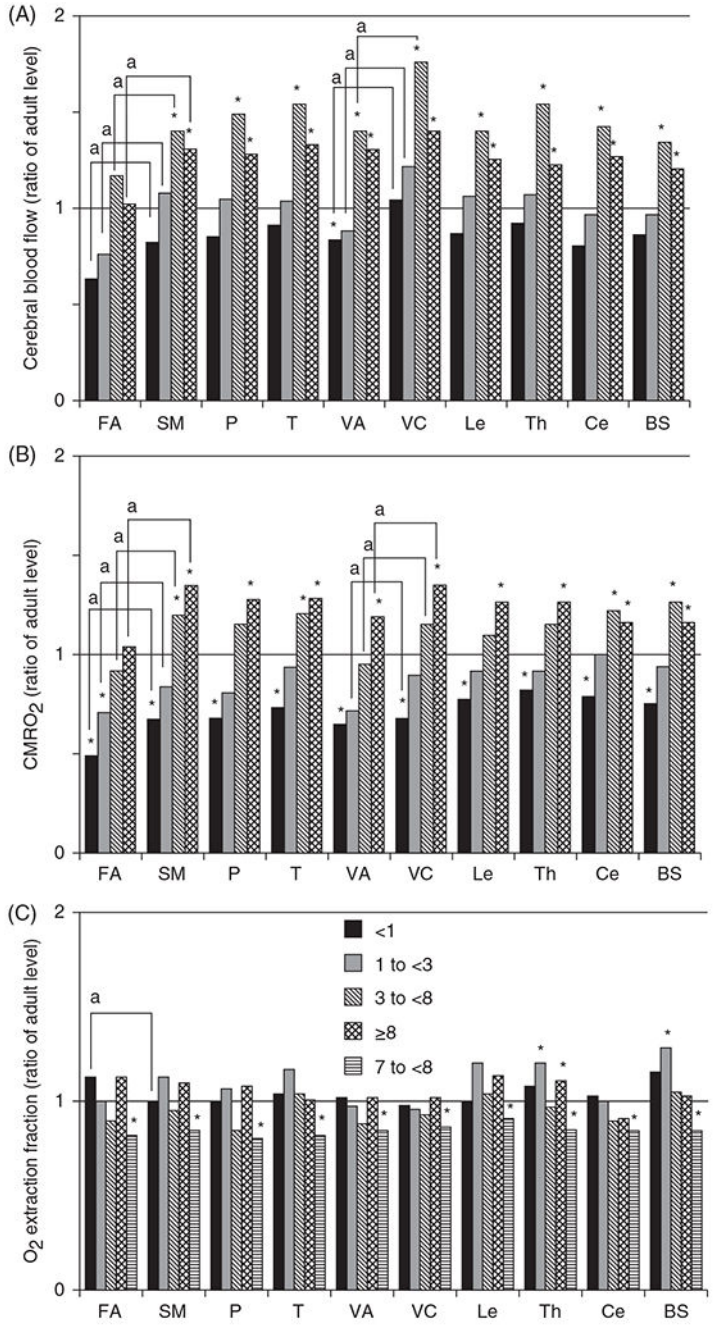


**Figure 3.**

Regional cerebral blood flow (CBF) (A) during development (relative to adult levels) paralleled regional developmental increases in cerebral metabolic rate of $O_2$ ($CMRO_2$) (B) with little change in $O_2$ extraction fraction (C). Measurements were made with PET imaging in children with neurosurgical disorders but with normal psychomotor development. Compared with CBF and $CMRO_2$ values in adults, low values were observed in the frontal association (FA), visual association (VA), and the sensorimotor (SM) areas in the less than 1-year-old group ($n = 10$) and in the FA area in the 1- to less than 3-year-old group ($n =$

5). In the 3- to less than 8-year-old group ($n = 7$) and in the greater than 8-year-old group (9-17-years old; $n = 8$ ), CBF and $CMRO_2$ exceeded the corresponding adult levels in all regions (*, $P < 0.05$ by Mann-Whitney U-test), except for the FA area. Consistent with delayed maturation in cortical association cortex, CBF and $CMRO_2$ values were lower in FA than in primary SM area, and CBF and $CMRO_2$ in VA cortex were lower than in the primary visual (VC) area (*a*, $P < 0.05$ by paired *t*-test), except in the ≥8-year-old group. P, parietal lobe; T, temporal lobe; Le, lenticulum nuclei; Th, thalamus; Ce, cerebellar hemisphere; BS, brain stem. Source: Adapted, with permission, from Takahashi T, et al., 1999 (408), © 1999, American Society of Neuroradiology.

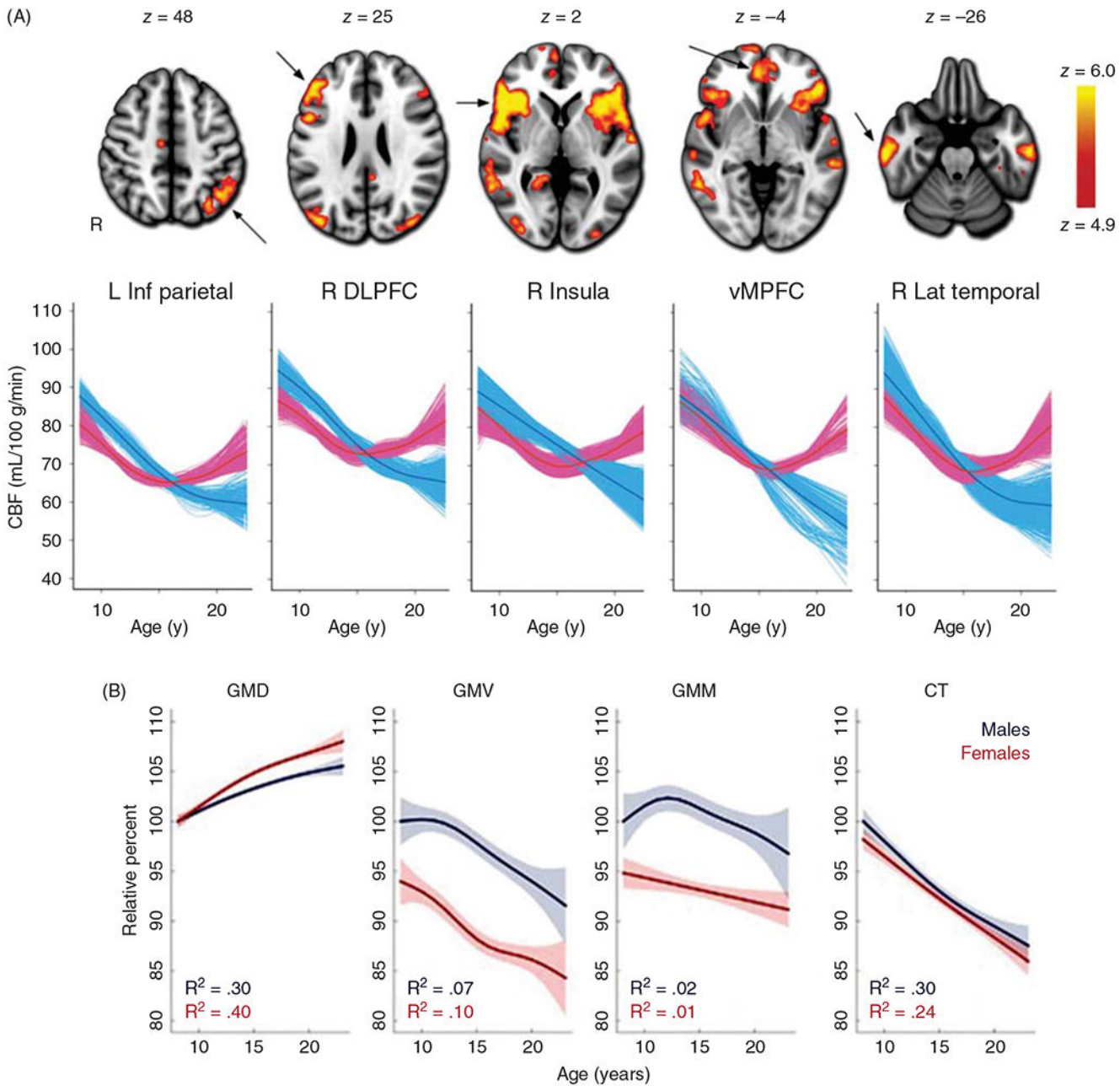


**Figure 4.**

(A) After reaching its peak level in preadolescents, cerebral blood flow (CBF) declines in male adolescents toward levels seen in young male adults. In females, CBF also declines in early adolescence but then increases in specific regions in late adolescence. These regions are denoted by arrows on the MR images; L Inf Parietal, left inferior parietal cortex; R DLPFC, right dorsolateral prefrontal cortex; R insula, right insula cortex; vMPFC, ventromedial prefrontal cortex; R Lat Temporal, right lateral temporal cortex. Source: Reused, with permission, from Satterthwaite TD, et al., 2014 (388). © 2014, National Academy of Sciences. Figure 2 from https://www.pnas.org/content/111/23/8643.

(B) Structural changes in cerebral cortex during adolescence. Gray matter density (GMD), determined from T1 MRI intensity averaged over the entire brain, increases in adolescence, while gray matter volume (GMV), gray matter mass (GMM=GMD × GMV), and cortical thickness (CT) largely decrease in males and females. Note that the higher CBF per unit mass in females at the end of adolescence is associated with higher GMD and is distributed to a lower gray matter volume and mass in females compared to males, thereby attenuating sex differences in volumetric blood flow to the entire cortical volume. Values are plotted as percentages of the fitted value for males at 8 years of age. Shaded bands correspond to two SE of the fit. Source: Adapted, with permission, from Gennatas ED et al., (156).

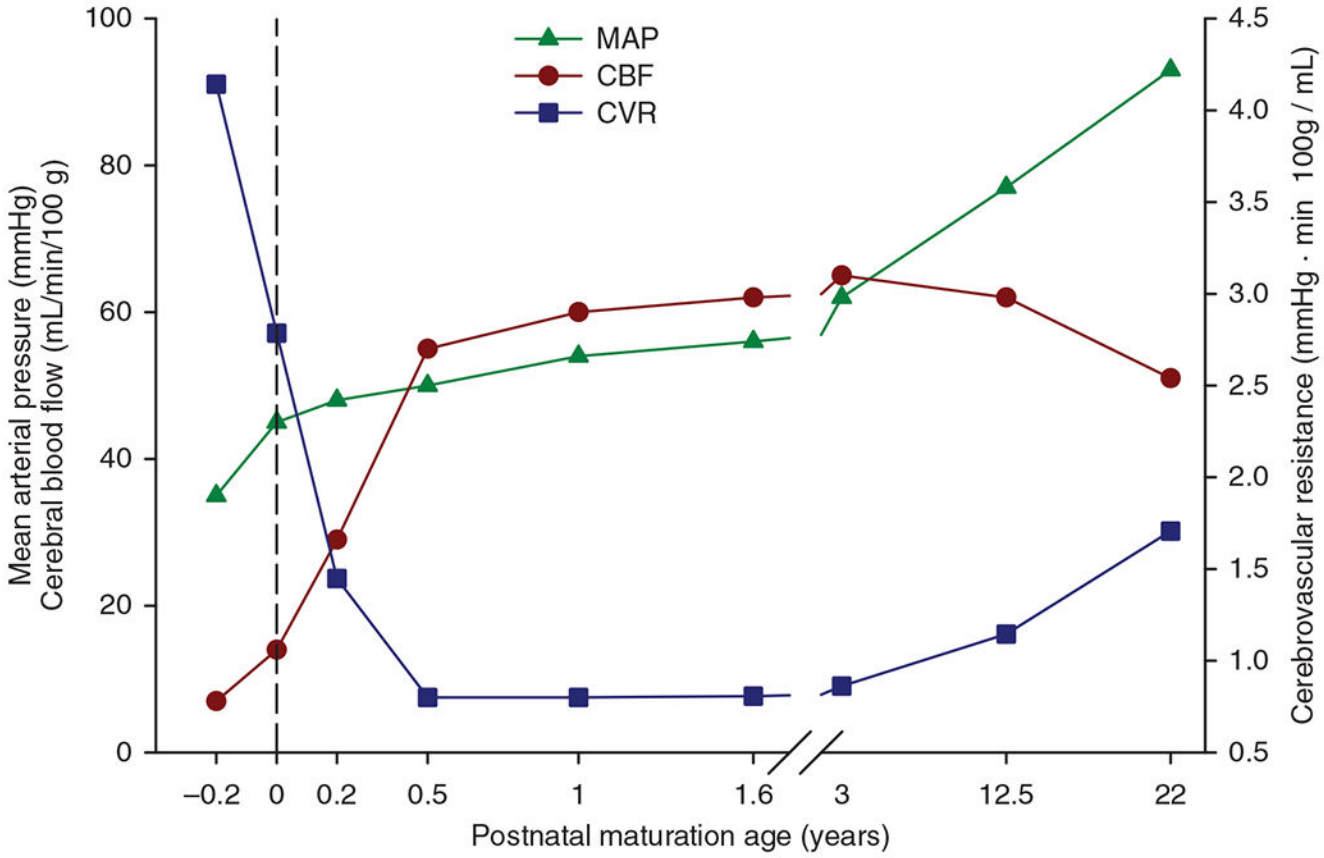


**Figure 5.**
Mean arterial pressure (MAP), cerebral blood flow (CBF), and cerebrovascular resistance (CVR) during human development. Source: Adapted, with permission, from Chiron C, et al., 1992 (96); De Vis JB, et al., 2014 (114), 2013 (115); Liu P, et al., 2014 (290); Ouyang M, et al., 2017 (343).

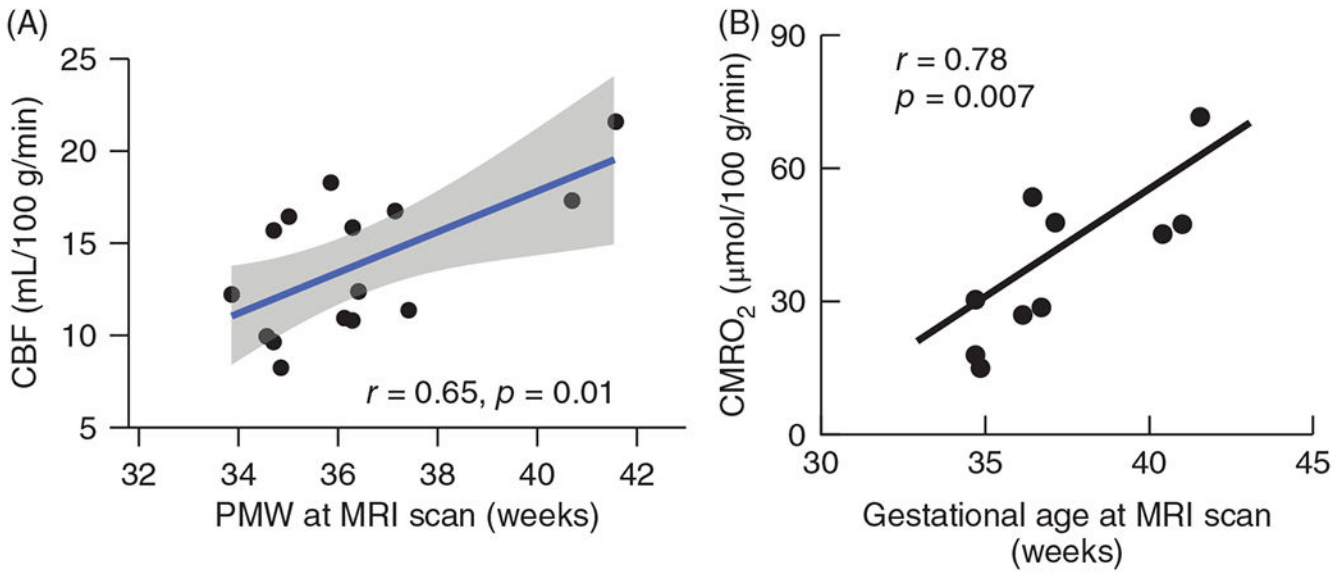


**Figure 6.**

(A) Global cerebral blood flow (CBF), derived from summation of phase-contrast MRI of internal carotid and vertebral arteries of 14 unsedated neonates studied about 2 to 3 weeks after birth, increased linearly with gestational age determined by postmenstrual weeks (PMW) at a rate of 1.22 mL/min/100 g/PMW. Source: Adapted, with permission, from Ouyang M, et al., 2017, (343). (B) Global cerebral metabolic rate of $O_2$ ($CMRO_2$), derived from MRI measurement of sagittal sinus $O_2$ saturation and CBF in 10 unsedated neonates, increased linearly with gestational age. Source: Adapted, with permission, from Liu P, et al., 2014 (290), © 2014, John Wiley & Sons.

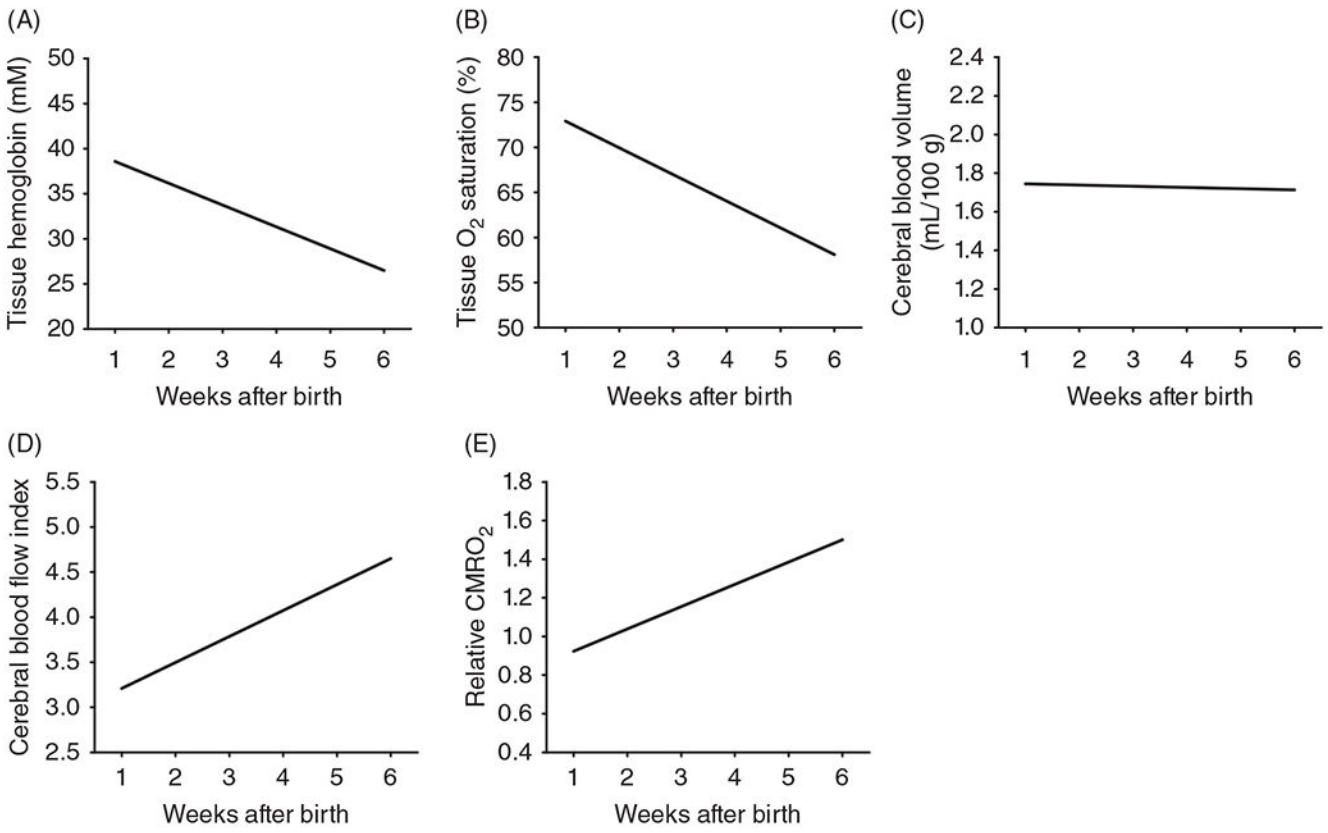


**Figure 7.**

Postnatal increases in cerebral blood flow are coupled to postnatal increases in cerebral metabolic rate of $O_2$ ($CMRO_2$) as determined by advance near-infrared spectroscopy (NIRS) modalities in prematurely born neonates over the first 6 weeks after birth. Noninvasive NIRS-based optical measures of tissue hemoglobin concentration (A), tissue $O_2$ saturation (B), cerebral blood volume (C), a cerebral blood flow index (D), and relative $CMRO_2$ determined with frequency domain NIRS plus diffuse correlation spectroscopy are expressed relative to the group average in human premature neonates born at 25 to 33 weeks PMA brains. The decreases in tissue hemoglobin concentration and tissue oxyhemoglobin saturation without an accompanying decrease in cerebral blood volume are attributed to a postnatal decrease in systemic hematocrit as high-$O_2$ affinity fetal hemoglobin-containing red blood cells are cleared faster than low-$O_2$ affinity adult hemoglobin-containing red blood cells are produced. Lines are linear regressions that were all statistically significant versus age, except for cerebral blood volume. Source: Reused, with permission, from Roche-Labarbe N, et al., 2010 (379).

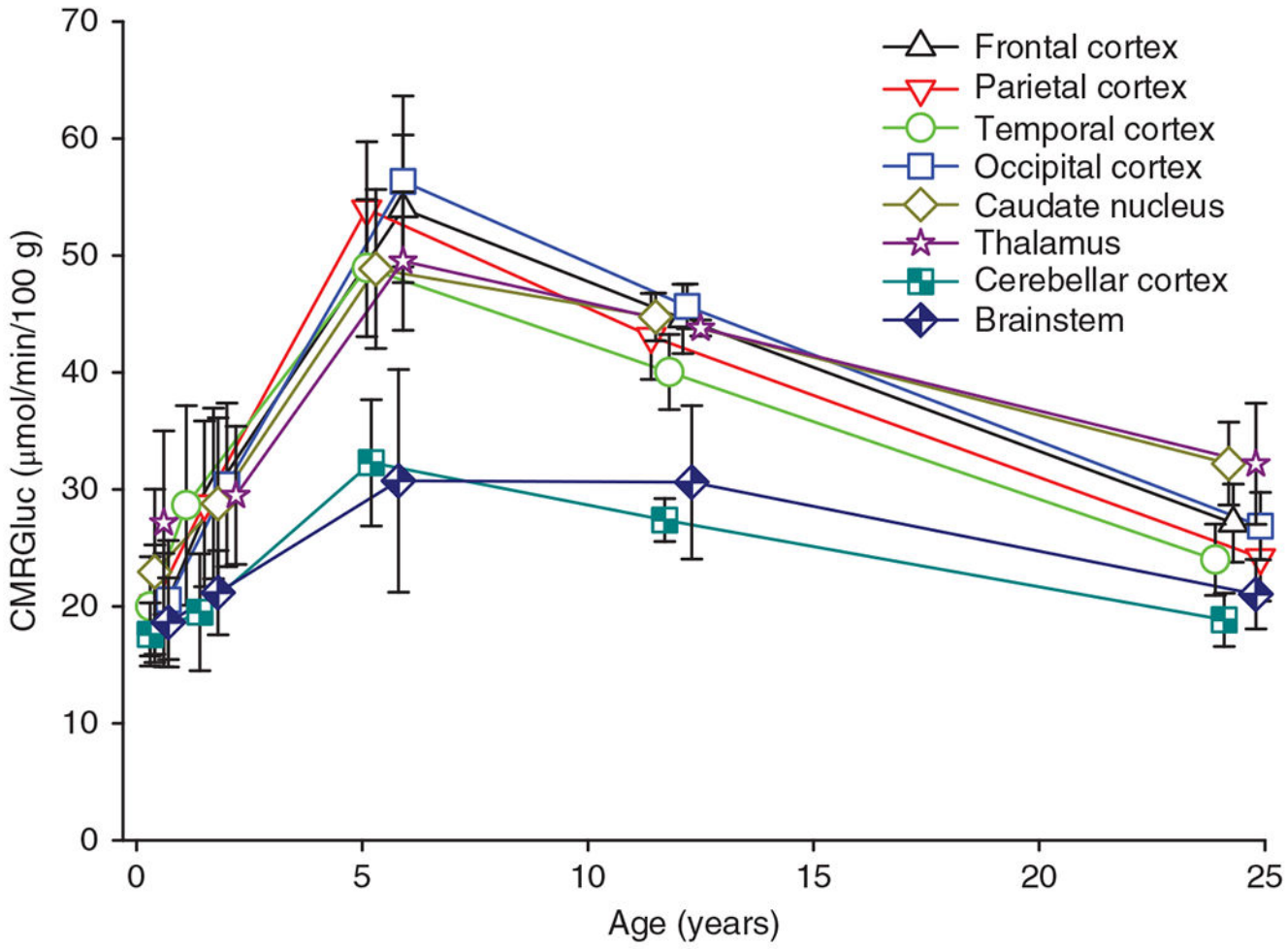


**Figure 8.**

Cerebral metabolic rate of glucose (CMRGluc) of various brain regions increases during early human development and then overshoots adult levels especially in forebrain regions. Source: Adapted, with permission, from Chugani HT, et al., 1987 (100).

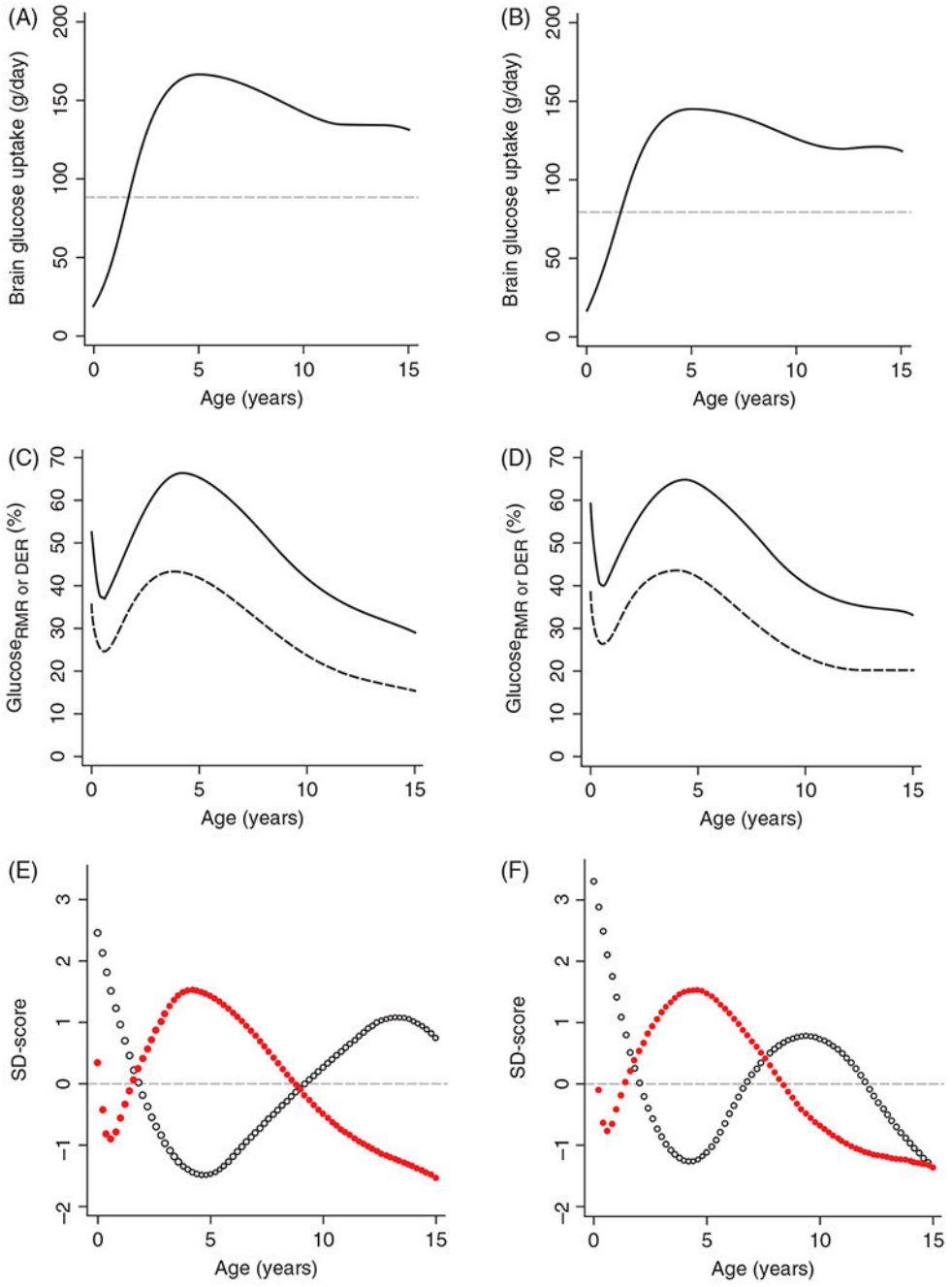


**Figure 9.**

Glucose utilization of the human brain by age in males (A) and females (B) and as a % of total body resting metabolic rate (rmr, solid line) and daily energy requirements (der, dashed line), expressed in glucose equivalents, for males (C) and females (D). Glucose utilization of the entire brain was estimated in units of g/day from the PET-derived glucose consumption for each brain region and the MRI-derived volume of each brain region at different stages of development. Through 5 years of age, the increase in total brain glucose utilization outpaces the increase in energy requirements for the entire body, whether based on resting caloric

demand or including caloric needs for daily activity. The brain glucose utilization, expressed as a percent of rmr (red dots), is out of phase with the body-weight growth rate (d*w*/d*t*, blue dots) in males (E) and females (F), suggesting an evolutionary adaptation to delay body growth so that limited caloric intake can be diverted to the prolonged period brain growth and development in humans. Glucose utilization as a percent of rmr and weight velocities are plotted as SD scores to allow unitless comparison. Source: Adapted, with permission, from Kuzawa CW, et al., 2014 (241), © 2014, National Academy of Sciences. Figures 1A-D and 2A-B from https://www.pnas.org/content/111/36/13010.

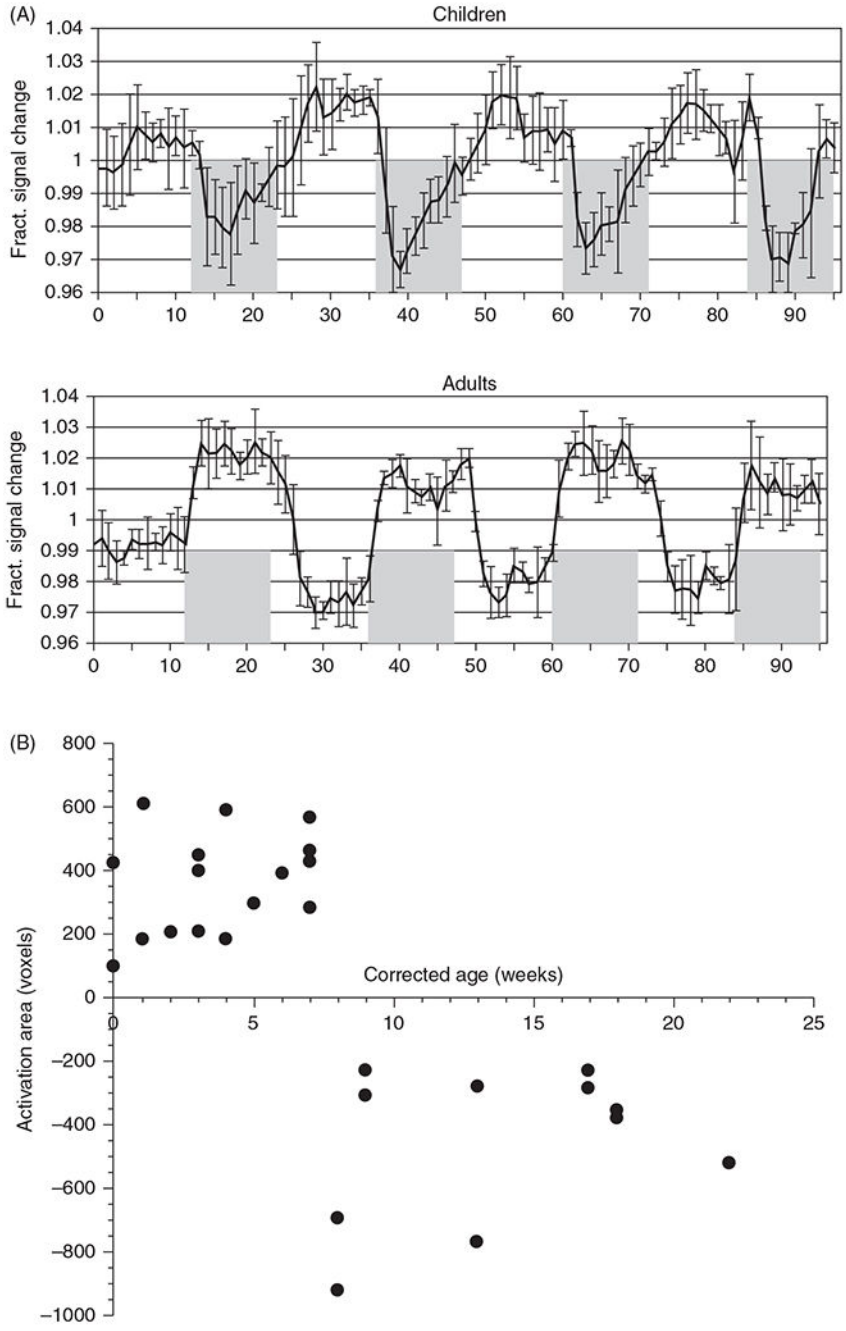


**Figure 10.**

Neurovascular coupling with visual stimulation. (A) Functional MRI BOLD response to visual stimulation (shaded area) in four children at age 4 to 71months is directionally opposite of the response in adults, with a negative BOLD response occurring in children. Perfusion MRI (not shown) indicated no increase in blood flow in infants, in contrast to a 20% increase in perfusion in adults. Source: Adapted, with permission, from Born AP, et al., 2002 (64), © 2002, Elsevier. (B) In response to visual stimulation, the area of significantly activated voxels in visual cortex displays a sharp transition from positive BOLD in neonates

to negative BOLD responses beyond 8 weeks of age. Source: Adapted, with permission, from Yamada H, et al., 2000 (468), © 2000, Wolters Kluwer.

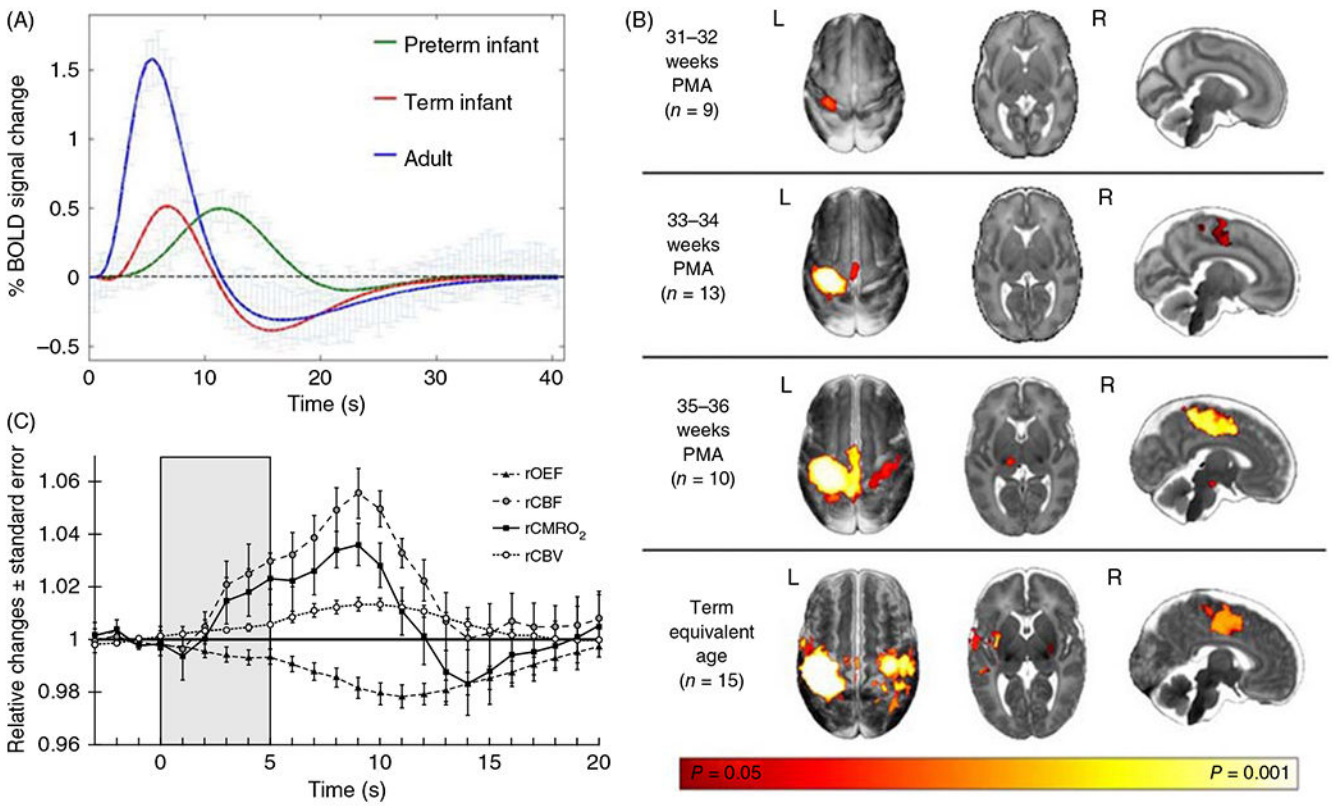


**Figure 11.**

Neurovascular coupling with tactile stimulation. (A) Functional MRI BOLD responses to 1-s somatosensory stimulation of the hand in adults ($n = 10$), infants at term ($n = 15$), and preterm infants at 34 weeks ($n = 10$). Positive BOLD responses are smaller and delayed in infants, and the post-stimulus undershoot is smaller in preterms. Source: Adapted, with permission, from Arichi T, et al., 2012 (14). Licensed Under CCBY 3.0 Unported. (B) In six preterm neonates born at 33 to 34 weeks PMA and studied 2.5 weeks after birth, NIRS-based measurements during 5 s of tactile stimulation show decreased $O_2$ extraction fraction (OEF) and increased CBF, $CMRO_2$, and cerebral blood volume (CBV), thereby indicating the presence of functional coupling in premature neonates. Source: Adapted, with permission, from Roche-Labarbe N, et al. 2014 (381), © 2014, Elsevier.

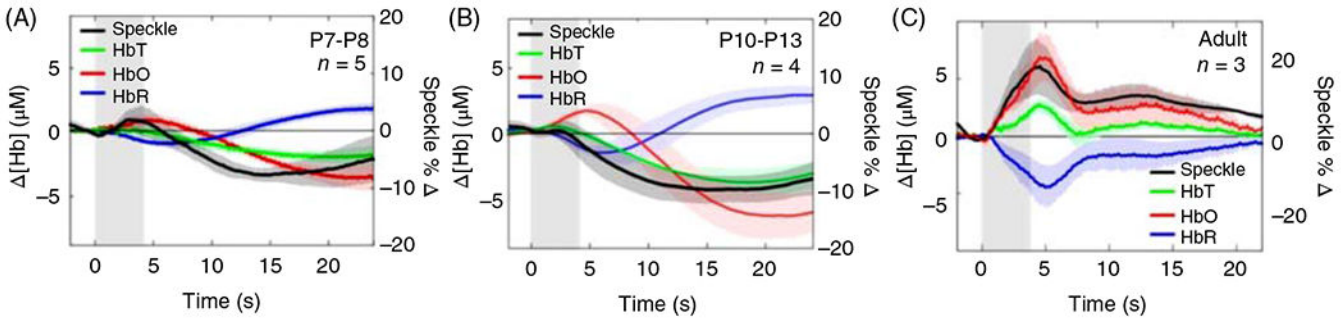


**Figure 12.**

Local cerebral blood flow, measured by laser-speckle imaging, does not increase in response to hindlimb stimulation in the neonatal mouse brain. (A-C) Averaged time courses of the change in oxyhemoglobin (Δ[HbO]), deoxyhemoglobin (Δ[HbR]), tissue hemoglobin (Δ[HbT]), and the percent change in laser-speckle flow (%Δ speckle) in the contralateral hindpaw region of the somatosensory cortex of mice in P7 to P8 (A), P10 to P13 (B), and adult (C) age groups ($n$ = 5, 4, 3, respectively). Source: Adapted, with permission, from Kozberg MG, et al., 2016 (236).

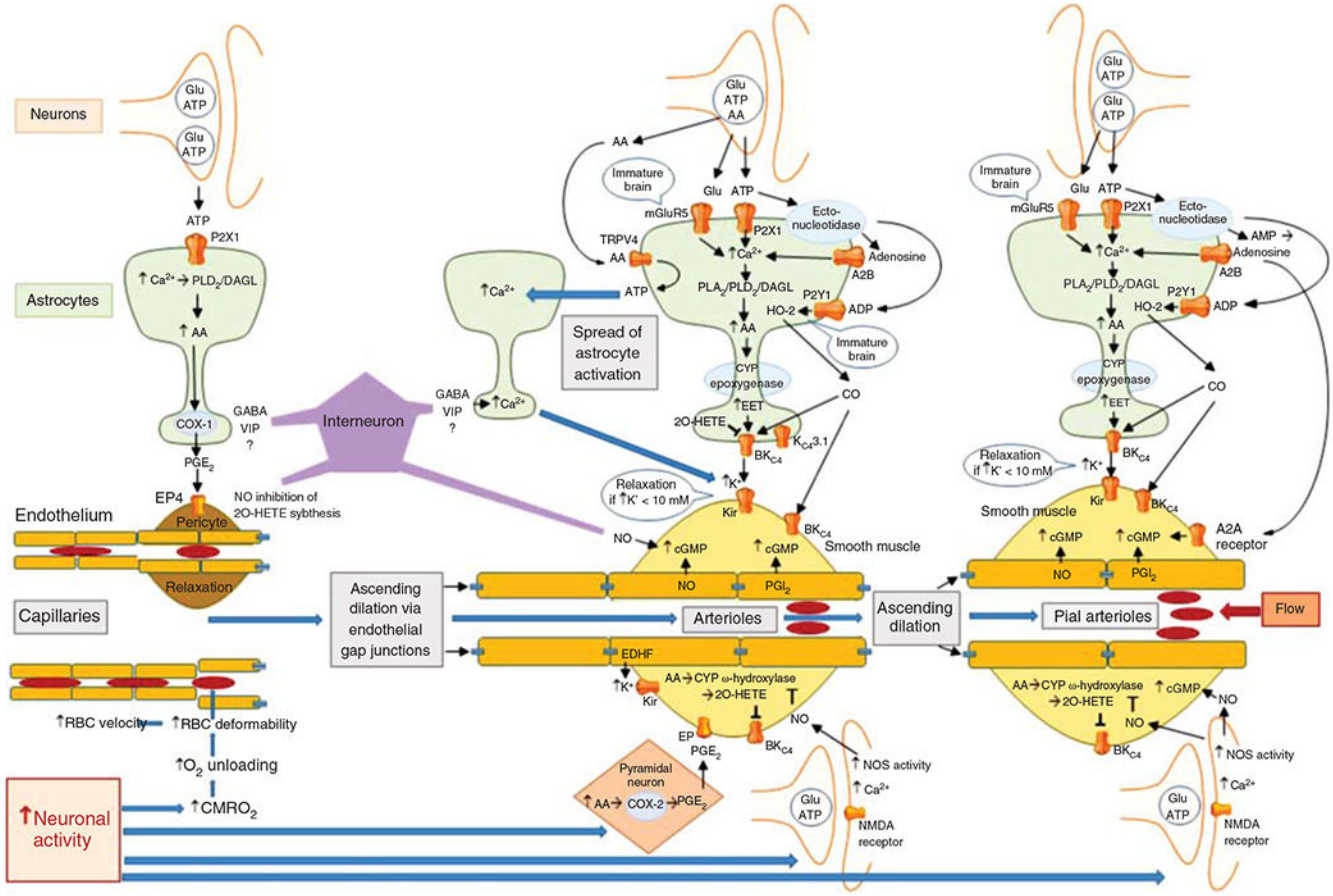


**Figure 13.**

Schematic diagram of the major signaling pathways involved in neurovascular coupling. With the initiation of neuronal action, the sequence of events proceeds from left to right, resulting in ascending vasodilation, part of which depends on conduction through endothelial gap junctions. The first step occurs with the increase in $CMRO_2$ leading to a transient increase in deoxyhemoglobin that results in an increase in red blood cell (RBC) deformability and velocity in capillaries. The second step involves release of the coneurotransmitter ATP acting on astrocyte P2X1 receptors to stimulate mobilization of arachidonic acid (AA) via phospholipase $D_2$ ($PLD_2$) and diacylglycerol lipase (DGL). $PGE_2$ is synthetized by cyclooxygenase-1 (COX-1) and released from the astrocyte foot process to induce relaxation of pericytes via EP4 receptors. Relaxation of circumferential pericytes increases capillary diameter in the vicinity of terminal arterioles, thereby increasing RBC flux. In addition to ATP, some interneurons in close proximity to astrocyte foot processes release GABA and VIP that either directly or indirectly act to increase $Ca^{2+}$ in the foot processes adjacent to pericytes and smooth muscle and that act to facilitate rapid vasorelaxation signaling. The third step is the action of neurotransmitters on astrocytes adjacent to vascular smooth muscle of intraparenchymal arterioles. In addition to the effects of ATP on astrocyte P2X1 receptors, glutamate can act on metabotropic glutamate receptor 5 (mGluR5) that is thought to be present on astrocytes of immature brain. Extracellular ATP can be metabolized by ectonucleotidases to adenosine, which

in sufficiently high concentration can activate the low-affinity adenosine A2B receptor. Together, these pathways may facilitate $Ca^{2+}$ wave transmission throughout the astrocyte network leading to mobilization of AA, which can act as a substrate for cytochrome P450 (CYP) epoxygenase to produce epoxyeicosatrienoic acids (EETs). EETs can activate $BK_{Ca}$ channels on the astrocyte foot process and release sufficient $K^+$ into the tight extracellular space between the foot process and smooth muscle to activate Kir channels on smooth muscle, resulting in hyperpolarization and relaxation. Furthermore, ATP can be metabolized by a different ectonucleotidase on astrocytes to ADP, which can lead to activation of heme oxygenase-2 (HO-2) expressed in astrocytes of immature brain. HO-2 generates CO, which in swine can facilitate the opening of $BK_{Ca}$ channels on smooth muscle and possibly on astrocytes. The intermediate conductance $K_{Ca}$ channel 3.1 and the TRPV4 channel on astrocytes also play a less well-defined role in the coupling process. AA can be released as a coneurotransmitter and serve as an agonist on TRPV4 channels that signal the release of ATP into the extracellular space where they can act on adjacent astrocyte processes to produce a $Ca^{2+}$ response. This slow spread of $Ca^{2+}$ waves in surrounding astrocytes presumably augments vasorelaxation signaling converging on smooth muscle. In addition to astrocyte-mediated vasodilation, neurons can exert direct effects on smooth muscle, including release of $PGE_2$ generated by COX-2 in select neurons and release of NO by neuronal NO synthase (NOS) mediated by NMDA receptors. The NO can stimulate guanylyl cyclase and increase vasorelaxant cGMP in smooth muscle. NO can also inhibit CYP ω-hydroxylase activity and the generation of 20-HETE that normally inhibits $BK_{Ca}$ channels. Some GABAergic interneurons have processes in close proximity to arterioles and capillaries and are thought to induce relaxation via an NO-dependent mechanism. The fourth step is dilation of pial arterioles to maintain the perfusion pressure for the penetrating arterioles serving the activated and nonactivated regions. This dilation involves some of the same mechanisms mediating penetrating arteriolar dilation, including NO generated by neuronal NOS and CO generated by HO-2 in astrocytes in the glia limitans. One difference is that the astrocyte-derived adenosine acts directly on pial arteriole smooth muscle A2A receptors to produce dilation.

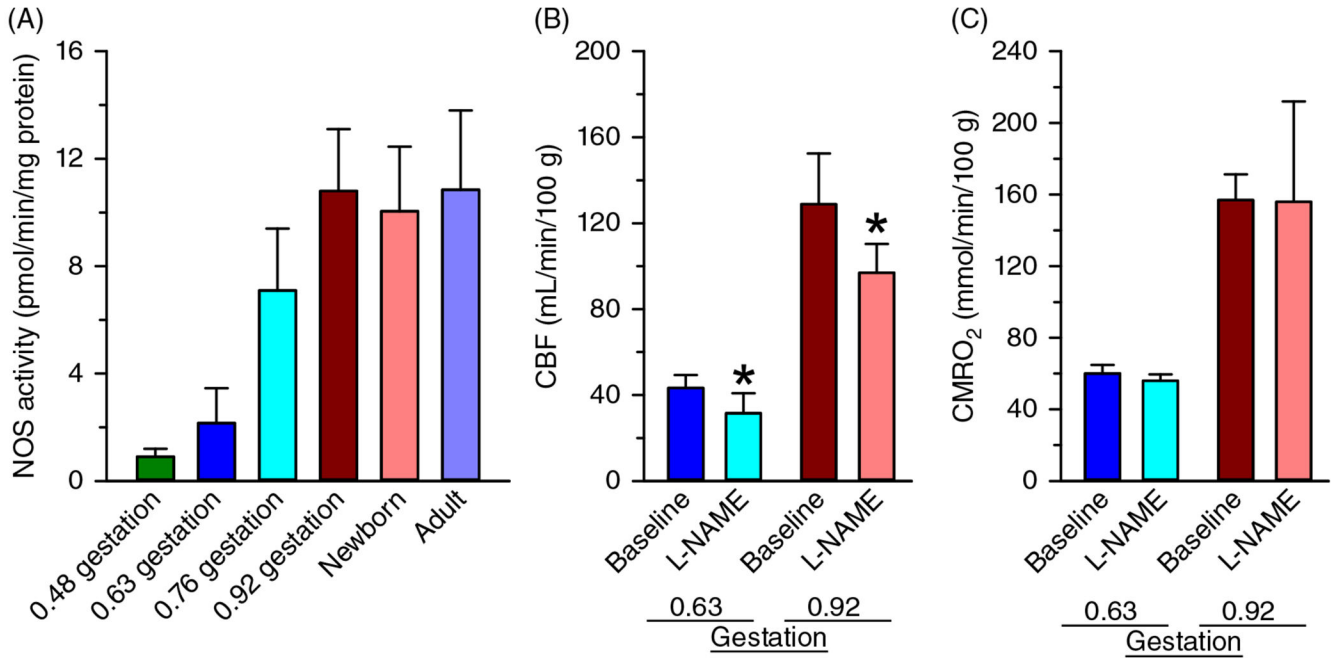


**Figure 14.**

Developmental increases in nitric oxide synthase (NOS) activity in sheep. (A) NOS catalytic activity, measured in fresh cortical samples, increased fourfold between 0.48 and 0.92 gestation in fetal sheep. CBF (B) and $CMRO_2$ (C) increase threefold between 0.63 and 0.92 gestation, and inhibition of NOS activity with nitro-L-arginine methyl ester (L-NAME) decreases CBF in unanesthetized fetal sheep at both gestational ages without reducing $CMRO_2$. These results imply that NO is tonically generated in quantities sufficient to induce vasodilation by midgestation in fetal sheep. Source: Modified, with permission, from Northington FJ, et al., 1997 (335).

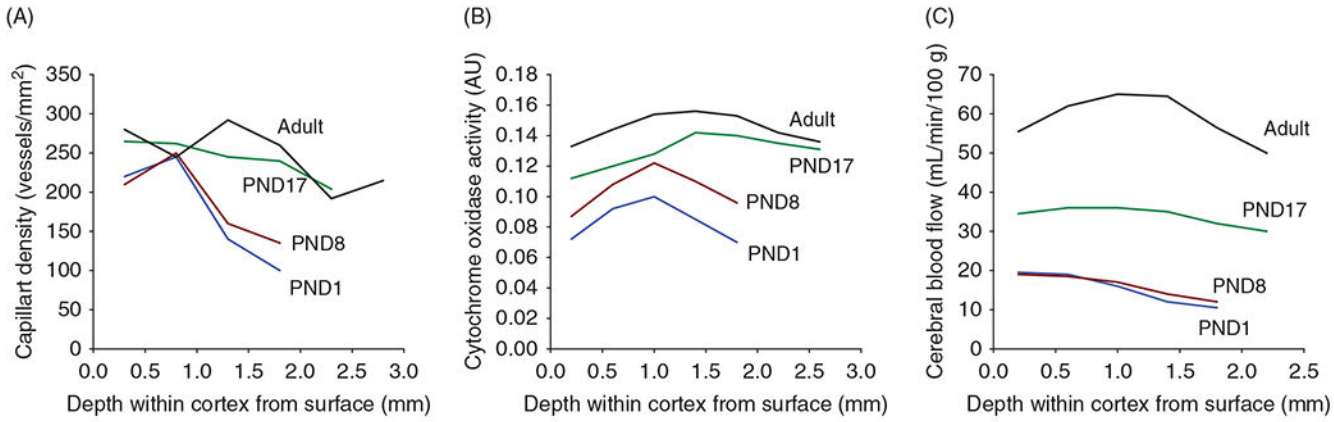


**Figure 15.**

Angiogenesis across cerebral cortical layers. In cerebral cortex of PND1 rabbits, capillary density and CBF are lower in deeper layers and increase during postnatal development. Cytochrome oxidase activity also increases in all cortical layers during development, but in relative terms, its spatial gradient is less than the spatial gradient of capillary density. This comparison suggests that increases in capillary density lag the increases in the mitochondrial capacity for energy metabolism. Source: Adapted, with permission, from Tuor UI, et al., 1994 (417).

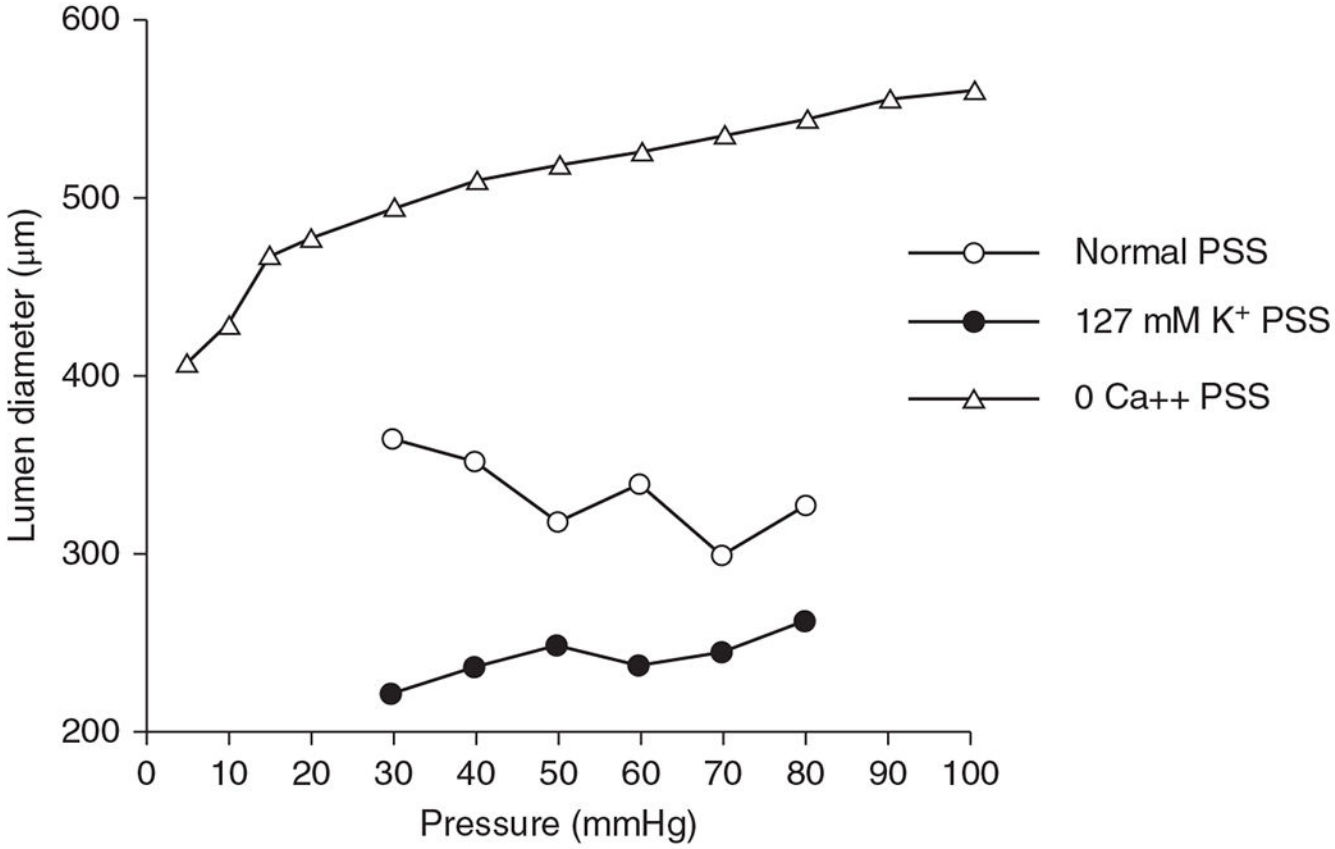


**Figure 16.**

Pressure-diameter relationship of human infant middle cerebral artery at 37 week gestation. The artery was subjected to changes in transmural pressure in random steps between 30 and 80 mmHg in physiologic salt solution (PSS). With increased transmural pressure, arterial diameter decreased (open circles), indicative of increased myogenic tone. In the presence of PSS containing 127 mmol/liter of KCl to induce depolarization and a maximum contractile state (closed circles), diameter increased slightly with increasing transmural pressure. In the presence of $Ca^{2+}$-free PSS containing 2 mmol/liter EGTA (triangles), the diameter increased passively at each pressure value. The difference between the passive and active curves indicates that the human middle cerebral artery is capable of generating a considerable myogenic response at this developmental age. Source: Adapted, with permission, from Bevan RD, et al., 1998 (58), © 1998, Springer Nature.

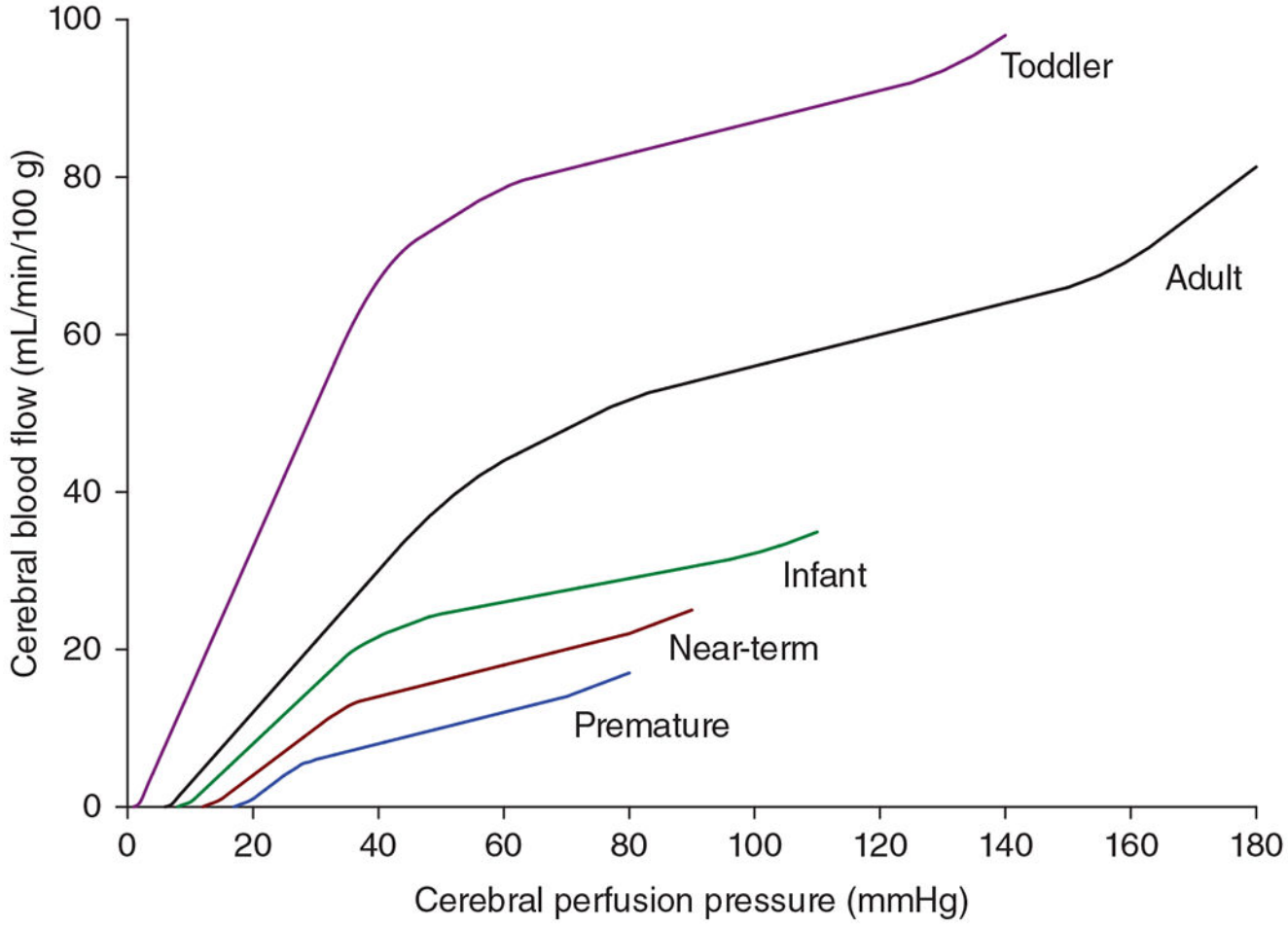


**Figure 17.**

Relationship of cerebral blood flow to cerebral perfusion pressure at different stages of human development. These idealized autoregulation curves are based on the limited number of studies of autoregulation in early human development and of studies of autoregulation in immature animals with extrapolation of the stage of brain maturation of the particular species to human development.

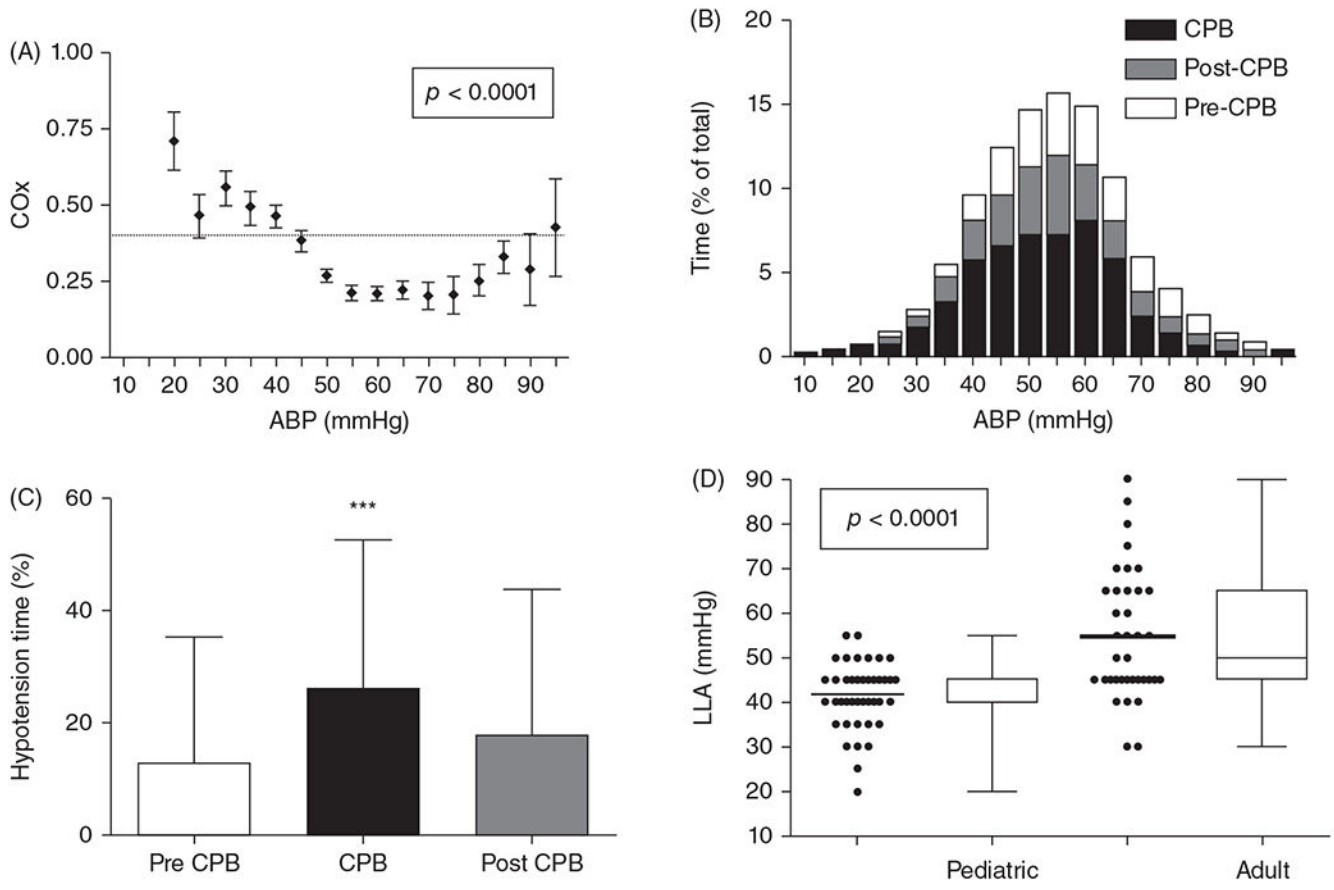


**Figure 18.**

(A) The distribution of the cerebral oximetry index (COx) across binned mean arterial blood pressure (ABP) in children undergoing cardiopulmonary bypass (CPB). Assuming a constant $CMRO_2$ during the sampling period, a low COx indicates a low correlation of tissue $HbO_2$ with variations in ABP (good CBF autoregulation), and a high COx indicates a high correlation of tissue $HbO_2$ with variations in ABP (poor CBF autoregulation). A COx value of 0.4 (horizontal dashed line) is assumed to correspond to the lower limit of autoregulation (LLA) threshold. (B) The distribution of percent of total monitoring time at each ABP before, during, and after CPB. (A, B) Source: Adapted, with permission, from Brady K, et al., 2010 (66). (C) The percentage of time spent below an ABP of 40 mmHg was greater during CPB than before or after CPB. (D) The average individual LLA with COx less than 0.4 for 42 pediatric patients was 42±7 mmHg compared with 55±14 mmHg for 37 adults patients undergoing cardiopulmonary bypass (±SD; $P < 0.0001$ between age groups).

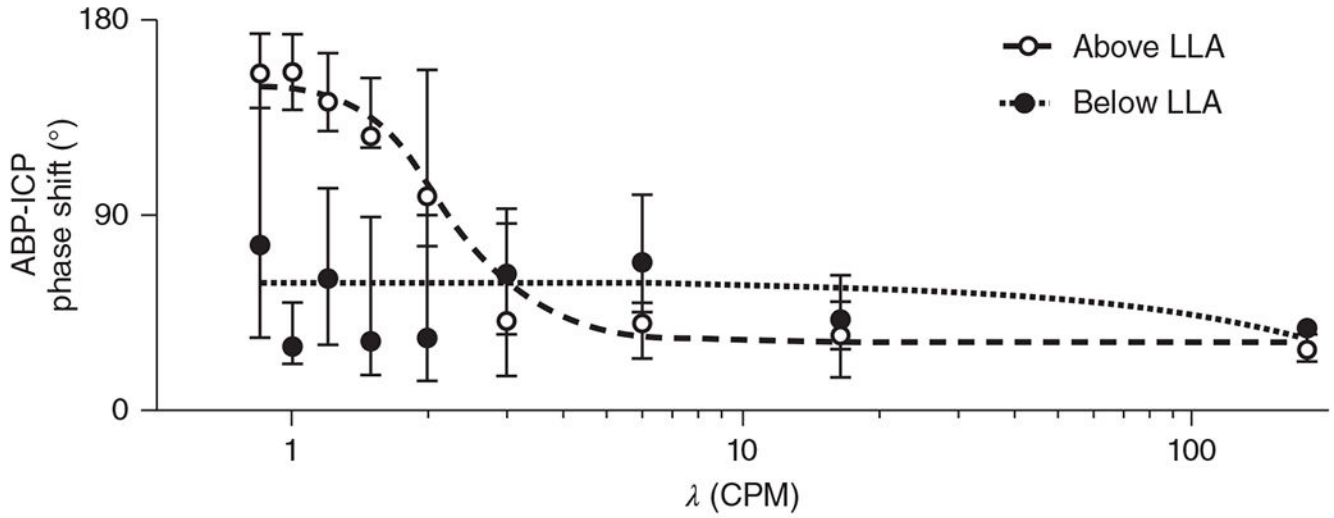


**Figure 19.**

Phase-angle relationship of the response of ICP to quasi-sinusoidal variations in arterial blood pressure (ABP) induced by frequency modulation of positive end-expiratory pressure in two-week-old piglets. When ABP was above the lower limit of autoregulation (LLA, open circles), the phase angle decreased when the ABP frequency increased from 1 to 6 cycles per minute (CPM). Assuming that ICP is related to cerebral blood volume, which is related to cerebral vasodilation and vasoconstriction responses, dynamic autoregulation is ineffective at periodicities less than 10 s. When ABP is below the LLA (closed circles), the phase angle is already reduced at low frequencies, confirming that frequency analysis at low ABP frequencies can be used to assess autoregulation. Source: Adapted, with permission, from Fraser CD, 2013 (144), © 2013, The American Physiological Society.

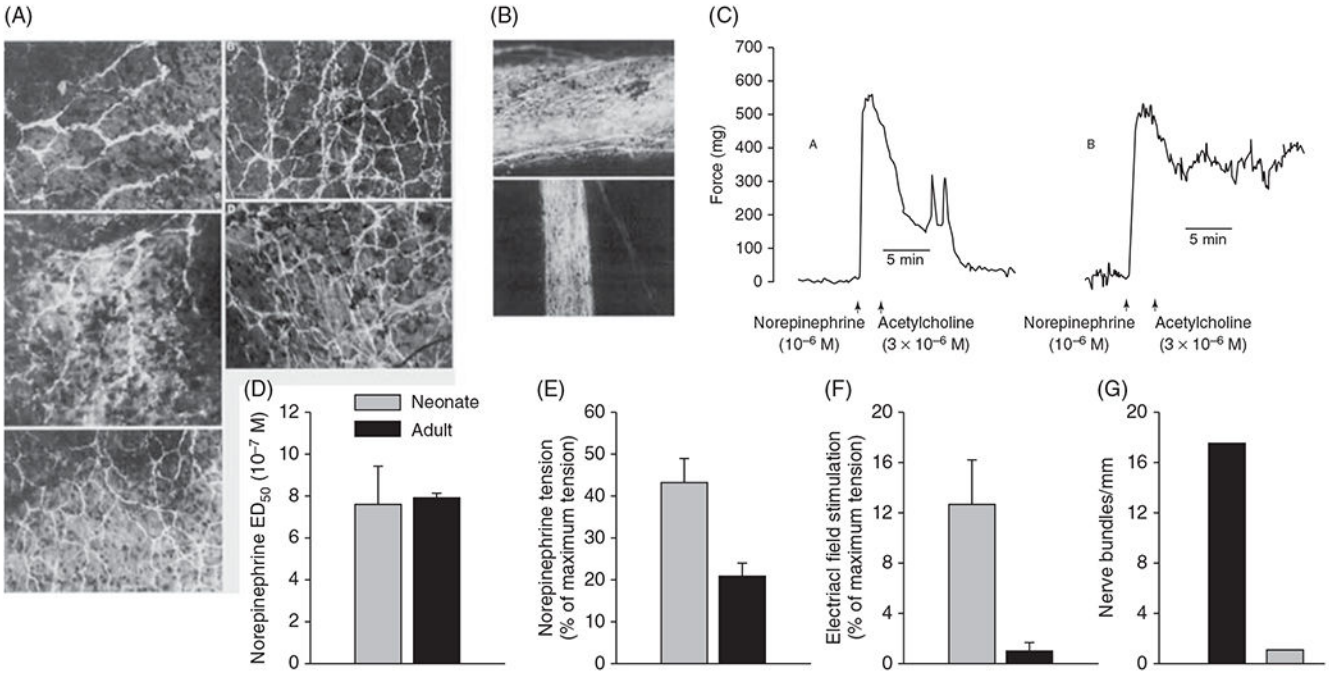


**Figure 20.**

Noradrenergic constriction is enhanced in human preterm cerebral arteries. (A) Catecholamine histofluorescence of perivascular nerves is prominent in proximal middle cerebral artery at gestational age 38 weeks (a) and term (b) and in basilar artery at gestational age 32 weeks (c), 5 weeks (d), and 38 weeks (e). (B) Catecholamine histofluorescence in perivascular nerves is also prominent at gestational age of 24 weeks in distal middle cerebral artery (a) and a branch of basilar artery (b). (C) The response of middle cerebral artery from infant of 24 weeks of gestation to norepinephrine before (left) and after (right) endothelium inactivation, which attenuated the relaxation to acetylcholine while preserving norepinephrine-induced contraction. Source: Adapted, with permission, from Bevan R, et al. 1998 (56), © 1998, Springer Nature. Comparison of the dose to produce constriction in 50% of cerebral arteries ($ED_{50}$) (D) and normalized tension generated in response to norepinephrine (E) and electrical field stimulation (F) of cerebral arteries studied within 2 days of autopsy in eight neonates at 23 to 38 weeks PMA and 21 adults (mean±SE). Comparison of the mean number of catecholaminergic nerve fibers per millimeter length of cerebral arteries in 2 neonates and 15 adults (G). Source: Adapted, with permission, from Bevan R, et al., 1998 (56).

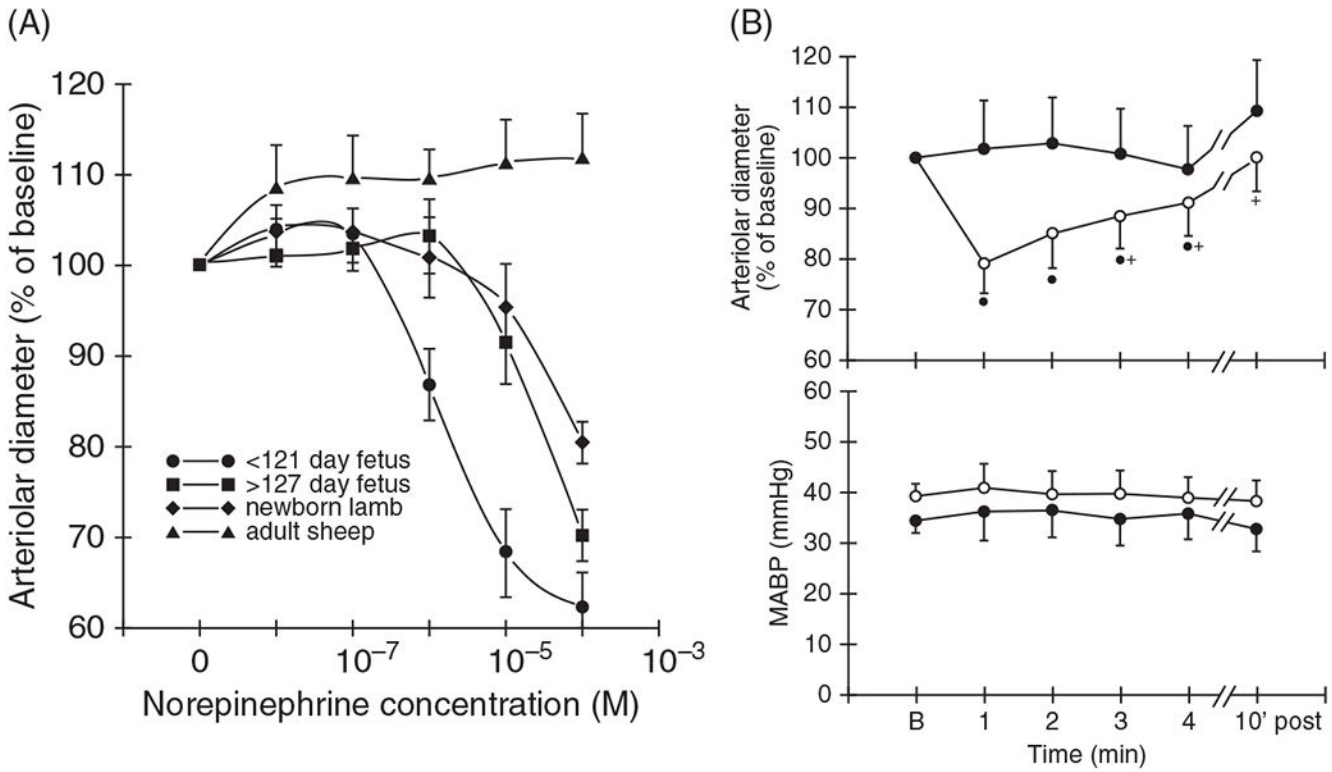


**Figure 21.**

Developmental changes in norepinephrine-induced constriction of pial arteries. (A) When applied through a closed cranial window, norepinephrine produced dose-dependent constriction in anesthetized fetal sheep and newborn lambs but not in adult sheep. The effect was most pronounced in fetuses less than 121 days gestation (<0.8 full term). (B) Electrical stimulation of the superior cervical sympathetic ganglion produced constriction of pial arteries that was blocked by the α-adrenergic antagonist prazosin. Source: Adapted, with permission, from Wagerle LC, et al., 1990 (442), © 1990, The American Physiological Society.

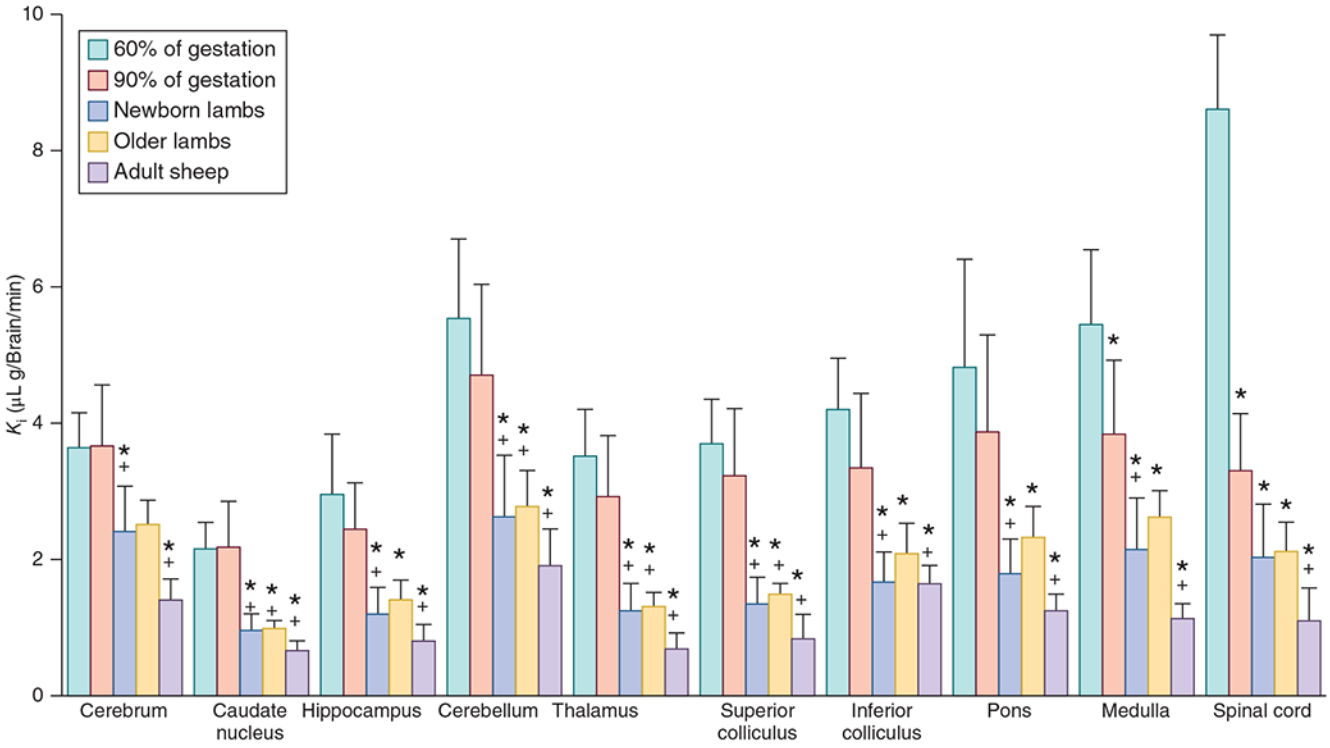


**Figure 22.**

Developmental changes in blood-brain barrier permeability in sheep. The influx transfer constant (Ki) for radiolabeled aminoisobutyric acid shows a progressive decrease from 60% of gestation in fetal sheep through adulthood in various brain regions. However, even at 60% of gestation, the transfer constant is not considered high and indicates that significant diffusion restriction is present for this metabolically inert small molecule. Source: Modified, with permission, from Stonestreet BS, et al., 1996 (402), © 1996, The American Physiological Society.

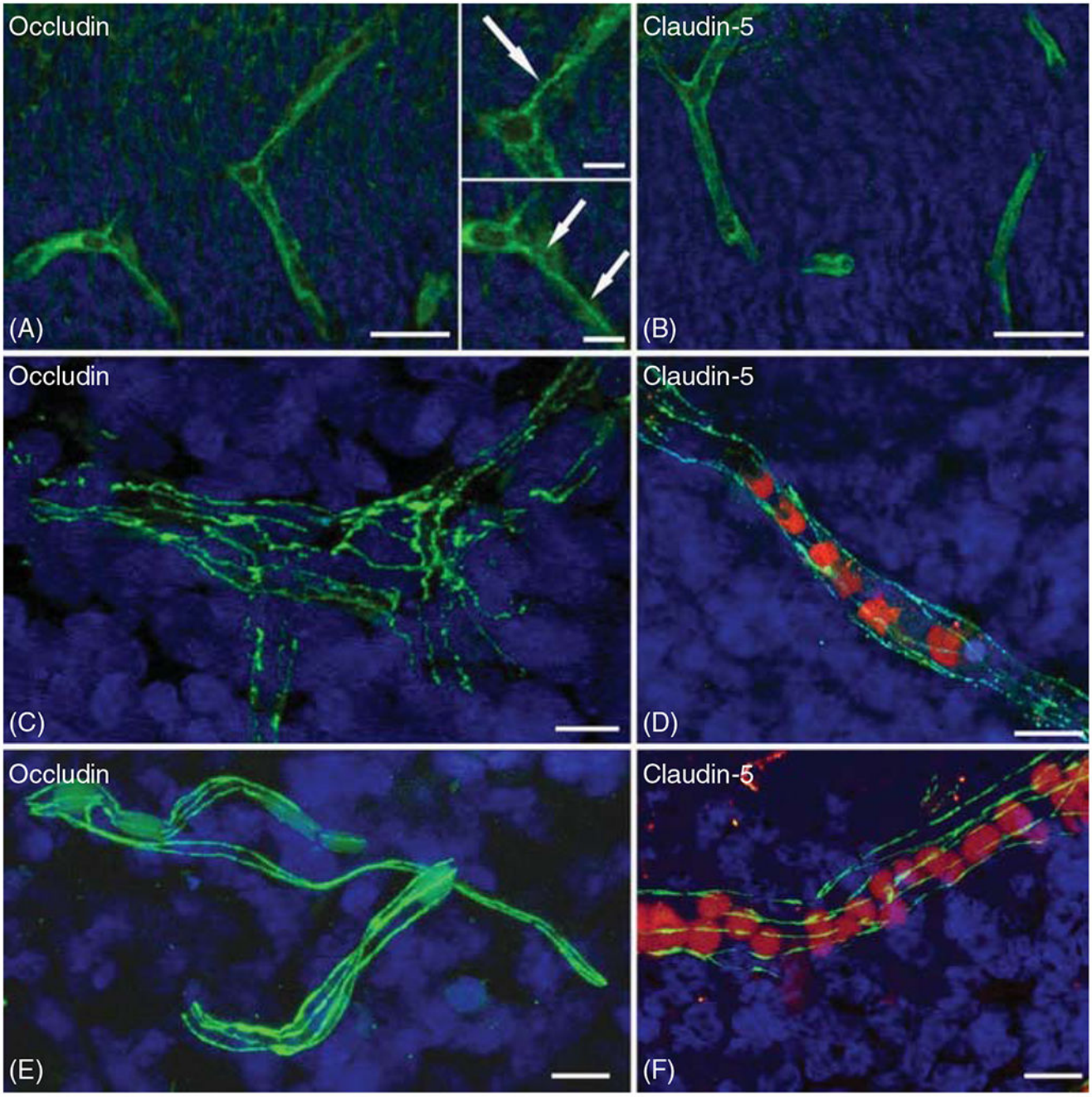


**Figure 23.**

Developmental changes in tight junction protein organization. Immunostaining of occludin and claudin-5 shows endothelial cytoplasmic staining with some linear cell membrane assembly of occludin present at 12 weeks PMA in human fetal telencephalon (A, B). By 14 weeks, linear beaded staining of occludin and claudin-5 becomes evident in the cell membrane (C, D). At 18 weeks, a more mature appearance of nearly linear immunostaining of occludin and claudin-5 occurs. Source: Adapted, with permission, from Virgintino et al. (434).

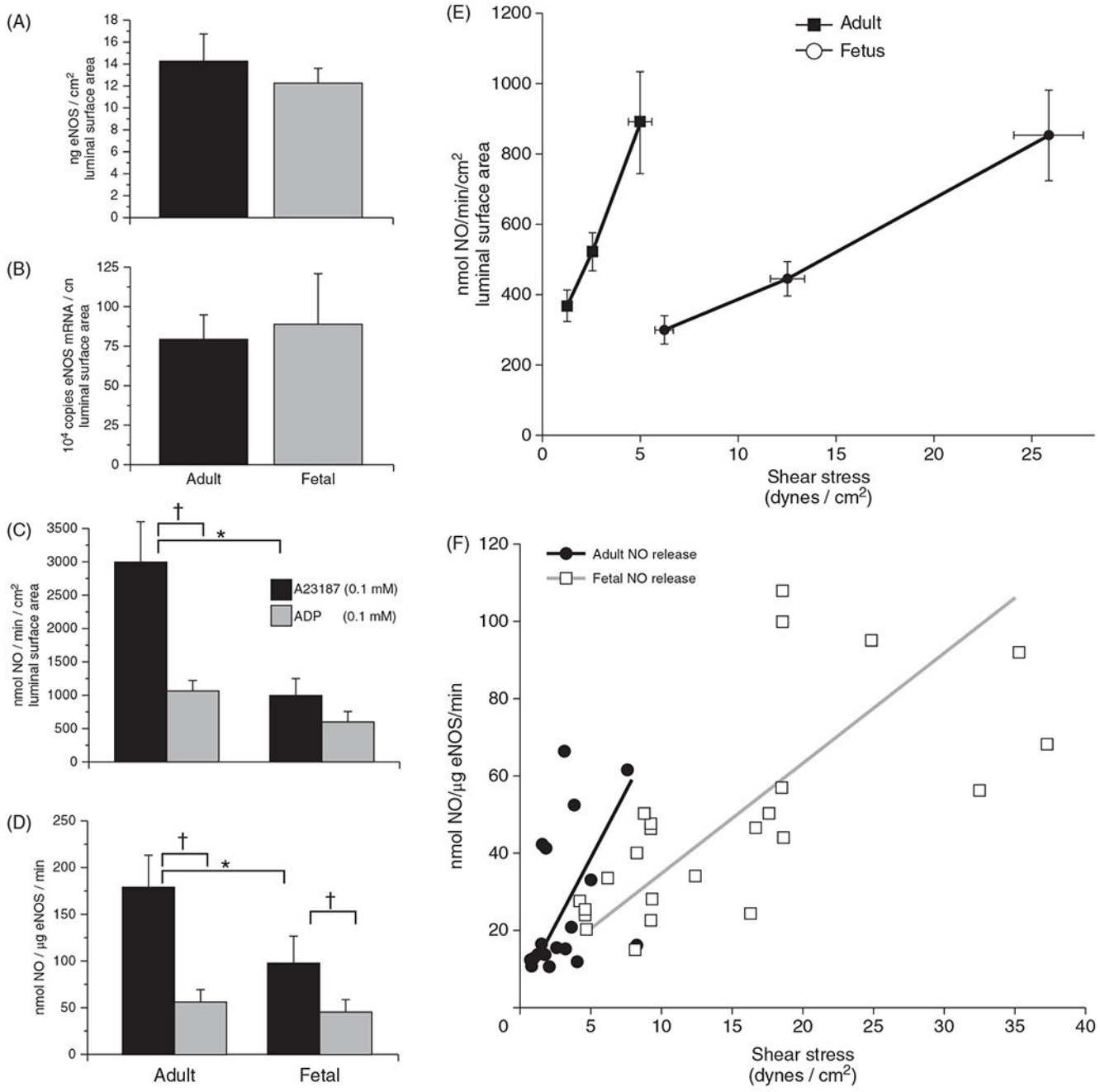


**Figure 24.**

Endothelial vasodilator function is depressed in fetal sheep carotid arteries. Postnatal maturation is associated with a moderately increased abundance of endothelial nitric oxide synthase (eNOS). However, when normalized by the luminal surface area or by eNOS concentration, the amount of NO generated in response to the calcium ionophore A23187 or to endothelial shear stress is greater in adult than in fetal arteries. In contrast, NO generation by ADP is not significantly different. Thus, eNOS coupling mechanisms are not fully mature in fetal sheep arteries, and maturation may depend on the nature of the stimulus. Mean±SE,

*n* = 6-8. Source: Adapted, with permission, from White CR, et al., 2005 (451), © 2005, The American Physiological Society.

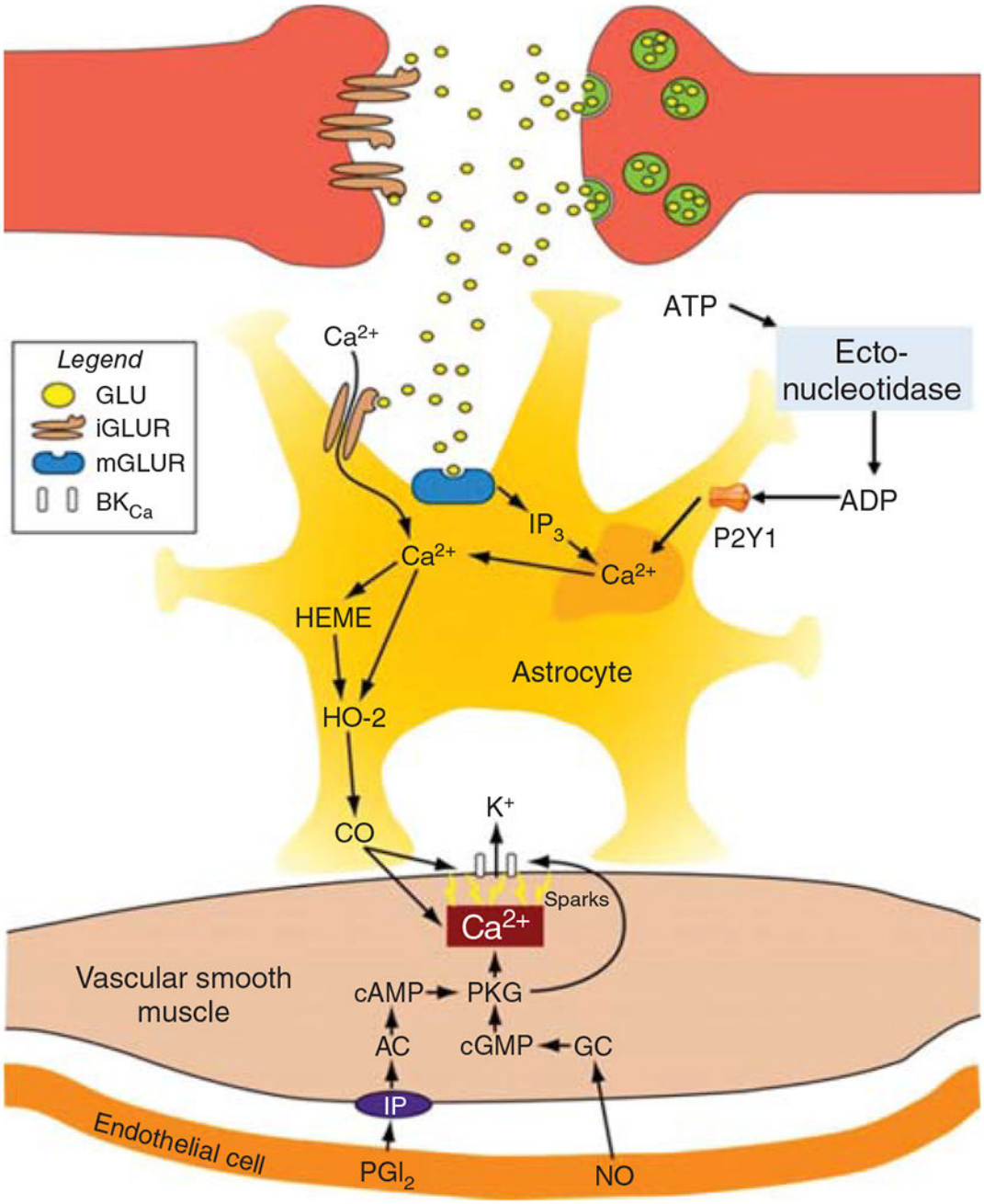


**Figure 25.**

Role of CO in immature neurovascular unit in glia limitans. Neurotransmitter glutamate binds to astrocyte ionotropic and metabotropic glutamate (GLU) receptors (iGLUR and mGLUR) expressed on immature astrocytes, elevating $[Ca^{2+}]_i$ that increases heme oxygenase-2 (HO-2 activity) and generates CO. The CO diffuses to pial artery vascular smooth muscle where it binds to a heme element that increases $Ca^{2+}$ spark-to-$BK_{Ca}$ channel coupling, thereby elevating $BK_{Ca}$ channel activity. In addition, CO increases $Ca^{2+}$ spark frequency, further increasing $BK_{Ca}$ channel activity. The resulting smooth muscle cell

hyperpolarization produces vasodilation. Furthermore, endothelial-derived NO and $PGI_2$ provide a minimal amount of guanylyl cyclase (GC) and cGMP and/or activation of $PGI_2$ receptors (IP), adenylyl cyclase (AC), and cAMP. The resulting protein kinase G (PKG) activity may phosphorylate sarcoplasmic reticulum RyRs, increasing $Ca^{2+}$ spark frequency and/or the $BK_{Ca}$ channel. In the intact vasculature, NO and $PGI_2$ can activate smooth muscle cell GC and AC directly, if a stimulus is sufficient at the endothelial cell. In addition to glutamate, neurons can release ATP from neurotransmitter vesicles, the ATP can be degraded to ADP by an astrocyte endonucleotidase, and the ADP can act on astrocyte P2Y1 receptors to also activate HO-2 (not shown). $IP_3$, inositol 1,4,5-trisphosphate. Source: Adapted, with permission, from Leffler CW, et al., 2011 (276), © 2011, The American Physiological Society.

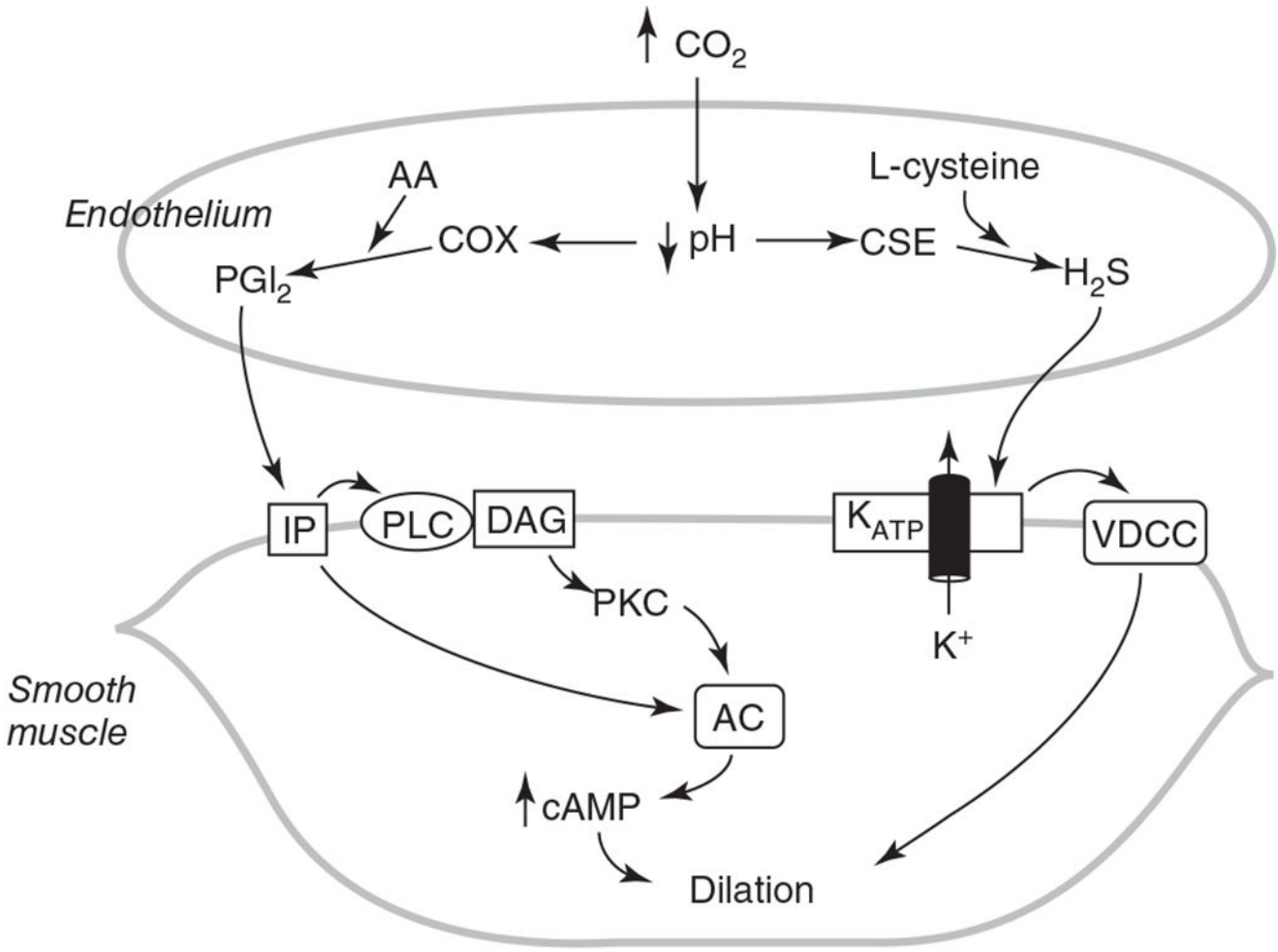


**Figure 26.**

Schematic diagram of endothelial-derived factors in dilation of pial arterioles to hypercapnia. Acidosis is thought to activate cystathionine γ-lyase (CSE) and generate $H_2S$, which activates $K_{ATP}$ channels and induces hyperpolarization and consequent inhibition of VDCC, voltage-dependent $Ca^{2+}$ channels (VDCC). $H_2S$ also promotes $Ca^{2+}$ sparks and activation of $BK^{Ca}$ channels (not shown), which also play a role in hypercapnic dilation. In addition, acidosis is thought to stimulate arachidonic acid (AA) release and cyclooxygenase (COX) activity and generate $PGI_2$, which then acts on the smooth muscle prostacyclin receptor (IP) to stimulate adenylyl cyclase (AC). Source: Adapted, with permission, from Leffler CW, et al., 2011 (274), © 2011, The American Physiological Society.

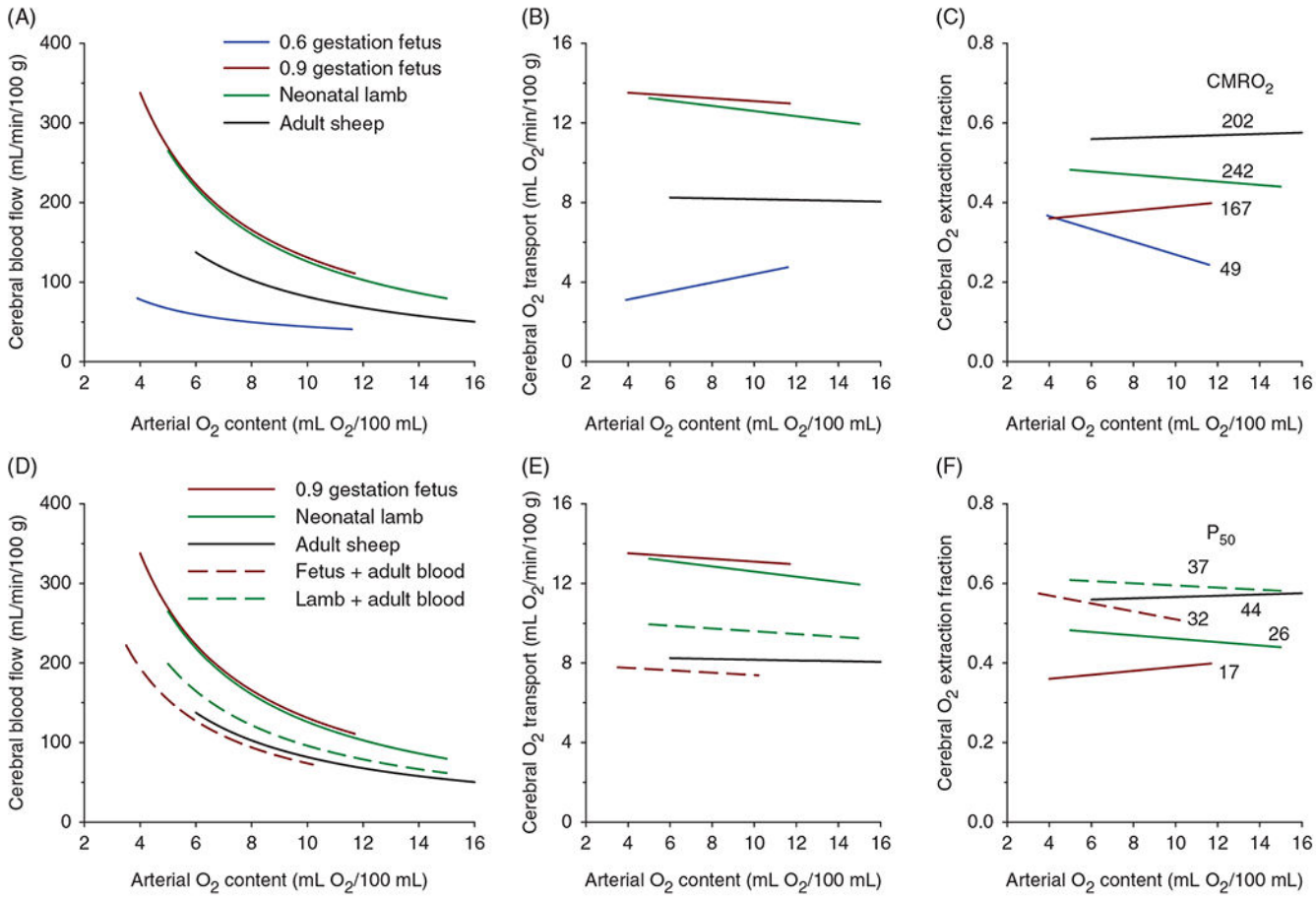


**Figure 27.**

Developmental changes in the cerebrovascular response to hypoxia in unanesthetized sheep. (A) Over a wide range of arterial $O_2$ content, cerebral blood flow (CBF) increases from 0.6 gestation to 0.9 gestation in fetal sheep, remains elevated after birth, and then decreases in adults. (B) At 0.6 gestation, the increase in CBF is inadequate to maintain cerebral $O_2$ transport, whereas the $O_2$ transport is maintained later in development during hypoxia. (C) $O_2$ extraction fraction, which is the ratio of $CMRO_2$ to $O_2$ transport, is also maintained during hypoxia later in development, although the level is highest in adults and lowest at 0.6 gestation. The levels of $O_2$ extraction fraction differed among groups despite normalization with the different levels of $CMRO_2$ (indicated as μmol $O_2$/min/100 g). (D-F) Fetal sheep at 0.9 gestation and neonatal lambs underwent a partial exchange transfusion with adult sheep blood having a $P_{50}$ ($PO_2$ at 50% oxyhemoglobin saturation) of 44 Torr to increase the $P_{50}$ from 17 to 32 Torr in fetal sheep and from 26 to 37 Torr in neonatal lambs. Compared to the pretransfusion responses to hypoxia, the CBF and $O_2$ transport responses were reduced, and the $O_2$ extraction fraction was elevated to levels closer to those seen in adult sheep. Source: Adapted, with permission, from Koehler RC, et al., 1986 (228), 1984 (230); Gleason CA, et al., 1990 (161); Rosenberg AA, et al., 1986 (382).

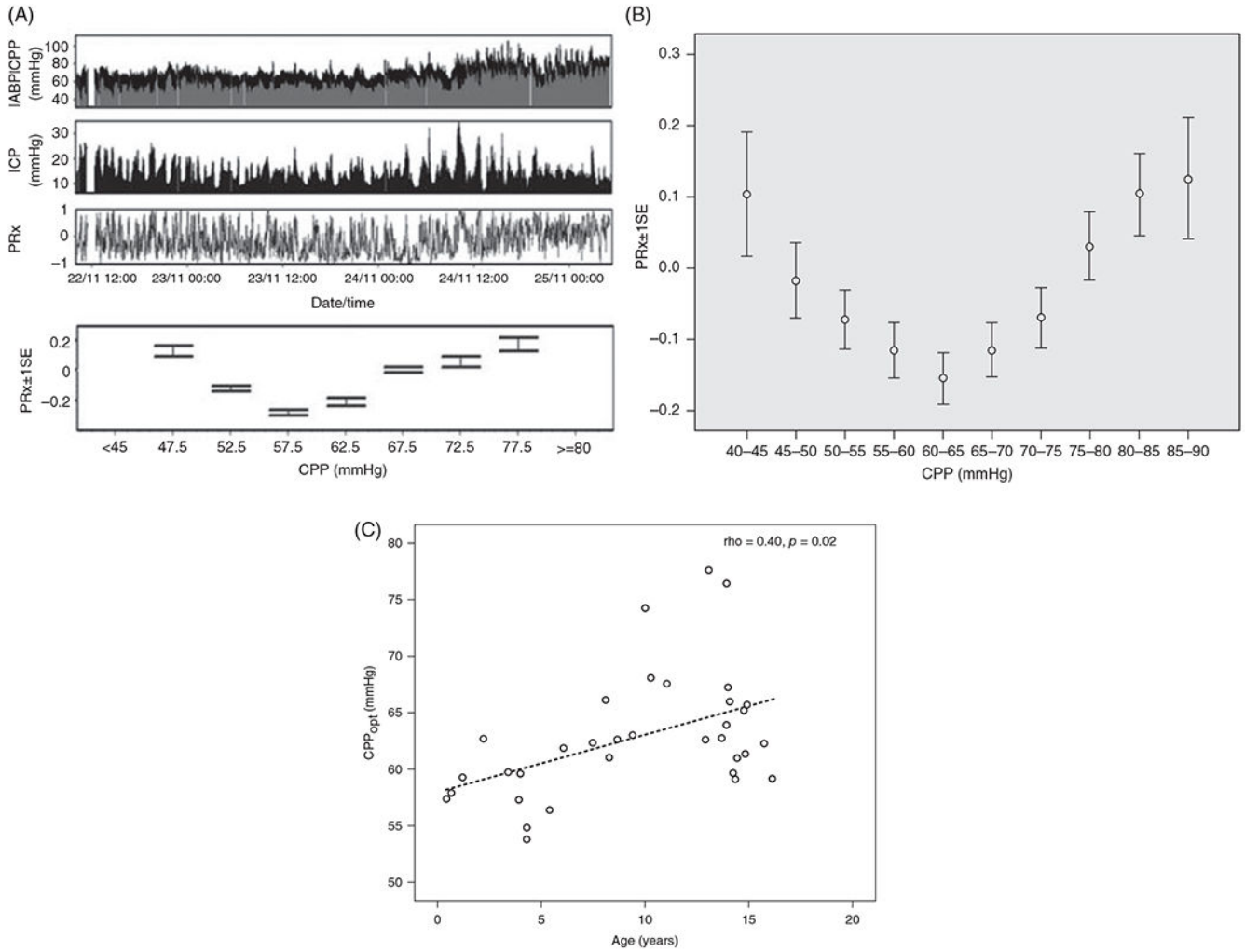


**Figure 28.**

(A) Example of real-time monitoring of pressure-reactivity index (PRx) for 72 h in a child after TBI. Top trace shows arterial blood pressure (ABP, black) and CPP (gray), second trace shows ICP, and third trace shows PRx. Bottom chart shows the PRx within 5 mmHg CPP bins averaged over 72 h for this single patient. An optimal CPP of 57.5 mmHg could be identified wherein PRx had a minimal value. (B) The average PRx for 36 children after TBI displays a U-shaped curve. (C) The optimal CPP ($CPP_{opt}$) in 34 TBI patients correlated with the patient's age. Source: Adapted, with permission, from Lewis PM, et al., 2015 (278), © 2015, Wolters Kluwer.

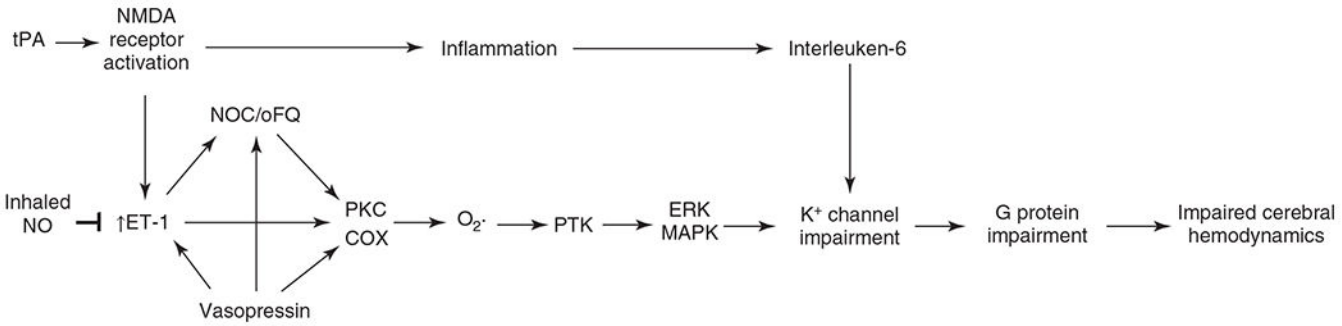


**Figure 29.**

Schematic diagram of potential mechanisms of impaired cerebrovascular regulation after hypoxia-ischemia, stroke, and fluid percussion injury in piglets. Endothelin-1 (ET-1) and vasopressin have been implicated in the release of the endogenous opioid nociception/orphanin FQ (NOC/oFQ) that can result in the generation of superoxide through a PKC signaling in concert with activation of cyclooxygenase (COX). Acting through protein tyrosine kinase (PKT) and ERK/MAPK signaling, superoxide generation results in impaired $K^+$ channel function. Focal stroke stimulates endogenous tissue plasminogen activator (tPA) that is known to augment activation of NMDA receptors. This pathway can result in increased ET-1 and activation of ERK/MAPK. It also produces an inflammatory response leading to increased interleukin-6 and impaired function of $K^+$ channels. Inhaled nitric oxide can block the increase in ET-1 and preserve autoregulation. Source: Adapted, with permission, from Pastor P, et al., 2019 (361); Armstead, WM, 2005 (34).

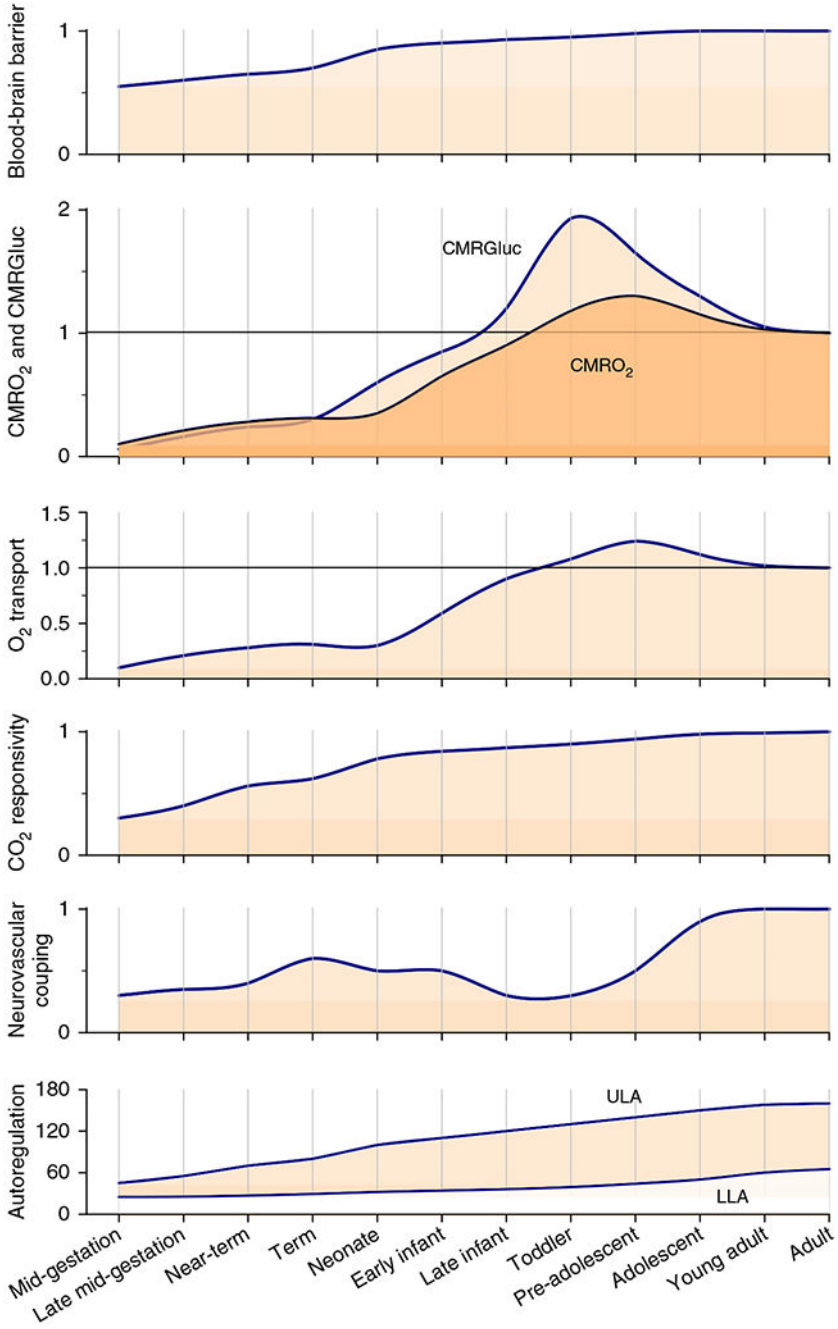


**Figure 30.**

Synthesis of the relative time course of developmental regulation of the cerebral circulation and energy metabolism. Blood-brain barrier (BBB) function, $CMRO_2$, CMRGluc, cerebral $O_2$ transport, CBF reactivity to $CO_2$, and neurovascular coupling are normalized relative to an adult value of 1. Autoregulation is displayed in terms of the upper (ULA) and lower (LLA) limits of autoregulation (mmHg) below and above which CBF is pressure passive. All lines are based on human data or, in the cases where human data are not available, on animal data. Interpolation was used in cases where no data are available for a particular

developmental stage. Note that energy metabolism and $O_2$ transport overshoot adult values between the infant and adolescent stages, whereas $CO_2$ reactivity does not. Also, $O_2$ transport has a postnatal dip, attributable to transient anemia and the decrease in hemoglobin $O_2$ affinity as fetal hemoglobin is replaced with adult hemoglobin. Neurovascular coupling is thought to have a transient increase near term and then decrease during the period of elevated CMRGluc. The range of autoregulation between the ULA and LLA progressively expands during development.